UNIVERSITAT POLITÈCNICA DE VALÈNCIA

EXPERIMENTAL STUDY OF THE FUEL EFFECT ON DIFFUSION COMBUSTION AND SOOT FORMATION UNDER DIESEL ENGINE-LIKE CONDITIONS

DOCTORAL THESIS

PRESENTED BY:
ALBA ANDREINA GARCÍA CARRERO

SUPERVISED BY:
JOSÉ VICENTE PASTOR SORIANO

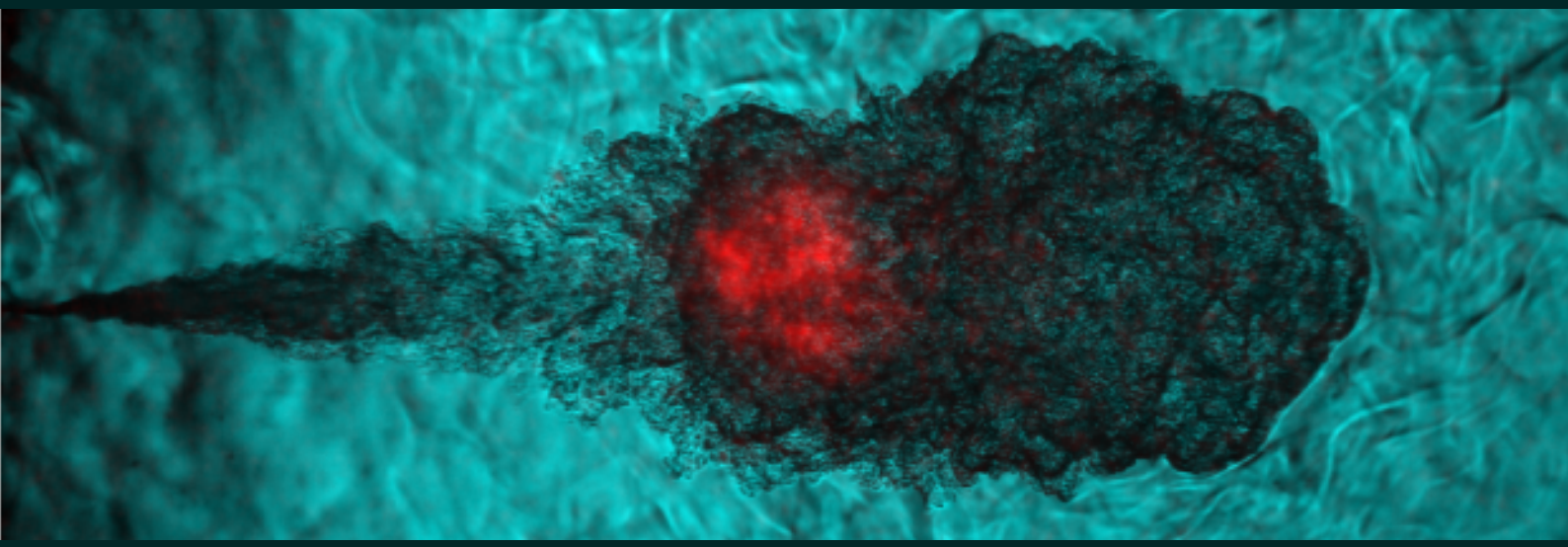

NOVEMBER 2021

DEPARTAMENTO DE MÁQUINAS Y MOTORES TÉRMICOS

Universitat Politècnica de València

Departamento de Máquinas y Motores Térmicos

EXPERIMENTAL STUDY OF THE FUEL EFFECT ON DIFFUSION COMBUSTION AND SOOT FORMATION UNDER DIESEL ENGINE-LIKE CONDITIONS

Doctoral Thesis

Presented by:

Alba Andreina García Carrero

Directed by:

Dr. José Vicente Pastor Soriano

Valencia, November 2021

Doctoral Thesis

EXPERIMENTAL STUDY OF THE FUEL EFFECT ON DIFFUSION COMBUSTION AND SOOT FORMATION UNDER DIESEL ENGINE-LIKE CONDITIONS

Presented by: Alba Andreina García Carrero

Directed by: Dr. José Vicente Pastor Soriano

Examining Board:

President: Prof. Jaime Gimeno García

Secretary: Prof. José Rodriguez Fernandez

Examiner: Dr. Cinzia Tornatore

Reviewing Board:

Prof. Magin Lapuerta Amigo

Dr. Francesco Concetto Pesce

Dr. Cinzia Tornatore

Valencia, November 2021

Abstract

CO_2 emissions in the transport sector have increased considerably in recent years due to global economic development. The growth of transport fleets, along with other factors, has contributed to the imbalance of the planet's carbon cycle. For that, CO_2 is considered a greenhouse gas from anthropogenic origin that must be reduced to avoid global warming.

Strategies to reduce CO_2 in the transport sector are focused on electrification and the use of neutral fuels or those with a low impact on the environment. However, an effective implementation of the latter requires a deep understanding of the combustion with those fuels. In this doctoral thesis, the combustion of different types of fuels has been experimentally characterized, including some with low impact on CO_2 emissions such as Hydrotreated Vegetable Oil (HVO) and two oxymethylene ethers (OME_1 and OME_x). Furthermore, due to their potential in reducing pollutants, blends of diesel and gasoline and HVO and Liquefied Petroleum Gas (LPG) have also been evaluated, which required adapting the injection system to avoid evaporation along the injection line.

All these fuels and blends have been injected with a single-hole nozzle and they have been evaluated using high speed visualization techniques under different thermodynamic conditions typical of a compression ignition engine operating under low-temperature combustion conditions in installations with optical accesses.

The effect of the physical-chemical properties of these fuels and blends on the characteristic parameters of a jet, such as the liquid length and the vapor penetration, has been analyzed. Combustion has been evaluated by characterizing the ignition delay, the heat release and the flame Lift-off length that is conditioned by the mixing process. Furthermore, the study of soot formation based on the fuel properties and the characteristics of the mixing process represents an important contribution of this thesis, showing that in addition to the benefits in CO_2 reduction provided by the different fuels and blends used in this study, these fuels also reduced the soot formation in the combustion chamber, highlighting among them the oxygenated fuels, especially OME_x which, in addition to not forming soot, was the most reactive in all conditions of operation evaluated.

Resumen

Las emisiones de CO_2 en el sector transporte se han incrementado considerablemente durante los últimos años debido al desarrollo económico mundial. El crecimiento de las flotas de transporte, junto con otros factores, ha contribuido al desequilibrio del ciclo de carbono del planeta. Es por ello que el CO_2 se considera un gas de efecto invernadero de origen antropogénico que debe ser reducido para evitar el calentamiento global.

Las estrategias para reducir el CO_2 en el sector transporte están enfocadas a la electrificación y al uso de combustibles neutros o de bajo impacto al ambiente. Sin embargo, una efectiva implementación de esta última requiere un profundo entendimiento de la combustión con tales combustibles. En la presente tesis doctoral, se ha caracterizado experimentalmente la combustión de diferentes tipos de combustibles, entre ellos, algunos de bajo impacto en emisiones de CO_2 como lo son el Aceite Vegetal Hidrotratado (HVO) y dos éteres de oximetileno (OME_1 y OME_x).Además, por su potencial en la reducción de contaminantes se han evaluado mezclas de diésel y gasolina y de HVO y Gas Licuado de Petróleo (LPG), lo que requirió adecuar el sistema de inyección para evitar la evaporación a lo largo de la línea.

Todos estos combustibles y mezclas han sido inyectados con una tobera mono-orificio y han sido evaluados mediante técnicas de visualización a alta velocidad bajo diferentes condiciones termodinámicas típicas de un motor de encendido por compresión operando en condiciones de combustión a baja temperatura, en instalaciones con accesos ópticos.

Se ha analizado el efecto de las propiedades físico químicas de estos combustibles y mezclas sobre los parámetros característicos de un chorro como lo son la longitud líquida y la penetración de vapor. La combustión ha sido evaluada mediante la caracterización del tiempo de retraso, de la liberación de calor y la longitud del despegue de la llama, que viene condicionada por el proceso de mezcla. Igualmente, el estudio de la formación de hollín en función de las propiedades del combustible y de las características del proceso de mezcla, representa un aporte importante de esta tesis. En adición a los beneficios en reducción de CO_2 que brindan los combustibles y mezclas utilizados en este estudio, estos también redujeron la formación de hollín en la cámara de combustión, destacándose entre ellos los combustibles oxigenados, especialmente el OME_x que además de no formar hollín, fue el de mayor reactividad en todas las condiciones de operación evaluadas.

Resum

Les emissions de CO_2 en el sector transport s'han incrementat considerablement durant els últims anys a causa del desenvolupament econòmic mundial. El creixement de les flotes de transport, juntament amb altres factors, ha contribuït al desequilibri del cicle de carboni del planeta. És per això, que el CO_2 es considera un gas d'efecte hivernacle d'origen antropogènic que ha de ser reduït per evitar l'escalfament global.

Les estratègies per reduir el CO_2 dins el sector transport, estan enfocades a l'electrificació i a l'ús de combustibles neutres o de baix impacte ambiental. No obstant això, una efectiva implementació d'aquesta última, requereix un profund coneixement del procés de combustió d'aquests combustibles. En la present tesi doctoral, s'ha caracteritzat experimentalment la combustió de diferents tipus de combustibles, entre ells, alguns de baix impacte en emissions de CO_2 com són l'Oli Vegetal Hidrotratat (HVO) i dos èters de oximetileno (OME_1 i OME_x) .A més , degut al seu alt potencial en la reducció de contaminants, s'han avaluat mescles de dièsel i gasolina, i de HVO i Gas Liquat de Petroli (LPG), el que va requerir adequar el sistema d'injecció per evitar l'evaporació al llarg de la línia.

Tots aquests combustibles i mescles han estat injectats amb una tovera mono-orifici i han estat avaluats mitjançant tècniques de visualització a alta velocitat a través dels accessos òptics del que disposa la instal·lació. Les diferents condicions termodinàmiques utilitzades son típiques d'un motor d'encesa per compressió operant en condicions de combustió a baixa temperatura.

S'ha analitzat l'efecte de les propietats fisicoquímiques d'aquests combustibles i de les mescles sobre els paràmetres característics d'un raig com són la longitud líquida i la penetració de vapor. La combustió ha estat avaluada mitjançant la caracterització del temps de retard, de l'alliberació de calor i de la longitud de l'enlairament de la flama que ve condicionada pel procés de mescla. A més, l'estudi de la formació de sutge en funció de les propietats del combustible i de les característiques del procés de mescla, representa una aportació important d'aquesta tesi evidenciant que a més dels beneficis en reducció de CO_2 que brinden tots aquests combustibles i mescles, també varen reduir la formació de sutge a la cambra de combustió, destacant-se entre ells els combustibles oxigenats, especialment el OME_x, que a més de no formar sutge, va ser el de major reactivitat en totes les condicions d'operació avaluades.

Funding and acknowledgments

This research has been partly funded by the Government of Spain and FEDER under TRANCO project (TRA2017-87694-R), by the European Union's Horizon 2020 Programme through the ENERXICO project, grant agreement n° 828947, and from the Mexican Department of Energy, CONACYT-SENER Hidrocarburos grant agreement n° B-S-69926 and by Universitat Politècnica de València through the Programa de Ayudas de Investigación y Desarrollo (PAID-01-18 and PAID-06-18).

I wish to acknowledge the financial support received by the institutions above mentioned.

Agradecimientos

Quiero reconocer ahora y para la posteridad a quienes me han acompañado en estos últimos años de manera presencial y digital. Estos años han sido análogos a una carrera de resistencia, donde parar, descansar o cambiar de piloto no fueron una opción. Sin embargo, tuve la suerte de contar con copilotos estupendos que me guiaron en los momentos en los que había perdido la ruta. Me facilitaron sus herramientas y sus estrategias en cada avería, y sobre todo me dieron ánimo cuando creía que no clasificaría. Fueron carreteras complicadas, y con clima muy variante a lo largo de la ruta. Ahora que estoy cruzando la línea de meta, no puedo dejar de reconocer mi esfuerzo, mi paciencia y mi disciplina a lo largo de estos años. Y menos aún puedo dejar de reconocer públicamente a todos los que han estado y han colaborado en este nuevo logro.

A toda la dirección del Instituto Universitario de Investigación CMT- Motores Térmicos: Prof. Francisco Payri, Prof. José María Desantes, Prof. Jesús Benajes y Prof. Vicente Macian, por recibirme en su centro de investigación y darme la oportunidad de involucrarme en el campo de la investigación. Me gustaría extender este agradecimiento al equipo administrativo, especialmente a Amparo, Habby y Elena. Gracias al equipo técnico que me ayudó en cada campaña experimental. Dani Lérida y Omar Huerta, gracias. De la misma manera, me gustaría agradecer a la Universitat Politècnica de València por el apoyo económico a través del Programa de Ayudas de Investigación y Desarrollo (PAID-01-18 and PAID-06-18) que me permitió realizar esta tesis doctoral.

Quiero darle mi más sincero agradecimiento a mi supervisor Dr José V. Pastor por su paciencia durante estos años, por su desborde continuo de enseñanza científica para conmigo, por enseñarme a ordenar las ideas, a cuidar los detalles y a ver siempre más allá de cada situación. Mil gracias Xevi.

Gracias al Dr. José María García por su cátedra constante y por contagiarme su pasión ante cada nuevo descubrimiento. También me gustaría agradecer al Dr Carlos Micó por el tiempo dedicado a enseñarme como mejorar mi trabajo. De la misma manera, quiero agradecer al Dr Antonio García por darme consejo en el momento más difícil de esta carrera de resistencia. Xevi, Xemary, Carlos y Antonio hacen un equipo estupendo. Ustedes son el “qué”, el “cómo”, el “dónde” y el “cuándo” necesario para el éxito de cualquier reto. Gracias de nuevo a todos.

Gracias al ETH-Zurich por darme la oportunidad de hacer la estancia en su prestigiosa institución. En especial al equipo del LAV dirigido por el Prof. Konstantinos Boulouchos, por permitirme trabajar con ustedes. A Walter Vera-Tudela por guiarme durante ese tiempo. Gracias

A mis compañeros del CMT- Motores Térmicos que me han regalado sus conocimientos, me han dado apoyo y ánimo en los momentos complicados, y con los que también he compartido momentos divertidos. Gracias Felipe Lewiski, Francisco Tejada,

Daiana de Leon, Tomas Montiel, Wei Wei Shang, Rafael Lago, Cássio Spohr, Augusto Trintinaglia, Ibrahim Barbery, María Martínez, Brayan Conde, Sushma Artham, y Antonio Jiménez.

Gracias a las personas que se convirtieron en amigos muy cercanos durante esta etapa: Maite Herreros, Noah Sánchez, Lina Balsamo, Santo Balsamo, Yipsi Pereira, Pilar Colomer, Pilar Galiana y Vicente Boronat. Gracias por darme un empujoncito adicional cuando quedaba poco combustible y por recordarme lo valiosa que soy. Gracias infinitas. También quiero agradecer a Leonardo Pachano, mi compañero de estudio y mi gran amigo. Gracias por ser mi psicólogo, mi consejero y mi amigo todos estos años. Gracias totales.

Y para finalizar, quiero agradecer a mi familia en Venezuela, en especial a mi mamá Morela Carrero y a mi ita Alba Márquez por darme ánimo día a día para cumplir mis objetivos. Gracias por recordarme los motivos por los que estoy donde estoy cuando a mí se me han olvidado. Gracias a mis amigos regados por el mundo por estar incluso en la distancia: Jhean Duarte, Yessika Torres, Karla Rodríguez, Marielis Zambrano, Sebastian Ramirez, Martha Viñas, José Minardo, entre muchos otros. Gracias Familia y Amigos por siempre ser mi “club de fans”.

“*Discipline will sooner or later defeat intelligence*”

Japanese proverb

Contents

List of figures

List of tables

Nomenclature

$(A/F)_{st}$	Stoichiometric air–fuel ratio
ASOE	After Start of Energizing
ASOI	After Start of Injection
ATDC	After Top Dead Center
BTE	Brake thermal efficiency
C	constant
CAD	Crank angle degree
CFD	Computational Fluid Dynamics
CI	Compression Ignition
ECN	Engine Combustion Network
d_o	Actual Nozzle Diameter
DPF:	Diesel Particle Filter
F	Focal length
FWHM	Full Width at Half Maximum
HCCI	Homogeneous Charge Compression Ignition
HD	High Density
HR	Apparent Heat Release
HT	High Temperature
HPHT	High Pressure and High Temperature Installation
HRF	High Reactivity Fuel
HVO	Hydrotreated Vegetable Oil
ICCD	Intensified Charge –Coupled Device
ID	Ignition Delay
KL	Integral value of the soot extinction coefficient along the light path
LED	Light-Emitting Diode
LD	Low Density
LHV	Low Heat Value
LL	Liquid Length

LOL	Lift-off Length
LO2	Low oxygen concentration
LPG	Liquid Petroleum Gas
LRF	Low Reactivity Fuel
LT	Low Temperature
LTC	Low Temperature Combustion
MT	Medium Temperature
NL	Natural Luminosity
NO	Nominal Operation
NO	Nitrogen Oxides
OH^*	Excited state of hydroxyl radical
OME_1	simplest molecular structure of oxymethylene ethers CH3–O–(CH2–O)n–CH3 n=1 or also known as Methylal
OME_x	A blend of oxymethylene ethers
PID	Proportional-Integral–Derivative controller
Pinj	Injection Pressure
PM	Particle Matter
RCCI	Reactivity Controlled Compression Ignition
RoHR	Rate of Heat Release
SA	smaller nozzle diameter
SD	bigger nozzle diameter
SOC	Start of Combustion
SOE	Start of Energizing
SOI	Start of Injection
TDC	Top Dead Centre
O_2	Oxygen concentration
r	Pixel-mm ratio (px/mm)
ρ	Density
$f_{(cl,LOL)}$	Fuel mixture fraction on the spray centerline
$\Phi_{(cl,LOL)}$	Equivalence ratio at the lift-off length location

s_{mass}	soot mas
λ	Wavelength
k_e	Dimensionless soot extinction coefficient
P_{amb}	Pressure in the chamber

Chapter 1

Introduction

Content

1.1 Introduction

This chapter addresses the global context of the research carried out in this dissertation, as well as the previous works carried out in the research group that have given way to the approach of this thesis. Next, the objectives and methodologies of this study will be described, as well as a brief resume of each chapter so that the reader can have an overview of the content of the document.

1.2 General Context

Internal combustion engines (ICE) are attractive due to their high power, low fuel consumption, high efficiency and the versatility of sectors in which they can be used, covering sectors such as land and sea transportation, agriculture, energy generation, among others. However, between 10 and 15% of greenhouse gases (GHG) come from land, air and sea transport [1]. Additionally, vehicle emissions such as particulates (PM), and nitrogen oxides (NO) are detrimental to human health [2]. For all this, legal regulations have been implemented around the world to reduce the levels of pollutant emissions, and with it the community of scientists and automotive manufacturers have had to devise different strategies that allow to ICE to maintain benefits and at the same time decrease pollutant emissions. Proof of this is that, in the early 90's, the allowed particle emissions for diesel passenger cars were 0.14 g/km, and currently, the legislation allows 0.0045 g/km in Europe [3]. This represents a reduction of 96% on PM emission. At the same time, there have also been improvements, although less significant, in fuel consumption and, consequently, in the CO_2 emissions from conventional fuel vehicles. However, the last years CO_2 emissions from the transport sector have increased considerably as a consequence of the increase in vehicles fleet required to cover the freight transport demand. This shows that medium and heavy duty vehicles are still the first choice in commercial activities. From 2010 to 2017 the annual registration of new trucks represented an increment of 45% [4]. As a disadvantage, recent data show that, the average emissions measured for new cars increased to 118.5 grams of CO_2/km in 2018 but the target for 2021 is maximum 95 g/km [5]. To face this, new strategies to reduce pollutant emissions have been investigated and worked without penalizing the power and efficiency of ICEs.

These strategies include the improvements in the systems responsible for the mixture formation and fuel supply, the redesign of the combustion chambers and exhaust ducts, exhaust gas recirculation schemes, mixture ignition approaches and the composition of the fuel used. These strategies are called active solutions since they are aimed at minimizing the pollutant formation at the source, while those strategies focused on containing the emissions of these pollutants once formed are known as passive solutions or after-treatment systems. Passive strategies are already implemented today but these elements imply an increase in the engine cost and operational costs along the engine life. Indeed, the aftertreatment systems for Compression Ignition (CI) engines require late post injections of fuel to stimulate an active

regeneration of the diesel particulates filter (DPF), increasing the fuel consumption. In this sense, active solutions have great interest and importance to the automotive research and development sector, since the lower formation of emissions requires after-treatment systems less sophisticated and therefore less expensive.

In the one hand, compression ignition (CI) engine has a big challenge due to the trade-off between nitrogen oxides (NO) and Particle Matter (PM) what makes it difficult to reduce both pollutants simultaneously. Therefore CI engines require the most sophisticated after-treatment systems and, consequently, the most expensive as it was previously mentioned. On the other hand, CI engines can delivery to the medium and heavy duty transport sector high power, high thermal efficiency and low fuel consumption. Thus, this doctoral thesis is frameworked on providing active solutions for the reduction of pollutant emissions in compression ignition engines, soot mainly, through the use of different types of fuel that are, or will be, available in the market with high potential for the medium and heavy duty vehicle's sector. The potential of alternative or renewable fuels is twofold: on the one side they can mean a significant contribution to CO_2 reduction; on the other, alternative fuels will allow to the transport sector to keep high performance (power and low fuel consumption) and the possibility to reduce its main pollutants such as PM and NO for the benefit of the environment and public health.

A number of strategies that have gained attention during the last decade are grouped under the generic name of Low Temperature Combustion strategies (LTC). They are focused on achieving lower combustion temperatures to keep NO emissions low and avoid local rich fuel equivalence ratios to keep soot production controlled. Thus, LTC can break the trade-off existing in pollutant emissions (NO and soot) while thermal efficiency is maintained. This achievement is possible due to the use of high rates of Exhaust Gas Recirculation (EGR) and longer mixing times compared with conventional combustion [6].

Within the LTC strategies, it could be considered, among others, the Homogeneous Charge Compression Ignition (HCCI) and the Partially Premixed Combustion Ignition (PCCI). Both strategies have been evaluated with different fuels and fuel blends, obtaining good results in reducing pollutant emissions. But the limitation of the load range (low and medium) is still present, and this is mainly due to the difficulty of controlling the combustion phase, which depends on the fuel reactivity [7–9]. To address the limitation of the engine's operating range, a combustion strategy called Reactivity Controlled Compression Ignition (RCCI) arises [10]. It is based on the regulation of ignition through the reactivity of the fuels used, diesel and gasoline mainly, whose reactivity properties are diametrically opposite. Despite the fact that with the RCCI the engine's load range is considerably extended for low and high loads, the use of two injection systems represent a technological limitation for its implementation, so that other combustion strategies continue to emerge that face the limitations mentioned above but they require deepening in the fundamentals of their combustion processes.

For a better understanding of the combustion processes of the different strategies for the fuel-air mixing formation, increasingly, computational models are developed. They are able to explain some phenomena that take place in the combustion chamber that cannot be visualized or analyzed only with the data obtained from the experimental tests. However, the mixing depends on the combustion strategies used which, on its side, depends on the characteristic of the fuel used and therefore it is necessary to extensively study the combustion behavior for different fuels. This is a field in which computational models are important for full understanding of whole phenomenon since it cannot be analyzed at all in experimentation.

In order to have a deep understanding of the combustion process, one of the most competent experimental ways is through visualization of the phenomenon with non-intrusive techniques in a steady and controlled thermodynamic environment. It has been studied in depth for diesel fuel where the combustion models have helped to optimize aspects as the interaction of spray and the chamber and thus achieving the high efficiency ranges and lower pollutant emissions. However, as it was mentioned above, each year the legal regulations on emissions are more and more restrictive, and it is necessary to expand the ways to reduce pollutants. One of them is the use of cleaner fuels. However to achieve this, it is necessary to investigate the behavior of alternative fuels.

Fuels such as natural gas, propane, hydrogen, and some alcohols such as ethanol, methanol, butanol and its derivatives are considered alternative fuels. Also vegetable and waste-derived oils, both under the generic name of biodiesel, or even blends of these fuels with traditional gasoline or diesel, are also considered as alternative fuels [11]. But the fact that petroleum-based fuel would still dominate transportation fuels for the next years has motivated the use of low-carbon alternative fuels which consider the entire life cycle (well to wheel) in order to reduce the greenhouse gas emissions caused by their production, transport and use in the engine, in addition to the plans already in place to make Europe the first climate-neutral continent [12]. The main objective is to accelerate the process of decarbonisation of the transportation sector. Currently, compression ignition (CI) engines powered by diesel and Liquefied Petroleum Gas (LPG) or Compressed Natural Gas (GNC) are easily available in the market. Although they show high performance in terms of reducing pollutant emissions, their main disadvantage lies in the power penalty and for minimize this, the fuel consumption increase [13–15]. However, the CO_2 benefit potential of Natural Gas with respect to diesel combustion could be as high as 20% [16].

In the same way fuels from vegetable source such as Biodiesel and Hydrotreated Vegetable Oil (HVO) are progressively incorporated in the market. Furthermore, the diesel blends with biodiesel do not require hardware modifications in the CI engine, because the characteristics of biodiesel are in general similar to those of diesel [13]. Biodiesel can be produced from waste oils, vegetable oils, sugars and biomass, using processes such as Fischer-Tropsch (FT), hydrogenation and hydro-treating. These processes to obtain synthetic

diesel by means of FT technology and hydrogenated animal fats or hydrogenated vegetable oils allow a wider panel of combustion approaches due to the specific fuel properties of these blend components, such as higher cetane number and low aromatics composition [17]. HVO and biodiesel have demonstrated to reduce the pollutant emissions without significant penalty on thermal efficiency and brake specific fuel consumption compared with conventional diesel [18,19].

Other novelty fuels such as the synthetic fuels produced by electrolysis of water with renewable electricity and CO_2 captured either from flue gases from an industrial site or via direct air capture, are beginning to emerge as substitute fuels for diesel, because they can achieve a great CO_2 reduction versus their equivalent fossil-based fuels. Moreover, they can be stored and transported easily and inexpensively compared to electricity. They can be kept in large-scale stationary storage over extended periods, and in mobile storage in vehicle tanks [20].

In recent years, the synthetic fuels, such as Oxymethylene ethers (OME) have been studied as alternative fuels for CI engine and they have demonstrated positive impacts on reduction of pollutants emissions [21–23]. Other studies have indicated that the main advantage of OME is the absence of PM-NO tradeoff [24]. In this sense, these fuels would be the solution to the main drawback of the compression ignition engine, i.e. the PM-NO tradeoff, and therefore the simplification or even the elimination of the required aftertreatment systems. However, their chemical composition has also disadvantages in terms of compatibility with some materials of engine elements [24]. Moreover, the infrastructure for its production is still small [13]. These disadvantages could be overcome or minimized by other research fields while its evaluation from the point of view of combustion has already been addressed and it becomes attractive to show the potential of using them in CI engines.

With these arguments, it is evident that to continue taking advantage of ICs on the global economic development is possible if the propulsion sources are combined or replaced by others with zero impact on the environment. However, there is still a long way to go in terms of research and development to achieve absolute compatibility between the current engines and the alternative fuels and thus ensure that the highest performance of both elements are obtained. Therefore, this doctoral thesis seeks to provide understanding about the behavior of alternative fuels from fossil, vegetable and synthetic sources under different combustion modes as well as to provide fundamental data for future works.

1.3 Background

In previous works carried out at CMT-Motores Térmicos, different combustion strategies have been studied in metal engines and optical vessels and using combustion models with the aim to provide alternative solutions to reduce pollutants emission, to expand the engine operation range and to keep and improve the engine performance. In these experiments and simulations, the most used fuels have been gasoline, diesel, and surrogates

of these. Nonetheless, some other alternative fuels have been considered in some of the studies, as follows.

In 2013 J.-G. Nerva [25] studied the effect of physical and chemical fuel properties on conventional combustion for blends of Rapeseed Methyl-Ester (first-generation biodiesel) and diesel and fuels produced from the FT process. The study was made in a vessel with optical access that mimics the conditions inside the combustion chamber of a diesel engine. One of the outputs of this study was the different statistic approaches made for the main parameters of each spray. The study showed a strong relationship between the ignition delay and the lift off length, as well as it was observed that the engine conditions and the proper oxygen content in fuel were determinant in the leaning of the mixture to the base of the flame for reducing soot production. Also, in a parallel way, V. Domenech [26] studied the effect of using gasoline in Partially Premixed Combustion (PCC), as a strategy to enhance the control and modulation of combustion in a single cylinder engine through the modification of fuel reactivity. The combustion results showed similarities between diesel and gasoline under partially premixed conditions and demontrated the potential of using low reactivity fuels at the start of combustion and combustion phasing under a wide range of engine operating conditions. Moreover, the high pressure gradient was reduced but it showed the need of improvements in terms of NO emissions and efficiency of the combustion process.

Afterward, in 2015 Vera-Tudela [27] studied the mixing and evaporation processes as well as the process of ignition and combustion but using blends of single component fuels as n-heptane, iso-octane, n-dodecane and others. The results showed that fuel properties do not have significant importance on vapor penetration but on the liquid length is more remarkable. Furthermore, in this study it was concluded that the fuel chemical properties and the ambient conditions (T,O_2, ρ) affect the reactivity of the mixture, therefore a more reactive blend (higher Cetane Number) leads to smaller ignition delay times, shorter lift-off lengths and more flame radiation.

Then, in 2016, J. Monsalve [28] deepened in the understanding of the dual-fuel combustion mode in compression ignition using diesel, gasoline and ethanol inside the chamber of a metal engine. Results showed that reducing the reactivity gradient between the low reactivity fuel and high reactivity fuel improves RCCI performance at low load and achieve NO under the EURO VI limit with low soot emissions. These results were in line with the findings made previously by Vera-Tudela in an optical vessel. However, Monsalve also showed that reducing fuel reactivity was not an adequate solution to extend the engine operation to higher loads.

As seen so far, fundamental and applied research have gone hand in hand confirming the results and finding alternative solution for each drawback. This is how in the field of applied research to fulfill the gap found by Monsalve, in 2018, V. Boronat [29] presented the concept Dual Mode and Dual Fuel (DMDF), also carried out in a metal engine using as fuel the dieseline (blend of diesel and gasoline). DMDF is based on the combination of dual fuel

combustion strategies that switches in function of the engine load. The results showed that is possible to work in the whole engine map but in some areas smoke emissions are higher. Continuing with the study of the DMDF strategy, in 2021, R. Lago-Sari [30] proposed the same DMDF concept in which, in addition to achieving cleaner combustion throughout the whole engine's operating map, with less HC and CO produced, a reduction of CO_2 was also proposed through the use of low-carbon alternative fuels in which the life cycle of the fuel or "well-to-wheel" concept is considered at the same time that its combustion behavior is evaluated.

On the other hand, and in parallel way, the field of fundamental research at CMT-Motores Térmicos has continued studying in depth the soot formation for diesel sprays. It is because of that in 2017, T. Xuan [31] characterized the in-flame soot formation under quiescent and not- quiescent conditions using single component fuels such as n-dodecane and n-heptane, and a blend of 80% n-heptane and 20% iso-octane (in mass) and using guidelines from ECN [32]. Both the in-flame soot volume fraction and temperature were obtained simultaneously. This work enabled, through the fundamental results, start the analysis of soot formation using CFD tools and thus allowed to L. Pachano [33], in 2020, validate the studies of the reactivity and mixing boundary condition variations on combustion and soot production in diesel sprays by means of equations soot models. This study was also carried out for the ECN Spray A condition and the fuel assessed was dodecane only. However, to continue gaining knowledge on soot production and how to mitigate it in the context of the ICE, it is necessary to improve in soot modeling. To achieve this, the fundamental study of the production of soot from other alternatives fuel such as diesel and gasoline blends and low-carbon alternative fuels is needed. This would let to assess the feasibility of these fuels to contribute to cleaner operation of ICEs. For that reason, parametric characterization of the behavior of alternative fuels and latest generation fuels is very important and therefore this work is proposed with the aim of generating experimental data under quiescent and no-quiescent environment, that in the near future can validate CFD models for a wide range of fuels under different diesel engine like conditions.

1.4 Objectives and methodology

The main objective of this thesis is twofold: on the one hand, to assess the potential of alternative fuels on the soot formation, through the identification and quantification of the effect of their physical and chemical properties in the different stages of the combustion process; on the other, to enlarge the experimental database with fundamental data that could be used as a reference for future development of combustion models and validation of CFD simulations with alternative fuels.

To achieve the fundamental objectives of this thesis, the following partial objectives were developed:

- To optimize the existing experimental methodology for the visualization of the injection and combustion process under controlled thermodynamic conditions that allows to quantify the influence of the fuel on combustion.
- To quantify the effect of the physical-chemical properties of Hydrotreated Vegetable Oil (HVO), Oxymethylene ethers with short and long chains, hereafter called as OME_1 and OME_x on the characteristic parameters of the spray, as well as on the start and development of combustion, and its influence on the soot formation compared with commercial diesel and its common surrogate, dodecane.
- To develop an experimental methodology to evaluate the injection system and the characteristics of the combustion process of biofuel blends: HVO in liquid phase and LPG in gaseous phase at ambient conditions. It also seeks to evaluate the influence of the different mixing proportions on the soot formation
- To study the spray and combustion characteristics of dual combustion of diesel and gasoline blends, their effect on combustion efficiency and soot formation in an installation that mimics characteristic timescales and thermodynamic parameters variations close to those of a compression ignition engine, whilst allowing optical access to the combustion chamber.

The methodology followed considered the literature review throughout the development of the thesis. It has served as the basis for the development of this. The bibliographic review has allowed establishing the fundamentals of mixing controlled combustion and pollutants formation and their relationship with the type of fuel used depending on its origin: fossil, vegetable or synthetic. The state of the art was established between different types of fuels, and different combustion modes. Initially, diffusive combustion has been studied. Then, the differences with Low Combustion Temperatures have been stablished. In both strategies, the mixture formation, the combustion development and the effect of each fuel on the soot formation has been studied. In the same way, a wide range of low-carbon alternative fuel have been explored in terms of their source, production, distribution, storage and engine performance. Later, the understanding of the optical facilities that allowed to study the combustion phenomena was needed, as well as it was also necessary to establish the fundamentals of the non-intrusive optical techniques available for the combustion study.

In the first experimental stage, the tests have been carried out with different types of fuels available on the current market. These fuels were dodecane, diesel, Hydrotreated Vegetable Oil (HVO), and two types of Oxymethylene ethers (OME): one of short-chain (OME_1) and another with long-chain (OME_x). Each one was studied in its pure state and in a highly controlled thermodynamic environment, such as the High Pressure and High Temperature facility (HPHT) belonging to CMT-Motores Térmicos. It is important to mention that dodecane and OME_1 have been experimentally evaluated due to their defined composition and chemical structure, which are useful for the development of combustion models. Boundary conditions such as temperature, oxygen concentration in the chamber, and rail pressure have been defined using the Engine Combustion Network (ECN) guidelines.

Likewise, the nozzles used are those already evaluated by the ECN for fundamental studies: nozzle A and nozzle D. During this stage, the auto-ignition characteristics and the spray structure have been studied for those fuels mentioned above. Furthermore, each one has been evaluated from the point of view of soot formation.

In a second stage, the dual combustion of fuel blends that require important modifications in a compression ignition engine was evaluated in the HPHT facility again. Since HVO and LPG (Liquefied Petroleum Gas) are in different physical states under atmospheric conditions (liquid and gas, respectively), the storage and injection system represent a challenge for immediate application. However, considering the availability in the market of HVO and LPG, these fuel coud be used in medium term. Both HVO and LPG can be considered as the low-carbon alternative of the dual combustion mode. The study was carried out in the High Pressure and High Temperature facility. The nozzle used was the same as used in the diesel-gasoline experiments. The boundary conditions were close to those of the ECN for the baseline conditions, and other injection temperatures and pressures were also assessed. The injection system was modified to inject the blends considering the physical state of both fuels. Special fuel tanks were used for the blends storage. During the experiments, different fuel ratios were evaluated regarding to the auto ignition characteristics and physical parameters of the spray as well as the effect on the soot formation.

In the third and last experimental campaign, the dual combustion of blends of the most common fuels used in internal combustion engines, diesel and gasoline, have been studied. The blends have been tested in an installation that mimics the thermodynamic conditions inside the combustion chamber of a compression ignition engine with optical accesses in order to evaluate the behavior of different proportions of diesel-gasoline blends, and also to evaluate the heat release under engine conditions and the fuel blend effect on soot formation, even in the transient regimes of the combustion, which is the advantage of using the facility mentioned. The injection system used was a common rail adapted to an injector already characterized and previously studied at CMT- Motores Térmicos [34]. The diesel and gasoline blends were prepared in volumetric proportion before being injected. Optical techniques were used to study the characteristics of the blends and the quantification of the soot formation.

Finally, a synthesis of the results obtained throughout the development of this thesis has been done, as well as future works have been proposed to continue deepening understanding and subsequent use of the low-carbon alternative fuels.

1.5 Thesis outline

The documents is structured in seven chapters, starting with this brief introduction (Chapter 1), that presented the general context, a summary of the previous studies developed by the CMT- Motores Térmicos research group and then the objectives and the methodology followed in this thesis to fulfil such objectives.

Chapter 2 is focused on describing the fundamental concepts of mixing controlled combustion, combustion strategies and its technical feasibility. The alternative fuels with high potential in terms of emission reduction and less environmental impact will be described in this chapter too.

Chapter 3 describes the facilities used. Each test rig is described with the corresponding measurement principle and procedure. Moreover, a brief summary of how optical techniques implemented have been used through the years to visualize and improve understanding of the combustion process will be given.

In chapter 4, the results of the spray characterization for diesel, dodecane, HVO, OME_1 and OME_x in conventional combustion are presented and analyzed. Parameters to characterize temporally and spatially the formation of the mixture, ignition and combustion will be presented in this chapter. Furthermore, this chapter includes soot formation analysis for the fuels tested.

In chapter 5, the results from the combustion behavior for blends of HVO and LPG are presented and discussed, as well as the description of the adapted injection system used to inject a blend of liquid and gaseous fuel. Results are presented in terms of the Ignition Delay and macroscopic combustion parameters. Furthermore, the soot formation is analyzed in a qualitative way.

Chapter 6 is centered on analyzing the results from dual combustion for blends of commercial fuels: diesel and gasoline. Results are given in terms of the combustion effectiveness, spray characteristics and the effect on soot formation.

Lastly, chapter 7 summarizes the research carried out, as well as the main conclusions of this thesis. Moreover, some ideas for future works are proposed from the experience and knowledge acquired during the development of this thesis.

To complement the brief description of each chapter, the Figure 1. 1 depicts the argument line followed from thesis definition until conclusions.

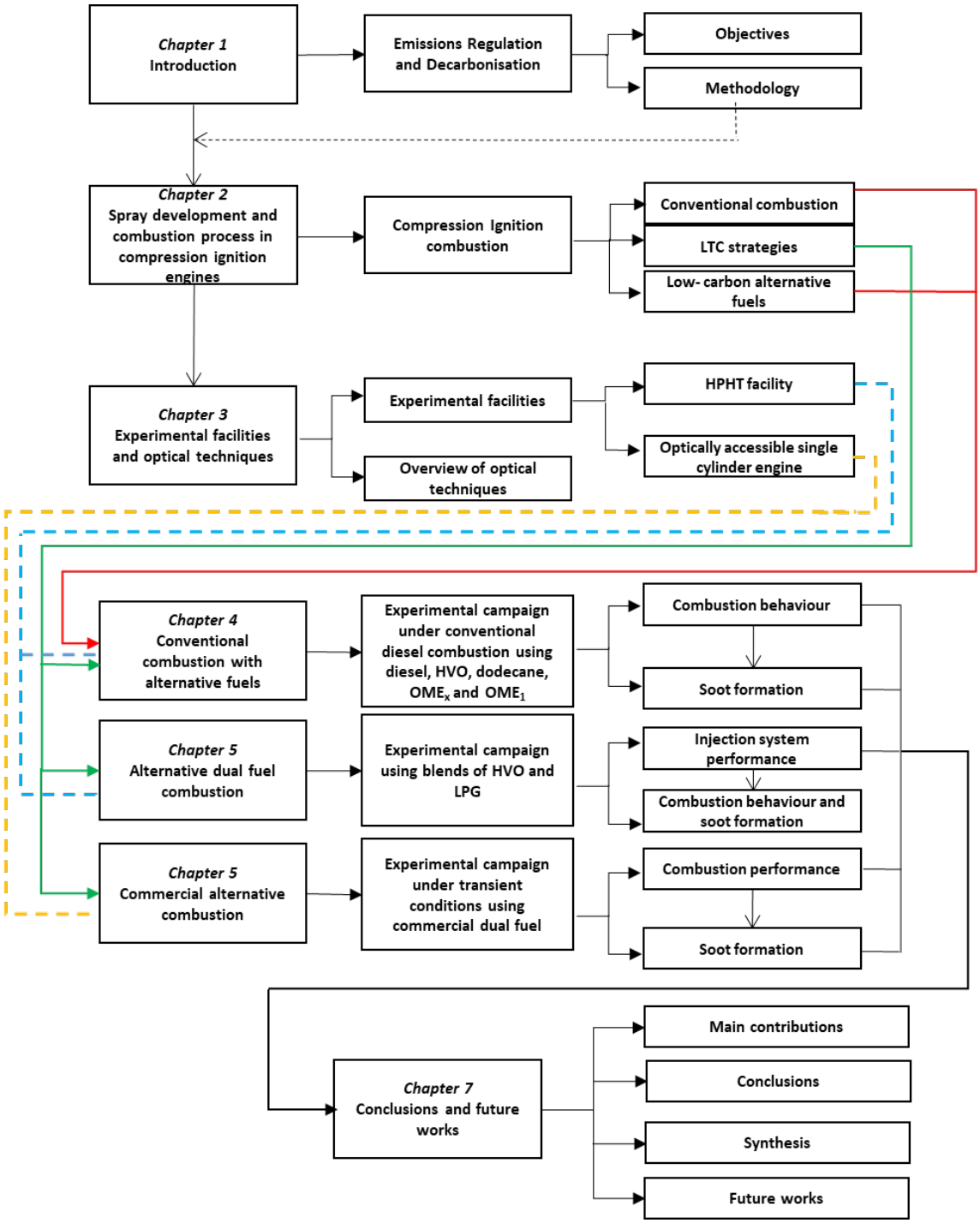

Figure 1. 1 Grafical representation of the argument line followed in this thesis

References

[1] Ritchie H, Roser M. CO_2 and Greenhouse Gas Emissions. Our World in Data, 2017.

[2] Review of evidence on health aspects of air pollution – REVIHAAP project: final technical report, 2017. http://www.euro.who.int/en/health-topics/environment-and-health/air-quality/publications/2013/review-of-evidence-on-health-aspects-of-air-pollution-revihaap-project-final-technical-report

[3] European Parliament and Council; Commission Regulation with respect to emissions from heavy duty vehicles (Euro VI). 2011.

[4] European Environment Agency, Carbon dioxide emissions from Europe's heavy-duty vehicles, 2018. https://www.eea.europa.eu/themes/transport/heavy-duty-vehicles/carbon-dioxide-emissions-europe.

[5] Reducir las emisiones de los automóviles: nuevos objetivos de CO2 | Noticias | Parlamento Europeo, 2018.

[6] Dec JE. Advanced compression-ignition engines—understanding the in-cylinder processes. Proceedings of the Combustion Institute 2009;32:2727–42. https://doi.org/10.1016/j.proci.2008.08.008.

[7] Lu X, Han D, Huang Z. Fuel design and management for the control of advanced compression-ignition combustion modes. Progress in Energy and Combustion Science 2011;37:741–83. https://doi.org/10.1016/j.pecs.2011.03.003.

[8] Inagaki K, Fuyuto T, Nishikawa K, Nakakita K, Sakata I. Dual-Fuel PCI Combustion Controlled by In-Cylinder Stratification of Ignitability, SAE Technical Paper 2006-01-0028; 2006. https://doi.org/10.4271/2006-01-0028.

[9] Manente V, Tunestal P, Johansson B, Cannella WJ. Effects of Ethanol and Different Type of Gasoline Fuels on Partially Premixed Combustion from Low to High Load, SAE Technical Paper 2010-01-0871; 2010. https://doi.org/10.4271/2010-01-0871.

[10] Kokjohn SL, Hanson RM, Splitter DA, Reitz RD. Experiments and Modeling of Dual-Fuel HCCI and PCCI Combustion Using In-Cylinder Fuel Blending. SAE International Journal of Engines, vol. 2, 2009, p. 24–39. https://doi.org/10.4271/2009-01-2647.

[11] European Commission. Directorate General for Research and Innovation. Alternative fuels: expert group report. LU: Publications Office; 2017.

[12] European Commission. A European Green Deal (2019). https://ec.europa.eu/info/strategy/priorities-2019-2024/european-green-deal_en (accessed July 15, 2021).

[13] Bae C, Kim J. Alternative fuels for internal combustion engines. Proceedings of the Combustion Institute 2017; 36:3389–413. https://doi.org/10.1016/j.proci.2016.09.009.

[14] Napolitano P, Alfè M, Guido C, Gargiulo V, Fraioli V, Beatrice C. Particle emissions from a HD SI gas engine fueled with LPG and CNG. Fuel 2020; 269:117439. https://doi.org/10.1016/j.fuel.2020.117439.

[15] Bayraktar H, Durgun O. Investigating the effects of LPG on spark ignition engine combustion and performance. Energy Conversion and Management 2005; 46:2317–33. https://doi.org/10.1016/j.enconman.2004.09.012.

[16] European Road Transport Research Advisory Council (ERTRAC) Working Group: Energy and Environment, Future Light and Heavy Duty ICE Powertrain Technologies, 2016.

[17] European Road Transport Research Advisory Council, Future Light duty Powertrain Technologies and Fuels, 2011.

[18] Bortel I, Vávra J, Takáts M. Effect of HVO fuel mixtures on emissions and performance of a passenger car size diesel engine. Renewable Energy 2019; 140:680–91. https://doi.org/10.1016/j.renene.2019.03.067.

[19] Dimitriadis A, Seljak T, Vihar R, Žvar Baškovič U, Dimaratos A, Bezergianni S, et al. Improving PM-NOx trade-off with paraffinic fuels: A study towards diesel engine optimization with HVO. Fuel 2020; 265:116921. https://doi.org/10.1016/j.fuel.2019.116921.

[20] Soler A. Role of e-fuels in the European transport system - Literature review. Brussels: Concawe; 2020.

[21] Wang Z, Liu H, Zhang J, Wang J, Shuai S. Performance, Combustion and Emission Characteristics of a Diesel Engine Fueled with Polyoxymethylene Dimethyl Ethers (PODE3-4)/ Diesel Blends. Energy Procedia 2015; 75:2337–44. https://doi.org/10.1016/j.egypro.2015.07.479.

[22] Härtl M, Seidenspinner P, Jacob E, Wachtmeister G. Oxygenate screening on a heavy-duty diesel engine and emission characteristics of highly oxygenated oxymethylene ether fuel OME1. Fuel 2015; 153:328–35. https://doi.org/10.1016/j.fuel.2015.03.012.

[23] García A, Monsalve-Serrano J, Villalta D, Lago Sari R, Gordillo Zavaleta V, Gaillard P. Potential of e-Fischer Tropsch diesel and oxymethyl-ether (OMEx) as fuels for the dual-mode dual-fuel concept. Applied Energy 2019; 253:113622. https://doi.org/10.1016/j.apenergy.2019.113622.

[24] Crusius S, Müller M, Stein H, Goral T. Oxy-methylen-di-methylether (OMEx) as an alternative for diesel fuel and blend compound: properties, additizing and compatibility with fossil and renewable fuels, Esslingen: 12th International Colloquium Fuels - Conventional and Future Energy for Automobiles; 2019, p. 8.

[25] Nerva J-G. An Assessment of fuel physical and chemical properties in the combustion of a Diesel spray. PhD thesis. Universitat Politècnica de València, 2013.

[26] Domenech Llopis V. Study of new strategies for combustion control in partially premixed modes in compression ignition engines (in Spanish). PhD thesis. Universitat Politècnica de València, 2013.

[27] Vera-Tudela Fajardo WM. An experimental study of the effects of fuel properties on diesel spray processes using blends of single-component fuels. PhD thesis. Universitat Politècnica de València, 2015.

[28] Monsalve Serrano J. Dual-fuel compression ignition: towards clean, highly efficient combustion. PhD thesis. Universitat Politècnica de València, 2016.

[29] Boronat Colomer V. Dual-Fuel Dual-Mode combustion strategy to achieve high thermal efficiency, low NOx and smoke emissions in compression ignition engines. PhD thesis. Universitat Politècnica de València, 2018.

[30] Lago Sari R. Dual-mode dual-fuel combustion implementation on a real medium duty engine platform. PhD thesis. Universitat Politècnica de València, 2021.

[31] Xuan T. Optical investigations on diesel spray dynamics and in-flame soot formation. PhD thesis. Universitat Politècnica de València, 2017.

[32] Engine Combustion Network | Engine Combustion Network Website, 2021. https://ecn.sandia.gov/.

[33] Pachano L. CFD modeling of combustion and soot production in diesel sprays. PhD thesis. Universitat Politècnica de València, 2020.

[34] Micó C. Development of measurement and visualization techniques for characterization of mixing and combustion processes with surrogate fuels. PhD thesis. Universitat Politècnica de València, 2015.

Chapter 2

Spray development and combustion process in compression ignition engines

Content

2.1 Introduction

This second chapter has the goal of giving a summary of many years of research and well established results in the field of Compression Ignition (CI) Engines. Firstly, this chapter will provide a description of the main physical and chemical processes that take place inside the combustion chamber of a direct injection diesel engine in a Conventional Diesel Combustion (CDC). Then, as a consequence of legal regulations for pollutant reduction, the Low Temperature Combustion strategies (LTC) emerged with the aim to reduce soot and NO mainly but it was observed that there was difference in the physical and chemical processes between CDC and LTC strategies. Therefore a combustion model for Low Temperature Combustion (LTC) introduced by Musculus [1] will also be described in this chapter and it will be contrasted with CDC model. Both combustion modes will be described through the comparison of the temporal evolution of the injected mass and the heat release rate (HRR). These parameters are calculated from the pressure signal in the cylinder using the First Law of Thermodynamics [2]. Furthermore, a description of the spatial flame structure and development in each case is also given

By last, at the end of this chapter a description of a wide range of different alternative fuels will be given, taking account that, for both combustion modes, the autoignition stage is dominated by physics and chemical reactions and the fuel characteristics play an essential role in this phase. For that, the alternative fuel section of this chapter seeks to highlight those fuels that in addition to contribute with the development of cleaner combustion modes also contribute to Well to Wheel (WTW) CO_2 reduction, which is a challenge nowadays. Biofuels of first, second and advanced generations will be presented. A brief description of their properties will be given as well as their feasibility to be implemented in internal combustion engine.

2.2 Conventional Diesel Combustion

The analysis of temporal evolution of the Heat Release Rate (HRR) is the easiest way to understand the different stages of the combustion process. For that, these phases will described in terms of the HRR in this thesis. Those stages are representative for conventional diesel conditions. In the Figure 2. 1 the HRR evolution is represented.

The first stage corresponds to the interval from the start of injection (SOI) up to the start of combustion (SOC). During this phase, complex mechanisms as atomization, air entrainment and evaporation take place and these allow that the fuel mixes with the air. Subsequently, and with oxygen in the ambient, low-intensity chemical pre-reactions appear which produce that fuel molecule breaks into shorter hydrocarbon chains, creating favorable conditions for the auto ignition. That delay time is what will be called as “Ignition Delay (ID)” in this thesis. The duration of this phase is highly dependent on numerous parameters such as injection pressure, nozzle diameter, temperature, density or fuel composition. The latter will be of great interest in this thesis. Furthermore, it is known that increasing injection

pressure, temperature and ambient density produce shorter ID. Likewise, smaller nozzle diameters shortens the ID [3,4].

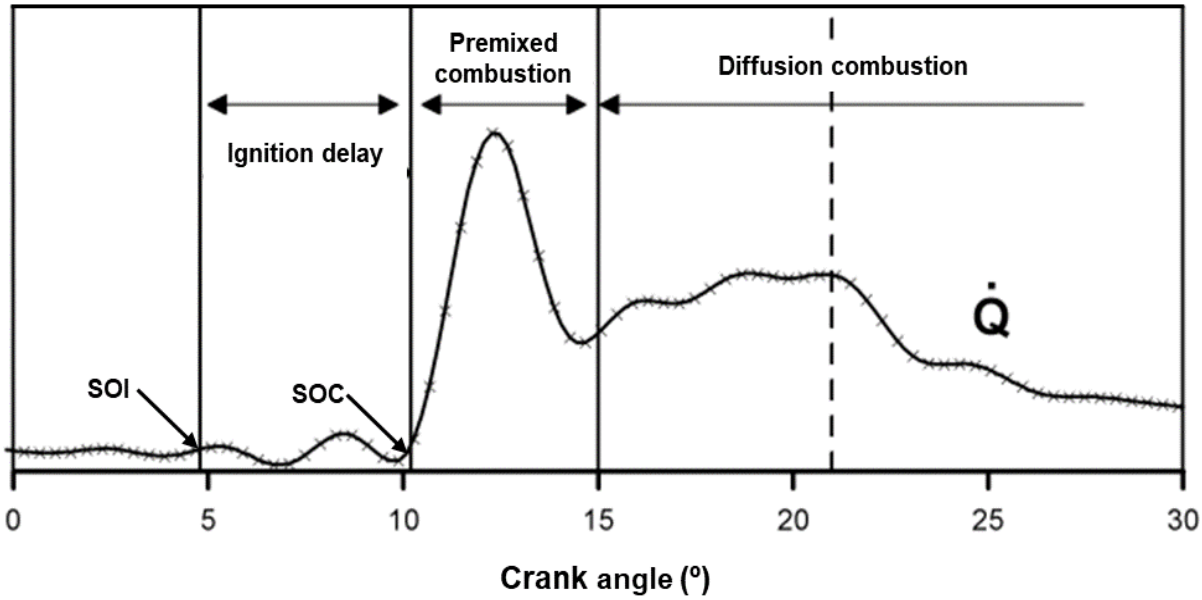

Figure 2. 1 Combustion phases in a Compression Ignition engine by means of Heat Release Rate (HRR) curve from [2]

The second stage, known as Premixed Combustion, is the phase in which the fuel that was not burned in the previous phase due to lack of conditions necessary to react, is burned quickly. Therefore, the heat is released at very high rate during the first instants. The duration of this phase is very similar to the ignition delay phase [2]. It starts with the jet ignition, that is when the HRR curve grows significantly and it finishes when the HRR achieves the first minimum value. Some author have stablished that main factors that control the premixed combustion phase are the injection rate, mixing rate and the ignition delay [5]. It is important to mention that, in this phase the soot precursor species such as Polycyclic Aromatic Hydrocarbons (PAHs) are formed [6].

Once the first minimum of the HRR curve is reached, at that point the third phase of combustion begins, this is known as diffusion combustion. From this moment, the combustion process has conditions that favor stable reactions. Then, the diffusion flame establishes, which will keep its basic structure throughout the rest of the combustion process as long as the injection process is maintained. In this phase, the jet experiences a “quasi-steady” period, with some fuel burning while more fuel is injected. This is what is known as mixing controlled process. Thus, after the end of injection, the analysis of flame structure and combustion characteristics is not interesting due to lack of process stability, although other process such as soot oxidation could be interesting after the end of fuel injection.

This quasi-steady period of diffusion combustion has been studied extensively over the years, thus providing the principles that allowed the development of the conceptual model

presented by Dec [7] in which the diffusion flame characteristics are defined. At the top of Figure 2. 2 an axial section of this model has been represented to explain the characteristics of the diffusion flame. It has been taken from [2].

The flame is formed by different parts or regions. To complete the detailed analysis of each one, the air fraction (Y_{O_2}), the dimensionless heat release (HR), the temperature (T/1000), the soot and the NO formed have been also depicted in the Figure 2. 2.

The first region is the closest to nozzle injector. In this stage, the mixture formation occurs, for that, the air entrainment or air fraction (Y_{O_2}) increases. Also, the temperature increases slightly. In this phase is where the atomization, air entrainment and evaporation take place. The jet velocity is high, therefore the flame is lift-off downstream of this zone. That length, from the nozzle to the base of the flame, is known as Lift off length (LOL) and it could be considered as the border between premixed combustion and diffusion combustion. The magnitude of the LOL and the equivalence ratio at the LOL are affected by many factors such as the fuel properties, ambient density, oxygen concentration, ambient gas temperature, injection pressure and nozzle size [4,8,9]. The analysis of this parameter is of great importance for this thesis.

In second region of the flame, the air-fuel mixture formed previously is being burned. The jet is expanded and it losses the conical shape that it had under non-reactive conditions. This expansion is a consequence of the temperature increment originated by the heat release. The change of both parameters (HR and T/1000) is seen in Figure 2.2, as well as it is observed that oxygen concentration (Y_{O_2}) drops to zero. The jet core is formed by the soot and unburned fuel, however the higher concentration of soot and particles are in the jet front. The jet core and front are surrounded by the reaction surface in which they are oxidized to CO_2 and H_2O [2]. Furthermore, outside of the reaction surface is where the nitrogen oxides (NO mainly) are formed according to what has been studied by Dec [7]. This zone has the necessary conditions to form NO via thermal mechanisms, as it can be seen in the bottom of Figure 2.2: high temperatures and high oxygen concentration (Y_{O_2}).

The third region of the flame can be found between both regions described above. This thin area has been represented in light blue in Figure 2. 2. Dec [7] indicates that it is the premixed reaction zone where the air entrainment is consumed. In this stage around 10 or 15% of heat is released [10]. Furthermore, in this region the soot precursor such as carbon monoxide (CO) and unburned hydrocarbons (HC) are formed.

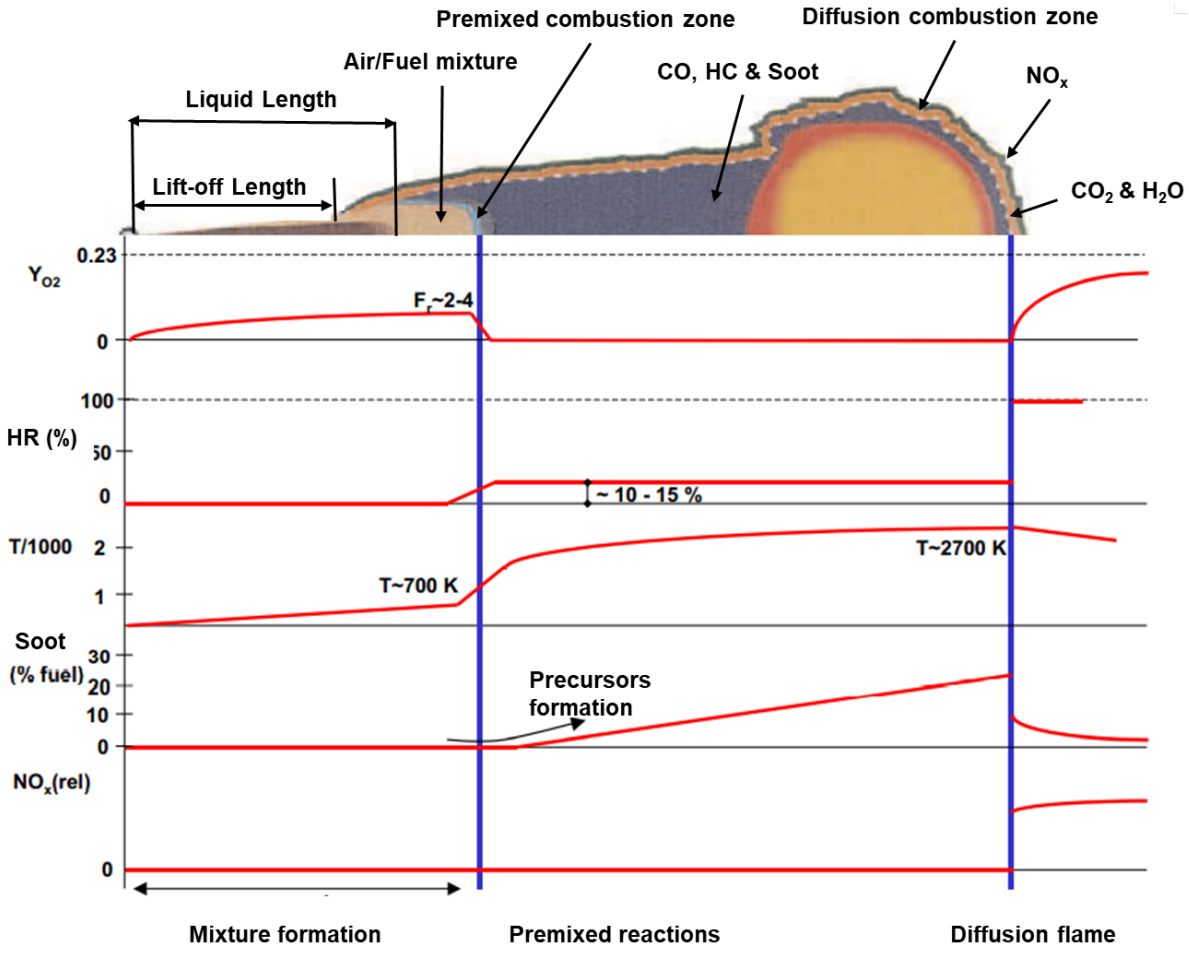

Figure 2. 2 Conceptual model for conventional diesel combustion during quasi-steady period from [2]

Other way to understand the evolution of combustion process is imaging a parcel of fuel that is injected, and describing what will occur to this parcel when it travels along the spray axis through the different regions mentioned above. Firstly, that parcel is atomized and mixed with other parcel of the air, forming a package of mixture. The air entrainment produces that temperature increases and the liquid fuel evaporates until it disappears at a certain distance from the nozzle. This distance is known as Liquid Length (LL) and it has been indicated in the Figure 2. 2. From LL, the fuel parcel in vapor phase continues to mix with the parcel of air until it reaches the premixed combustion zone where the equivalence ratio is around 4 and the temperature is around 700 K [10]. In this moment there is not available oxygen surrounded the package, therefore there are a lot of partial products of fuel oxidation, mainly CO and HC which are the species that lead the Polycyclic Aromatic Hydrocarbons (PAHs) that constitute the soot precursors [7,10]. According to Flynn studies [10] in this process, around 10-15% of the chemical energy contained in the fuel is released. Then, that fuel-air mixture package enters in the diffusion zone (orange line in the Figure 2.2) where the mixing and air entrainment process continue, but there are not free oxygen,

therefore there are not heat release inside of this zone [2]. However, when that package that is burning, reaches the front of the flame, the temperature increases (~2700 K) and that combined with the products of fuel oxidation make that small soot particles appears in the flame. They grow in size as they approach to the flame front. When the package finally crosses the diffusion flame front, the partial products of combustion are burned due to the contribution of oxygen by diffusion coming from the outer part of the front. Thus, the rest of chemical energy (~ 85%) is released. With this, the maximum temperature is reached on this front. The formed soot is also oxidized due to high temperature and the presence of the OH radical [11,12]. This radical constitutes a fundamental mechanism of soot oxidation while high temperature conditions exist, even when the injection process has already finished [2].

Knowing the processes involved in a conventional diesel combustion (CDC) where soot and NO are the main drawbacks, new combustion strategy that modify some of these processes has been conceptualized and consequently it is possible to reduce polluting emissions. This will be described in the next section of this chapter.

2.3 Low Temperature Combustion (LTC)

As it was mentioned before, soot formation and NO are the main issue of the Compression Ignition (CI) engines. On one hand, the soot is formed as a consequence of the lack of oxygen and high temperatures inside the jet, which makes that the jet core is composed by fuel and partially oxidized products that will later become soot. On the other hand, the high temperatures at the jet periphery and the existence of oxygen in the environment contribute with the NO formation.

As a result of the deep understanding of the processes in which these pollutants are formed, strategies to mitigate them have emerged. In the case of soot formation, a lean fuel-air equivalence ratio ($\Phi \leq 1$) reduce it. As well as, the soot can be reduced using alternative fuels without aromatics in its compositions or with high oxygen concentration in its molecular structure.

In the case of NO, a lower temperature combustion reduces its formation. It can be achieved by means of high levels of EGR or high levels of dilution of the mixture [13]. However, a trade-off between soot and NO exists, that means that if the temperature is reduced, the NO decreases but the soot increases and vice versa. Thus, with these premises Low Temperature Combustion (LTC) strategies born. LTC produces low levels of NO. Moreover the lower temperatures enhance the homogeneity of the mixture which reduce the propensity for soot formation because fuel rich zones are minimized [14–16].

Kamimoto and Akihama [17,18] described the close relationship between the fuel-air equivalence ratio (Φ) and the temperature. These studies mapped in terms of Φ and temperature, the zones where soot and NO are produced. It was identified that the development of Conventional Diesel Combustion (CDC) takes place both in the zone of high soot formation and in the NO zone, which leads to high levels of emissions. This means that

the equivalence ratios (Φ) in which the combustion starts are very high but the temperature is still low, these are favorable conditions for soot formation. Furthermore, as the flame evolves, Φ decreases but the temperature increases. In this zone defined as jet periphery or stoichiometric surface in previous section, is where the partial products of combustion are oxidized at high temperatures and then, the NO is produced [13]. So, the LTC strategies seek that the combustion development takes place at low temperatures (T <1500 K) for a wide Φ range. Or, on the contrary, it operates at lower Φ (Φ <4) but with temperatures near or below 2300 K, as long as the combustion efficiency is comparable with the CDC.

To deepen understanding of LTC strategies, it is necessary to study the in-cylinder processes. Some authors observed that LTC strategies are diluted or partially premixed [13] and therefore the combustion development is not equal to CDC. The first difference appears in the ignition stage because dilution, premixing or cooler in-cylinder gases delay the reactions. In other words, the reactions occur at slower rate. Therefore, the three stages of combustion defined above, as well as the structure of the diffusion flame are not fully valid for LTC strategies. To fill this gap, some authors [1,19] have studied the combustion development also in terms of the heat release rate, for different scenarios that are considered as LTC strategies. In this thesis, the explanation about the Heat Release Rate (HRR) profile will be given for a LTC strategy at low load (~4 bar of gross indicated mean effective pressure) with early injection that means that the Start of Injection (SOI) is around 22º After Top Dead Center (ATDC). This data corresponds to the study developed by Musculus [1]. Moreover, this profile can be extended to other variations of the LTC strategies.

In Figure 2. 3 the HRR profile for both combustion modes (CDC and LTC) is compared with the aim to observe the differences between them. As can be seen, in both cases the evaporation process manifests with a slight decrease in the HRR curve (until point 1 and 4) due to the reduction of the thermal energy of the ambient gases [1]. So far, the two modes of combustion are similar. However, the differences appear from now on. It is important to mention that, when the injection is early, the ambient gases are colder and less dense than in a CDC. So the fuel takes longer time to evaporate. In Figure 2. 3, it is observed how the evaporation for the LTC is prolonged (until point 4), and the reactions occur at a lower rate, therefore the ignition is delayed even more. And that is why two stages are observed in the ignition phase. The first one is shown as a small bump in the HRR curve (ponit 5) and it is known as the stage of low temperature reactions.

Next, the second stage of ignition takes place (point 6). It becomes clear, that in LTC strategies the ignition delay is increased and consequently allows the fuel to mix for a longer time before the second ignition stage. It is important to clarify at this point that in the CDC, the ignition also occurs in two stages, only that the reactions are so fast that it is not possible to appreciate a variation in the HRR profile. In the LTC, after the start of combustion, the fuel also continues to mix, so a mixing-controlled combustion heat release phase is also observed (point 7) but to a lesser extent than in the CDC.

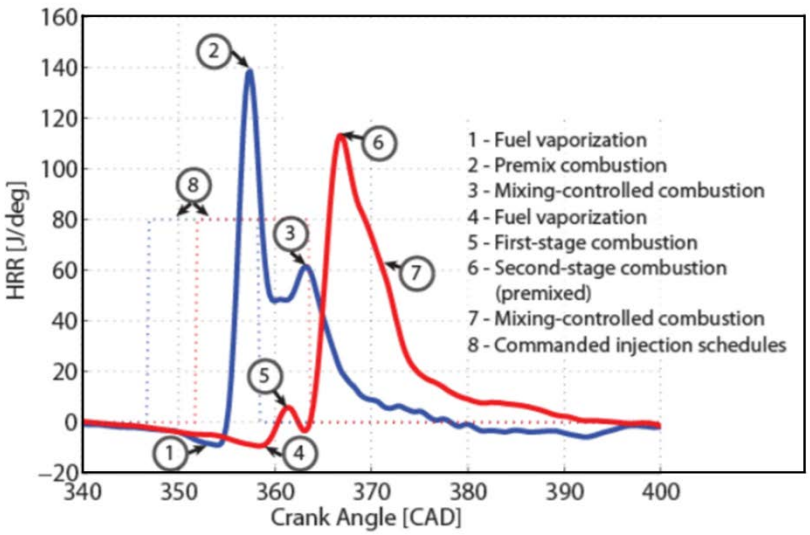

Figure 2. 3 Comparison of HRR profile for conventional diesel combustion (CDC) and Low Temperature Combustion (LTC) strategy [19]

For late injections (SOI~ 1.25º ATDC), the HRR shows similar characteristics to those of early injections. One difference arise in the maximum of HRR which it is slightly lower that for early injection. Another difference is that the mixing controlled combustion heat release is more significant than for early injections [1].

As the in-cylinder processes for LTC are different to those of the CDC, a conceptual model for LTC strategies was developed by Musculus [1,20]. This has been depicted in Figure 2. 4. The LTC model was defined considering a case with the following characteristics: Exhaust Gas Recirculation (EGR) between 10 and 15%, early fuel injection (SOI~ 22º ATDC), small-orifice diesel nozzles and the fuel is injected in a single injection event. Therefore, the ambient temperature and density are low when the fuel is injected. As a consequence of this the liquid length (LL) is longer compared with the LL of the CDC. However when the injection is late, these difference is not significant [1] because the in-cylinder gases have density and temperature comparable to conventional diesel conditions.

Another remarkable difference of the flame structure under a LTC strategy is its shape. The conical jet obtained in CDC is indistinguishable. As well as the high soot concentration is not distinguished in the jet core due to the premixed burn (green area) evolves throughout near-stoichiometric mixtures [20]. The soot forms further from the injector and it forms only in the head vortex where the mixture is relatively rich. Those soot lobes are slowly oxidized as the cycle progresses [1]

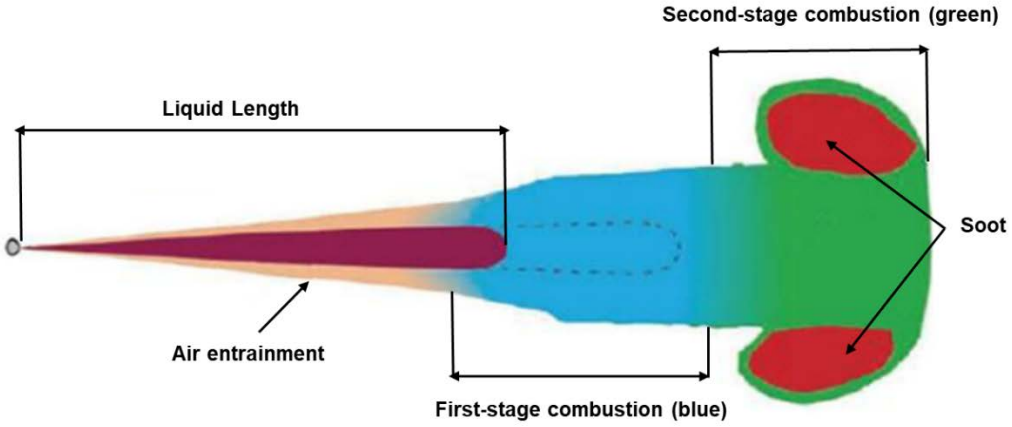

Figure 2. 4 Low Temperature Combustion model [21]

The characteristics and differences of the two conceptual models have been established since the experimentation carried out in this doctoral thesis will use their basic principles for the analysis. At first, combustion will be analyzed under conventional conditions but varying the type of fuel used. Ignition characteristics could have an impact due to these are dependent on fuel composition, as well as the soot formation could be modified. In the same way, the composition of the fuel can change the characteristics of the premixed and diffusion stage. Therefore, all these combustion characteristics will be studied in this thesis. Moreover, it is also important to highlight that these models were built starting from a diesel surrogate with a simple molecular structure in order to avoid the physical-chemical uncertainties that appear as a result of the different compositions that traditional diesel have. Finally, it will be experimented with fuel blends in different proportions. Some of these fuels are in different physical phases at ambient conditions. In these campaigns, the characteristics of the flame will also be analyzed.

2.4 Alternatives fuels with high potential for different combustion modes

Internal combustion engines (ICE) can be actioned by multiple fuel types from different sources as it can be seen in Figure 2. 5. Fossil sources have been the most used for power generation. In the case of crude oil, the diesel and the gasoline have been the leading fuels in the automotive sector. Other fossil source such as Natural Gas (NG) has been incorporated recently into the automotive sector due to its high potential to CO_2 reduction [25]. Fuels such as Liquefied Petroleum Gas (LPG), Compressed Natural Gas (CNG) and Liquefied Natural Gas (LNG) have been implemented and tested in ICE. Conversion process involved in most fossil fuels production is the refining. Additionally, in recent years, others

fuels have begun to be used for combustion engines propulsion. As can be seen in Figure 2.5, fuels such as biodiesel, biogas, synthesis gas (syngas) and Hydrotreated Vegetable Oil (HVO), among others, can be used in ICE. These are known as alternative fuels. They come from renewable sources such as biomass, recycled carbon dioxide (CO_2) and solar and wind energies. Different conversion processes are implemented to obtain renewable fuels. The most common are steam forming, partial oxidation, gasification, chemical looping, electrochemical reaction, electrolysis, transesterification, esterification, hydrogenation and fermentation. Each one is applied depending on the source from which they come. Furthermore, the blends between fuels from fossil and renewable sources, are also considered alternative fuels. Figure 2. 5 has been presented in this thesis in order to give a general context of the available sources, as well as to illustrate only a small sample of the variety of fuels that could be obtained from them. The represented fuels have been considered the most interesting for this thesis.

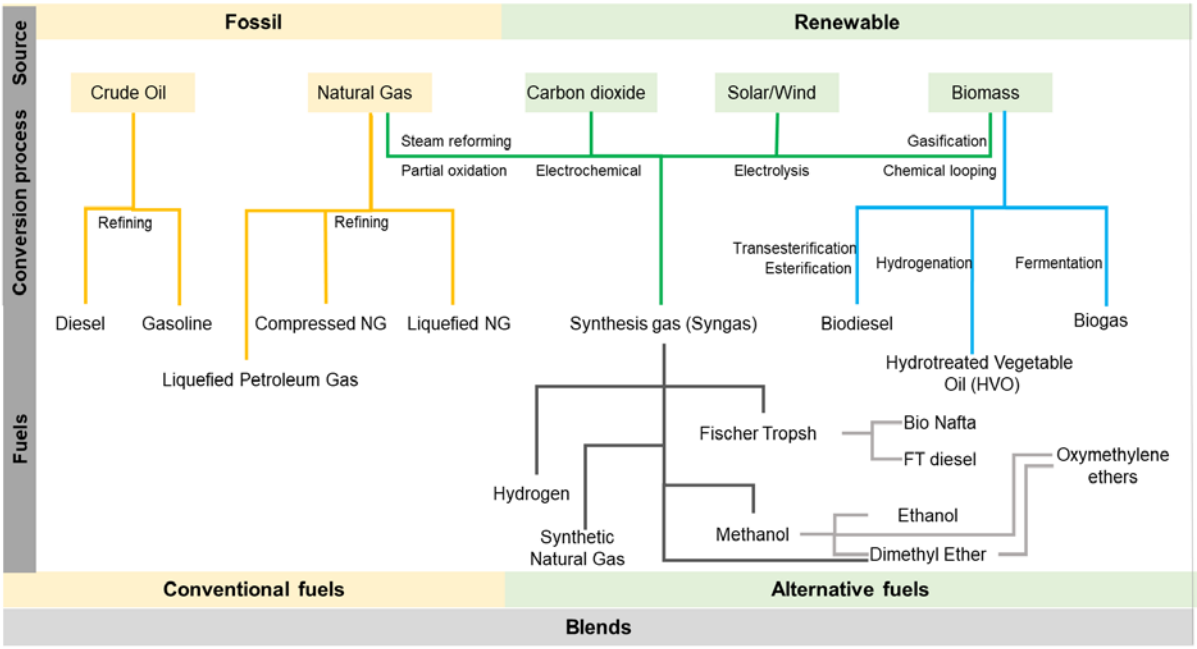

Figure 2. 5 Sources for conventional and alternative fuels. Adapted from [22–24]

To obtain fuels, source conversion processes include steam reforming, partial oxidation or overall refining for those of fossil origin. Gasification or chemical looping are used for those from biomass, and electrolysis for wind and solar sources and also for recycled CO_2 [26]. As seen in Figure 2. 5, many fuels are obtained from the synthesis gas (syngas), which is considered the first step in the renewable sources transformation.

Synthesis gas or syngas is composed mainly of H_2 and CO. It contains most of the chemical energy of the raw material from which it comes. Syngas can be produced from any hydrocarbon feedstock, including crude oil, coal, natural gas, and biomass. This latter is the most interesting in terms of CO_2 reduction. The biomass is placed in a reactor and it is

subjected to a high temperature and high pressure and under the presence of a gasification agent such as oxygen [25]. This process is known as gasification. The other way to obtain syngas is through chemical looping process as it was mentioned previously. This process uses two or more reactions to perform the oxidation of hydrocarbon-based fuels. This method can achieve both an increase in power station efficiency simultaneously with low energy penalty carbon capture [27]. However, gasification is the most common process to obtain syngas due to the simplicity of the process and the low process cost.

One of the advantages of fuels from renewable sources is that their overall carbon footprint is lower. Conversely, the life cycle of gasoline and diesel (from raw material until exhaust gases) usually generates high polluting emissions. On the one hand, these emissions include the particle matter (PM) and the NO produced in the engine. On the other hand, the emissions also include the carbon dioxide (CO_2) produced from the combination of steps necessary to turn a resource into a fuel and also the CO_2 from combustion.

Although the CO_2 is not dangerous to human health, the increment of this gas in the atmosphere has produced an unbalance in the carbon cycle. Nowadays, production of CO_2 is higher than its absorption. Therefore its concentration in the atmosphere is constantly increasing. Thus, all the efforts made to reduce CO_2 emission and thus reach a balance between "generation and absorption" of this gas are essential.

A useful tool to determine the impact of fuel's life cycle on the environment is the Well-to-Wheels (WTW) analysis. It covers from the source until the vehicle has burned the fuel. In the case of crude oil, the WTW analysis includes its extraction, the transport, the refining, distribution, retail and by last, the engine performance and the emissions generated by the engine. In this analysis it is needed to calculate the total energy required to produce the fuel and the total Green House Gas (GHG) emitted. However, these results need to be evaluated along with other aspects such as volume potential, feasibility, reasonable costs, and customer acceptance to determine if a fuel has potential for massive use.

In this thesis, the aspect to evaluate is the performance in the combustion process of these fuels that are attractive in terms of soot and NO reduction, as well as being attractive in terms of CO_2 reduction. The fuels described below offer a significant GHG reduction potential, in addition to their potential in terms of behavior in the combustion process which will be also explained. They will be described in terms of physicochemical properties, feasibility to be implemented and previous studies carried out in compression ignition engines (CI) in order to evidence their performance. Some of them will be evaluated in this thesis.

2.4.1 Natural Gas (NG)

Natural Gas (NG) is a blend of hydrocarbons around 87-97% of methane (CH_4). Also, NG contains nitrogen (N_2) or carbon dioxide (CO_2) which are considered impurities. This fuel can be obtained from fossil sources or from renewables such as waste, advanced

feedstocks or synthetic methane. When NG comes from renewable energies, it is known as Biogas. In both fossil or renewable cases, NG is considered a clean fuel because it has low carbon content and the CO_2 tailpipe emissions are low compared with others hydrocarbon [28]. These characteristics make NG an attractive fuel to help to reduce GHG emissions. This fuel has been considered a good option to achieve the European Union (EU) target of moving towards a decarbonization and the crude oil substitution for the transport sector as described ERTRAC Working group years ago [25]. Criteria as sustainability, economic and technical are fulfilled with this fuel because reserves are estimated up to 150 years in Europe [25].

With the aim to increase energy density, NG can be converted into compressed or liquefied gas, modifying the storage pressure or temperature. Hence the term Compressed Natural Gas (CNG) or Liquefied Natural Gas (LNG) respectively. However, a big challenge is the storage tank, since five liter of CNG at 200 bar has the same energy content than one liter of diesel at ambient pressure. Conversely, the LNG can provide the same energy than diesel, just in 1.8 liters [25]. The main issue to use LNG could be the on-board storage solutions, which mean that cryogenic tanks are required. Despite this, in 2019, 1.8% of total vehicles (light, medium and heavy duty) produced in Spain, corresponded to Spark ignition engines powered by GNC and LPG [29]. Moreover, shipping companies such as Balearia has nine ships powered by NG within its fleet in 2020 [30]. Caterpillar-MaK, MAN, MTU, Rolls-Royce, Siemens, Wärstilä and YANMAR are committed to developing natural gas engines [31]. To support this, there are many research works about the combustion behavior of NG in compression ignition (CI) engines for transportation using different combustion strategies. L. Wei [28] studied the addition of NG into the intake air upstream of the manifold and then ignited by the direct injection of diesel in the cylinder, this combustion strategy is known as Dual Fuel operation mode. It was found that ignition delay and the burning time were longer than the conventional diesel fuel while the maximum in-cylinder pressure was lower. In terms of emissions, the CO_2, NO, and PM decreased. However CO and unburned HC increased significantly. Moreover, the engine power as well as the brake thermal efficiency (BTE) also decreased when the load was low and intermediate. Only at high load, BTE was higher than conventional diesel mode. However, Wannatong [32] observed that increasing the intake temperature at constant engine speed and engine load, the maximum in-cylinder pressure increased considerably and the ignitión delay was shortened.However the engine knock also increased.

Yang [33] led a parametric study of Natural Gas port injection and diesel pilot injection on the combustion characteristics in a turbocharged common rail dual fuel engine. He found that flame propagation and the combustion efficiency can be improved when the natural gas injection is retarded at low and part loads. Moreover, shorter ignition delay, combustion duration and BTE can be achieved modifying parameters such as pressure, timing and injection duration. However, increasing the NG substitution rate would require hardware optimization, as injector nozzle [34], or optimizing injections parameters [35] but the soot-NO trade-off is still a challenge. Therefore, engine control and aftertreatment

technology require additional investments. However, NG has low carbon-hydrogen ratio which is an advantage for soot reduction. For that, the use of NG or LPG is extended currently. These fuels are used in marine engines by means of dual fuel mode (NG or LPG in lesser ratio) or by means of High-Pressure Direct-Injection. In this last technology, the NG or LPG is the primary fuel and diesel acts as a pilot ignition source. NG and LPG have great potential in terms of technical feasibility and combustion performance to be extended to other sectors.

2.4.2 Biodiesel

Biodiesel or Fatty Acid Methyl Ester (FAME) are esters which come from fatty acids. They are generated from animal fats, vegetable oils or waste oils with alcohols by esterification and transesterification processes. The term “biodiesel” was implemented to refer to mixtures of diverse fatty acid methyl esters.

Physical characteristics of biodiesel vary depending on the type of vegetable oil used in the transformation process. In general terms, this fuel has an acceptable cetane number (CN), usually over 50. This is an advantaged over fossil diesel. Other feature slightly different from diesel is its higher viscosity which could represent an issue in terms of fluidity. Therefore biodiesel requires special additives to avoid excessively high viscosity values. Regarding flash point, non-toxicity and biodegradability, these characteristics are similar or better than diesel. Moreover, this fuel does not contain Sulphur or aromatics and it has oxygen in its molecular structure [36,37] which makes it very attractive to reduce the soot formation. However, features such as low-temperature operation ability and lower oxidative stability are drawbacks to be overcome. Other drawback is that biofuel contains metal impurities and this generates damages such as nozzle coking. Therefore, biodiesel is less attractive to fully replace diesel due to the damage that it can cause to engine hardware [25]. Furthermore, biofuel may lead to deterioration of oil quality since the distillation range is smaller and the boiling point is higher compared to diesel [37]. Knowing that and for avoiding engine damage, biodiesel has been tested in different substitutions ratio in compression engines.

In terms of logistical feasibility, biodiesel has great advantages, since distribution and storage can be similar to diesel. Currently, the cost is dominated by feedstock. Considering that this fuel could be obtained from waste oils, the cost results attractive for the customer [38]. However, depending on source from which it comes, biodiesel fuels require special handling to prevent high water content due to the risk of corrosion and microbial growth [36]. Currently, these drawbacks have been overcome and biodiesel is commercially distributed in Europe. In filling stations, customers can choose different types of diesel: B7 or B10. The number refers to the amount of biodiesel that diesel has in its composition, 7% and 10% respectively. Previous studies with biodiesel have demonstrated that its use leads to the substantial reduction in unburned HC, PM, and CO emissions. The emission reduction can be attributed to presence of oxygen in its molecular structure, as it was mentioned previously. However at partial loads or at cold temperatures, higher PM emissions were detected. This

could be related to the condensed hydrocarbons since HC and aldehyde emissions were high after cold-start [39], this also as a consequence of biodiesel's properties.

The power loss could be almost imperceptible. However, the fuel consumption is high due to the lower calorific value of biodiesel fuel, as well as the NO emission increased. The thermal efficiency is not affected when substituting diesel by biodiesel fuel either pure or blended [40]. The main technical drawback could be the problems related to its higher density, viscosity, poor filtration and lower volatility.

2.4.3 Hydrotreated Vegetable Oil (HVO)

Hydrotreated Vegetable Oil (HVO) is a paraffinic bio-based liquid fuel, its chemical composition and physical properties are very similar to those of fossil diesel, but HVO is free of aromatics, oxygen and Sulphur [41]. HVO is produced from waste animal fats or vegetable fats pathways. HVO is considered a second generation biofuel because it comes from non-food feedstocks, therefore it does not affect the human food chain. The production process starts with fatty oils. Firstly, these oils are treated with hydrogen. The resulting products are monoglycerides, diglycerides and acids. Then, these intermediate products are converted into alkanes through decarboxylation and hydrogenation processes [42]. HVO is also known as renewable diesel or green diesel due to the fact that it comes from renewable sources but its properties are similar to those of conventional diesel [43]. For these characteristics, the HVO is a good drop-in fuel which means that no hardware modifications are required to be used in a compression ignition engine [43]. Furthermore, its reasonable distillation range, good winter properties, high cetane number and low amount of ash forming components make it an attractive fuel to be used in diesel engines [44]. However, HVO requires additives to balance the lubricity and thus to prevent damage in the existing diesel engine technology.

The energy content of HVO is slightly higher than diesel fuel. Therefore the storage tank and vehicle fuel tank sizes could be maintained. Also, the driving autonomy of HVO vehicles could be similar to that of diesel vehicles. These are advantages over the rest of fuels that come from biomass. For some authors [45], the HVO is considered as the best renewable fuel from biomass source. However, the biggest challenge continues to be the raw materials. Currently, the largest volume of production is held by Neste. However, companies such as Preem and Eni have also been incorporated to HVO production

In terms of implementation feasibility, HVO does not present great technological challenges due to this fuel can be delivered to consumers using the current diesel fuel logistic system. Furthermore, as it was mentioned previously, the characteristics of fuel tank could be maintained. Regarding production technology, HVO could be used in large commercial scale in Europe [25], due to the fact that the catalytic processes to obtain HVO are similar to those used to refine the traditional oil, therefore, they are available from many suppliers.

HVO has been extensively studied in CI engines for its similarity to diesel in terms of physical and chemical properties, but being from a renewable source makes HVO more

attractive. Bortel [46] tested the effect of this fuel in passenger car, using different substitution ratio, pure HVO (100% of HVO) and a blend of 30% of HVO and 70% of diesel. The results showed a reduction of 10% on CO, unburned HC, and PM emissions. In some operating condition the influence was neutral both on emissions and on engine performance. The effect on NO emission was positive but marginal. The power output increased in order of substitution rate but it was necessary to adjust operating parameters such as EGR, injection pressure, injection timing among others. Other studies conducted in heavy duty diesel engines demonstrated that particles (PM) was reduced by 30–51% when running on HVO compared to diesel fuel [41,47,48]. All results indicate that HVO can be adopted in CI engines even at various blend ratios [45]. Additionally, the benefits in PM, and NO emissions open a new possibilities for optimization of Electronic Control Unit (ECU) strategy for NO-PM trade-off [46].

With these improvements shown on engine performance, HVO could be considered the most immediate substitute for diesel, because in addition to improving or maintaining the engine performance, consumption and emissions, HVO does not require new distribution and storage logistics, neither big investments in engine manufacturing process. Companies such as DAF, Volvo and MAN have confirmed that their most recent trucks can use HVO without problem [49]. The constraint has been a shortage of waste-based feedstock supply. The collection systems need to be improved [50].

2.4.4 Alcohols fuels

Alcohols as fuels have gained attention because they can be produced from renewable sources such as biomass through the synthesis gas process as shown in Figure 2.5. Moreover, alcohols can also be obtained from natural gas and coal. Therefore, the demand can be fully met due to the production capacity [51].

In the case of spark ignition (SI) engines, ethanol (C_2H_5OH) has been used as a gasoline surrogate. Even, in the filling station it can be found gasoline with 5% and 10% of ethanol, identified as E5 and E10 respectively. In Europe, cars manufactured after 2000 usually offer E5 and E10 compatibility [52]

In the case of compression ignition engines, methanol (CH_3OH) has been the most used alcohol. Furthermore, in many cases, both fuels have been blended to be tested in CI engines. Both fuels share similar properties as alcohol fuels. These fuels are oxygenated hydrocarbons with lower viscosity compared to diesel or gasoline, as well as the boiling point is lower which favors the evaporation process, therefore the spray structure is directly influenced by this property. Regarding energy, the Low Heat Value (LHV) of these alcohols is lower than LHV of gasoline and diesel. At atmospheric conditions, methanol and ethanol are liquids. Therefore, minor modifications are required and the current infrastructure could be used. The storage, handle and transport are easier than for gaseous alternative fuels [51].

Although alcohols can be produced from renewable sources, some studies showed contradictory debatable results about the life cycle assessment referred to the benefit and cost of alcohol production, considering its use in internal combustion engines. These studies indicated that energy efficiency, the GHG emission reduction and environmental sustainability are low, when the air pollution, soil and groundwater contamination issues are taken into account [51,53]. For that a careful feedstock selection would be required.

Methanol and ethanol have been tested in compression ignition engine in different ratios even with full replacement ratio. For both fuels, the spray has shown faster evaporation and diffusion velocity under high temperatures in the combustion process as a consequence of their properties [51]. Furthermore, methanol and ethanol retard the combustion phase but they do not affect the combustion stability at all [51,54]. In some studies, the smoke emissions decreased [55]. Other authors have stablished that at lower load or higher load the emission trend is variable, even the unburned HC and CO result higher than those obtained with conventional diesel when some parameters such as temperature, injection pressure or timing injection are changed. However, the NO emission decreased or remained equal to those obtained with diesel. The fuel consumption increased since LHV is lower compared to diesel [51]. The thermal efficiency is often higher due to the higher octane numbers of these fuels. Furthermore, the latent heat of vaporization is also high which allows to enhanced charge cooling effects.

2.4.5 Dimethyl Ether (DME)

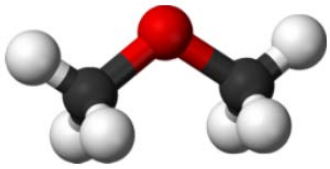

Figure 2. 6 Molecular structure of Dimethyl Ether (DME). The white color represents the hydrogen molecule, the black is the carbon and the red corresponds to the oxygen molecule. [56]

The molecular structure of Dimethyl Ether (DME) has been depicted in Figure 2. 6 to evidence the absence of Carbon–Carbon bonds. Each atom has been represented with colors, the black represents the carbon, the white indicates hydrogen and the red illustrates the oxygen. These are in the following proportion: CH_3OCH_3. As can be seen, DME contents oxygen which makes it an interesting candidate fuel for replacing diesel in CI engines because these properties produce smokeless combustion, low formation and high oxidation rates of particulates. At ambient conditions DME is gaseous fuel, but it can be converted into a liquid fuel when it is subjected to pressure over 5 bar or when it is cooled. Therefore, the handling characteristics are similar to those of liquefied petroleum gas [57]. Furthermore, its low boiling point leads a quick evaporation what improve the air-fuel mixing process [58]. The high cetane number (>55) indicates its fast autoignition. However, DME has lower LHV

compared to diesel so that more fuel is required to achieve the same amount of energy than diesel. That indicates that fuel consumption increases. Moreover, its low viscosity and lubricity could cause damages to fuel supply and injection systems. [58]. Therefore, the material sealing made of conventional elastomers should be replaced with anticorrosive materials compatible with DME. Materials such as polytetrafluoroethylene and the methyl vinyl silicone rubber have been identified as compatible material with DME [58,59]. Regarding environmental characteristics, DME can be hazardous due to it is a volatile organic compound, but it has been demonstrated that DME is non-carcinogenic, non-toxic and biodegradable product [60].

DME can be obtained through two methods as it shown in Figure 2.5. The first is by means of direct synthesis gas and the second is by dehydration of methanol [57]. In the near future, DME could be produced from captured CO_2 and hydrogen (H_2) from electrolysis, which makes it an attractive fuel to balance the CO_2 emissions.

In terms of jet characteristics, DME is similar to diesel jet. However, some differences arise. The fuel droplets brake up before than diesel and the evaporation process is also faster due to its lower boiling point. Therefore, the atomization process is improved when DME is used. Furthermore, DME evaporation characteristics enhanced the mixture formation. That represents an advantages for better engine performance and for reducing the pollutant emissions. In the same way, the liquid length results shorter, so the fuel impingement on the cylinder wall could be reduced. The ignition delay and the combustion duration are shorter for DME compared to diesel. That contributes to slightly higher NO emissions because the charge temperature in the cylinder increases. It is important to mention that main factors that promote NO formation are the long combustion duration, high combustion temperature and low oxygen content, being the first two, disadvantageous characteristics for DME. However, those NO emission can be overcome by maintaining the current EGR systems. Furthermore, the CO and unburned HC emissions have been lower than those from diesel [58]. Regarding the soot formation, DME does not form soot. Thus, the lower pollutant emission of DME (unburned HC, CO and PM) are a results of its high oxygen content and the absence of C-C bonds which improve the air-fuel mixing process avoiding the rich fuel regions [61].

Regarding thermal efficiency, this is similar to that obtained with diesel, although it is needed more fuel to achieve it due to its lower LHV. However, combustion efficiency is better because lower incomplete combustion products [62].

In general, DME is very attractive for CI engines, due to its low emission formation, thermal efficiencies comparable to diesel, and its high potential to reduce CO_2 emission, not only because it is obtained from renewable sources but it also has low carbon content and lower LHV. These characteristics determine CO_2 emissions during combustion.

Currently, DME is used just for research purposes because engines require new storages and fuel delivery systems and it remains to solve the compatibility problems between

the materials as it was previously mentioned. Thus, the most challenge aspects are related to DME physical properties. These issues are outside the scope of this thesis.

2.4.6 Oxymethylene ethers (OME_n)

Oxymethylene ethers also known as polyoxymethylene dimethyl ethers, are alternative fuels produced from renewable resources. They are commonly abbreviated as OME_n, PODE or POMDME [56]. In this thesis, these fuels will be abbreviated as OME_n. Its molecular structure is CH_3-O-$(CH_2$-$O)_n$-CH_3. This includes several (n) oxymethylene groups (-O-CH_2-) in the molecule, being the simplest molecule, the one with n = 1. The longest will be the one with n = 6. Therefore, n indicates the molecule chain length. Moreover, it could be possible to stablish that the oxymethylene ethers with n equal to 0 is, in fact, the DME fuel [63].

Oxymethylene ethers can be produced from methanol or from DME as it is shown in Figure 2.5. In the first case, processes such as oligomerization, transesterification or partial oxidation can be applied to synthesize oxymethylene ethers. In these processes, formaldehyde is added to obtain oxymethylene ether with longer chains [63]. In the case of DME as raw material, the conversion processes for obtaining OME_n could be by means of a non-oxidative process or by means of partial oxidation [64].

Regarding oxymethylene ethers physico-chemical properties, these are strongly dependent on the chain length. OME_n with $n \geq 2$ have cetane number (CN) over 60, therefore they have fast ignitability. However, for OME_n with n=1, the CN is 28, but its appeal lies in the potential for low emissions formation [65]. Furthermore, oxymethylene ethers contain over 40 % of oxygen in their molecular structure [65]. Both characteristics (high CN and oxygen content) make them attractive to replace diesel. Nevertheless, characteristics such as corrosiveness, viscosity and lubricity are similar to those of DME, therefore those problems that DME presents due to these properties are also present when oxymethylene ethers is used. To overcome the lubricity problem of these fuels, mixtures of oxymethylene ethers have been made and are known as OME_x. These OME_x blends are normally made with different proportions of various oxymethylene ethers, with the major contributors being OME_n with n between 3 and 6. It has been observed that by mixing these molecules, lubricity properties become similar as those of diesel. Moreover, the CN of OME_x normally exceeds the value of CN of diesel [65]. An advantage of OME_n and OME_x over DME is the fact that they are liquid fuels under ambient conditions which enables easy storage and transportation.

Regarding oxymethylene ethers behavior in CI engines, these fuels has been tested both pure or in different blend ratios. In this thesis, the term "OME_x" will be used for any blend made from several OME_n ($1<n<6$). OME_n will be used only when it refers to a pure substance. It is worth to mention that the most interesting fuel for CI engines is the OME_x because lubricity properties as it was mentioned before.

In either cases, mixtures or pure fuel, these fuels (oxymethylene ethers) require longer injection duration due to lower LHV. With this, it can be indicated that the combustion phase is faster since the oxygen content allows to quickly reach the conditions necessary (air-fuel ratio) for combustion. As a consequence of this, the combustion duration is shorter [65]. However, when higher load are tested, OME showed longer combustion duration than diesel since when the load increases, a higher nozzle flowrate is required and this is already the maximum for OME to compensate disadvantageous properties (mainly viscosity and LHV). Further investigations are necessary to optimized injector configuration. However, with this limitation is possible to indicate that oxymethylene ethers lead slightly higher indicated efficiency until medium loads [65,66].

In terms of pollutant emission, oxymethylene ethers are promising fuels due to absence of carbon-carbon bonds and high oxygen content. CO and volatile organic compounds (VOC) are lower than diesel [65]. Furthermore, it has been observed that no soot formation occurred during combustion process [67]. Other studies have indicated that NO remained almost unchanged without further changes to the engine control. That gives the possibility to reduce NO without a NO – soot trade-off [65].

It is evident that oxymethylene ethers are the alternative fuels with high potential for the simultaneous reduction of CO_2 and the main pollutants of ICE: NO and soot. Therefore, a fundamental study of them will be carried out in this thesis.

2.4.7 Renewable Hydrogen

Hydrogen (H_2) is the most abundant chemical substance in the universe. Although it is available almost everywhere, its extraction with a certain degree of purity is not always easy or viable. However, and depending on the degree of purity required, H_2 can be obtained from syngas which, as indicated in Figure 2.5, can be obtained from multiple sources such as natural gas, recycled CO_2, solar or wind energy and biomass by means of steam reforming, partial oxidation, electrochemical, electrolysis, gasification, or chemical looping [57,68]. It contains much more energy than other hydro-carbon fuel [68]. For that, H_2 is an attractive fuel for transportation applications. However, the storage technology for using hydrogen in ICE is the main challenge. A way to hydrogen storage can be through compressed systems using high pressure tanks, the disadvantage lies in high cost installation, electricity consumption and the required cost for its maintenance [69]. Other way could be transforming gaseous H_2 into liquid H_2 by cryogenic method. This way offers high volumetric energy density but fails as being an energy extensive method, other issue is the corrosion as a consequence of ice formed in the tank [68]. The great advantage of hydrogen in combustion processes is that H_2 is considered as zero-emission fuel. Its combustion does not produce pollutant emissions, it only releases water vapor into the environment [57,68].

Hydrogen has a viable application for spark ignition engines due to high octane number, however, some studies have indicate that at compression ratios over 17 the H_2 can be implemented in compression ignition engines [70,71]. Hydrogen has been used as an

additive for combustion improvement, even the H_2 has been implemented with an external ignition source (pilot injected high cetane fuel) in CI engines because it improves the combustion rate. Some automobile manufacturers such as Toyota, Hyundai and Honda already produce hydrogen-fueled vehicles, others companies are still exploring this technology concept [72]. However, it needs strong investment in infrastructure.

In compression ignition engines, a stable operation at low load can be achieved, avoiding combustion anomalies such as misfiring and knocking [71,73]. In terms of power, some results have indicated that hydrogen can produce higher power than diesel due to the absence of smoke emissions [74]. Furthermore, NO emission can be reduced. However, the indicated efficiency was about 90% of that obtained with diesel at moderate loads. At low load, the efficiency of the hydrogen-fueled engine decreases compared to that at moderate loads [70,71]. Another potential use of hydrogen is as a medium for the energy storage by means of fuel cells. This is an electrochemical device in which a continuous flow of fuel, generally hydrogen due to properties described before, and oxidant directly supplies electrical current to an external circuit. Currently, Honda and Toyota are the only companies that have obtained approval in Japan, the United States and Europe to market their vehicle "*FCX Clarity*" and "*Toyota Mirai*" powered by hydrogen fuel cell.

Hydrogen has high potential in the engine propulsion systems both for its high energy content and for its low environmental impact. But it need further research in terms of combustion behavior, storage, distribution and handling mainly, which are out of scope of this thesis.

2.5 Summary

Firstly, in this chapter, a description of the combustion process under conventional condition has been made using the Heat Release (HR) curve. The fundamental processes and the parameters of interest have been identified. In the same way, the stages that are affected due to the change in the engine operating conditions and boundary conditions have also been indicated, as well as the changes resulting from the fuel chemical composition.

Secondly, the combustion process for LTC strategies has been described since mixing controlled process and low combustion temperatures allow low soot formation and low NO emissions. Moreover, it has been evidenced that LTC strategies are more attractive if alternative fuels or blends of them are implemented. For that, in the last part of this chapter, multiple fuels have been described. These have potential in terms of engine performance and pollutant reduction. Furthermore, these fuels also have benefits in CO_2 reductions from their manufacture to the tank (WTT). For that, the fuels to analyze in this thesis will be HVO, OME_x, OME_1 and dual fuel mixtures of conventional diesel and gasoline and alternative blends of HVO and LPG.

In the next chapter, the facilities used for the experimental campaigns will be described. In addition a general review of optical techniques implemented to visualize the combustion process will also be given.

References

[1] Musculus MPB, Miles PC, Pickett LM. Conceptual models for partially premixed low-temperature diesel combustion. Progress in Energy and Combustion Science 2013;39:246–83. https://doi.org/10.1016/j.pecs.2012.09.001.

[2] García Oliver JM. Contributions to the study of the j turbulent combustion process of jets in direct injection diesel engines (in Spanish). PhD thesis. Universitat Politècnica de València, 2004.

[3] Gimeno J, Martí-Aldaraví P, Carreres M, Peraza JE. Effect of the nozzle holder on injected fuel temperature for experimental test rigs and its influence on diesel sprays. International Journal of Engine Research 2018;19:374–89. https://doi.org/10.1177/1468087417751531.

[4] Benajes J, Payri R, Bardi M, Martí-Aldaraví P. Experimental characterization of diesel ignition and lift-off length using a single-hole ECN injector. Applied Thermal Engineering 2013;58:554–63. https://doi.org/10.1016/j.applthermaleng.2013.04.044.

[5] Plee SL, Ahmad T. Relative Roles of Premixed and Diffusion Burning in Diesel Combustion, SAE Technical Paper 831733; 1983. https://doi.org/10.4271/831733.

[6] Dec JE, Espey C. Chemiluminescence Imaging of Autoignition in a DI Diesel Engine, SAE Technical Paper 982685; 1998. https://doi.org/10.4271/982685.

[7] Dec JE. A Conceptual Model of DI Diesel Combustion Based on Laser-Sheet Imaging, SAE Technical Paper 970873; 1997. https://doi.org/10.4271/970873.

[8] Siebers D, Higgins B. Flame Lift-Off on Direct-Injection Diesel Sprays Under Quiescent Conditions, SAE Technical Paper 2001-01-0530; 2001. https://doi.org/10.4271/2001-01-0530.

[9] Pickett LM, Siebers DL, Idicheria CA. Relationship Between Ignition Processes and the Lift-Off Length of Diesel Fuel Jets, SAE Technical Paper 2005-01-3843; 2005. https://doi.org/10.4271/2005-01-3843.

[10] Flynn PF, Durrett RP, Hunter GL, zur Loye AO, Akinyemi OC, Dec JE, et al. Diesel Combustion: An Integrated View Combining Laser Diagnostics, Chemical Kinetics, And Empirical Validation, SAE Technical Paper 1999-01-0509; 1999. https://doi.org/10.4271/1999-01-0509.

[11] Dec JE, Coy EB. OH Radical Imaging in a DI Diesel Engine and the Structure of the Early Diffusion Flame, SAE Technical Paper 960831; 1996. https://doi.org/10.4271/960831.

[12] Kosaka H, Aizawa T, Kamimoto T. Two-dimensional imaging of ignition and soot formation processes in a diesel flame. International Journal of Engine Research 2005;6:21–42. https://doi.org/10.1243/146808705X7347.

[13] Dec JE. Advanced compression-ignition engines—understanding the in-cylinder processes. Proceedings of the Combustion Institute 2009;32:2727–42. https://doi.org/10.1016/j.proci.2008.08.008.

[14] Jacobs TJ, Assanis DN. The attainment of premixed compression ignition low-temperature combustion in a compression ignition direct injection engine. Proceedings of the Combustion Institute 2007;31:2913–20. https://doi.org/10.1016/j.proci.2006.08.113.

[15] Murugesa Pandian M, Anand K. Comparison of different low temperature combustion strategies in a light duty air cooled diesel engine. Applied Thermal Engineering 2018;142:380–90. https://doi.org/10.1016/j.applthermaleng.2018.07.047.

[16] Asad U, Divekar P, Zheng M, Tjong J. Low Temperature Combustion Strategies for Compression Ignition Engines: Operability limits and Challenges, 2013, p. 2013-01–0283. https://doi.org/10.4271/2013-01-0283.

[17] Kamimoto T, Bae M. High Combustion Temperature for the Reduction of Particulate in Diesel Engines, SAE Technical Paper 880423; 1988. https://doi.org/10.4271/880423.

[18] Akihama K, Takatori Y, Inagaki K, Sasaki S, Dean AM. Mechanism of the Smokeless Rich Diesel Combustion by Reducing Temperature, SAE Technical Paper 2001-01-0655; 2001. https://doi.org/10.4271/2001-01-0655.

[19] O'Connor J, Musculus M. Optical Investigation of Multiple Injections for Unburned Hydrocarbon Emissions Reduction with Low-Temperature Combustion in a Heavy-Duty Diesel Engine. vol. 1, 8th US National Combustion Meeting 2013. Western States Section/Combustion Institute; 2013, p. 467–91.

[20] Musculus MPB. Multiple Simultaneous Optical Diagnostic Imaging of Early-Injection Low-Temperature Combustion in a Heavy-Duty Diesel Engine, SAE Technical Paper 2006-01-0079; 2006. https://doi.org/10.4271/2006-01-0079.

[21] Low Temperature Combustion 2021. https://dieselnet.com/tech/engine_ltc.php (accessed April, 2021).

[22] European Road Transport Research Advisory Council, Future Light duty Powertrain Technologies and Fuels, 2011.

[23] European Road Transport Research Advisory Council (ERTRAC) Working Group: Energy and Environment, Future Light and Heavy Duty ICE Powertrain Technologies, 2016.

[24] Reif, K. Gasoline Engine Management. Wiesbaden: Springer Fachmedien Wiesbaden; 2015. https://doi.org/10.1007/978-3-658-03964-6.

[25] ERTRAC Working Group. Energy Carriers for Powertrains for a clean and efficient mobility. European Road Transport Research Advisory Council (ERTRAC) Working Group: Energy and Environment; 2014.

[26] Syngaschem BV. https://www.syngaschem.com/ (accessed April, 2021).

[27] Chemical looping combustion. Wikipedia, 2021.

[28] Wei L, Geng P. A review on natural gas/diesel dual fuel combustion, emissions and performance. Fuel Processing Technology 2016;142:264–78. https://doi.org/10.1016/j.fuproc.2015.09.018.

[29] ANFAC | Informe Anual, 2019. https://anfac.com/informe-anual-2019/ (accessed June, 2021).

[30] FolletoCorporativo_Balearia, 2021. https://www.balearia.com/es/grupo-balearia/#page=12 (accessed June, 2021).

[31] Motores marinos a gas natural. Gasnam, 2021. https://gasnam.es/maritimo/motores-marinos-a-gas-natural/ (accessed June, 2021).

[32] Wannatong K, Akarapanyavit N, Siengsanorh S, Chanchaona S. Combustion and Knock Characteristics of Natural Gas Diesel Dual Fuel Engine, SAE Technical Paper 2007-01-2047; 2007. https://doi.org/10.4271/2007-01-2047.

[33] Yang B, Xi C, Wei X, Zeng K, Lai M-C. Parametric investigation of natural gas port injection and diesel pilot injection on the combustion and emissions of a turbocharged common rail dual-fuel engine at low load. Applied Energy 2015;143:130–7. https://doi.org/10.1016/j.apenergy.2015.01.037.

[34] Lee S, Kim C, Lee S, Lee J, Kim J. Diesel injector nozzle optimization for high CNG substitution in a dual-fuel heavy-duty diesel engine. Fuel 2020;262:116607. https://doi.org/10.1016/j.fuel.2019.116607.

[35] Yuvenda D, Sudarmanta B, Wahjudi A, Muraza O. Improved combustion performances and lowered emissions of CNG-diesel dual fuel engine under low load by optimizing CNG injection parameters. Fuel 2020;269:117202. https://doi.org/10.1016/j.fuel.2020.117202.

[36] Singh D, Sharma D, Soni SL, Inda CS, Sharma S, Sharma PK, et al. A comprehensive review of biodiesel production from waste cooking oil and its use as fuel in compression ignition engines: 3rd generation cleaner feedstock. Journal of Cleaner Production 2021;307:127299. https://doi.org/10.1016/j.jclepro.2021.127299.

[37] Saxena P, Jawale S, Joshipura MH. A Review on Prediction of Properties of Biodiesel and Blends of Biodiesel. Procedia Engineering 2013;51:395–402. https://doi.org/10.1016/j.proeng.2013.01.055.

[38] McCormick RL, Graboski MS, Alleman TL, Herring AM, Tyson KS. Impact of Biodiesel Source Material and Chemical Structure on Emissions of Criteria Pollutants from a Heavy-Duty Engine. Environmental Science & Technology 2001;35:1742–7. https://doi.org/10.1021/es001636t.

[39] Aakko P, Nylund N-O. Particle Emissions at Moderate and Cold Temperatures Using Different Fuels, SAE Technical Paper 2003-01-3285; 2003. https://doi.org/10.4271/2003-01-3285.

[40] Xue J, Grift TE, Hansen AC. Effect of biodiesel on engine performances and emissions. Renewable and Sustainable Energy Reviews 2011;15:1098–116. https://doi.org/10.1016/j.rser.2010.11.016.

[41] Aatola H, Larmi M, Sarjovaara T, Mikkonen S. Hydrotreated Vegetable Oil (HVO) as a Renewable Diesel Fuel: Trade-off between NOx, Particulate Emission, and Fuel Consumption of a Heavy Duty Engine, SAE Int. J. Engines 1(1):1251-1262; 2008. https://doi.org/10.4271/2008-01-2500.

[42] Huber GW, O'Connor P, Corma A. Processing biomass in conventional oil refineries: Production of high quality diesel by hydrotreating vegetable oils in heavy vacuum oil mixtures. Applied Catalysis A: General 2007;329:120–9. https://doi.org/10.1016/j.apcata.2007.07.002.

[43] Bjørgen KOP, Emberson DR, Løvås T. Combustion and soot characteristics of hydrotreated vegetable oil compression-ignited spray flames. Fuel 2020;266:116942. https://doi.org/10.1016/j.fuel.2019.116942.

[44] Hartikka T, Kuronen M, Kiiski U. Technical Performance of HVO (Hydrotreated Vegetable Oil) in Diesel Engines, SAE Technical Paper 2012-01-1585; 2012. https://doi.org/10.4271/2012-01-1585.

[45] Sugiyama K, Goto I, Kitano K, Mogi K, Honkanen M. Effects of Hydrotreated Vegetable Oil (HVO) as Renewable Diesel Fuel on Combustion and Exhaust Emissions in Diesel Engine, SAE Int. J. Fuels Lubr. 5(1):205-217; 2011. https://doi.org/10.4271/2011-01-1954.

[46] Bortel I, Vávra J, Takáts M. Effect of HVO fuel mixtures on emissions and performance of a passenger car size diesel engine. Renewable Energy 2019;140:680–91. https://doi.org/10.1016/j.renene.2019.03.067.

[47] Murtonen T, Aakko-Saksa P, Kuronen M, Mikkonen S, Lehtoranta K. Emissions with Heavy-duty Diesel Engines and Vehicles using FAME, HVO and GTL Fuels with and without DOC+POC Aftertreatment, SAE Int. J. Fuels Lubr. 2(2):147-166; 2010. https://doi.org/10.4271/2009-01-2693.

[48] Wu Y, Ferns J, Li H, Andrews G. Investigation of Combustion and Emission Performance of Hydrogenated Vegetable Oil (HVO) Diesel. SAE International Journal of Fuels and Lubricants, SAE Int. J. Fuels Lubr. 10(3):2017; 2017. https://doi.org/10.4271/2017-01-2400.

[49] Bredenoord. HVO diesel as a sustainable solution. Bredenoord, 2019. https://www.bredenoord.com/en/knowledge/hvo-diesel/ (accessed July, 2021).

[50] Renewable Diesel / HVO: Why are we not heading to a Malthusian trap? | LinkedIn, 2021. https://www.linkedin.com/pulse/renewable-diesel-hvo-why-we-heading-malthusian-trap-fabien-hillairet-1e/ (accessed July, 2021).

[51] Zhen X, Wang Y. An overview of methanol as an internal combustion engine fuel. Renewable and Sustainable Energy Reviews 2015;52:477–93. https://doi.org/10.1016/j.rser.2015.07.083.

[52] Ministerio para la Transición Ecológica y el Reto Demográfico - ¿Qué gasolina debo repostar?, 2021. https://energia.gob.es/Gasolinas/Paginas/tipos-gasolina.aspx (accessed July, 2021).

[53] Niven RK. Ethanol in gasoline: environmental impacts and sustainability review article. Renewable and Sustainable Energy Reviews 2005;9:535–55. https://doi.org/10.1016/j.rser.2004.06.003.

[54] Oh H, Bae C, Min K. Spray and Combustion Characteristics of Ethanol Blended Gasoline in a Spray Guided DISI Engine under Lean Stratified Operation. SAE International Journal of Engines, SAE Int. J. Engines 3(2):213-222; 2010. https://doi.org/10.4271/2010-01-2152.

[55] Cairns A, Stansfield P, Fraser N, Blaxill H, Gold M, Rogerson J, et al. A Study of Gasoline-Alcohol Blended Fuels in an Advanced Turbocharged DISI Engine. SAE Int J Fuels Lubr 2009;2:41–57. https://doi.org/10.4271/2009-01-0138.

[56] Dimethyl Ether, 2021. https://dieselnet.com/tech/fuel_dme.php (accessed May, 2021).

[57] Bae C, Kim J. Alternative fuels for internal combustion engines. Proceedings of the Combustion Institute 2017;36:3389–413. https://doi.org/10.1016/j.proci.2016.09.009.

[58] Arcoumanis C, Bae C, Crookes R, Kinoshita E. The potential of di-methyl ether (DME) as an alternative fuel for compression-ignition engines: A review. Fuel 2008;87:1014–30. https://doi.org/10.1016/j.fuel.2007.06.007.

[59] Crusius S, Müller M, Stein H, Goral T. Oxy-methylen-di-methylether (OMEx) as an alternative for diesel fuel and blend compound: properties, additizing and compatibility with fossil and renewable fuels, Esslingen: 12th International Colloquium Fuels - Conventional and Future Energy for Automobiles; 2019, p. 8.

[60] Semelsberger TA, Borup RL, Greene HL. Dimethyl ether (DME) as an alternative fuel. Journal of Power Sources 2006;156:497–511. https://doi.org/10.1016/j.jpowsour.2005.05.082.

[61] Park SH, Lee CS. Combustion performance and emission reduction characteristics of automotive DME engine system. Progress in Energy and Combustion Science 2013;39:147–68. https://doi.org/10.1016/j.pecs.2012.10.002.

[62] Kim MY, Yoon SH, Ryu BW, Lee CS. Combustion and emission characteristics of DME as an alternative fuel for compression ignition engines with a high pressure injection system. Fuel 2008;87:2779–86. https://doi.org/10.1016/j.fuel.2008.01.032.

[63] Ulrich A, Kathrin H, Philipp H, Jörg S. Refuels – Raw Materials, Processes and Applications for Synthetic Fuels. COMSYN European 2nd Generation Biofuels - Opportunities and Applications 2018.

[64] Niethammer B, Wodarz S, Betz M, Haltenort P, Oestreich D, Hackbarth K, et al. Alternative Liquid Fuels from Renewable Resources. Chemie Ingenieur Technik 2018;90:99–112. https://doi.org/10.1002/cite.201700117.

[65] Pélerin D, Gaukel K, Härtl M, Jacob E, Wachtmeister G. Potentials to simplify the engine system using the alternative diesel fuels oxymethylene ether OME1 and OME3−6 on a heavy-duty engine. Fuel 2020;259:116231. https://doi.org/10.1016/j.fuel.2019.116231.

[66] Liu H, Wang Z, Zhang J, Wang J, Shuai S. Study on combustion and emission characteristics of Polyoxymethylene Dimethyl Ethers/diesel blends in light-duty and heavy-duty diesel engines. Applied Energy 2017;185:1393–402. https://doi.org/10.1016/j.apenergy.2015.10.183.

[67] Härtl M, Seidenspinner P, Jacob E, Wachtmeister G. Oxygenate screening on a heavy-duty diesel engine and emission characteristics of highly oxygenated oxymethylene ether fuel OME1. Fuel 2015;153:328–35. https://doi.org/10.1016/j.fuel.2015.03.012.

[68] Niaz S, Manzoor T, Pandith AH. Hydrogen storage: Materials, methods and perspectives. Renewable and Sustainable Energy Reviews 2015;50:457–69. https://doi.org/10.1016/j.rser.2015.05.011.

[69] Syed MT, Sherif SA, Veziroğlu TN, Sheffield JW. An economic analysis of three hydrogen liquefaction systems. International Journal of Hydrogen Energy 1998;23:565–76. https://doi.org/10.1016/S0360-3199(97)00101-8.

[70] Jeon J, Bae C. The effects of hydrogen addition on engine power and emission in DME premixed charge compression ignition engine. International Journal of Hydrogen Energy 2013;38:265–73. https://doi.org/10.1016/j.ijhydene.2012.09.177.

[71] Heindl R, Eichlseder H, Spuller C, Gerbig F, Heller K. New and Innovative Combustion Systems for the H2-ICE: Compression Ignition and Combined Processes. SAE International Journal of Engines, SAE Int. J. Engines 2(1):1231-1250; 2009. https://doi.org/10.4271/2009-01-1421.

[72] Hydrogen vehicle. Wikipedia 2021.

[73] Guo H, Hosseini V, Neill WS, Chippior WL, Dumitrescu CE. An experimental study on the effect of hydrogen enrichment on diesel fueled HCCI combustion. International

Journal of Hydrogen Energy 2011;36:13820–30. https://doi.org/10.1016/j.ijhydene.2011.07.143.

[74] Welch AB, Wallace JS. Performance Characteristics of a Hydrogen-Fueled Diesel Engine with Ignition Assist, SAE Technical Paper 902070; 1990. https://doi.org/10.4271/902070.

Chapter 3

Experimental facilities and optical techniques

Content

3.1 Introduction

In the previous chapter, the spray structure was described for conventional diesel combustion and for low temperature combustion, as well as it was described a wide range of promising fuels for both combustion modes and committed with Green House Gas (GHG) reduction. This third chapter comes to describe the tools and methods available to evaluate the main parameters of each stage of combustion for alternative fuels.

It is important to have on mind that combustion process inside the engine combustion chamber is quite complex. This is influenced by different phenomena such as the changes of the thermal-dynamic conditions, the turbulence in the cylinder flow field, the interaction of the spray with the piston wall, the interaction spray to spray, and also the transient regimes that take place in the CI engine. All these factors could be a big challenge for the combustion analysis when all phenomena occur at the same time. For that reason, with the aim to avoid these effects and thus deepen into the combustion analysis of alternative fuels, in this research two facilities with highly controlled boundary conditions have been selected. In both facilities, the ambient gas conditions are representative of those in a diesel engine during the injection and combustion process. In this sense, all the experiments have been carried out with a single-hole nozzle. One of these facilities is a constant pressure vessel, known as High Pressure and High Temperature installation (HPHT). In this facility, the boundary conditions are stationary and the spray develops freely. The second installation is an optically accessible single cylinder engine, so that the cycle-to-cycle variation and the transient regimes can be evaluated. In this installation, by means of a transducer pressure it is possible to record the instantaneous pressure curve and applying the first principle of thermodynamics, thus it is possible to estimate the heat release. Both installations have optical accesses that allow the visualization of the combustion phenomena facilitating the evaluation of the injection and combustion processes by means of non-intrusive optical techniques which have contributed throughout the years to improve the understanding on combustion process. Some of these techniques are based on the visualization of flame radiation and on the interaction of the jet with the medium surrounding it.

In this chapter, the facilities used to evaluate the alternative fuels will be described first. Then, a background of the common optical techniques available to study combustion phenomena will be given. In this section the most widely used optical techniques will be also addressed in a general way, since these techniques have helped to describe each phase of the combustion and thus building the currently known combustion models [1,2]. Some of the imaging techniques visited will be used in the experiments of this thesis.

3.2 Experimental facilities

As it was mentioned in chapter 1, in this thesis the experiments were performed in three different campaigns. All of them were made with single injectors with the aim to avoid spray-spray interaction. The first campaign related with the analysis of conventional fuels

and single alternative fuels, was carried out in the High Pressure and High Temperature (HPHT) installation. Also, in this facility, the blends of biofuels were tested in a second campaign. That means that two-thirds of experimental campaigns of this thesis were carried out in the HPHT facility. By last, with the aim to analyze the blends of commercial fuels, in particular diesel and gasoline, a third experimental campaign was carried out in an optically accessible single cylinder engine. Therefore, the HPHT installation and the optically accessible single cylinder engine will be described below.

3.2.1 High Pressure and High Temperature installation (HPHT)

The High Pressure and High Temperature (HPHT) is a facility in which the thermodynamic conditions are similar to a diesel engine at the instant of injection. This vessel is classified as a constant-pressure flow (CPF) facility [3], as the conditions are reached by a continuous flow of high-pressure and high temperature gas through the chamber. The chamber have three windows. Two of them are located opposite each other and they have 128 mm of diameter. The other window has 181 mm of diameter and it is perpendicular to the others two windows.

Parameters such as the temperature of the ambient gas, the composition of the gas, the oxygen concentration and the pressure can be controlled independently to obtain the desired values. In Figure 3. 1, a schematic diagram that includes all the control system of the vessel is presented. The test chamber can run as an open circuit with air or, for reducing O_2 concentration, as a closed loop circuit with a mixture of air and nitrogen. In the open circuit the valves are set so that air is filtered, compressed and stored in the high-pressure reservoirs. The air humidity is lowered using a high-pressure industrial dryer. Then, the dry air enters to the test chamber through a 30 kW electric heating system. Hot gases exit the vessel. Then they are cooled and thrown into the atmosphere. To control the gas flow, a valve is located downstream of the chamber. It is manually operated. Thus, combining the circuit valves correctly, the closed loop mode can be used to simulate exhaust gas recirculation (EGR) as was mentioned above, by the addition of nitrogen and continuous monitoring of the oxygen concentration.

The test rig control system regulates both chamber temperature and pressure, both signals are measured inside the test chamber. The heaters are controlled by a Proportional–Integral–Derivative controller (PID) regulated by a temperature set-point that is fixed at the desired level. The chamber pressure is also regulated by a PID system through a flow control valve that is the responsible for increasing the air pressure. The heaters are protected by maintaining a minimum gas flow value, a maximum output temperature and a minimum coolant flow. Firstly, a cooling unit regulates the temperature of the combustion chamber, o-ring seals, and the thermos regulator unit. A pump drives the coolant (ethyleneglycol) from the reservoir to the HPHT's room. Then, the coolant is sent to the chiller by means of another pump and it is sent back to the reservoir. The temperature of the fluid is around 17º C. Then, a second circuit controls and keeps constant the temperature of the injector throughout the

experimentation time. Moreover, as the injection frequency is low, the fuel temperature is the same that the temperature of nozzle tip. Therefore, to control the injector temperature, an aluminum cap was installed. This acts as a conductor between the coolant chamber around the injector and the nozzle tip. Thus, both fuel and nozzle tip temperature are under control [5].

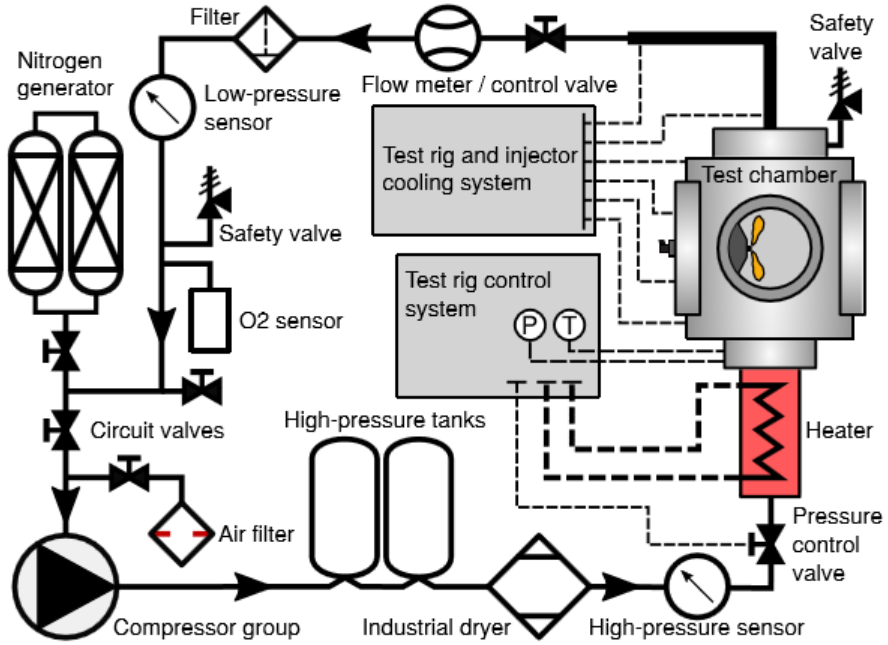

Figure 3. 1 Schematic diagram of High Pressure and High Temperature installation from [4]

The HPHT reaches temperatures up to 1100 K and 15 MPa. The test section has a volume of 15 liters approximately. It has a thick insulation layer to minimize the heat transfer between the inner wall and the external wall or vice-versa. Thus, the inner wall helps to control the temperature inside the chamber and the external helps to tolerate the structural loads. To improve the temperature distribution in the test section, the heated gas exits through four steel tubes. Then they enters to the combustion chamber through a swirler-diffuser.

The most important characteristics of the HPHT facility are been summarized in Table 3. 1 and the wide description and characterization of the vessel can be found in [4,6].

Facility type	CPF
Chamber diameter	200 mm
Chamber height	250 mm
Maximum pressure	15 MPa

Maximum temperature	1100 K
Main heater power	30 kW
Gas velocity	<0.3 m/s

Table 3. 1 Main characteristics of the High Pressure and High Temperature installation

3.2.2 Optically accessible single cylinder engine

One-third of the experimental campaign were carried out in an optically accessible single cylinder engine. A more extensive description of the facility can be found in [7]. This facility is inspired by a 2-stroke single cylinder engine (Jenbach JW 50). The displacement is three liters.

The facility was designed for research purposes as the large displacement limits the effect of liquid vaporization and the spray combustion processes on the pressure trace. However, it is not able to develop enough work each cycle to keep running by itself. Therefore, an asynchronous electric motor (37 kW) is used to start and keep the desired working conditions. The engine is motored at maximum 500 rpm which is a low speed, with the aim to minimize the variation of in-cylinder conditions during a relatively long period if it is compared with typical DI diesel injection durations. A diagram of the engine is depicted in Figure 3. 2. Both air intake and exhaust are handled by transfers on the cylinder liner. The cylinder head was specially designed to provide optical access to the test chamber. The shape is cylindrical, to avoid wall impingement when single hole nozzles are utilized. The effective compression ratio was kept at 15.6 [8,9]. The chamber presents an upper port, where the injector is mounted, and four lateral accesses. A pressure transducer is installed in one of them, whereas the other three are equipped with oval-shaped quartz windows with a thickness of 28 mm. The high and length of quartz windows are indicated in *Table 3. 2*. The cylinder head and the block temperature are controlled by a coolant recirculation system. Their temperature was set to 353 K, to guarantee good lubricity.

Intake and exhaust processes are handled by transfers on the liner. The control of the engine conditions is done with intake air pressure and air temperature. The first one is regulated by an external compressor while a set of electrical resistors at the intake line is used to achieve the desired temperature. A characterization of the engine was carried out, to determine the needed values to achieve any combination of pressure and temperature at top dead center (TDC).The full description about this characterization can be found in [10]. The method is based on determining thermodynamic conditions inside the cylinder, for a variety of points that covers the entire operating range of the engine. In-cylinder temperature and density are calculated from in-cylinder pressure signal, using a first-law thermodynamic analysis and accounting for heat transfer, mechanical stress and blow-by [7,11]. In First, the trapped mass is estimated using intake temperature, pressure, and volume at intake valve

closure (IVC). The mass that leaked through blow-by is calculated as the difference between the trapped mass (at IVC) and the mass at exhaust valve opening (EVO) at exhaust pressure and temperature. The blow-by mass is distributed all along the cycle via a simple algorithm based on Bernoulli's equations for the flow through a nozzle. The equation of state is applied again, with the new "instantaneous mass", geometric volume and experimental pressure, to estimate temperature and density all along the cycle [12]. The mechanical stress applied to the rod can lead to a correction on the instantaneous geometric volume. In this specific engine, no significant deformation was detected [12,13].

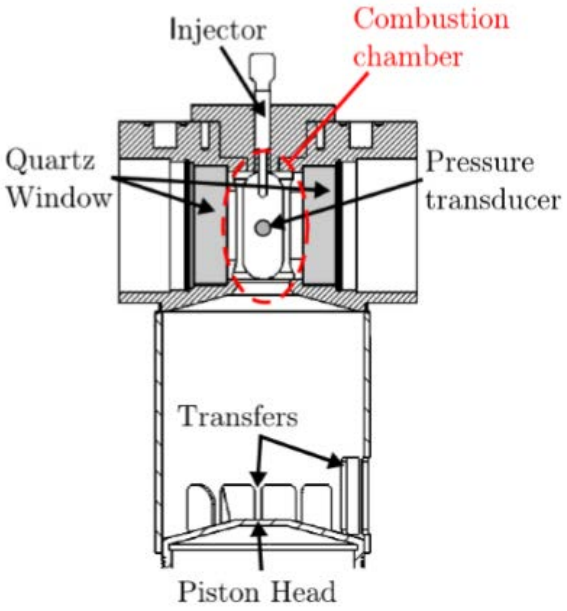

Figure 3. 2 The cross-sectional view of cylinder head from [9]

Because of compression, air temperature and density vary with crank angle along the engine cycle, and consequently, ambient conditions are not constant during the whole injection event. However, in this study it was assumed that the temperature of the air interacting with the spray was constant and homogeneous, and the values of temperature and density are averaged during a given time interval. For the purpose of this study, the average interval was considered to be between the start of injection and ignition. During such interval, temperature variation was always lower than 1%.

The in-cylinder ambient conditions are kept constant for each repetition because there is no remaining residual gas from previous combustion cycles, since the injection occur every thirty cycles. During engine operation, the block temperature is controlled by an external heating-cooling system. The facility can be operated in either open or closed loop. The second mode allows modifying oxygen concentration to simulate EGR conditions. Due to the low amount of fuel injected per cycle, N_2 needs to be used to partially replace oxygen in

the air. During each test, the O_2 concentration is monitored to ensure that it is kept close to the desired value.

An electronically controlled Bosch common-rail was used in these experiments. It is capable to achieve injection pressures up to 160 MPa. The common rail was equipped with a piezoelectric injector of single-hole nozzle. The outlet diameter is 140 μm with a conical shape (K factor of 1.5), which has also been used in different studies by the authors [14–17]. The injection frequency is low during operation and the injector holder is cooled, which allows the nozzle tip and injected fuel temperature to be constant. The injection was placed 3 CAD after TDC and the energizing time was 3 msec.

In *Table 3. 2*, the optically accessible single cylinder engine characteristics have been summarized

Type	single cylinder two stroke
Displacement	3 L
Bore	150 mm
Effective Stroke	108 mm
Speed	500 rpm
Chamber diameter	45 mm
Chamber height	91 mm
Window height	88 mm
Window width	37 mm
Line of sight area	78 mm x 29 mm

Table 3. 2 Main characteristics of the optically accessible engine

3.3 Optical techniques for the study of spray and combustion phenomena

In this thesis, the optical techniques will be used as a method to study the main combustion parameters of a selection of alternative fuels with the aim to contribute to the understanding of the physical and chemical process for each one of them as well as the effect of these fuels on soot production. For that, in this chapter, a background of the optical techniques used to define the combustion models will be given.

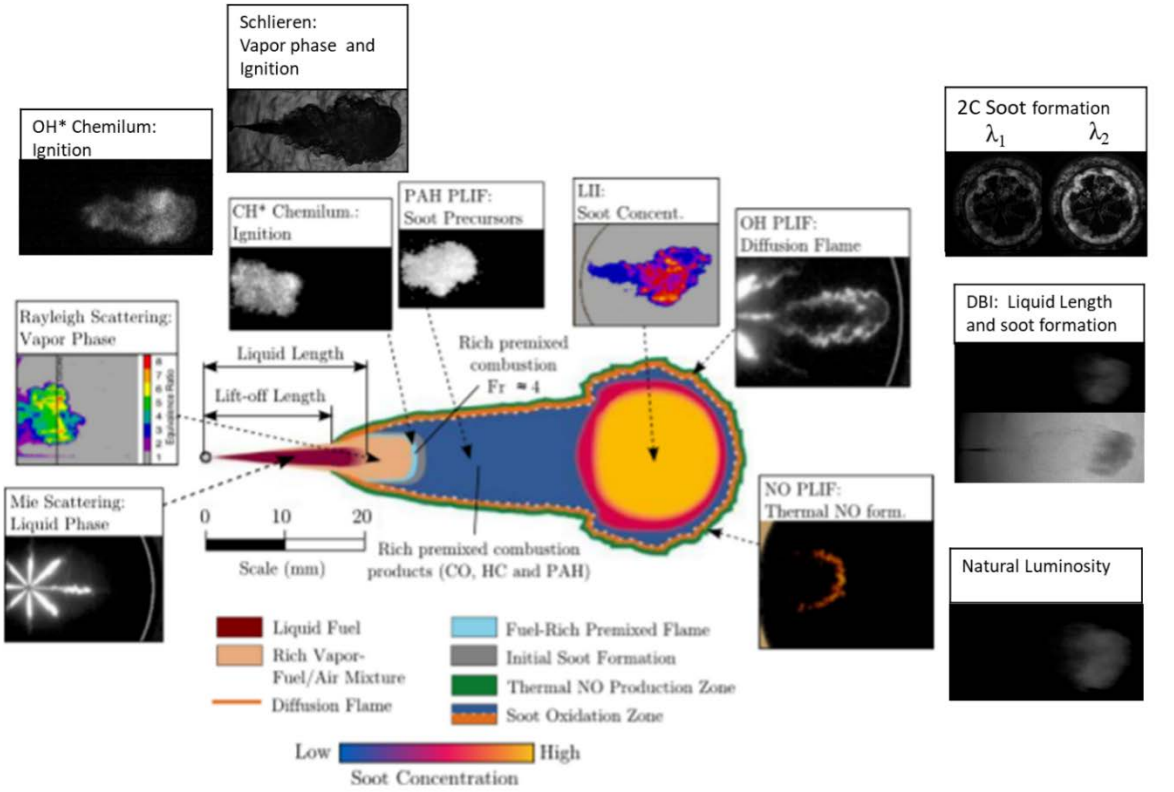

Figure 3. 3 Schematic of direct injection diesel spray and the optical techniques available for diagnostics of each characteristics adapted from [1,9]

Throughout the years, multiple visualization techniques have been used to understand the combustion process. Each combustion stage and each characteristic of the spray and flame have been studied using optical techniques. That knowledge is reflected in the combustion conceptual models presented in Chapter 2.

In Figure 3. 3, it has been depicted some of the optical techniques that were used to measure the spray parameters and to visualize the whole combustion process. The data corresponds to the study presented by Dec and others authors [1,18,19] and the instant drawn corresponds to the period prior to the end of injection. For the development of these models, the techniques applied were mostly laser based techniques. However, there are other techniques that are useful to analyze the main combustion characteristics, therefore these have also been included in Figure 3. 3. A brief summary of some optical techniques to study the non-reactive phase, autoignition, flame development and soot formation will be given in the following items.

- Non-reactive phase.

This phase covers from the start of injection until the start of combustion. Characteristics such as the liquid length (LL) and the vapor penetration (S) can be evaluated. Techniques such as Mie scattering, Diffused Backlight Illumination (DBI) and those techniques based on

the visualization of the fluorescence radiation known as Laser Induced Fluorescence (LIF) have been applied to quantify the liquid phase [20–22]. Mie is based on the light scattered by particles, in this case the particles will be the fuel liquid droplets which are, at least, the size of the wavelength. The scattering signal intensity is influenced by the ratio of the refraction index between the particle and the ambient medium, the shape, size and orientation of the particle. The particles scatter the light under the hypothesis of kinetic energy conservation (elastic collision) and most of this light is scattered in the same direction of the incident beam. The light source can be continuous or pulsed but it must be of high intensity or the detectors such as cameras, must have high-sensitivity. However, in the past, pulsed illumination was more common. Nowadays, when Mie scattering is applied, continuous light is often used because current cameras have a greater capacity to capture light, therefore, the handling of lasers, whose manipulation is a bit more complex, is avoided. Furthermore, as was mentioned before, the LL can also be measured with DBI technique. This technique consists of continuously and uniformly illuminating the jet and registering the shadow or attenuation that it has produced. This attenuation is produced because the intensity of light that propagates in the direction of the original light source reduces due to it is scattered in all directions by fuel droplet [9]. Therefore, that shadow that is generated corresponds to the location of the liquid phase of the jet. In addition to Mie scattering and DBI, other techniques such as LIF can be used to identify both the liquid phase and the vapor phase of the jet. LIF techniques are based on the fluorescence emitted by the molecules when they are excited with a laser pulse at a certain wavelength [23]. The molecules absorb part of incident radiation and reemit a new electromagnetic radiation at a longer wavelength. Unlike Mie scattering, the principle of fluorescence is inelastic since the wavelength of the emitted light is not that of the incident one [24]. In the case of implementing LIF for liquid phase visualization, it is usually combined with planar elastic-scatter imaging techniques such as Mie [20,23] because with calibration procedures and correction methods it is possible to determine maps of relative Sauter Mean Diameter of the droplets or, in the case of evaporating sprays, to discriminate between the liquid and vapor phase. However, this technique is most used to measurements in vapor phase.

In the past, Mie and LIF were most used to describe the fuel spray development and fuel-air interaction. Thus, the works that contributed to the development of the combustion models presented in Chapter 2 used these techniques to study the liquid and vapor phase. Nowadays, DBI has gained advantage over Mie and LIF techniques as a results of technological advances such as camera sensors with high sensitivity and more powerful light sources. Furthermore, DBI does not require sophisticated methods to obtain accurate data and the processing methods are not complex. Nevertheless, when DBI is implemented, two aligned optical accesses are needed. One to illuminate the field and the other to collect the images [25–27]. Another advantage of DBI is the possibility of measuring other parameter such as the spatial distribution of soot particles in the flame [26]. For that, in Figure 3. 3it has been indicated that DBI measures LL and soot formation. Later, this last will be discussed.

The other phase that can be measured during the inert period is the vapor phase. In this phase, important information such as the mixture fraction can be obtained. Techniques such as Rayleigh scattering, LIF or Schlieren have been implemented to visualize and measure this phase. Rayleigh scattering is the elastic scattering of light by particles that are much smaller than the wavelength of the incident light. Rayleigh signal intensity is directly proportional to the incident laser intensity, the molecular number density and the Rayleigh scattering cross-sections of the molecules in the study region [28]. Parameter such as vapor fuel concentration and the adiabatic mixing temperatures can be obtained using the Rayleigh technique. This technique contributed to the construction of the known combustion models. It was identified that the equivalence ratio prior to ignition was from 2 and 4 for conventional combustion [29]. However, the optical set up required special care to avoid interference from the particle and background scattered light, beam steering at high temperatures or variations in laser intensity produced by shot-to-shot [28,29], which made it a complex technique to be implemented later, despite the fact that this technique, with regard to obtaining the measurements, does not require additional processing methods or additional calibrations. Nowadays, advanced image processing methodologies have been implemented to mitigated Rayleigh issues such as particle contamination (dust in air or some liquid droplets), laser intensity variation and beam steering [30]. Therefore, time-resolved mixing and estimated temperature measurements can be obtained. As it was mentioned previously, LIF technique can also be implemented for measuring the vapor concentration [31]. Sometimes, to measure liquid and vapor phase simultaneously, a dopant molecule or fluorescence tracer can be used [32]. However, this could represent a drawback since vaporization properties must be equal to those of fuel because it allows to mimic the fuel vaporization process. Nevertheless, the advantages of LIF techniques are the high intensity of the fluorescence radiation compared with techniques sucha s Rayleigh and its proportionality to the concentration of the substance under study [31]. LIF requires complex methods to obtain accurate measurements. A technique that can face these issues related with signal interference, beam steering and undesired fluorescence for vapor phase characterization, is the schlieren technique. This is based on the refraction phenomenon [33]. When a beam passes through a medium with refractive index gradients, it suffers a deflection. This technique is useful to detect spray boundaries and thus evaluate macroscopic spray characteristics such as vapor penetration under inert and reactive conditions. Although Schlieren does not allow to quantify the vapor fuel concentration, it does provide an overview of the jet that includes both liquid and vapor phase without distinction between them. Furthermore, the temporal evolution of vapor penetration can be measured. Another advantage of schlieren is the ease of being implemented due to the experimental set up does not require sophisticated optical elements [33].

- Autoignition

Although the ignition time is defined as the moment when the pressure increases in the chamber, some light emissions have been observed previous to the variation in the pressure

curve is detected [34]. Some species such as hydroxil (OH^*), formaldehyde (CH_2O^*) and methylidyne (CH^*), emit a spontaneous radiation at characteristic wavelengths. This radiation is known as chemiluminescence. This chemiluminescence has also been used to define the ignition process. In the first stage of ignition known as "cool flame", when the temperature is still low, the radiation comes mainly from CH_2O^* and CH^*. They emit strong chemiluminescence at 355 nm and 430 nm respectively [35,36]. Then, the appearance of the OH^* characterizes the second stage of ignition (ignition at high temperature). Some authors indicate that the most intense peaks of OH^* chemiluminescence occur at 281 nm and 306 nm [36]. Most recent studies indicated that the peak intensity takes place at 309 nm [37].

Some authors compared the curves of heat release with the curves of chemiluminescence intensity for both radicals and they found that the maximum value of OH^* chemiluminescence is reached near the maximum value of the pressure curve, while CH^* is slightly delayed respect to OH^* maximum [36]. For that, OH^* has been identified as a good tracer for the ignition event. However, the radiation of these radicals have a weak signal, for that an intensifier is needed to amplify it. Furthermore, band pass interference filters centered at the desired wavelength are also require to register the radiation emitted. Nowadays, the techniques to visualize the chemiluminescence are characterized by high spatial resolution, high sensitivity and high repetition rates since high-speed image intensifiers and high speed cameras are used.

Other most recently studies analyzed the evolution of the spray and flame geometry to determine the auto ignition through the change in the cone angle by means of schlieren technique. Schlieren images showed that the jet seems to disappear when the low temperature heat release started and then the jet suffers an expansion when the ignition at high temperature takes place [38]. That was easily detectable since the optical arrangement included high speed cameras with high sensitivity and high acquisition rates. For that, in the last years, schlieren has been widely used to characterize both non-reactive and reactive phase due to the simple optical set up needed, in addition to the fact that it is possible to obtain an overview of the injection and combustion process during all stages [39]. In addition, the techniques that allow to determine the spatial and temporal location of ignition, which provide high-fidelity data, are very useful for the development of quality numerical models. These data allow to validate them and at the same time, to improve them.

- Flame development and soot formation

After ignition, the flame development and soot formation can be studied. Thus, different visualization techniques have been applied to define the diffusion combustion flame and then to establish the models that were described in Chapter 2.

In Figure 3. 3 the conventional combustion model [34] and the optical techniques available to define each stage have been shown.

Characteristics such as lift-of length (LOL), which is the distance from the tip injector until the reaction zone where the flame stabilizes after autoignition, can be measured by means of OH^* chemiluminescence. In the past, temporal resolution of this parameter was not possible but nowadays due to the existence of high speed intensifiers, this is possible. With OH^* chemiluminiscence both ignition delay and LOL can be obtained.

As it can be seen in Figure 3. 3, the jet core (blue zone) is formed by intermediate combustion products mainly CO, HC and PAH. This zone is surrounding by a stoichiometric surface known as the diffusion flame front (orange line) where there is a high concentration of OH radical. Then, at jet periphery (green line), the NO are produced. To obtain a spatial distribution of these molecules at a certain plane within the flame, techniques such as Planar Laser Induced fluorescence (PLIF) have been applied [35,40,41].To visualize PAH, some authors [34,35] have used laser beams with wavelengths of 355 nm and 387 nm to induce the fluorescence of these particles. However, distinguishing PAH is complex because in these wavelengths the fluorescence of CH_2O or CH^* also appears at these wavelengths. For that reason, narrow band pass filters are necessary to isolate the desired fluorescence. Furthermore, special care is required to analyze the results considering the complexity of PAH fluorescence spectra [35] assuming that the fluorescence near of front of the flame corresponds to PAH since fluorescence in the jet core could be from PAH or formaldehyde. Thus, to identify the specific PAH species in flames is still a big challenge. Therefore, studying the soot formation by means of the flame radiation gains advantage over the observation of its precursors.

Analyzing the flame radiation provides qualitative information about soot production. However, it must be considered that other species present in the flame also emit spontaneous radiation as it was indicated previously. To better understanding, in Figure 3. 4 the spectral emission during the combustion process has been represented. It can be observed that excited molecules and radicals emit radiation in a limited spectral range. Conversely, the continuous radiation come from thermally excited soot [42], so the intensity of radiation increases as combustion evolves. Furthermore, it can be seen that some species overlap each other. This last explains the spectra issues mentioned above regarding PAH visualization. Moreover, it can also be seen that the highest soot radiation occurs from the visible spectrum (λ>380 nm). This allows to use simple optical set up to visualize only the soot radiation. That means that the signal is intense, therefore intensifiers are no required.

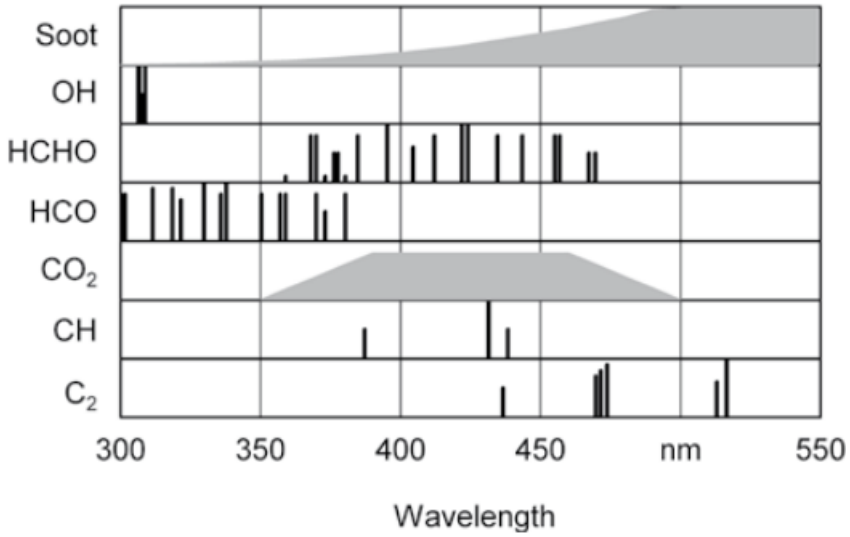

Figure 3. 4 Spectral emission during the combustion process in a diesel engine [42]

One of the techniques for visualizing the soot radiation is the Natural Luminosity. This technique is based on the broadband radiation registered by the camera without spectral filtering. Therefore registered light will be almost entirely the thermal radiation arising from small soot particles at high temperature present in the flame [43]. However, brighter flame could be the consequence of a higher temperature or of a higher soot concentration, or both. For that, this technique allows only qualitative analysis of the soot formation. Diagnosis with this technique has demonstrated to be useful as a first step in describing the general features of combustion process when studying new fuels, engines, and operating conditions [43,44]. Therefore, Natural flame luminosity will be used in this thesis.

Other techniques that do allow to quantify the soot production can be classified into techniques based on thermal radiation of soot particles or in techniques based on light extinction caused by absorption and scattering by the soot particles.

Among the techniques based on the thermal radiation, it can be found the Two-color method (2C) and the Laser-induced incandescence (LII). Both techniques use the theory of thermal radiation which states that the intensity of radiation emitted by soot is proportional to the radiation emitted by a black body at the same temperature. Additionally, both techniques assume that, during combustion, the temperature of the soot particle and the flame temperature are approximately the same [32]. One the one hand, the 2C can separate temperature and soot influences on the radiation by measuring the radiance at two wavelengths (one image for each wavelength) and expressing the emissivity of the particles in terms of soot concentration. 2C is an integrated measure along the line of sight. One of the drawbacks of this method is the low sensitivity to variation of thermodynamic conditions and fuel properties [9]. Furthermore, if the distribution of temperature in the flame is severely non-uniform, this can easily underestimate the soot concentration measured [32]. On the other hand, LII has been often used to obtain soot distribution on the flame symmetry plane

[14,45]. The cloud of soot is illuminated with an intense laser light. The soot particles are heated to a temperature well above the surrounding gas temperature due to the absorption of laser energy. Thus, the heated soot particles will emit black body radiation corresponding to the elevated soot particle temperature. The magnitude of this signal can be related with the soot volume fraction in the detection region. However, the acquired signal requires a careful calibration of the system. Furthermore, the light attenuation and signal trapping effects could have influence on the measurements [46,47]. In terms of simplicity to be applied, LII requires laser sources and imaging systems [48] unlike other techniques that can be implemented with simpler light sources.

The other group of techniques used to study soot formation are those based on light extinction caused by absorption and scattering from the soot particles. These have the advantage that the measured signal depends only on soot distribution. The influence of the flame temperature does not exist. Furthermore, these techniques do not require a previous calibration. Although it is true that these techniques have the disadvantage of beam steering effects caused by the refractive index gradients inside the combustion chamber, they can be corrected and their influence on soot measurement is low [8]. Laser Extinction Method (LEM) and Diffused Back Illumination (DBI) belong to this group. Both LEM and DBI techniques assume that the extinction properties of soot are constant along the soot cloud. LEM allows quantify the soot formed just in the volume defined by the light beam which means that the soot spatial distribution cannot be detailed. Conversely, DBI allows quantify, in addition to liquid length, the soot in the entire flame and during all combustion event. Other difference between both techniques is the light source. LEM uses laser illumination and DBI light source is provided by diffused light, that cover the whole spray area [8]. With the DBI technique both good spatial and temporal resolution can be obtained using simple hardware. Additionally, thanks to the diffused illumination background is possible reducing light steering effects [49,50]. DBI requires two optic accesses, one for introducing the diffused light and the other to collecting it. For that, this technique is generally applied in facilities that simulate diesel operation conditions instead of optical engines. However, in this thesis the used facilities have wide optical accesses and this is an advantages to apply DBI technique.

Continuing with the study of the flame structure, the diffusive flame front (orange line in Figure 3. 3) can be visualized by means of PLIF with excitation near 280 nm, known as OH PLIF. As it was mentioned previously, this technique uses fluorescence of the OH radical to define the jet structure. Sometimes, this technique has difficulties since the signal is usually interfered by other signals such as laser elastic scattering, fluorescence from PAH, laser-induced incandescence from soot and other spontaneous radiation from jet [35]. However, the PLIF for OH visualization is less noisy compared with PAH PLIF since in the wavelength that OH appears, not many more species of combustion appear too (see Figure 3. 4). Therefore, OH PLIF requires optical filter centered in the desired wavelength. In the case of NO visualization, PLIF can also be used to determine the spatial distribution of this

pollutant. However, this signal can be noisy due to the interference from other radiations. The optical filters must suppress elastic scattering, flame luminosity and the radiation of other substances such as O_2 which is likely to be present with the NO and both molecules fluoresce at close wavelength [51].

In summary, PLIF techniques require specifically designed correction strategies to consider radiation losses and interferences signals regardless of the molecule to be visualized.

It is worth to note that laser techniques mentioned previously are characterized by the fact that the temporal resolution to visualize the evolution of the spray depends on the frequency of the laser, unless highly sophisticated laser sources and imaging systems are implemented [48], while continuous lighting transfers responsibility for the acquisition frequency to performance of the camera. Furthermore, laser hardware and the sheet laser alignment represent an additional challenge in the experimental campaigns. Therefore, in this research, making a trade-off between the advantage of high speed cameras and the optical access available in the facilities, the selected optical techniques have been: Schlieren, OH^* chemiluminescence, Natural Luminosity and DBI. In Chapter 4, these optical techniques will be described in depth as well as the image processing methods.

3.4 Summary and conclusions

Through this chapter, the facilities used in this thesis have been described. Firstly, it was described the High Pressure and High Temperature (HPHT) vessel. It has wide optical accesses that allow to evaluate the combustion process in a stationary regime and under ambient conditions similar to those obtained in the combustion chamber of a compression ignition engine. In this facility, two of the three experimental campaigns of this thesis have been carried out. The first of them was carried out with single fuels and will be discussed in Chapter 4. The second campaign, which will be described in Chapter 5, was also carried out in the HPHT facility. This study will deal with the combustion of blends of two fuels with very different physical characteristics. Issues related to the blends preparation, the fuel handling and the control of the injection process will treated in due time

Also, in this chapter, the optically accessible single cylinder engine has also been described. In this vessel the third experimental campaign will be carried out, therefore transient regimes were considered

By last, in this chapter, an overview of some of the optical techniques available to study the spray and combustion characteristics was given with the aim to stablish a theoretical background of the advantages or drawbacks of each technique mentioned. The details of the techniques used for the experiments carried out this thesis and the details of the arrangements done for the simultaneous use of several techniques, will be duly given in the respective chapters.

References

[1] Dec JE, Coy EB. OH Radical Imaging in a DI Diesel Engine and the Structure of the Early Diffusion Flame, SAE Technical Paper 960831; 1996. https://doi.org/10.4271/960831.

[2] Musculus MPB, Miles PC, Pickett LM. Conceptual models for partially premixed low-temperature diesel combustion. Progress in Energy and Combustion Science 2013;39:246–83. https://doi.org/10.1016/j.pecs.2012.09.001.

[3] Baert RSG, Frijters PJM, Somers B, Luijten CCM, de Boer W. Design and Operation of a High Pressure, High Temperature Cell for HD Diesel Spray Diagnostics: Guidelines and Results, SAE Technical Paper 2009-01-0649; 2009. https://doi.org/10.4271/2009-01-0649.

[4] Viera A. Effect of multiple injection strategies on the Diesel spray formation and combustion using optical diagnostics. PhD thesis. Universitat Politècnica de València, 2019.

[5] Payri R, García-Oliver JM, Bardi M, Manin J. Fuel temperature influence on diesel sprays in inert and reacting conditions. Applied Thermal Engineering 2012;35:185–95. https://doi.org/10.1016/j.applthermaleng.2011.10.027.

[6] Payri R, Gimeno J, Cardona S, Ayyapureddi S. Experimental study of the influence of the fuel and boundary conditions over the soot formation in multi-hole diesel injectors using high-speed color diffused back-illumination technique. Applied Thermal Engineering 2019;158:113746. https://doi.org/10.1016/j.applthermaleng.2019.113746.

[7] Bermúdez V, García JM, Juliá E, Martínez S. Engine with Optically Accessible Cylinder Head: A Research Tool for Injection and Combustion Processes. SAE Technical Papers, SAE Technical Paper 2003-01-1110; 2003. https://doi.org/10.4271/2003-01-1110.

[8] Xuan T. Optical investigations on diesel spray dynamics and in-flame soot formation. PhD thesis. Universitat Politècnica de València, 2017.

[9] Micó C. Development of measurement and visualization techniques for characterization of mixing and combustion processes with surrogate fuels. PhD thesis. Universitat Politècnica de València, 2015.

[10] Nerva J-G. An Assessment of fuel physical and chemical properties in the combustion of a Diesel spray. PhD thesis. Universitat Politècnica de València, 2013.

[11] Payri F, Pastor JV, Nerva J-G, Garcia-Oliver JM. Lift-Off Length and KL Extinction Measurements of Biodiesel and Fischer-Tropsch Fuels under Quasi-Steady Diesel Engine Conditions, SAE Int. J. Engines 4(2):2278-2297; 2011. https://doi.org/10.4271/2011-24-0037.

[12] Pastor JV, Payri R, Gimeno J, Nerva JG. Experimental Study on RME Blends: Liquid-Phase Fuel Penetration, Chemiluminescence, and Soot Luminosity in Diesel-Like Conditions. Energy & Fuels 2009;23:5899–915. https://doi.org/10.1021/ef9007328.

[13] Pastor JV, Pastor JM, Gimeno J, Nerva J-G. The effect of Biodiesel fuel blend rate on the Liquid-phase fuel penetration in Diesel engine conditions, SAE Technical Paper 2009-24-0051; 2009. https://doi.org/10.4271/2009-24-0051.

[14] Pastor JV, García-Oliver JM, García A, Micó C, Möller S. Application of optical diagnostics to the quantification of soot in n -alkane flames under diesel conditions. Combustion and Flame 2016;164:212–23. https://doi.org/10.1016/j.combustflame.2015.11.018.

[15] Pastor J, Garcia-Oliver JM, Garcia A, Nareddy VR. Characterization of Spray Evaporation and Mixing Using Blends of Commercial Gasoline and Diesel Fuels in Engine-Like Conditions, SAE Technical Paper 2017-01-0843; 2017. https://doi.org/doi:10.4271/2017-01-0843.

[16] Pastor JV, García-Oliver JM, García A, Pinotti M. Effect of laser induced plasma ignition timing and location on Diesel spray combustion. Energy Conversion and Management 2017;133:41–55. https://doi.org/10.1016/j.enconman.2016.11.054.

[17] Pastor JV, García-Oliver JM, García A, Pinotti M. Laser induced plasma methodology for ignition control in direct injection sprays. Energy Conversion and Management 2016;120:144–56. https://doi.org/10.1016/j.enconman.2016.04.086.

[18] Dec JE, Espey C. Chemiluminescence Imaging of Autoignition in a DI Diesel Engine, SAE Technical Paper 982685; 1998. https://doi.org/10.4271/982685.

[19] Flynn PF, Durrett RP, Hunter GL, zur Loye AO, Akinyemi OC, Dec JE, et al. Diesel Combustion: An Integrated View Combining Laser Diagnostics, Chemical Kinetics, And Empirical Validation, SAE Technical Paper 1999-01-0509; 1999. https://doi.org/10.4271/1999-01-0509.

[20] Uhl M, Schießl R, Maas U, Dreizler A. Time Resolved Spray Characterisation in a Common Rail Direct-Injection Production Type Diesel Engine Using Combined Mie/LIF Laser Diagnostics, SAE Technical Paper 2003-01-1040; 2003. https://doi.org/10.4271/2003-01-1040.

[21] García Oliver JM. Contributions to the study of the j turbulent combustion process of jets in direct injection diesel engines (in Spanish). PhD thesis. Universitat Politècnica de València, 2004.

[22] Pastor JV, Payri R, Garcia-Oliver JM, Briceno FJ. Analysis of transient liquid and vapor phase penetration for diesel sprays under variable injection conditions. Atomization and Sprays 2011;21:503–20. https://doi.org/10.1615/AtomizSpr.2011003721.

[23] Pastor JV, López JJ, Juliá JE, Benajes JV. Planar Laser-Induced Fluorescence fuel concentration measurements in isothermal Diesel sprays. Opt Express, OE 2002;10:309–23. https://doi.org/10.1364/OE.10.000309.

[24] Manin J. Analysis of mixing processes in liquid and vaporized diesel sprays through lif and rayleigh scattering measurements. PhD thesis. Universitat Politècnica de València, 2011.

[25] Gimeno J, Martí-Aldaraví P, Carreres M, Peraza JE. Effect of the nozzle holder on injected fuel temperature for experimental test rigs and its influence on diesel sprays. International Journal of Engine Research 2018;19:374–89. https://doi.org/10.1177/1468087417751531.

[26] Manin J, Bardi M, Pickett LM. Evaluation of the liquid length via diffused back-illumination imaging in vaporizing diesel sprays, Fukuoka, Japan: The Eighth International Conference on Modeling and Diagnostics for Advanced Engine; 2012.

[27] Ghandhi JB, Heim DM. An optimized optical system for backlit imaging. Review of Scientific Instruments 2009;80:056105. https://doi.org/10.1063/1.3128728.

[28] Adam A, Leick P, Bittlinger G, Schulz C. Visualization of the evaporation of a diesel spray using combined Mie and Rayleigh scattering techniques. Exp Fluids 2009;47:439–49. https://doi.org/10.1007/s00348-009-0673-y.

[29] Espey C, Dec JE, Litzinger TA, Santavicca DA. Planar laser rayleigh scattering for quantitative vapor-fuel imaging in a diesel jet. Combustion and Flame 1997;109:65–86. https://doi.org/10.1016/S0010-2180(96)00126-5.

[30] Manin J. High-speed mixing measurements, ECN 5, 2017.

[31] Desantes JM, Pastor JV, Pastor JM, Juliá JE. Limitations on the use of the planar laser induced exciplex fluorescence technique in diesel sprays. Fuel 2005;84:2301–15. https://doi.org/10.1016/j.fuel.2005.05.009.

[32] Zhao H, Ladommatos N. Optical diagnostics for soot and temperature measurement in diesel engines. Progress in Energy and Combustion Science 1998;24:221–55. https://doi.org/10.1016/S0360-1285(97)00033-6.

[33] Settles GS. Schlieren and Shadowgraph Techniques: Visualizing Phenomena in Transparent Media. Springer Science & Business Media; 2012.

[34] Dec JE. A Conceptual Model of DI Diesel Combustion Based on Laser-Sheet Imaging, SAE Technical Paper 970873; 1997. https://doi.org/10.4271/970873.

[35] Bruneaux G. Combustion structure of free and wall-impinging diesel jets by simultaneous laser-induced fluorescence of formaldehyde, poly-aromatic hydrocarbons, and hydroxides. International Journal of Engine Research 2008;9:249–65. https://doi.org/10.1243/14680874JER00108.

[36] Reyes M, Tinaut FV, Giménez B, Pastor JV. Effect of hydrogen addition on the OH* and CH* chemiluminescence emissions of premixed combustion of methane-air mixtures.

International Journal of Hydrogen Energy 2018;43:19778–91. https://doi.org/10.1016/j.ijhydene.2018.09.005.

[37] Zhao M, Experimental and Numerical Study of OH Chemiluminescence in Hydrogen Diffusion Flames. Combustion and Flame 2018;197:369–77. https://doi.org/10.1016/j.combustflame.2018.08.019.

[38] Pastor JV, Payri R, Garcia-Oliver JM, Briceño FJ. Schlieren Methodology for the Analysis of Transient Diesel Flame Evolution. SAE International Journal of Engines, SAE Int. J. Engines 6(3):1661-1676; 2013. https://doi.org/10.4271/2013-24-0041.

[39] Pastor JV, Payri R, Garcia-Oliver JM, Nerva J-G. Schlieren Measurements of the ECN-Spray A Penetration under Inert and Reacting Conditions, SAE Technical Paper 2012-01-0456; 2012. https://doi.org/10.4271/2012-01-0456.

[40] Kosaka H, Aizawa T, Kamimoto T. Two-dimensional imaging of ignition and soot formation processes in a diesel flame. International Journal of Engine Research 2005;6:21–42. https://doi.org/10.1243/146808705X7347.

[41] Singh S, Musculus MPB, Reitz RD. Mixing and flame structures inferred from OH-PLIF for conventional and low-temperature diesel engine combustion. Combustion and Flame 2009;156:1898–908. https://doi.org/10.1016/j.combustflame.2009.07.019.

[42] Pittermann R. Spectroscopic Analysis of the Combustion in Diesel and Gas Engines. MTZ Worldw 2008;69:66–73. https://doi.org/10.1007/BF03227907.

[43] Pastor JV, Garcia-Oliver JM, Garcia A, Pinotti M. Soot Characterization of Diesel/Gasoline Blends Injected through a Single Injection System in CI engines, SAE Technical Paper 2017-24-0048; 2017. https://doi.org/10.4271/2017-24-0048.

[44] Mueller CJ, Musculus MP. Glow Plug Assisted Ignition and Combustion of Methanol in an Optical DI Diesel Engine, SAE Technical Paper 2001-01-2004; 2001. https://doi.org/10.4271/2001-01-2004.

[45] Pastor JV, García JM, Pastor JM, Buitrago JE. Analysis Methodology of Diesel Combustion by Using Flame Luminosity, Two-Colour Method and Laser-Induced Incandescence, SAE Technical Paper 2005-24-012; 2005. https://doi.org/10.4271/2005-24-012.

[46] Smallwood GJ, Clavel D, Gareau D, Sawchuk RA, Snelling DR, Witze PO, et al. Concurrent Quantitative Laser-Induced Incandescence and SMPS Measurements of EGR Effects on Particulate Emissions from a TDI Diesel Engine, SAE Technical Paper 2002-01-2715; 2002. https://doi.org/10.4271/2002-01-2715.

[47] Naccarato F, Potenza M, de Risi A. Simultaneous LII and TC optical correction of a low-sooting LPG diffusion flame. Measurement 2014;47:989–1000. https://doi.org/10.1016/j.measurement.2013.09.013.

[48] Sjöholm J. High Repetition Rate Laser Diagnostics for Combustion Applications. PhD thesis. Lund University, 2012.

[49] Manin J, Pickett LM, Skeen SA. Two-Color Diffused Back-Illumination Imaging as a Diagnostic for Time-Resolved Soot Measurements in Reacting Sprays. SAE International Journal of Engines, SAE Int. J. Engines 6(4):1908-1921; 2013. https://doi.org/10.4271/2013-01-2548.

[50] Skeen SA, Manin J, Dalen K, Pickett LM. Extinction-based Imaging of Soot Processes over a Range of Diesel Operating Conditions. Internal combustion and gas turbine engines, 2013, p. 1–13.

[51] Dec JE, Canaan RE. PLIF Imaging of NO Formation in a DI Diesel Engine, SAE Technical Paper 980147; 1998. https://doi.org/10.4271/980147.

Chapter 4

Effect of fuel composition and nozzle diameter on a diffusion combustion spray

Content

4.1 Introduction

This chapter will report the results of the experimental study of the influence of the chemical and physical structure of fuel and the effect of changing the nozzle diameter on the combustion processes and on soot formation. The fuels tested in this campaign will be classified into alkanes and oxygenated in this thesis, according to their molecular structure. The nozzle diameter corresponds to those characterized by the ECN [1] belong to the Spray A and Spray D conditions. All these experiments were carried out in the optically accessible High Pressure and High Temperature (HPHT) rig under diffusion combustion conditions for a single jet and under steady regimens. Firstly, in this chapter, the fuels and nozzles characteristics will be shown. Then, the optical arrangement and the operating conditions will be described. Next, the results will be analyzed for Spray A conditions in four parts: maximum liquid length, ignition delay, spray tip and flame penetration and flame lift-off length. Then, these parameters will be compared with those of another nozzle diameter for evidencing the effect of combining fuels and different nozzles at the same time. Moreover, the effect of fuels and nozzles on soot formation will be also analyzed. Lastly, this chapter ends with the conclusions of the study.

4.2 Experimental methodology

This experimental campaign was carried out in the optically accessible High Pressure and High Temperature (HPHT) rig described in the Chapter 3. In this installation is possible to replicate the in-cylinder thermodynamic conditions of an internal combustion engine when the fuel is injected. Furthermore, as the temperature field is homogeneous and constant in the area of interest, the uncertainties that could be associated to engine transients are reduced.

On the other hand, the common-rail used is capable to achieve injection pressures up to 230 MPa. It is worth mentioning that the injection system pump used is made by polymerizing tetrafluoroethylene material. This material has shown compatibility with oxymethylene ether fuels according to the investigation reported in [2].

Fuels and nozzles characteristics will be described below. Then, the visualization techniques and the optical setup will be explained. By last, the operating conditions tested will be shown.

4.2.1 Fuels and nozzles characteristics

A set of two different groups of alternative fuels were tested and compared to a low sulfur diesel fuel without biodiesel, which was used as reference. First, two alkanes or paraffinic fuels with different molecular structure: a renewable hydrotreated vegetable oil (HVO) and a single component n-paraffin fuel (dodecane) were tested. The last is used as standard surrogate for diesel by the Engine Combustion Network (ECN) [1] and, in this work, dodecane is tested to compare the results with ECN database and to validate the current

experiments. Then, two oxymethylene ethers, with the general structure $CH_3–O–(CH_2–O)_n–CH_3$ were tested under the same thermodynamic conditions as HVO and dodecane. The first one was a single component one corresponding to the shortest carbon chain (n= 1) of the family, which will be denoted here as OME_1. The second one is a multi-component fuel, which will be denoted here as OME_x, which is a blend of components of different chain lengths. Table 4. 1 compiles the main properties for all five fuels and Table 4. 2 shows the OME_x actual composition.

Characteristics	**Diesel**	**Dodecane**	**HVO**	**OME_1**	**OME_x**
Density [kg/m^3] (T= 15 °C)	835.2	751.2	779.1	866.7	1057.1
Viscosity [mm^2/s] (T= 40 °C)	2.8	1.44	2.7	0.36	1.08
Cetane number [-]	54.18	74	75.5	28	68.6
Lubricity [µm]	386	563	316	747	320
Flash point [ºC]	-	83	70	<40	65
Lower heating value [MJ/kg]	39.79	44.2	43.9	19.25	19.21
Initial Boiling Point [ºC]	155.1	214	185.50	37.4	144.9
Final Boiling Point [ºC]	363.1	218	302	38	242.4
Total contamination [mg/kg]	<24	-	6	<1	<1
Carbon content [% m/m]	85.3	84	85.7	48.4	44.2
Hydrogen Content [% m/m]	13.4	16	14.3	10.4	8.8
Oxygen content [% m/m]	0	0	0	42.1	45
$(A/F)_{st}$ at 21% of O_2	14.39	14.92	14.55	7.22	5.89
$(A/F)_{st}$ at 15% of O_2	19.98	20.72	20.2	10.03	8.18

Table 4. 1 Fuel properties

Molecule	**Content (wt%)**
OME_1	0.01
OME_2	<0.01
OME_3	57.9
OME_4	28.87
OME_5	10.08
OME_6	1.91

Table 4. 2 Composition of OME_x used in this thesis

Also, in this experimental campaign two injectors with different nozzle geometry were used with each fuel. These nozzles will be called as SA and SD in this thesis. Both of them have a single-hole nozzle and they are considered as standard injectors for diffusive combustion studies. Furthermore, "*the injector specifications are for modern advanced injection systems with high pressure capability*" [1]. No cavitation problems have been observed in these nozzles for the fuels that have been already tested [1,3]. The main characteristics of these injectors are summarized in Table 4. 3

	SA	**SD**
Number of holes	1	1
Hole outlet diameter (d_o) (μm)	89.4	189
Nozzle K factor	1.5	1.5
Discharge coefficient (Cd)	0.86	0.86
Hole angular orientation	axial	axial

Table 4. 3 Main characteristics of the injectors used in this study

4.2.2 Operating condition

For the five tested fuels, a set of parametric studies was performed. Oxygen concentration, ambient temperature and injection pressure were defined as variables. Table 4.6 shows the test matrix.

The nominal condition is based on nominal specification from the ECN [1]. It corresponds to 900 K as ambient temperature, 15% of oxygen concentration and 1500 bar as injection pressure and air density of 22.8 kg/m^3 which are conditions of low-temperature combustion with moderated EGR. These guidelines have been followed considering that ECN seeks standardized the experimentation and modeling of engine combustion events in order to "*provide a framework for collaborative comparisons of measured and modeled results*" [1].

The whole test matrix is shown in Table 4. 4. It represents 36 operating points for each fuel. A single injection was used as injection strategy. The energizing time was 2000 μs which provides an injection event long enough to study the spray evolution and flame development under stabilized mixing controlled combustion.

Oxygen concentration (%)	**Temperature [K]**	**Injection Pressure [bar]**
15/ 21	800/900/1000	500/1000/1500

Table 4. 4 Variation of parameters to evaluate for each fuel

4.2.3 Optical Set up

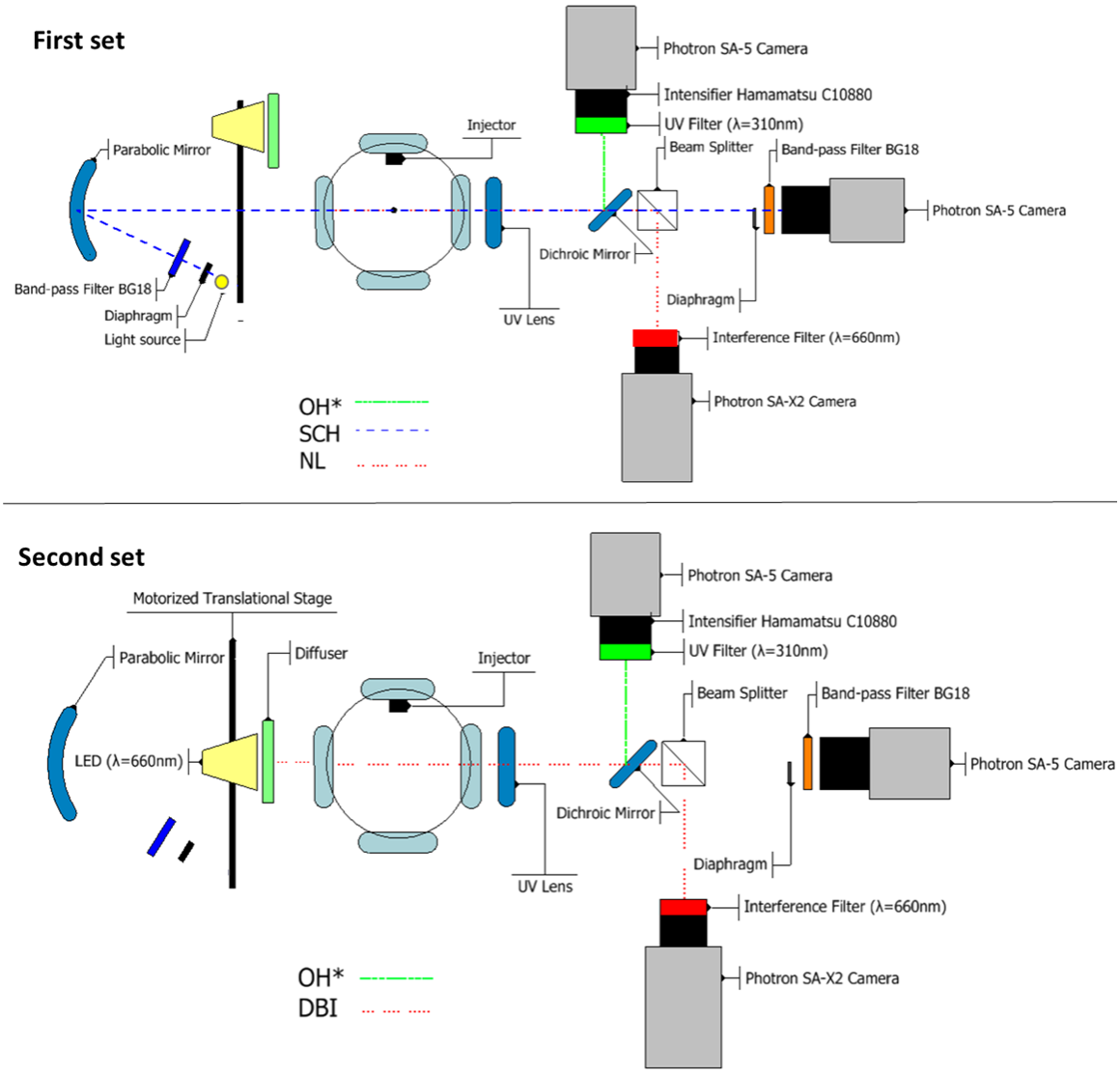

Figure 4. 1 Optical arrangement for the first set up (top) and second setup (bottom)

Aiming to analyze the spray development, the ignition delay, the combustion behavior and the soot formation for each fuel and each nozzle, four visualization techniques have been implemented using the two opposed optical access windows in the installation. The measurements were carried out in two sets with the slightly different setups shown in Figure 4. 1. In the first set, images of schlieren, OH^* chemiluminescence and natural luminosity were recorded. After saving the images, in a second set, by means of motorized translational stage, the LEDs were placed in front of the window in few seconds and images of DBI and OH^* chemiluminescence were recorded. The time between both injections was very short, therefore it can be assumed that measurements will all the techniques were

performed nearly simultaneously for any given condition of the test matrix. To verify this, later some parameters measured in both set will be compared.

In the next section, the configuration for each technique will be explained.

4.2.3.1 Schlieren Imaging

The schlieren technique is based on the deviation suffered by a light beam, due to refraction, when crossing a media with refractive index gradients [4]. Consequently, it allows recording as an image any variations of refractive index, such as those produced by the injection of fuel spray in liquid and vapor phases, as well as the density variations provoked locally by the fuel auto ignition or flame development.

The schlieren technique has different arrangements. In this experimental campaign, a high-speed single-pass schlieren imaging configuration was implemented to visualize the spray and flame boundaries at any operating conditions. The optical arrangement could be divided in two different sections: the illumination and collection side.

On the illumination side, light from a xenon lamp is driven with a liquid light guide into an iris diaphragm, to generate a point light source at the focal length plane of a parabolic mirror (f = 610 mm, D = 150 mm) so that the measurement area is illuminated with a collimated beam. In addition, to avoid interference and restrict the spectrum of the xenon lamp in the DBI and NL images commented later, a BG18 band pass filter was used. On the other side of the chamber, the collection side, a spherical lens (f = 750 mm) was placed very close to optical access. This lens focusses the light onto the focal point, also known as Fourier plane where an iris diaphragm with a cut-off diameter of around 3 mm was located. Additionally, another BG18 band pass filter was placed just before the Photron Fastcam SA-5 camera to minimize undesired light from sources other than the schlieren illumination lamp. The camera was equipped with a Carl Zeiss Makro-Planar T 100 mm f/2 ZF2 camera lens. Images were recorded at 25 kfps. The shutter time was 4.24 µs and it was kept constant throughout all the experiments. The resolution was 800 × 320 pixel with a total magnification of 6.9 pixel/mm. 20 injection cycles per test were recorded in all cases.

The schlieren images have been used to describe the spray tip penetration under nonreactive, as well as the penetration under reactive conditions and the ignition delay. First, the geometry configuration was stablished, then an image segmentation from the background has been performed by using the standard methodology developed by ECN [1]. To help with the understanding of that procedure, Figure 4. 2 has been depicted. Firstly, a dynamic subtraction of the background is obtained. That means that the background for an image in an instant *"i"* (Figure 4. 2.a) is updated constantly as consequence of the slight changes that the background undergoes throughout the combustion event. This dynamic background is composed by two areas. The biggest area (Figure 4. 2.b) is composed by the pixels that are not considered as spray in the instant *"i-1"*. The other area occupied by the spray (Figure 4. 2.c) is filled with the background obtained before the injection. Thus, the dynamic

background is obtained (Figure 4. 2.d). Then, this dynamic background is subtracted from image in the instant *"i"* (Figure 4. 2.e) for detecting the jet contours. To detect them, a threshold between the spray and the background by means of a binarization is used. Therefore, the contours correspond to the coordinates of the boundaries between the white and black regions of the binarized image. A more detailed description of this procedure can be found in [5].

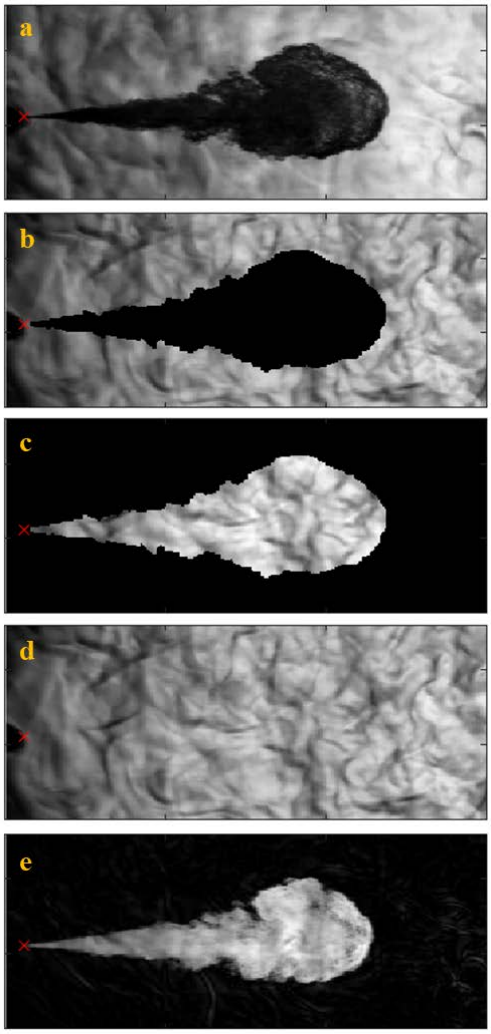

Figure 4. 2 Background segmentation procedure. The image corresponds to Dodecane using Spray A

Once the contours are determined, the vapor penetration is measured at any time as the distance from the nozzle until the furthest coordinate of the contour in the axial direction. In Figure 4. 3 some frames of dodecane under the nominal condition (Spray A, 900 K, 1500 bar and 15 % of O_2) have been presented. The interval time has been selected to depict the intensity changes that the jet undergoes during auto-ignition process. The red line indicates

the jet contours. The blue line indicates the furthest coordinate of jet contour and the yellow line indicates the measurement of vapor penetration for that time.

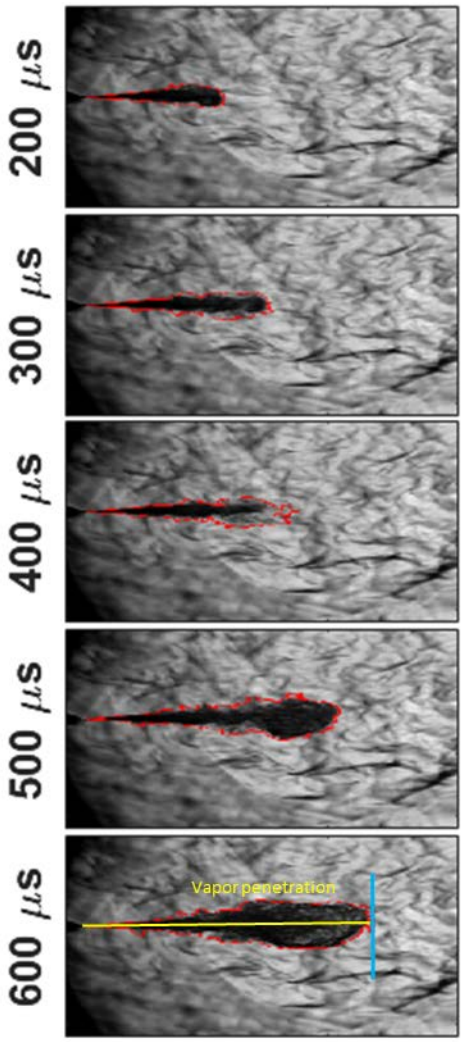

Figure 4. 3 Spray evolution during the ignition period for dodecane with SA under nominal operating condition

As it can be found in literature [6] and seen in Figure 4. 3, at 200 μs, the jet in liquid or vapor phase has a dark shape. Then (300 μs) the first stage of the auto ignition process, also called the cool flame stage, makes the spray contrast of the Schlieren images to vanish, so the intensity decreases in the jet front. After that, in the following frame (400 μs), a slightly intensity increment appears. That indicates that the second stage of ignition process is starting. Then, the high temperature ignition stage, provokes spray radial expansion and spray tip acceleration [7] and the local increase of temperature enhances again the contrast in the images (from 500 μs). Using these observations, the timing when ignition occurs can be determined from the Schlieren movies. This is achieved by determining the maximum accumulated intensity level of the spray for each step time "*i*" and then deriving it for

obtaining the intensity increment. The change in the slope of the curve, determines the ignition delay. That has been depicted in Figure 4. 4. This figure shows a plot of the accumulated intensity increment between consecutive frames for the same fuel and operation condition represented before. The regression of the spray intensity increment reveals the occurrence of the cool flame, which is followed by a step increase associated to the occurrence of the high temperature ignition stage. In this thesis, the ignition timing has been determined as the mean value between the cold flame minimum and the easily detectable maximum after ignition. With this criterion, the ignition times measured are much more suited to the ignition times observed in the images collected in the experiments than with the criterion used previously by other partners from the same research group [8] where the ignition delay is chosen as the time where the maximum intensity increment occurs. It was observed here that at the time when the maximum intensity increment occurs, the jet has already widened showing that the combustion process has started moments before.

Observing the Figure 4. 3 again, the ignition seems to occur very close to 400 µs as it was mentioned before. If the criterion defined in [8] is used for this case, the maximum intensity increment (see purple vertical line in Figure 4. 4) occurs closer to 500 µs (486.5 µs to be exact). That means that the ignition delay would be overestimated. However, when the new criterion of 50% of the time (red vertical line) between the minimum intensity (blue vertical line) and the maximum (purple vertical line in Figure 4. 4) is used, the ignition delay occurs at 406.5 µs, this is much closer to what was seen in the schlieren images. This criterion has been verified for all conditions and fuels and it fits quite well for all.

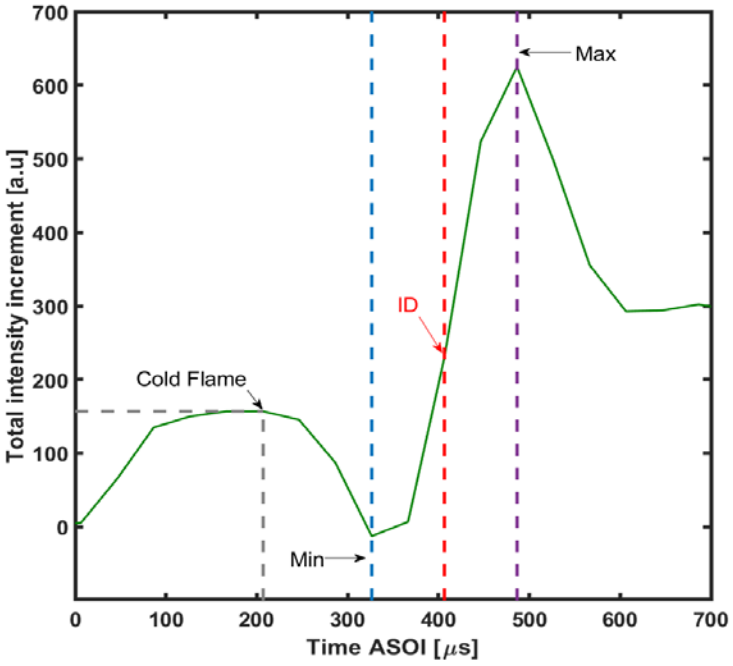

Figure 4. 4 Description of method used to define ignition delay based on the total intensity increment

4.2.3.2 High-speed OH^* chemiluminescence imaging

The OH^* chemiluminescence is a technique based on collecting the radiation of the excited OH radical (OH^*). When the molecule OH reaches this excitation state (OH^*), it absorbs photons and these produce the chemiluminescence phenomenon. The OH^* radical has the strongest emittance band around 310 nm [9]. This radical OH is released during hydrocarbon oxidation and raised to an excited electronic state (OH^*) by exothermic reactions. OH^* results from chemical reactions in near-stoichiometric, high-heat-release regions. For that, OH^* radicals are known to be a good tracer of high temperature combustion regions in a flame [10]. The distance from the injector until this region is known as Lift-off length (LOL). This parameter will be studied throughout this thesis for the different fuels and different operating conditions by means of the visualization of OH^* chemiluminescence. This technique has been implemented as a standard technique by the Engine Combustion Network (ECN) [1] to study this combustion parameter. This technique requires a signal intensifier coupled to a camera with an optical filter centered at then wavelength at which OH^* chemiluminescence appears to avoid non desired flame radiation.

The image processing method to determine LOL consists of tracking a threshold intensity defined as a percentage of camera dynamic range (between 5% and 10% depending of each case). For that, the flame is divided through its axis into a top and bottom profile. For each half, the spatial location where this intensity appears is registered. To represent this, the Figure 4. 5 is shown. It corresponds to OH^* chemiluminescence image for dodecane using SA at nominal operating condition at 3360 µs ASOI. At top, a raw image with the spray axis has been depicted. At bottom, the signal intensity profile has been depicted for both halves of the jet. The vertical lines represent the LOL values obtained for both profiles.

As can be seen in Figure 4. 5, the spatial location where this intensity appears is registered but it fluctuates for each half, therefore the Engine Combustion Network (ECN) recommends to find the distances between the injector tip and the first axial locations above and below the spray centerline with intensity greater than 50% of the intensity peak of that zone [1]. The average of these top and bottom distances is defined as the LOL and it has been depicted as the blue vertical line in the Figure 4. 5

Additionally, with OH^* chemiluminescence technique is possible to determine the ignition delay (ID) if a high speed intensifier is used. This is the case of this experimental campaign. This parameter was computed determining the first frame with light intensity. The results obtained with the schlieren technique were contrasted with these of OH^*. Both techniques agree perfectly. This will be shown later.

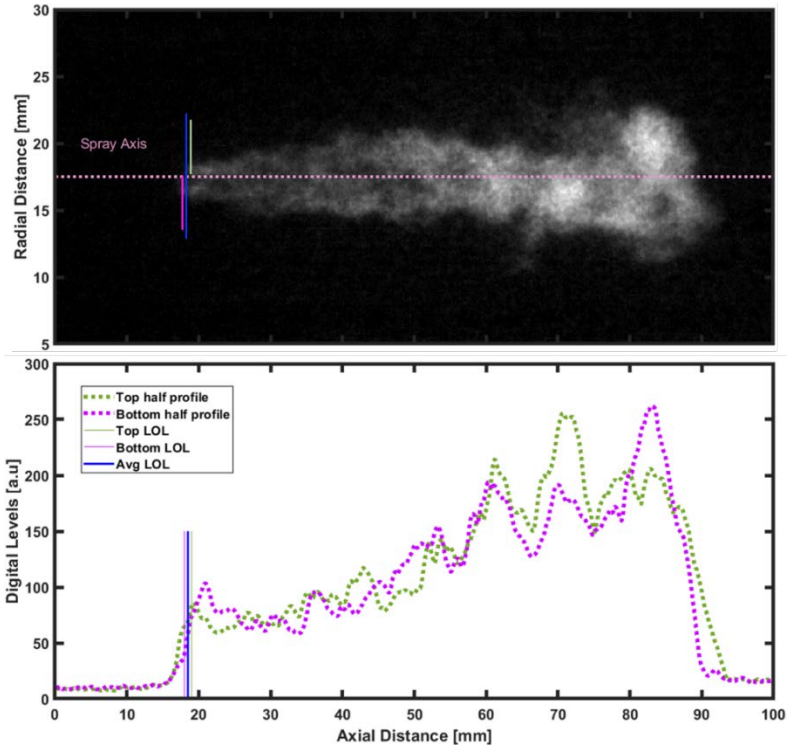

Figure 4. 5 Lift-off length definition using OH^* chemiluminiscence signal. Top: raw image. Bottom: Intensity profile for top (orange dashed line) and bottom (purple dashed line) half. Vertical lines with the same color represent the LOL determined with each profile. Blue vertical line represents the method used in this thesis to define the LOL. The case represented corresponds to the instant 3360 μs belonging to the Spray A using dodecane at 900 K, 1500 bar and 15% of O_2

Regarding to the optical arrangement shown in Figure 4. 1, the light emitted by the jet passes through a UV lens and it is reflected to the camera by means of a dichroic filter. The filter used in these experiments belongs to Thorlabs and the reference code is DMSP805. This filter allow to pass a small range of wavelengths while allows to reflect other range. The transmission and reflectance curve of this filter is shown in Figure 4. 6. It can be seen that maximum transmission range occurs between 400 and 800 nm, while reflectance range occurs between 300 nm and 400 nm and 800 nm 1400 nm. This explains the use given to dichroic filter in this thesis. The signal between 300 nm and 400 nm has been reflected to the the system used to capture this signal. It is formed by a high speed image intensifier (Hamamatsu C10880), coupled to a high speed camera (Photron Fastcam SA5) with a 1:1 relay lens, equipped with a UV f/4 100 mm focal length lens (OUC 2.50 by Bernhard Halle Nachfl.). An interference filter centered at 310 nm (10 nm FWHM) was placed in front of the camera to remove most of the radiation of the flame while keeping OH^* chemiluminescence.

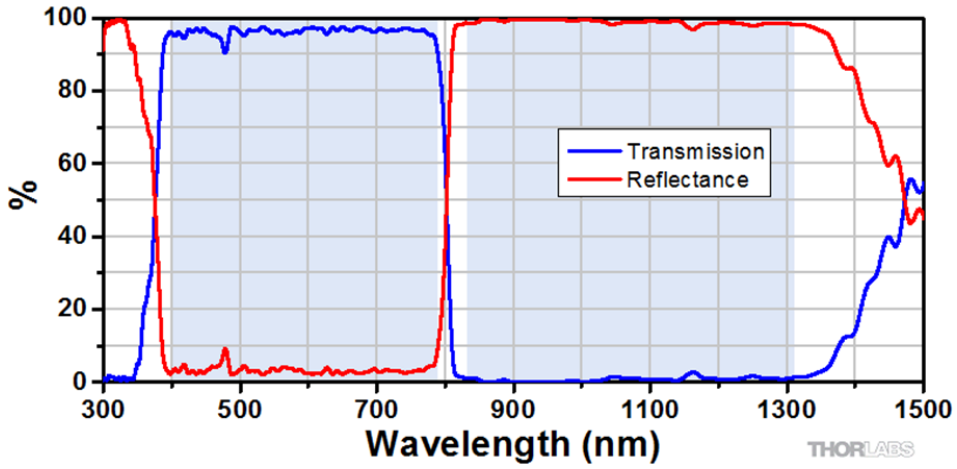

Figure 4. 6 Transmission and reflectance curve for Thorlabs dichroic filter DMSP805 taken from Thorlabs [11]

Images were taken at a fixed frequency of 15 kfps, with a resolution of 320x536 pixel, and a magnification of 3.4 pixel/mm. Shutter time was fixed in 33 μs and care was taken to ensure that light saturation, whenever occurred, did not affect the measurement of the LOL and was low enough as to not imply any risk for the intensifier safety. Again, 30 valid injection cycles per test were recorded in any case, at least.

4.2.3.3 Diffused back illumination

Diffused back-illumination (DBI) is a way to illuminate a field. For that, DBI technique is based on measuring the amount of light attenuated by liquid droplets or by soot particles within the flame, which is related to the liquid and soot concentration, respectively. The light attenuation can be related with the optical properties of the soot cloud by means of Lambert-Beer's law, as described in Equation 4.1:

$$e^{-KL} = \frac{I_{on} - I_{off}}{I_o} \tag{4.1}$$

where $I_{on}$is the light intensity recorded by the camera when the LED is on, i.e., the sum of the transmitted LED intensity and the flame luminosity. I_{off} is the intensity of the flame acquired when the LED is off. $I_o$is the LED light intensity obtained from images recorded before the start of injection (SOI). K is the soot dimensional extinction coefficient and L is the light beam path length through the soot cloud. Thus, the product KL represents the integral value of the soot extinction coefficient along the light path, which is related with the soot concentration [12].

Besides determining soot production through the *KL* factor, DBI is also suggested as an experimental standard to measure the liquid length (LL) of fuels by ECN [1]. The method uses the extinction produced by the spray droplets to provide a quantitative parameter related

to the liquid volume fraction along the path of the light. It is assumed that there is no attenuation in the dark image (I_{off}). That means that the image with intensity flame (I_{off}) is not considered to determine the extinction. Therefore, the Equation 4.1 can be rewritten as follows:

$$e^{-KL} = \frac{I_{on}}{I_o} \tag{4.2}$$

To differentiate the integral value of the soot extinction coefficient along the light path (KL) from the light extinction (τ) produced by the liquid jet, the equation used to determine the liquid length is written with the following nomenclature:

$$\tau = -\ln\left(\frac{I_{on}}{I_o}\right) \tag{4.3}$$

In Figure 4. 7, the extinction profile (τ) has been represented for dodecane under 800 K, 1000 bar of injection pressure and 15% of O_2 using the Spray A. It is possible to see that the beam steering caused by cold vapor droplets does not allow that the extinction curve reach zero. It represents around 3% of the maximum extinction value. Therefore, a linear fitting is applied to the extinction curve to determine the cut with the axis. Thus, this interception at zero defines the liquid length (red vertical line). The extinction values downstream of this location correspond to beam steering produced by vapor as it was mentioned previously.

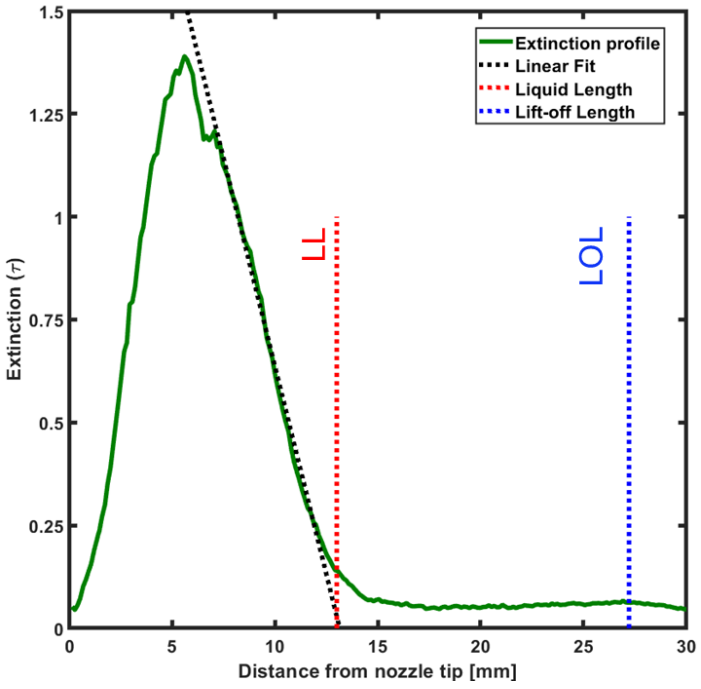

Figure 4. 7 Method to determine the liquid length from extinction profile for dodecane with spray A at 800 K, 1000 bar of injection pressure and 15% of O_2

ECN recommends also taking care with vapor phase beam steering from temperature gradients, which could disturb the measurement. In the current work, the liquid length has been determined only at 800 K and 900 K. It was observed that at these temperatures, the flame lift-off (blue vertical line in Figure 4. 7) is not close to the liquid jet zone. Moreover, at these temperatures the beam steering is low (less than 3% of maximum value). Therefore, the measurement is more accuracy. However, at higher temperatures the uncertainty in the LL measurement is higher because it is closer to LOL and the beam steering in this zone represents around 10% of the maximum value of extinction. For that reason, in this work the LL was determined just for 800 K and 900 K.

Regarding optical configuration, a high power red LED Engin LZ1-10R202-0000 (λ= 660 nm), was used in these experiments as the light source (see Figure 4. 1) to create short flashes synchronized with the camera frames. This wavelength was chosen in this study to reduce the uncertainties of the dimensionless extinction coefficient (***ke***) which is determined through the ratio of scattering and absorption cross-sections which is used in small particle Mie theory. This coefficient will be used later to determine the soot mass. Xuan [13] observed that strong uncertainty of ***ke*** exists when shorter wavelength of the background light is used. For that reason and taking advantage of that study, in this thesis 660nm was selected as wavelength to illuminate the measurement field.

An engineered diffuser RPC Photonics was placed in front of the LED to create a diffused Lambertian intensity profile. That means that diffused light is directly proportional to the cosine of the angle θ between the direction of the incident light and the surface normal [14]. In other words, the engineered diffuser is capable of homogenizing the light while the light is distributed in space.

On the collection side, the transmitted light from the LED and the flame radiation went through a beam splitter with a 50% reflection rate. Then, half of the light was collected by the Photron SA-X2 camera. The exposure time was 1 μs and the resolution was 896x384 with a magnification of 6.85 pixel/mm. The sampling frequency was 25 kfps.

The images taken were analyzed considering that the total light registered by the camera has two contributions: the transmitted LED light intensity and the flame radiation. Due to the use of a bandpass filter centered at 660 nm (FWHM = 10 nm), the crosstalk of flame radiation into the DBI signal is minimized. However, the flashing frequency of the LED was set as quarter of the camera frame rate to capture a LED image between every three consecutive dark images. Thus the image will contain one image with LED and three without LED. This configuration has been called “1 to 3” throughout this thesis. To better understanding of this configuration, Figure 4. 8 is shown. In this study, the camera frequency was 25 kfps, every 40 μs a frame is captured. Therefore, with the “1 to 3” configuration, the LED signal appears every 120 μs. This configuration was used to deal with the non-ideal CMOS sensor behavior that occurs when the camera is exposed to a sudden change in light intensity between two consecutive frames [15]. The flame luminosity from dark image before

the LED image (third dark image: I_{off}) was quantified and used to isolate the transmitted LED light from the total registered radiation.

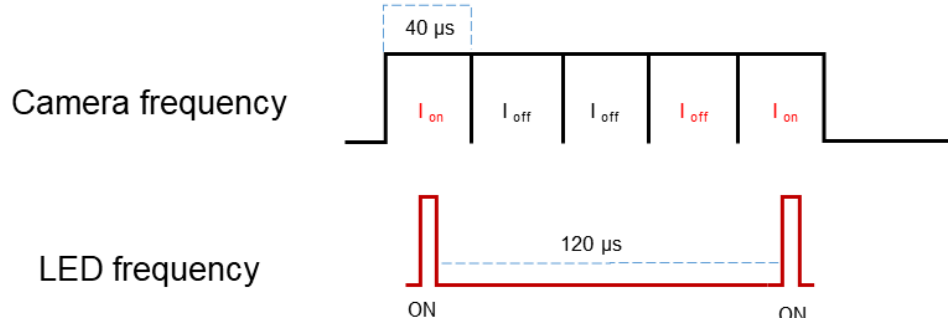

Figure 4. 8 Camera and LED signal synchronization

The image processing method to get KL was based on creating a mask from the third dark image I_{off} (indicated as red I_{off} in Figure 4. 8) with the aim of collecting the information only corresponding to flame radiation. The attenuation of the light was calculated only in the area defined by that mask, so the attenuation produced by the liquid phase did not disturb the KL calculation. Based upon this mask, attenuation ($I_{on}-I_{off}$) is calculated, from which Equation 4.1 is applied. This attenuation was calculated for each instant of time. Then, over the N repetitions, these images were averaged.

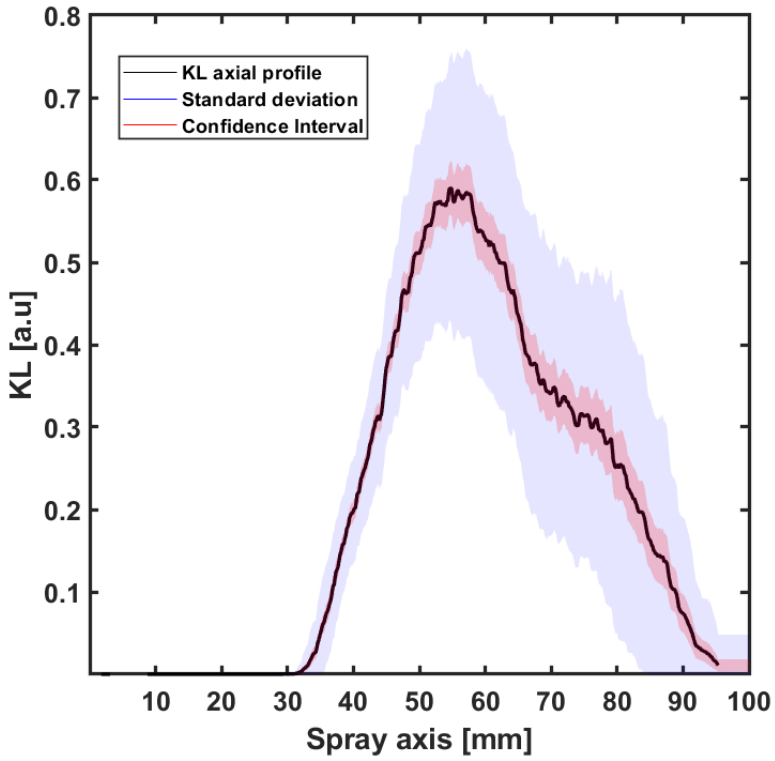

Figure 4. 9 KL profile on the spray axis for diesel at nominal case in the time instant 3500 µs

Figure 4. 9 shows a KL profile along the spray axis at a time instant where the flame is well developed (3500 µs), within the quasi- steady period chosen in this study (between 3000 µs and 4000 µs). The confidence interval at 95% (red shadow) for the measurement of the ensemble averaged KL value and the standard deviation (blue shadow) have been represented. The operating condition shown is the nominal case and the fuel chosen is the diesel.

Similarly, the total soot mass ($\boldsymbol{s_{mass}}$) at a given time was determined from Equation 4.4 as the sum of the values of over all the pixels of the average image taken at that time, and corrected with the other factors indicated. In this equation, $\boldsymbol{\rho_{soot}}$ corresponds to the soot density defined as 1.8 g/cm^3 by Choi [16], $\boldsymbol{\lambda}$ is the wavelength used in the current work (660 nm), $\boldsymbol{r}$ is the pixel-mm ratio (6.85 in this work) and $\boldsymbol{ke}$ is the dimensionless extinction coefficient equal to 7.27 determined in this study through the ratio of scattering and absorption cross-sections which is used in small particle Mie theory as it was mentioned previously:

$$\boldsymbol{s_{mass} = \frac{\sum KL \cdot \rho_{soot} \cdot \lambda}{ke \cdot r^2}} \tag{4.4}$$

In Figure 4. 10 the temporal evolution of total soot mass for diesel at nominal condition is shown. The standard deviation (blue shadow) and confidence interval at 95% for the ensemble average soot mass value (red shadow) have been represented too. In the results section, these values will be shown for the other fuels and operating conditions tested.

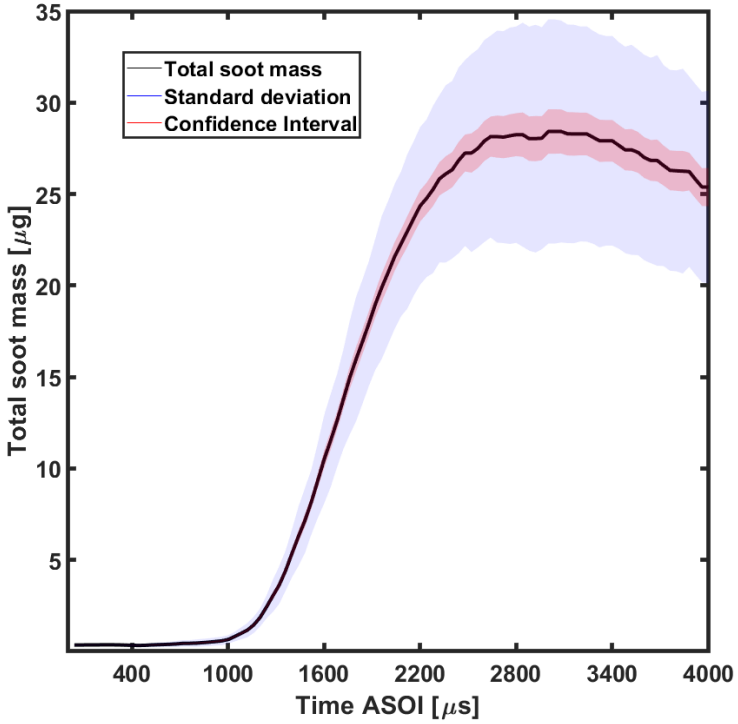

Figure 4. 10 Total soot mass for the diesel at nominal condition

4.3 Effect of fuel composition on global combustion parameters

Before entering the quantification and detailed analysis on the effect that fuel and nozzle have upon the spray characteristics, the combustion process and soot formation for the new fuels studied here, a comparison between results for the dodecane fuel from current study and from similar study available in the ECN database [1] is presented.

Table 4. 5 summarizes the mean values obtained under the nominal conditions (15% of Oxygen concentration, 900 K of temperature and 1500 bar of injection pressure) for both nozzle diameters tested in this experimental campaign. These results have been compared with others obtained by Sandia National Laboratory (SNL).This comparison has been made with the aim to give support to the results obtained for the entire test matrix, assuming that, if the values are in the pertinent range in the nominal case, the others will be as well.

Parameter	Current work SA	SNL SA	Current work SD	SNL SD
LL[mm]	10.0	9.60	24.85	21.83
ID [µs]	410	430	620	590
LOL [mm]	18.89	17.66	29.54	25.98

Table 4. 5 Comparison of main spray parameters between database available in the ECN [1] and current work for dodecane at 900 K, 1500 bar and 15 % O_2 for both nozzles

Observing Table 4. 5, it can be concluded that the results obtained in the current study for dodecane are in the range of those obtained by other researchers. Therefore, the techniques and methods used for the images analysis can be considered valid for the other fuels at different operating conditions. Starting from this premise, firstly, the macroscopic parameters and soot formation will be analyzed for the smallest nozzle. It will be called as "SA" (d_o= 89.4 µm) for all fuels to identify just the fuel effect. Then, it will be analyzed if changing the nozzle diameter (SD with d_o=189 µm) has the same effect for all fuels.

4.3.1 The nozzle A

It was previously commented that the test matrix has been defined following the ECN guidelines in order to provide experimental data that allows comparisons with other experimental or modelling studies. In the same way, the injectors have also been selected with this premise. Both of them are considered as standard injectors for diffusive combustion studies. Their characteristics are for modern advanced injection systems with high pressure capability.

It is well known that SA (smaller nozzle diameter) has been extensively studied for diesel surrogates so its behavior is well characterized. Therefore, with the aim to expand

engine datasets for other conditions and other fuels, this chapter will first analyze the behavior of all fuels for SA and thus be able to evidence the differences respect to diesel surrogates. To facilitate analysis and comparisons, the dodecane, which is the most common diesel surrogate, has also been tested in this experimental campaign. After this, a comparison with SD (bigger nozzle diameter) will be carried out.

4.3.1.1 Maximum liquid length

Spray liquid length (LL) is the maximum axial penetration of the liquid phase fuel. Previous studies have demonstrated that a shorter spray liquid length leads to a better air-fuel mixing, because the fuel vaporization is completed before the fuel reaches the combustion region [17]. On the other hand, too long liquid length leads to fuel wall impingement on the cylinder, which could produce more soot emission with reduced engine efficiency [18]. Figure 4. 11 shows the liquid length at 800 K and 900 K for fuels tested. The injection pressure is 1500 bar and the oxygen concentration is 15%. The LL is constant in time, therefore the values correspond to an average between 800 µs and 4000 µs. From this figure, it can be seen that the spray liquid length of OME_1 is shorter, which could be due to the lower distillation temperature of OME_1 (37.4ºC) compared to the other fuels. Additionally, as Kook indicated in a previous study [19], low viscosities and high densities lead to shorter liquid lengths. This could explain that OME_x (υ=1.082 mm^2/s; ρ=1057.1 kg/m^3) shows shorter LL than diesel and HVO (υ=2.7 mm2/s; ρ=779.1 kg/m^3).

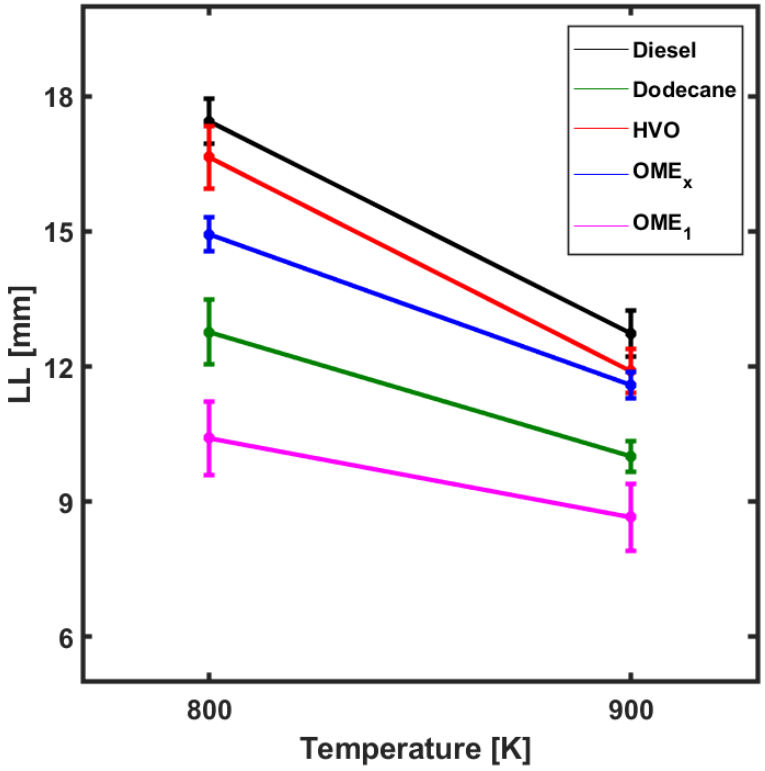

Figure 4. 11 Liquid length for 15% O_2 and 1500 bar of injection pressure

4.3.1.2 Ignition delay time

Ignition delay (ID) is defined as the time elapsed from the Start of Injection (SOI) to the start of combustion (SOC). Figure 4. 12 shows the ignition delay comparison obtained from Schlieren technique and from OH^* chemiluminescence imaging. It can be seen that ID values for both techniques are almost identical, therefore, whatever ID value used in the current work is valid. Hereafter, the represented ID values correspond to those from the schlieren technique.

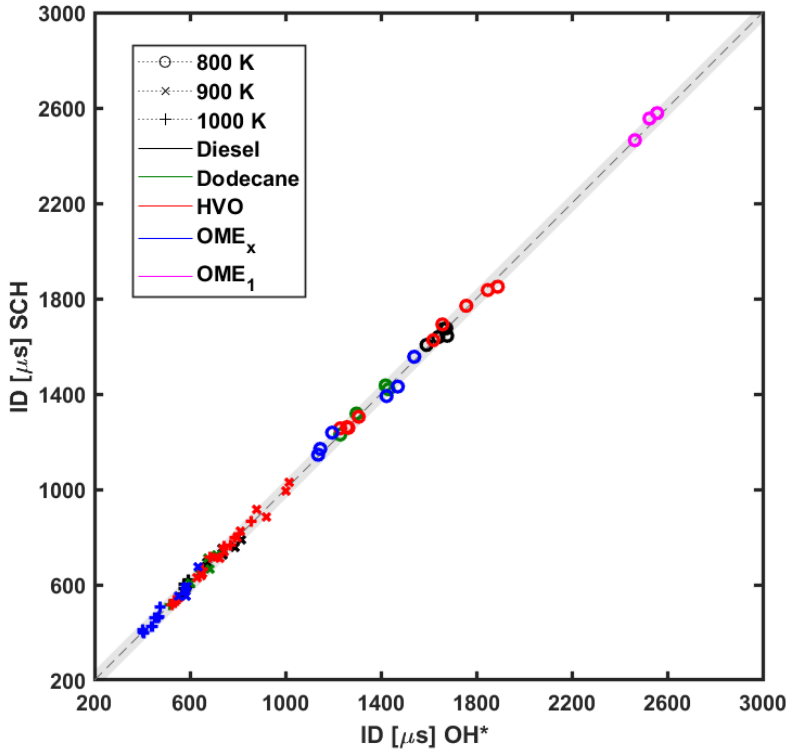

Figure 4. 12 Comparison between Ignition Delay measured from Schlieren and from OH^* chemiluminescense images

In Figure 4. 13, ID for dodecane, HVO, OME_x and OME_1 have been compared against diesel. All the operation conditions have been represented with their standard deviation. The results attend to the trend found in previous studies [20,21]. When the air temperature, injection pressure and ambient oxygen concentration are increased, the ID values decrease. It is a common behavior for all the fuels tested. Furthermore, Figure 4. 13 shows that dodecane, HVO, and OME_x ignite before diesel does. The three fuels have a higher cetane number than diesel (see Table 4. 1 Fuel properties), and the results confirm the relevance of this parameter on autoignition. Based on this, one could expect OME_x to ignite later than HVO and dodecane. However, its molecular structure has high oxygen content which makes it more reactive. This explains that OME_x ignites earlier than HVO and dodecane, despite its lower cetane number. For OME_1, although its molecular structure also contains oxygen, its

cetane number is much lower when compared to the other fuels tested. Thus, it is the last one to ignite as shown in Figure 4. 13. It is important to mention that the OME_1 at 800 K and 15% of O_2 does not ignite and at 21% of O_2, the ignition occurs very late (around 2400 µs).

Furthermore, in Figure 4. 13, it can be seen the effect of ambient temperature. For all fuels increase the temperature, reduce the ignition delay

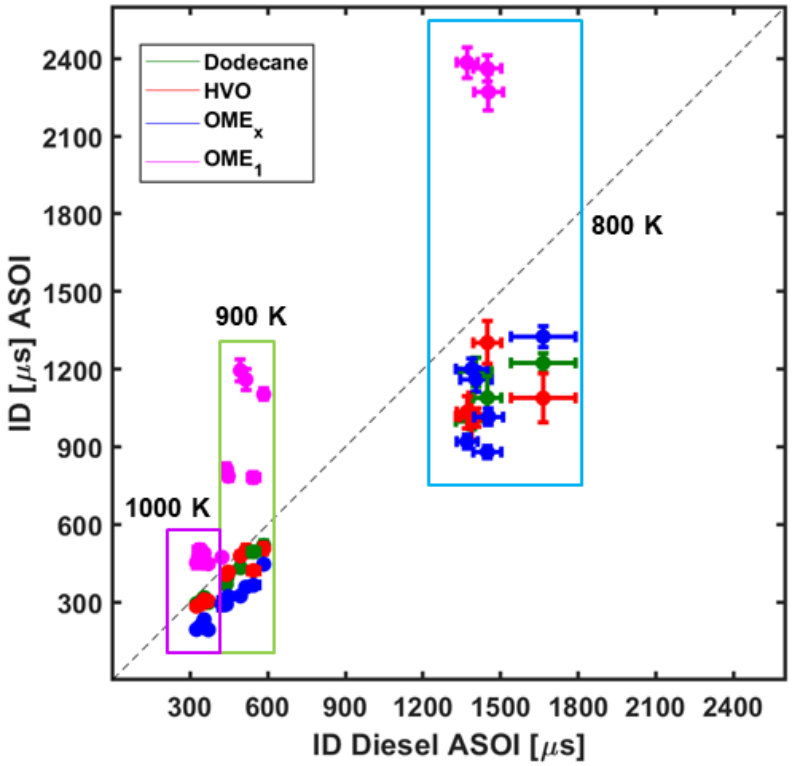

Figure 4. 13 Comparison between Ignition Delay of diesel and the ignition delay for the other fuels tested

To clearly demonstrate the effect of other parameters such as injection pressure and oxygen concentration on ID, the Figure 4. 14 is shown. The temperature of 900 K has been chosen as reference temperature for this representation. At the left side, the oxygen concentration of 15% is represented and at the right 21% of O_2. Each bar represents the value of ID for each injection pressure. It can be seen that reducing the oxygen concentration increases the ID for all fuels. This agrees with what was previously defined in the literature [20,21]. Higher oxygen concentration accelerates the oxidation reactions. Regarding the effect of injection pressure on ID, it can be seen that for OME_x, dodecane, HVO and diesel, the effect is as expected, higher injection pressures shorten ID. However, for OME_1 this trend is inverse. Increasing the injection pressure generated longer ID. That means that for OME_1 increasing the injection pressure produces slower fuel-air mixing. It could be the result of the low reactivity of the fuel combined with a faster mixing rate, which makes the mixture hard to burn.

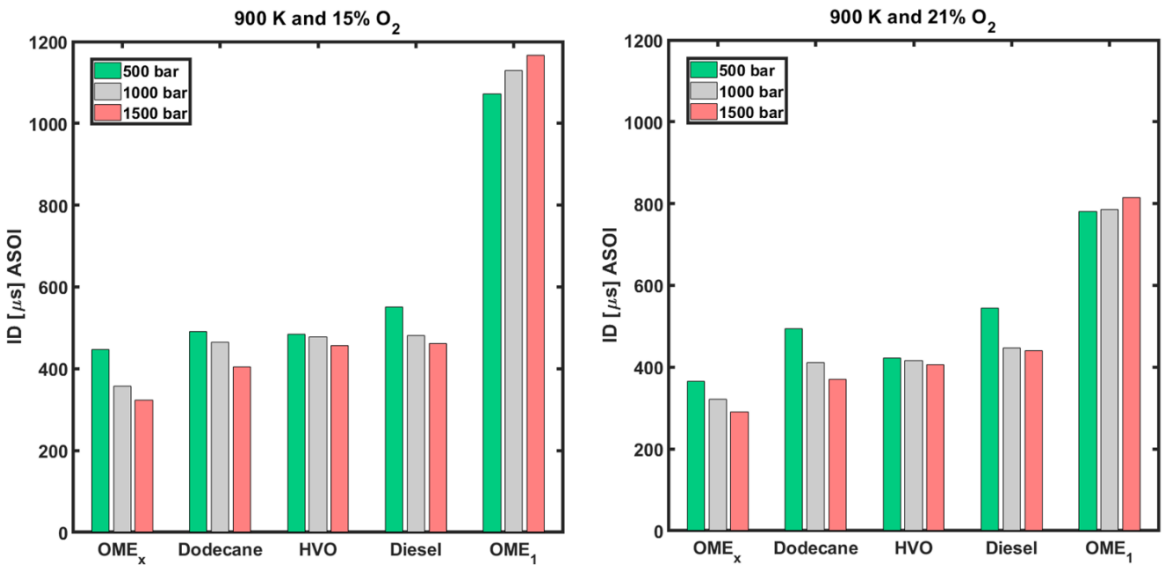

Figure 4. 14 Effect of oxygen concentration and injection pressure on Ignition Delay. At the left 15% of O_2. At the right 21% of O_2. In both cases, the temperature represented is 900 K

4.3.1.3 Spray tip and flame penetration

The temporal evolution of vapor penetration and LOL, as well as the ignition delay (ID) for all the fuels at nominal condition have been shown in Figure 4. 15. The vapor penetration and ID have been measured from schlieren images and LOL from OH^* chemiluminescence, as was mentioned previously. The standard deviation for each parameter is represented by shaded areas. A first stage from start of injection until ignition can be observed, where vapor penetration is identical for all the fuels. Only at certain time after ignition differences appear. This first stage corresponds to the ignition delay phase which extends for each fuel until combustion starts. The ignition delay time has been marked in the figure as a dashed vertical line for each fuel. During the period until ignition, there are not effects on the spray behavior, as expected because the penetration is governed by the momentum flux at the nozzle [19] which only depends on the pressure drop across the nozzle and on the orifice area, fuel effects are negligible. Also, in Figure 4. 15 the effect of the different fuels upon the indicated parameters can be observed. The dashed-dot horizontal lines correspond to the temporal evolution of LOL. After the ignition, the fuel that ignites first, penetrates faster than the others. In general, it is possible to see that while OME_x has similar behavior to the alkane fuels, OME_1 is quite far from them.

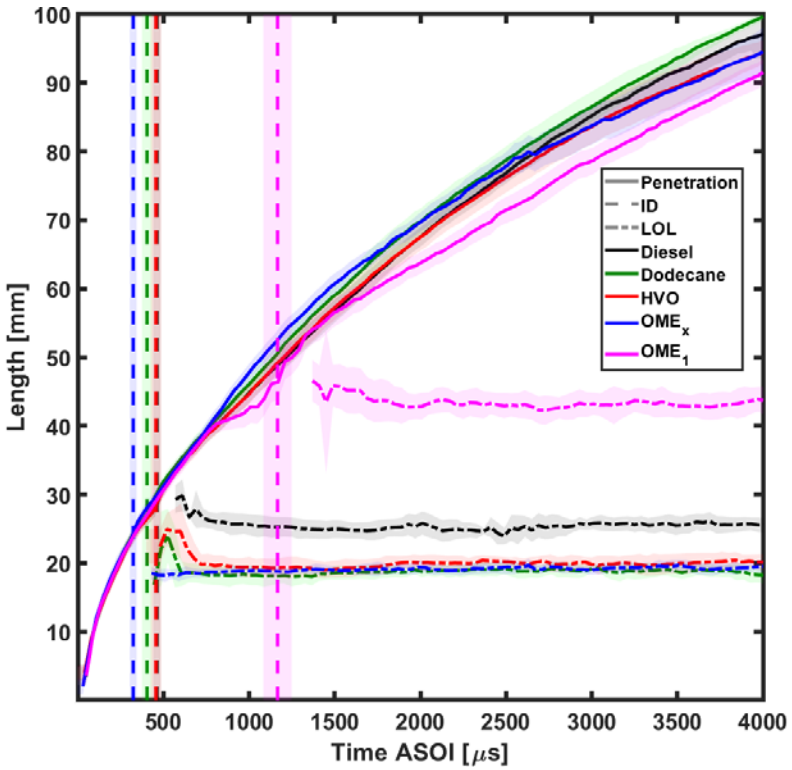

Figure 4. 15 Spray tip penetration and Lift-off length at 900 K 15% O_2 and 1500 bar (Spray A condition by ECN). Ignition delay is represented by vertical dashed lines

On the other hand, from OH^* images, the flame tip penetration can be measured also from the high-speed OH* chemiluminescence imaging as the axial distance from tip injector until the flame front. In Figure 4. 16, the temporal evolution of the flame penetration for all fuels at 900 K and 1500 bar and both oxygen concentrations have been represented. The solid lines correspond to the case of 15% of oxygen concentration and the dotted lines to 21% case From this figure, flame tip penetration is seen to undergo a similar time evolution as spray tip penetration during most of the injection period. However, for all cases flame tip becomes constant after a given period, which depends on fuel type and oxygen concentration. For oxygenated fuels, this occurs between 1000 µs to 1500 µs, while for all other paraffinic fuels it happens close to the end of injection event (around 4200 µs). During that period, the stoichiometric reacting surface stabilizes and hence the maximum distance where OH^* chemiluminescence is recorded does not change with time. For constant ambient and injection conditions this distance has been shown to scale with the stoichiometric mixture fraction, i.e. directly with the $(A/F)_{st}$ ratio [22,23], which depends on oxygen concentration and fuel composition. Table 4. 1 shows stoichiometric air-fuel ratios, from which one can observe that paraffinic fuels have similar values, resulting in the similar long stabilization distance, while the oxygenated fuels approximately a 50% lower $(A/F)_{st}$, resulting in a much shorter flame length.

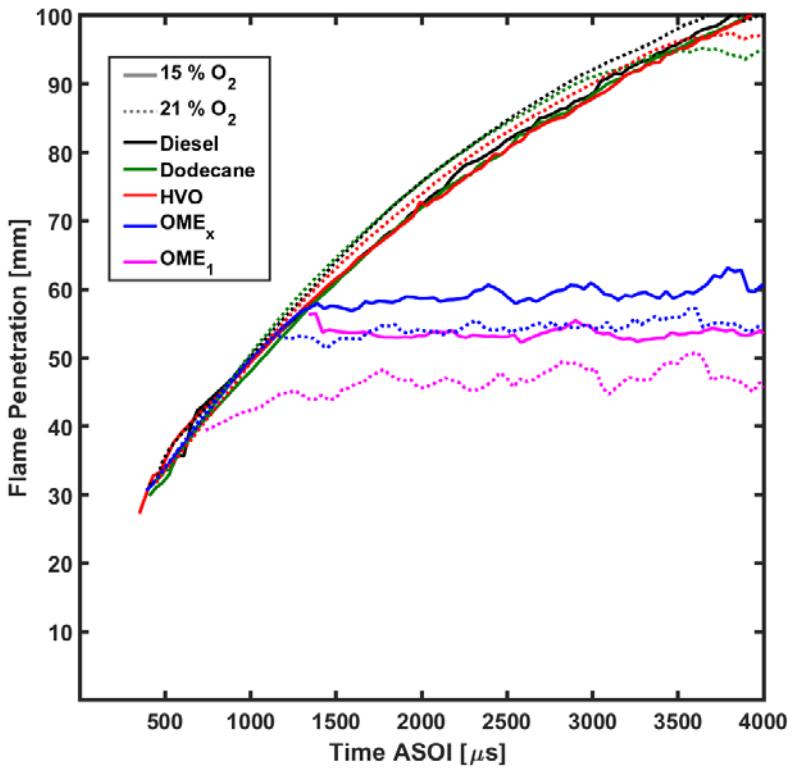

Figure 4. 16 Flame penetration at 900 K and 1500 bar. The solid lines correspond to 15% of O_2 and dotted lines to 21% of O_2

Furthermore, differences among alkanes fuels: Diesel, HVO, Dodecane are small, in agreement with the small $(A/F)_{st}$ differences, OME_1 shows a consistently roughly 10% shorter penetration compared to OME_x.

Figure 4. 17 has been used to depict the differences in flame structure for each fuel at the nominal operating condition in an instant of time where the combustion is quasi steady (3500 µs). Such images confirm the previously plotted trends among fuels in stabilized flame length, with paraffinic fuels having a similar length and a shorter one is observed for oxygenated fuels. On the other hand, observed differences in Lift-off length also point out at interesting features. As shown above, this quantity is quite similar for all paraffinic fuels and OME_x, while it is far longer for OME_1. The equivalence ratio at the Lift-off length ($\Phi_{cl,LOL}$) can be estimated for all fuels using Equation 4.4 and the values are shown in the Figure 4. 17

$$\boldsymbol{\Phi_{cl,LOL}} = \frac{\boldsymbol{f_{cl,LOL}}}{\mathbf{1} - \boldsymbol{f_{cl,LOL}}} \cdot \boldsymbol{(A/F)_{st}} \tag{4.4}$$

In the Equation 4.5, the term $f_{cl,LOL}$ represents the fuel mixture fraction on the spray centerline at the Lift-off length location and it is calculated using the Equation 4.5, where K is a constant equal to 7, d_o is the actual nozzle diameter and ρ_f and ρ_a correspond to the density of the fuel and the ambient respectively.

$$f_{cl,LOL} = \frac{K \cdot d_o \cdot \sqrt{\frac{\rho_f}{\rho_a}}}{LOL} \tag{4.5}$$

Results show that the flame is rich at the Lift-off length for all fuels except for the OME_1 and hence a typical lifted diffusion flame stabilized at stoichiometric conditions is observed for all fuels except for the latter one. OME_1 flame stabilizes at lean conditions where all needed air is already available, which explains the previously observed differences in flame length between OME_x and OME_1. Similar lean stabilized flames were observed for an oxygenated fuel (70% tetraethoxy-propane 30% Heptamethyl-nonane) with a 100 µm orifice at 21% O_2, 850 K and 14.8 kg/m^3 ambient conditions in [24].

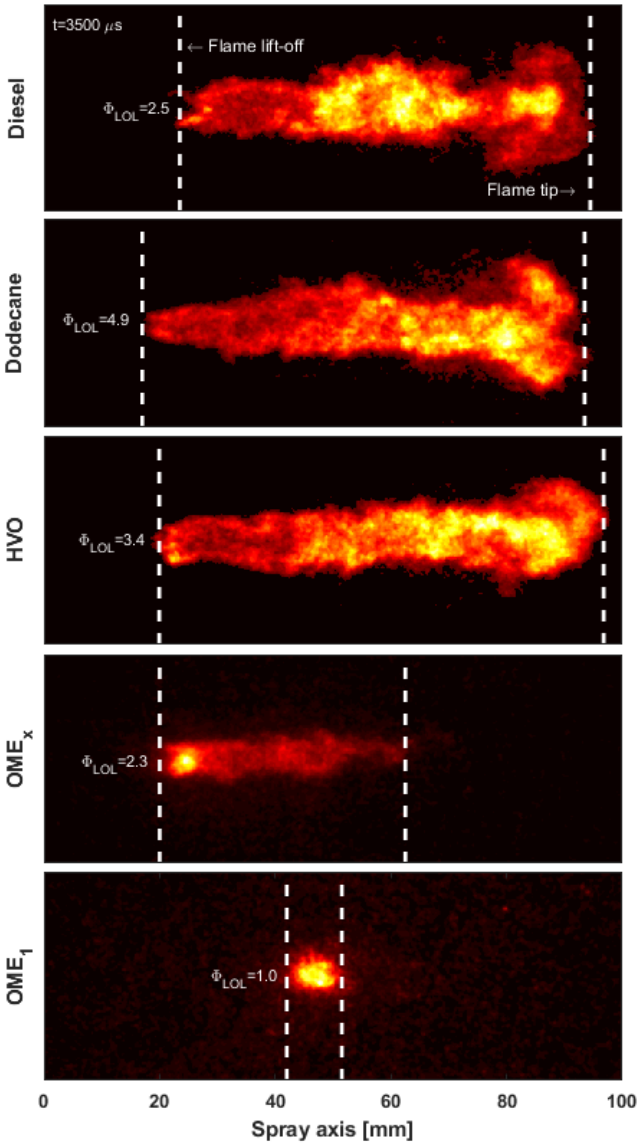

Figure 4. 17 Flame images from OH^* chemiluminescence for all fuels at the nominal operating condition at 3500 µs ASOI

4.3.1.4 Flame Lift-off length

An important parameter in the combustion and soot production processes is the flame lift-off length (LOL). This is strongly related with the amount of fuel–air mixing upstream the combustion region. Enough air entrained reduces the average equivalence ratio at the LOL [25] and this result in less soot production. Consequently, flame LOL is worth to be studied for the different fuels tested in current work.

As previously done with the ignition delay, the LOL for the diesel compared to the other fuels is shown in the Figure 4. 18. The interval time to average the LOL corresponds to that in which the flame is "quasi steady" (between 3000 µs and 4000 µs). The HVO and dodecane present a very close behavior, showing smaller LOL than diesel. However, the tendency is not so clear for OME_x since at 800 K its LOL is slightly longer that diesel, at 900 K it is similar but at 1000 K is smaller, close to HVO and dodecane. It is also possible to observe that at 800 K and 15% of O_2 the LOL of OME_x has the highest standard deviation, indicating a lower combustion stability. The OME_1 cases show longer LOL than the other fuels as a consequence of its lower reactivity (higher ignition delay). However, at 1000 K the difference between LOL of diesel and LOL of OME_1 is smaller compared with the other operating conditions.

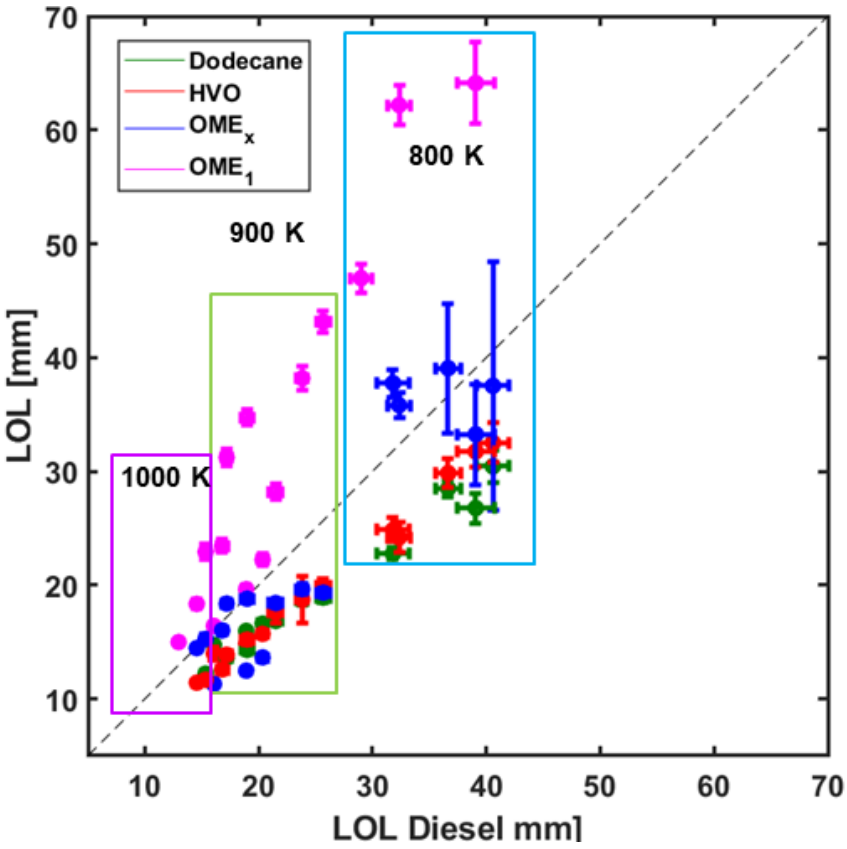

Figure 4. 18 Comparison between Lift-off length (LOL) of diesel and the other fuels tested

4.3.1.5 Soot production

As was indicated previously, the DBI technique was used to determine the soot production. The DBI images were collected after schlieren. However, OH^* chemiluminescence was recorded with the two sets. To verify that both sets are consistent and there are no experimental discrepancies among them, the results obtained for ID from OH^* images measured with the first and in the second set are compared in Figure 4. 19. The grey shadow in the bisector represents the uncertainty associated to the time interval between consecutive frames. It can be observed that ID differences between both sets are always less than the time elapsed between two consecutives frames (40 µs). Thus, it is possible to conclude that both sets are consistent and results can be analyzed together.

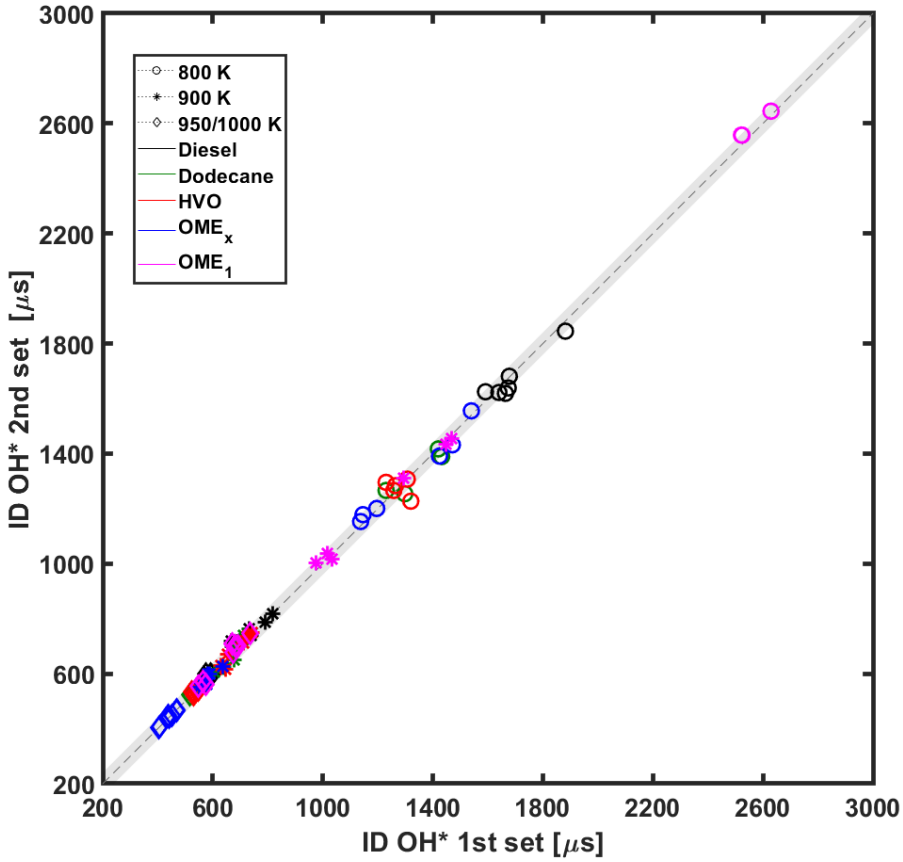

Figure 4. 19 Comparison of Ignition Delay (ID) obtained in the first set and in the second one

DBI images were processed to calculate the flame soot in terms of the optical thickness (KL). KL maps were constructed to depict soot evolution throughout the combustion event by calculating the KL for each axial distance and time-step. A good way to evaluate the evolution of KL temporally and spatially is transforming the KL map at any given instant into a 1D vector where KL values at any given cross section from the nozzle are accumulated into a single value. Thus, each KL map at any instant is converted into a

vector of “accumulated KL” values along the flame axis. By compiling those vectors at every time step (i.e. at every frame), a plot such as those of Figure 4. 20 can be obtained. In any of those plots, the abscissa axis reads for time, the ordinates axis indicates axial distance from the nozzle and the color at any point (X,Y) in the plot indicates the accumulated KL at a cross section at distance Y from the nozzle, belonging to those frames taken at time X after SOI.

In Figure 4. 20 the accumulated KL has been represented for the operating condition with greater tendency to soot formation, that is, at the highest temperature (1000 K), the lowest injection pressure (500 bar) and the lowest oxygen concentration (15%). Dashed lines have been used to depict ID, vapor penetration and the flame Lift off length. In this figure, it is possible to observe that soot production for OME_1 and OME_x is below the detection threshold. In fact, the color scale for these two fuels has been modified in other to enhance this fact. Therefore, a sootless flame seems to be established. This holds for all operating conditions and, consequently, KL values for those fuels cannot be analyzed further. Dodecane, HVO and OME_x show smaller KL values than diesel. As for the time evolution, it can be observed that initially the largest soot amount is located at the spray tip, in the head vortex area, but when reaching a distance around 70 mm, this soot disappears due to the establishment of the quasi-steady flame The highest KL region appears for the three fuels from 40 to 50 mm from the nozzle.

For a given fuel composition, the soot production is related to the amount of air entrainment that occurs upstream of the Lift-off [25]. Longer LOL suggests less soot formation but this depends also on fuel composition. This can be observed in Figure 4. 20, where diesel has the longest Lift-off length but also the largest soot formation. The stoichiometric air-fuel ratio (m_a/m_f) for dodecane and OME_1 is quite different. At 15% of oxygen concentration, stoichiometric air-fuel ratio for dodecane is 20.72 versus 10.03 for OME_1 indicating that oxygenated fuels require less air to oxidize. This explains that OME_x, although with LOL closer to diesel, does not produce soot. This statement is supported by the equivalence ratio (Φ) at LOL. For dodecane, Φ is 4.9 at baseline operating condition, while for the OME_1 is 1. Furthermore, OME fuels do not have carbon-carbon (C-C) bonds which contribute to the absence of soot.

In the case of HVO, its aromatic free composition suggests that less polycyclic aromatic hydrocarbons (PAH) are formed [26]. This could explain the lower soot production for HVO compared to diesel, as they can be considered as the building blocks for particulates in flames [27].

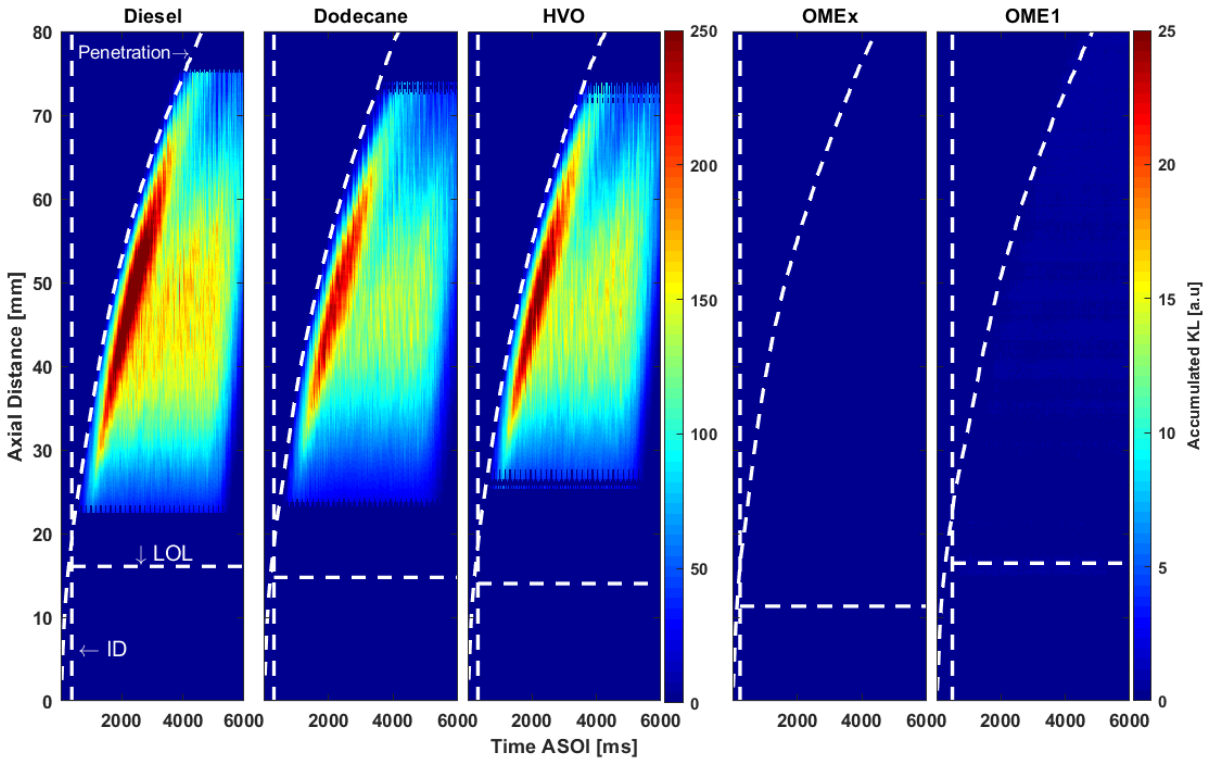

Figure 4. 20 Accumulated KL map at the operating condition with the greatest tendency to soot formation (1000 K of temperature, 500 bar of injection pressure and 15% of O_2)

The total soot mass production was calculated from instantaneous KL, following the procedure described previously in the section 4.2.3.3. *Figure 4. 21* depicts the total soot mass for diesel, dodecane and HVO at different operating conditions with the aim of showing the effect of decreasing temperature, increasing injection pressure and increasing the ambient oxygen content. The shown temperatures are 1000 K and 900 K, from top to bottom; the injection pressures are 500 bar and 1000 bar, from left to right; and 15% and 21% of oxygen have been represented for 900 K and 500 bar at the bottom of the figure.

It can be seen that when decreasing the temperature from 1000 K to 900 K (from top to bottom, at the left side of the figure), the maximum value of soot production is reduced 40% for diesel and 30% for dodecane and HVO. When the injection pressure is increased from 500 bar to 1000 bar (from left to right at the top of figure), the soot reduction is around 30% for all fuels. When the oxygen concentration is increased from 15% to 21% (from left to right at the bottom of figure) the total average soot production is reduced 30% for diesel, 40% for HVO and 50% for dodecane. Results for all conditions show that the parametric variation in terms of soot tendency always holds, with diesel showing the largest soot production, while HVO and dodecane present similar soot production. In fact, considering all results presented in this chapter regarding combustion and soot formation characteristics, it can be concluded that n-dodecane is a good surrogate to model the HVO due to its similarities.

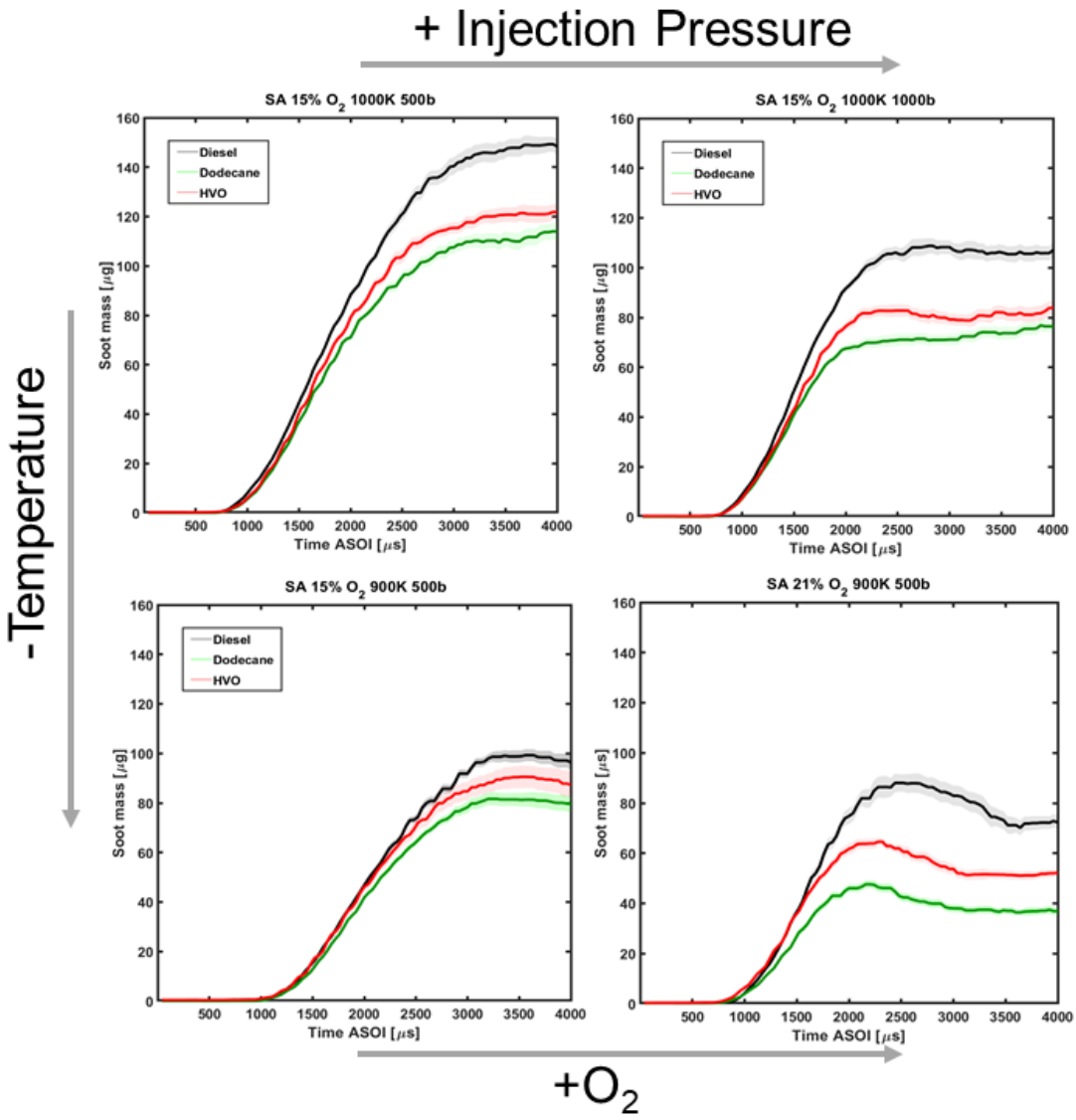

Figure 4. 21 Influence of the variation of injection pressure, temperature and oxygen concentration on the total soot mass

4.3.2 Effect of combining different nozzle diameter on combustion behavior

In this section, a qualitative description about observed differences between nozzle A and nozzle D, SA and SD hereafter, using schileren and OH^* chemiluminescence images will be given.

Figure 4. 22 shows overlaid schlieren (black) and OH^* (red) images for the nominal operating condition for all fuels and both nozzles for the quasi-steady phase of the reacting spray evolution (3015 µs ASOI). The first thing that can be observed is that the oxygenated fuel flames as defined from the OH^* signal for both nozzles are shorter and narrower than for the other fuels, consistently with the lower stoichiometric A/F ratio (Table 4. 1). This is

especially evident in SA images, where the observation window spans over the whole flame for all fuels due to the smaller nozzle diameter.

OH^* images for diesel, dodecane and HVO show a typical cylindrical diffusion flame starting at the Lift-off location [28] within a conical spray flow, as derived from the schlieren images. Moving from SA to SD, the spray flow increases in radius, the Lift-off length location moves further away from the nozzle (as previously discussed) and there is a noticeable increase in OH^* signal intensity within the reaction zone compared to the smaller nozzle case. This intensity increases with axial distance to the orifice, which hints at an interference from soot broadband radiation. As results will show below, soot formation is much larger in the larger nozzle and most probably this creates a strong signal that overlaps with the OH^* one at 310 nm. All in all, fuel effects on flame radiation are not noticeable with these three fuels and the transition from SA to SD is also similar for all of them. However, for the oxygenated fuels OH^* radiation distribution is pretty different. This is especially evident for OME_1 and the two nozzles, where the highest intensity all over the flame is observed at the Lift-off location with intensity dropping abruptly further downstream. This is consistent with results found by Pickett and Siebers [24], where flames with small nozzle diameter and oxygenated fuels were investigated. Under such conditions, lean equivalence ratio values were found at the flame base, in line with the results presented here for SA in Figure 4. 17 (later, $\Phi_{cl,LOL}$ will be evaluated for both nozzles). Hence, the whole combustion process is occurring at locally fuel-lean conditions. This result rules out the presence of a stoichiometric flame front, and hence some sort of lean-burn mixing-controlled combustion can be hypothesized in the same way as Pickett and Siebers [24]. This reaction front location is pretty much the same for both nozzles with the flame base moving from around 45 mm for SA to around 60 mm for SD. Other than that, there is no major difference between both nozzles.

For OME_x, some sort of in-between situation can be observed, with a LOL similar to the conventional fuels, and more luminosity downstream of this location. The equivalence ratio at the Lift-off length is richer than for OME_1, and hence the possibility of a stabilized diffusion flame front around stoichiometric locations still exists.

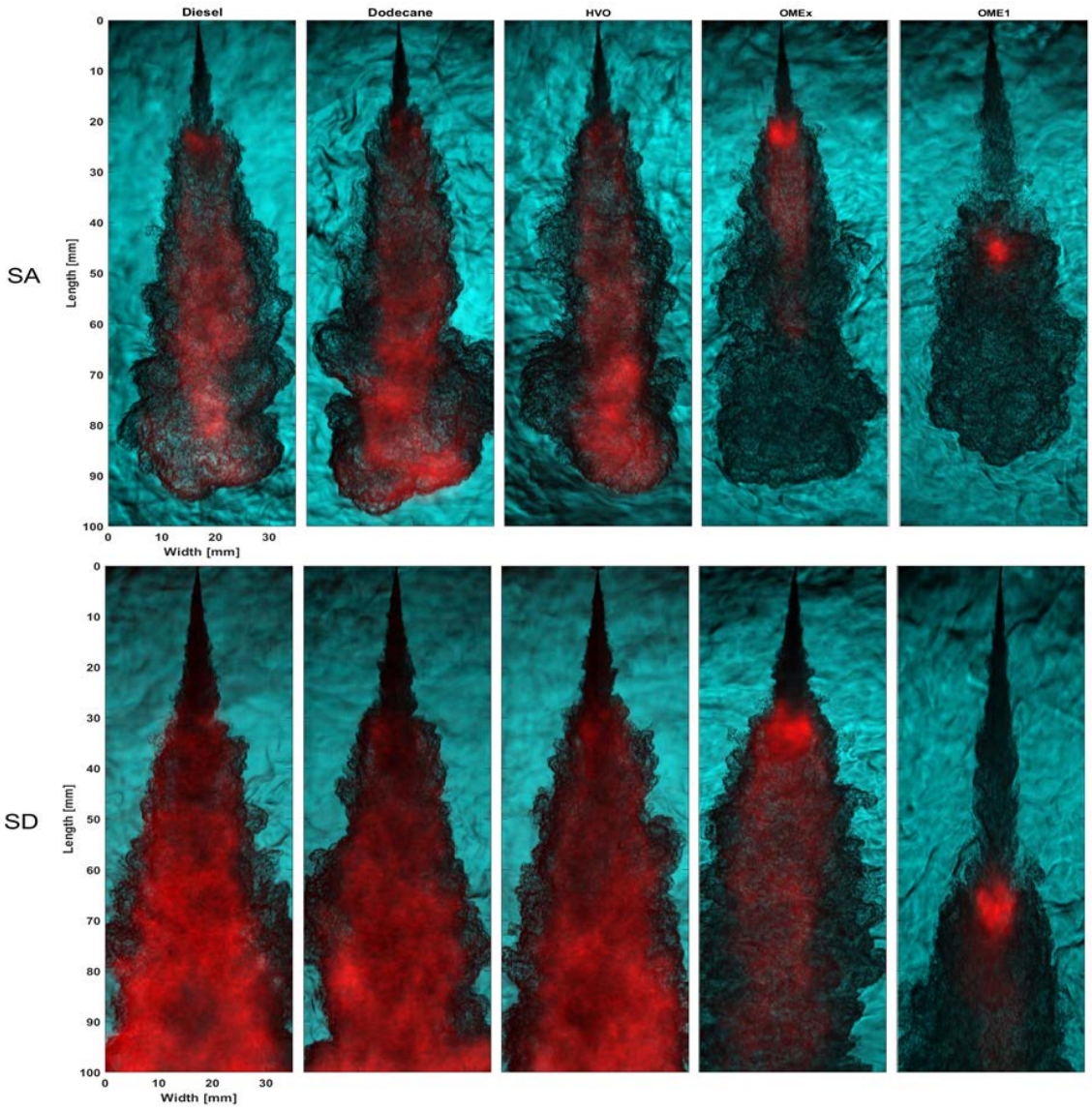

Figure 4. 22 Overlaid images of schlieren and OH^* chemiluminescence for different fuels and nozzle diameters at 900 K, 1500 bar of injection pressure and 15% of O_2 during the time interval equal to 3015 μs

Other remarkable difference is the length and width of the flame observed with the OH^* chemiluminescence signal. For dodecane, a big difference is observed between nozzles. With SD, the radiation covers almost the entire region of the spray shown by the schlieren image.

To analyze the combustion behavior in quantitative terms, in the Figure 4. 23 the temporal evolution of vapor penetration, liquid length and Lift-off length is shown, as well as the ignition delay obtained with both nozzles under the reference operating condition: 900 K, 15% of O_2 and 1500 bar of injection pressure. For sake of better understanding, at the top of the figure, the alkanes fuels are been depicted. At the bottom, the oxygenated fuels. The

red lines represent to SD and the black lines to SA. The shadow in each parameter represents its standard deviation.

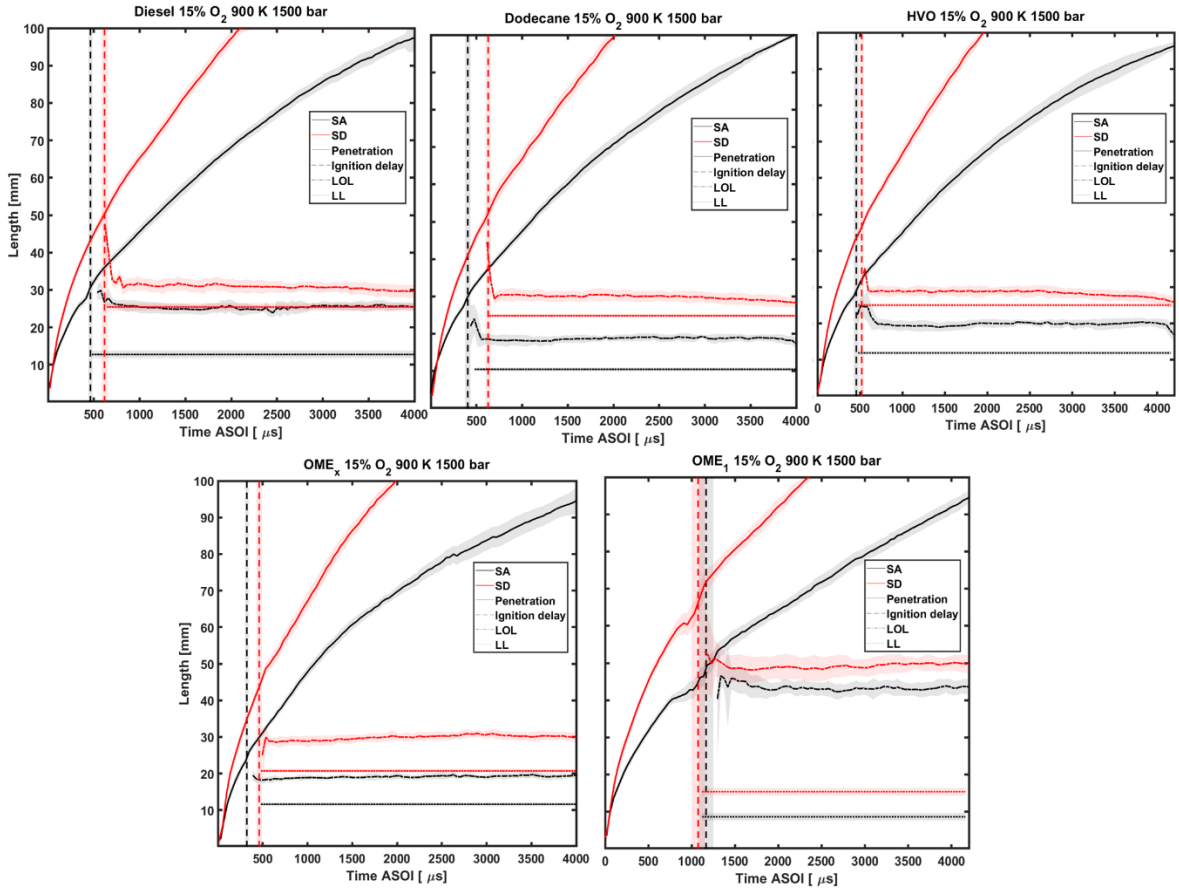

Figure 4. 23 Comparison of the effect of nozzle diameter for all fuels on the characteristic spray parameters.

For both types of fuels, it can be seen that SD produces faster penetration than SA, as expected. The differences observed between injectors with respect to vapor penetration are the result of the momentum flux increment which is dependent on nozzle diameter. Only in the first instants, when the injector section is still controlled by the needle lift, both nozzles behave similar.

The stabilized liquid length (LL) as well as the Lift-off length (LOL) are longer for SD. Additionally, ignition delay (ID) is also longer for this nozzle. As ambient conditions and fuel are exactly the same for both nozzles, these results suggest a slower mixing process for SD. That means also a slower vaporization process, which causes the ignition conditions to be achieved later.

When comparing fuels, it is possible to see that the nozzle geometry does not have the same effect on both types of fuels. Regarding liquid length, for dodecane, which is the

reference fuel for the ECN, the SA shows a 60% reduction in comparison to SD. However, for OME_1 only a 44% reduction is observed. When comparing ID, dodecane shows a reduction of 35% when comparing SA to SD. On contrary, for OME_1 the trend is inverted. The SA provides a 9% larger ID than SD. The reason of this reverse trend will be analyzed in the following paragraphs. Finally, when focusing on the LOL, a reduction of 35% when comparing SA and SD has been measured for dodecane while only a 12% difference is observed for OME_1.

Considering these results, it can be stated that the effect of the nozzle diameter is not the same for both types of fuels. The change of the nozzle affects less the oxygenated fuels less than the alkane one. This can be explained by the fact that, in the case of alkanes, more air entrainment is needed in the mixing process to reach equivalence ratios that lead to combustion, due to their chemical structure with carbon-carbon bonds. In contrary, the oxygen content in the oxymethylene ethers molecule makes the mixing process to be not as decisive as it is for the dodecane. Therefore, when this process is modified through the change in the nozzle diameter, it does not affect the start and development of combustion so much. For oxygenated fuels, the chemical processes play as important a role as physical processes play in alkanes fuels.

The behavior reported in the previous paragraphs can be extended to the other fuels tested in this work. On one hand, diesel and HVO show a 50% reduction liquid length, 20% in ID and 20% in LOL when comparing SA and SD. On the other hand, OME_x showed a similar behavior to OME_1. The main difference between the two oxygenated fuels is that the first one shows a similar trend to dodecane in terms of ID when comparing SA and SD.

In order to perform a more detailed analysis of the main spray and ignition parameters is performed in the following paragraphs. In Figure 4. 24 the maximum liquid length for SD (LL_{SD}) versus SA (LL_{SA}) has been compared. The data corresponds to 800 K and 900 K, 1500 bar of injection pressure and 15% of O_2. The variation of injection pressure has no effect on this parameter [29–31]. For that reason, just one pressure has been depicted. Each fuel has been identified with a color, and the temperature with a symbol for easy understanding. The standard deviation has been represented with error bars. The dashed line has a slope equal to the ratio of actual diameters (d_o) of both nozzles, as derived from Table 4. 4. At constant operating conditions, this would be the theoretical relationship between the liquid length of both nozzles, according to scaling laws in [31,32]. In agreement with this scaling law, LL is longer for the SD. It is known that with bigger orifice diameters mixing slows down and atomization worsens [33]; as a consequence, the vaporization process slows down, too. The data corresponds to conditions with the longest separation between liquid and Lift-off lengths (800 K and 900 K, 1500 bar injection pressure and 15% of O_2) to ensure that the liquid length is not affected by combustion characteristics and then it can be considered as that of an inert spray. The variation of injection pressure has no effect on this parameter [29,30]. For that reason, just one pressure has been depicted.

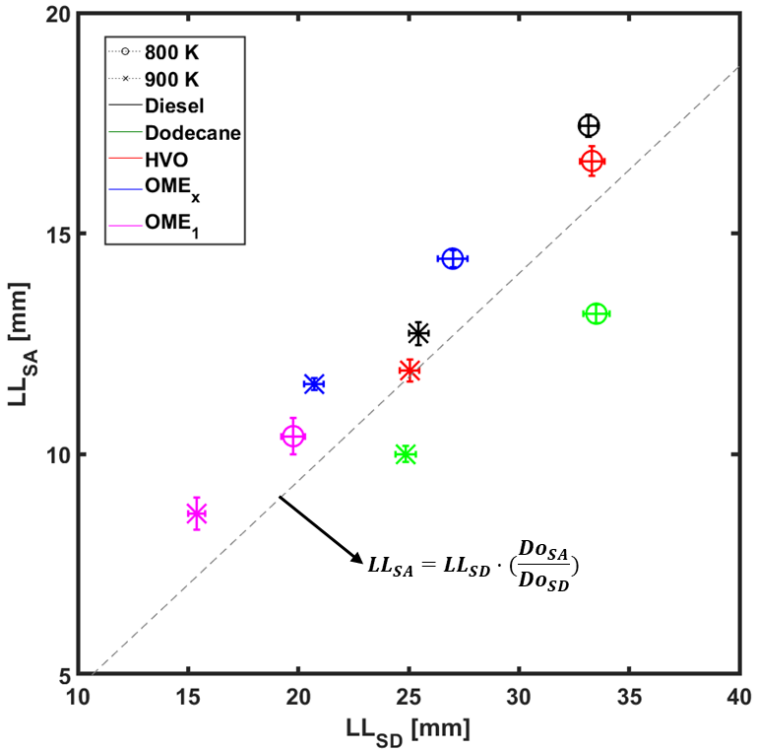

Figure 4. 24 Liquid length comparison for SA and SD for Diesel, HVO, OME_x and OME_1. The operating conditions correspond to 800 K and 900 K at 15% of O2 and 1500 bar of injection pressure

Firstly, it can be observed that LL is closely linked to fuel composition as it has been reported previously [29]. Diesel, dodecane and HVO show similar values, while the OME_x and OME_1 have shorter LL. The fuels with lower distillation temperatures show shorter LL values as the vaporization process requires less energy to evaporate the fuel. This is coherent with the conclusions of Vera-Tudela [29] who stated that, after ambient temperature, the second greatest influence on the maximum liquid length is the enthalpy of vaporization. In the cases where this parameter is not available, the evaporation temperature or boiling point can be used instead [19,29]. The results in this study are in agreement with this statement, since the lowest average boiling point (arithmetic average of the initial and final boiling point of the Table 2) corresponds to OME_1 and then to OME_x, being HVO the fuel with higher boiling point of those represented. Regarding the differences between nozzle diameters, the LL is longer for the SD. It is known that with bigger orifice diameters the mixing slows down and also worsens the atomization process [33]. As a consequence, the vaporization process worsens, too. The effect of nozzle diameter variation on the LL was lower for the oxygenated fuels because of the more similar volatility characteristics.

Making a detailed observation on the ignition delay (ID) results, in Figure 4. 25 this parameter has been compared for SA and SD. The operating conditions correspond to 800 K, 900 K and 1000 K at two extreme injection pressures: 500 bar and 1500 bar. The different

temperatures have been identified with symbols and the fuels with colors. Error bars correspond to the standard deviation. The gray shadow around the dashed line indicates a variation of ±40 µs, which was the high-speed camera shutter time used in this study, to represent the uncertainty related to the time resolution of the measurements. SD is shown to have around 20% longer ignition delay than SA for Diesel and HVO and 30% for dodecane and OME_x, except for OME_1 for most of the operating points. No special effect of fuel properties is observed. This trend has also been observed for dodecane in previous studies [3,34–36] and can be explained in terms of the slower mixing rate with the larger nozzle, which results in longer residence times needed to reach the mixture fraction values that are most favorable for ignition and hence a longer ignition timing.

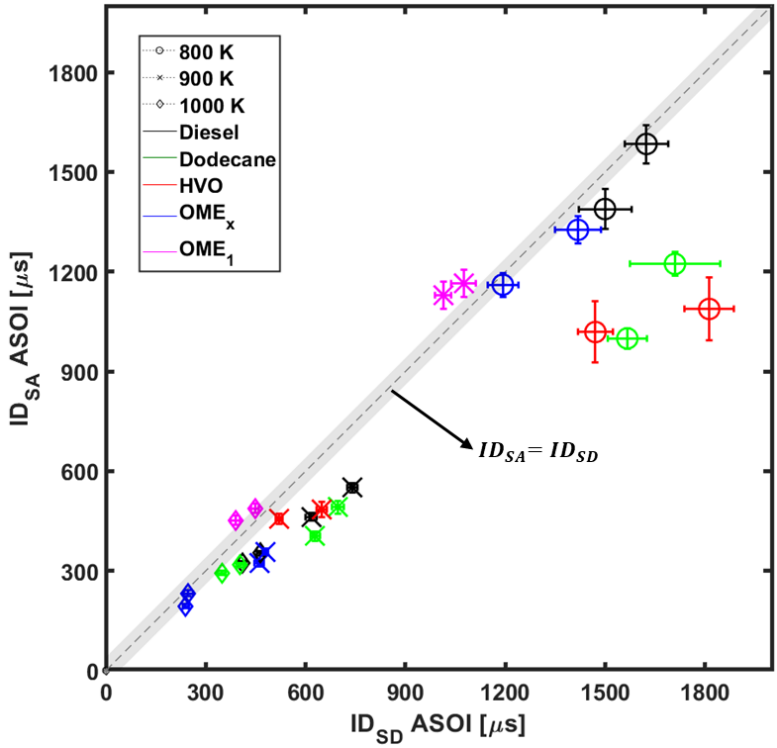

Figure 4. 25 Ignition delay comparison between SA and SD for Diesel, HVO, OME_x and OME_1. The data depicted corresponds to 900 K and 1000 K at 500 and 1500 bar of injection pressure and 15% of O_2

However, the previous trend is not maintained for OME_1, where SA ignites later than SD. The larger nozzle provides an ID 9% shorter than the smaller one. Recent CFD computational results [37] have shown that for the nominal SA condition OME_1 combustion development occurs under highly lean conditions compared to dodecane. This is a consequence of the low reactivity of the fuel, coupled to the oxygen present in the fuel, which decreases the amount of stoichiometric air needed and hence result in a high degree of premixing at ignition sites. At the same time, concurrent homogeneous reactor calculations have also shown that from a purely chemical point of view the most reactive mixtures are

close to stoichiometry, or even slightly rich. For this oxygenated fuel there seems to be a trade-off between the need to spend time in highly reactive mixtures for ignition to occur and the inherent fast mixing. In this context, the use of a larger nozzle diameter such as SD, which decreases mixing rate, means that more time can be spent on richer mixtures, which helps reduce ignition delay compared to the smaller nozzle. This is also consistent with results found in other studies [38] where it was indicated that for smaller nozzles diameter the ignition delay of oxygenated fuels is dominated by lean mixtures due to the fast air-fuel mixing. Figure 4. 25 also shows that differences in ignition delay between nozzles for OME_1 reduce as ambient temperature increases, due to the higher reactivity, but results are never similar to those of the other fuels.

In Figure 4. 26, Lift-off length for SA and SD has been compared at different operating conditions. The different temperatures have been identified with symbols and the fuels with colors. The error bars represent the standard deviation. For all cases, LOL is higher when the SD is used. The dashed line represents the relation in which Lift-off length is expected to vary with the nozzle diameter, as it was stablished by Siebers and Higgins [25]. They indicated that LOL is proportional to orifice diameter to the power of 0.34. The proportionality seems to fit the scatterplot on a global scale, but plenty of scattering can be observed, especially for low temperature cases (i.e. long LOL). Error bars indicate that fluctuations become important for LOL values longer than 35 mm, due to the low reactivity.

In global terms, LOL follows the ID trend for diesel, dodecane, HVO and OME_x, which is in line with previous studies [20,39], meaning that longer ignition delays produce longer Lift-off lengths. However, it must be noted that for OME_1, LOL follows the same trend with respect to nozzle diameter as the other fuels, although this was not the case for ID, as discussed before.

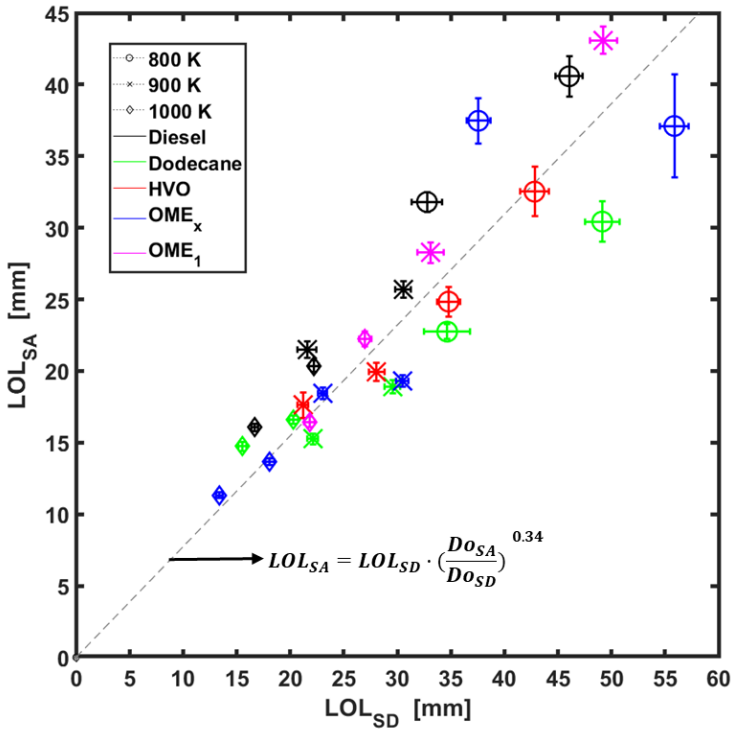

Figure 4. 26 Lift-off length comparison between SA and SD for 900 K and 1000 K and two injection pressures: 500 bar and 1500 bar. All cases at 15% of O_2

To provide more insight into this behavior, the equivalence ratio at the Lift-off length location ($\Phi_{cl,LOL}$) was calculated also for the SD under the baseline operating conditions (900 K, 1500 bar and 15% of O_2 concentration) to Equation 4.4 and the results have been summarized in *Table 4. 6*

Fuel	$\boldsymbol{\Phi_{cl,LOL\_SA}}$	$\boldsymbol{\Phi_{cl,LOL\_SD}}$
Dodecane	4.9	7.2
HVO	3.4	5.7
Diesel	2.5	5.2
OME_X	2.3	3.5
OME_1	**1**	**2**

Table 4. 6 Equivalent ratio ($\Phi_{cl,LOL}$) for each fuel at 900 K, 1500 bar and 15% of O_2 for both SA and SD

For all the fuels, SD nozzle provides richer $\Phi_{cl,LOL}$ values than SA. As Equation 4.4 shows, in spite of the longer LOL values, the larger nozzle diameter results in richer $\Phi_{cl,LOL}$ values for SD than for SA. It must be noted that equivalence ratio value on the axis is an

upper limit for the value that may be found at the lift-off location, as the actual flame is radially displaced from the axis, and hence even leaner values are expected. For oxygenated fuels, results confirm that even for the larger nozzle, $\Phi_{cl,LOL}$ values can reach values close or below 2, which are in the range of non-sooting regimes.

In terms of soot production, in Figure 4. 27 the time-averaged (from 3 to 4 ms ASOI) KL distribution is shown for 900 K, 1500 bar of injection pressure and 15% O_2 for SD, which represents the quasi-steady combustion phase for all fuels. Maximum KL values are around 4 for diesel, with slightly lower values for dodecane and HVO. However, not enough signal was found for OME_1 and OME_x, which confirms that these are non-sooting fuels as discussed in a previous work [40]. The molecular structure of these oxygenated fuels, without carbon-carbon bonds, avoid the soot formation [41,42] even under rich conditions as obtained for large nozzles as SD. In this figure it is also possible to see that the most sooting fuel is diesel, followed by dodecane and then HVO as the less sooting fuel of these three. This result is in agreement with results presented in [40] for the SA.

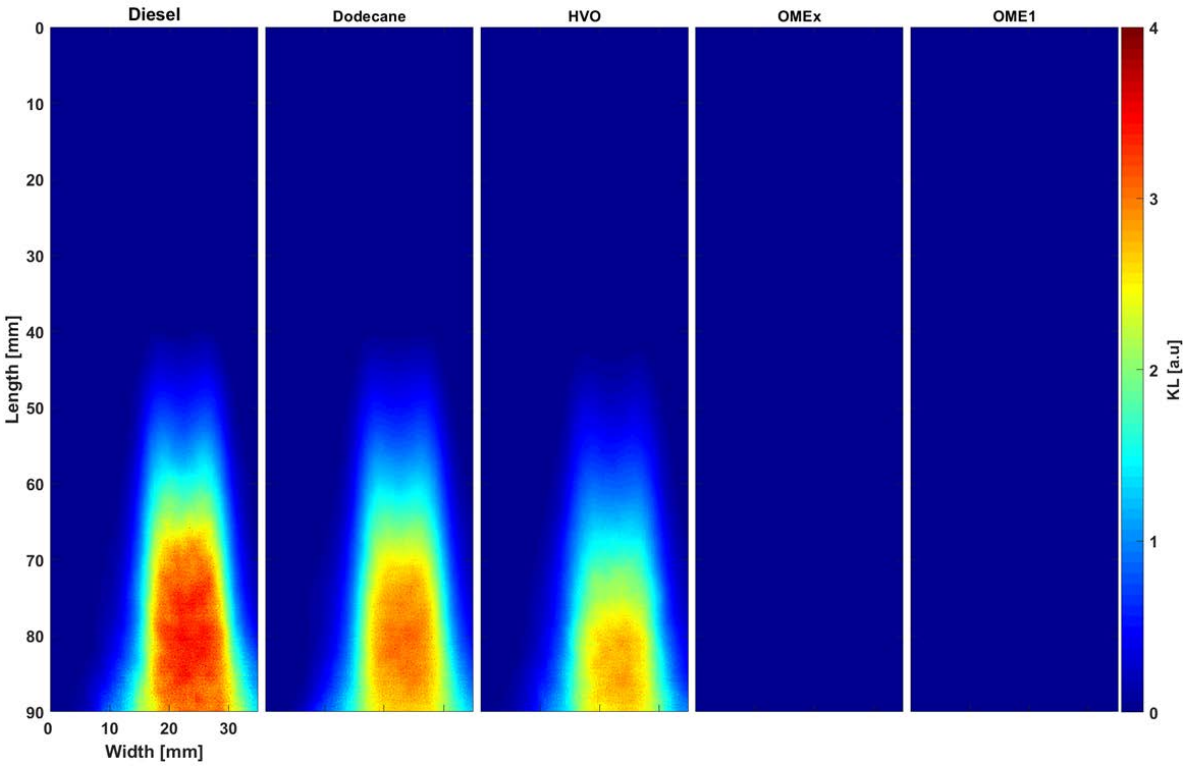

Figure 4. 27 Average soot KL values for SD during the quasi-steady phase of the flame, between 3 ms and 4 ms. The operating condition corresponds to 900 K, 1500 bar of injection pressure and 15% of O_2

Figure 4. 28 depicts the evolution of accumulated soot mass for diesel, dodecane and HVO at 900 K, 500 bar of injection pressure and 15% of O_2 for SA (continues lines) and SD (doted lines). The shadows correspond to the confidence interval of the average at 95%. With

SD, soot production increases seven to ten times with respect to the quantities obtained with SA. However, if the equivalence ratio values at LOL (Table 4. 6) are compared between both nozzles, it is possible to see that $\Phi_{cl,LOL}$ for SD increased two times as much in comparison to SA. Thus, the differences in mixture formation do not justify the increase of soot formation between both nozzles. However, it was previously stated that bigger orifice diameter promotes longer local residence time of fuel. This allows a greater formation of soot precursor species [33] and could be the reason for the differences observed in this work.

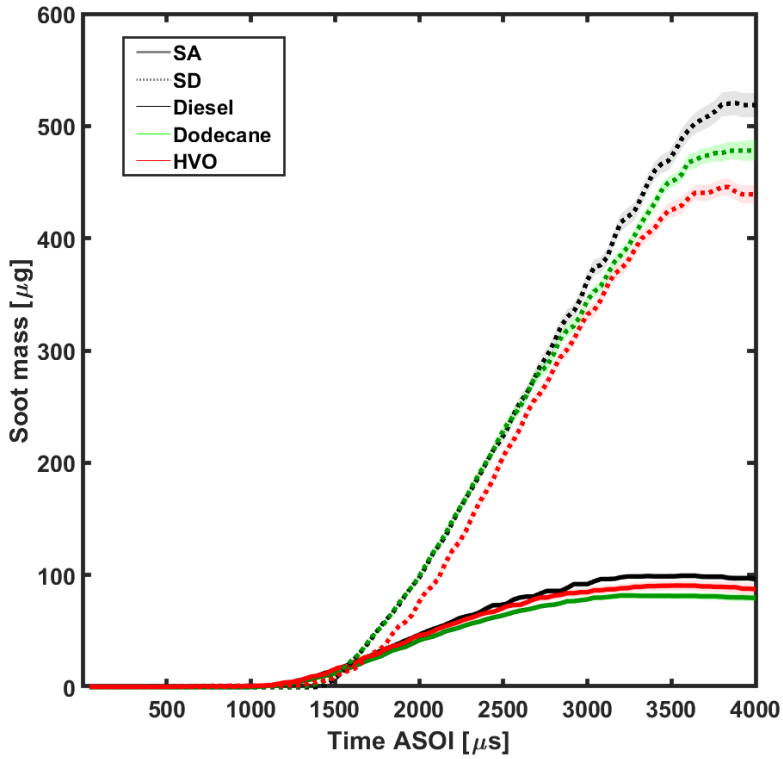

Figure 4. 28 Comparison of accumulated soot mass production evolution of Spray A and Spray D. The operating conditions are 900 K, 1000 bar and 15% of O_2

4.4 Summary and conclusions

In this chapter the main spray parameters and combustion characteristics for diesel, HVO, dodecane, OME_x and OME_1 were evaluated for two nozzles namely SA and SD, with orifice diameter of 89.4 µm and 189 µm respectively at High Pressure and High Temperature installation, with controlled oxygen concentration. The parameters studied were liquid and spray tip penetration, ignition delay, flame Lift-off length, flame length, flame tip penetration and soot production. These were assessed using high-speed imaging based optical techniques: schlieren, OH^* chemiluminescence and diffused back illumination. The operating condition were defined using as baseline the targets recommended by the Engine Combustion Network (ECN). Results obtained for the dodecane with both nozzle A and nozzle D at the baseline condition (900 K 1500 bar and 15% of O_2) for ignition delay, liquid

length and flame Lift-off length are consistent with those found in the ECN database, which provides confidence in the reliability of the results of this study.

The main conclusions of this study are summarized below:

- To change the nozzle diameter produces the same effect for all fuels but not in the same proportion. This proportion will depend on the chemical composition of the fuel. In the case of oxygenates fuels, as the combustion takes place in a lean stoichiometric environment, the effect of changing the nozzle is not very significant in terms of characteristic spray parameters.
- The maximum liquid length of all five fuels correlates with the corresponding distillation temperature, stratified in increasing order: OME_1-Dodecane-OME_x-HVO-diesel. The liquid length is longer for the SD than for SA. This evidence that the evaporation process is slower for the SD due to the atomization process worsen with the increment of nozzle diameter.
- During the period until ignition, all fuels show the same behavior in terms of penetration, since the spray tip penetration is known to be governed by the momentum flux conservation at the nozzle orifice, which only depends on the pressure drop across the nozzle and the orifice area. Thus, SD penetrates faster than SA since the SD has bigger orifice diameter than SD.
- ID trend matches the cetane number rating of paraffinic fuels. HVO and dodecane ignite very close and earlier than diesel. However, OME_x ignites before the other fuels although its cetane number is not the highest, but its shorter ID is due to the oxygen in its molecular structure which improves its ignition. The only fuel that ignites after diesel does is OME_1. However, at 1000 K, OME_1 shows a similar behavior than diesel. The ID for SD is higher than for SA. It is due to the SD has longer residence times and therefore the mixing process is slower. At the baseline operating condition, for the spray A, using dodecane, the ID was 35% smaller than using spray D. However, for the OME_1, this reduction was not observed, since at the same operating condition, the ID for SD was 9% smaller than for SA. This could be consequence of its chemical composition, since for SA the equivalent ratio in the reaction zone is less or equal to 1, which means that there is an overmixing.
- The longest flame Lift-off length is for OME_1 and at 800 K and 900 K, which is quite far from OME_x and paraffinic fuels. Conversely, OME_x has a closer behavior to paraffinic fuels in all operating conditions. The LOL follows the ID trend for diesel, dodecane, HVO and OME_x. Higher ID produced longer LOL. However, for OME_1 although the SD had shorter ID than SA, when the LOL was analyzed, the LOL was longer with the SD. That means that LOL increases when the nozzle diameter increases too. However, increasing the orifice diameter worsen the air entrainment, this result in an increase of the equivalent ratio ($\Phi_{cl,LOL}$). Therefore, for smaller orifices diameters the mixing process improves, it means that vaporization process improves and the amount of air entrainment increases too, producing leaner mixtures.

- The difference of flame penetration between paraffinic fuel and oxygenated fuel is very marked. Oxygenated fuels stabilize early while paraffinic fuels reach the flame stabilization later as a consequence of the fuel's stoichiometry. Furthermore, an important difference between OME_1 and OME_x at nominal operating condition exists due to the OME_1 flame stabilizes at lean air-fuel ratio.
- The OME_1 has typical equivalent ratios ($\Phi_{cl,LOL}$) of the premixed combustions, those are less than approximately two as the literature indicates [43]. This allows to conclude that the combustion characteristics of OME_1 can be more identified with a premixed phenomenon than with a diffusive one.
- Regarding soot production, the oxygenated fuels (OME_x and OME_1) did not produce detectable soot at any operating condition tested for both nozzles. This can be explained by the very low equivalence ratio at lift-off owing to the oxygen content in the molecule as well as by the absence of C-C bonds.
- HVO produces less soot than diesel for SA. This behavior can be related with the absence of aromatic compounds in HVO formulation. In the case of diesel and HVO, the soot production with SD was nine and seven times higher than SA. That was a result of slower mixing process that it is obtained when bigger orifice diameter was used.

References

[1] Engine Combustion Network | Engine Combustion Network Website, 2021. https://ecn.sandia.gov/.

[2] Crusius S, Müller M, Stein H, Goral T. Oxy-methylen-di-methylether (OMEx) as an alternative for diesel fuel and blend compound: properties, additizing and compatibility with fossil and renewable fuels, Esslingen: 12th International Colloquium Fuels - Conventional and Future Energy for Automobiles; 2019, p. 8.

[3] Pastor JV, Garcia-Oliver JM, Garcia A, Morales López A. An Experimental Investigation on Spray Mixing and Combustion Characteristics for Spray C/D Nozzles in a Constant Pressure Vessel, SAE Technical Paper 2018-01-1783; 2018. https://doi.org/10.4271/2018-01-1783.

[4] Settles GS. Schlieren and Shadowgraph Techniques: Visualizing Phenomena in Transparent Media. Springer Science & Business Media; 2012.

[5] Viera A. Effect of multiple injection strategies on the Diesel spray formation and combustion using optical diagnostics. PhD thesis. Universitat Politècnica de València, 2019.

[6] Siebers DL. Liquid-Phase Fuel Penetration in Diesel Sprays, SAE Technical Paper 980809; 1998. https://doi.org/10.4271/980809.

[7] Desantes JM, Pastor JV, García-Oliver JM, Briceño FJ. An experimental analysis on the evolution of the transient tip penetration in reacting Diesel sprays. Combustion and Flame 2014;161:2137–50. https://doi.org/10.1016/j.combustflame.2014.01.022.

[8] Payri R, Viera JP, Pei Y, Som S. Experimental and numerical study of lift-off length and ignition delay of a two-component diesel surrogate. Fuel 2015;158:957–67. https://doi.org/10.1016/j.fuel.2014.11.072.

[9] Gaydon AG. The Spectroscopy of Flames. Dordrecht: Springer Netherlands; 1974. https://doi.org/10.1007/978-94-009-5720-6.

[10] Reyes M, Tinaut FV, Giménez B, Pastor JV. Effect of hydrogen addition on the OH* and CH* chemiluminescence emissions of premixed combustion of methane-air mixtures. International Journal of Hydrogen Energy 2018;43:19778–91. https://doi.org/10.1016/j.ijhydene.2018.09.005.

[11] Thorlabs - Search, 2021. https://www.thorlabs.com/search/thorsearch.cfm?search=shortpass%20dichroic%20mirror (accessed July, 2021).

[12] Xuan T, Desantes JM, Pastor JV, Garcia-Oliver JM. Soot temperature characterization of spray a flames by combined extinction and radiation methodology. Combustion and Flame 2019;204:290–303. https://doi.org/10.1016/j.combustflame.2019.03.023.

[13] Xuan T. Optical investigations on diesel spray dynamics and in-flame soot formation. PhD thesis. Universitat Politècnica de València, 2017.

[14] Lambert's cosine law. Wikipedia 2021.

[15] Bjørgen KOP, Emberson DR, Løvås T. Combustion and soot characteristics of hydrotreated vegetable oil compression-ignited spray flames. Fuel 2020;266:116942. https://doi.org/10.1016/j.fuel.2019.116942.

[16] Choi MY, Mulholland GW, Hamins A, Kashiwagi T. Comparisons of the soot volume fraction using gravimetric and light extinction techniques. Combustion and Flame 1995;102:161–9. https://doi.org/10.1016/0010-2180(94)00282-W.

[17] Li D, He Z, Xuan T, Zhong W, Cao J, Wang Q, et al. Simultaneous capture of liquid length of spray and flame lift-off length for second-generation biodiesel/diesel blended fuel in a constant volume combustion chamber. Fuel 2017;189:260–9. https://doi.org/10.1016/j.fuel.2016.10.058.

[18] Lequien G, Berrocal E, Gallo Y, Themudo e Mello A, Andersson O, Johansson B. Effect of Jet-Jet Interactions on the Liquid Fuel Penetration in an Optical Heavy-Duty DI Diesel Engine, SAE Technical Paper 2013-01-1615; 2013. https://doi.org/10.4271/2013-01-1615.

[19] Kook S, Pickett LM. Liquid length and vapor penetration of conventional, Fischer–Tropsch, coal-derived, and surrogate fuel sprays at high-temperature and high-pressure ambient conditions. Fuel 2012;93:539–48. https://doi.org/10.1016/j.fuel.2011.10.004.

[20] Benajes J, Payri R, Bardi M, Martí-Aldaraví P. Experimental characterization of diesel ignition and lift-off length using a single-hole ECN injector. Applied Thermal Engineering 2013;58:554–63. https://doi.org/10.1016/j.applthermaleng.2013.04.044.

[21] Payri R, Salvador FJ, Manin J, Viera A. Diesel ignition delay and lift-off length through different methodologies using a multi-hole injector. Applied Energy 2016;162:541–50. https://doi.org/10.1016/j.apenergy.2015.10.118.

[22] Pickett LM, Siebers DL. Orifice Diameter Effects on Diesel Fuel Jet Flame Structure. J Eng Gas Turbines Power 2005;127:187–96. https://doi.org/10.1115/1.1760525.

[23] Pastor JV, García-Oliver JM, López JJ, Vera-Tudela W. An experimental study of the effects of fuel properties on reactive spray evolution using Primary Reference Fuels. Fuel 2016;163:260–70. https://doi.org/10.1016/j.fuel.2015.09.064.

[24] Pickett LM, Siebers DL. Non-Sooting, Low Flame Temperature Mixing-Controlled DI Diesel Combustion, SAE Technical Paper 2004-01-1399; 2004. https://doi.org/10.4271/2004-01-1399.

[25] Siebers D, Higgins B. Flame Lift-Off on Direct-Injection Diesel Sprays Under Quiescent Conditions, SAE Technical Paper 2001-01-0530; 2001. https://doi.org/10.4271/2001-01-0530.

[26] Aatola H, Larmi M, Sarjovaara T, Mikkonen S. Hydrotreated Vegetable Oil (HVO) as a Renewable Diesel Fuel: Trade-off between NOx, Particulate Emission, and Fuel Consumption of a Heavy Duty Engine, SAE Int. J. Engines 1(1):1251-1262; 2008. https://doi.org/10.4271/2008-01-2500.

[27] Marinov NM, Pitz WJ, Westbrook CK, Vincitore AM, Castaldi MJ, Senkan SM, et al. Aromatic and Polycyclic Aromatic Hydrocarbon Formation in a Laminar Premixed n-Butane Flame. Combustion and Flame 1998;114:192–213. https://doi.org/10.1016/S0010-2180(97)00275-7.

[28] Dec JE, Coy EB. OH Radical Imaging in a DI Diesel Engine and the Structure of the Early Diffusion Flame, SAE Technical Paper 960831; 1996. https://doi.org/10.4271/960831.

[29] Vera-Tudela Fajardo WM. An experimental study of the effects of fuel properties on diesel spray processes using blends of single-component fuels. PhD thesis. Universitat Politècnica de València, 2015.

[30] Pastor J, Garcia-Oliver JM, Garcia A, Nareddy VR. Characterization of Spray Evaporation and Mixing Using Blends of Commercial Gasoline and Diesel Fuels in Engine-Like Conditions, SAE Technical Paper 2017-01-0843; 2017. https://doi.org/doi:10.4271/2017-01-0843.

[31] Siebers DL. Scaling Liquid-Phase Fuel Penetration in Diesel Sprays Based on Mixing-Limited Vaporization, SAE Technical Paper 1999-01-0528; 1999. https://doi.org/10.4271/1999-01-0528.

[32] Pickett LM, Kook S, Williams TC. Transient Liquid Penetration of Early-Injection Diesel Sprays, SAE Int. J. Engines 2(1):785-804; 2009. https://doi.org/10.4271/2009-01-0839.

[33] Pachano L. CFD modeling of combustion and soot production in diesel sprays. PhD thesis. Universitat Politècnica de València, 2020.

[34] Desantes JM, Garcia-Oliver JM, Novella R, Pachano L. A numerical study of the effect of nozzle diameter on diesel combustion ignition and flame stabilization. International Journal of Engine Research 2020;21:101–21. https://doi.org/10.1177/1468087419864203.

[35] Maes N, Skeen SA, Bardi M, Fitzgerald RP, Malbec L-M, Bruneaux G, et al. Spray penetration, combustion, and soot formation characteristics of the ECN Spray C and Spray D injectors in multiple combustion facilities. Applied Thermal Engineering 2020;172:115136. https://doi.org/10.1016/j.applthermaleng.2020.115136.

[36] Pérez-Sánchez EJ, Garcia-Oliver JM, Novella R, Pastor JM. Understanding the diesel-like spray characteristics applying a flamelet-based combustion model and detailed large eddy simulations. International Journal of Engine Research 2020;21:134–50. https://doi.org/10.1177/1468087419864469.

[37] Benajes J, Garcia-Oliver JM, Pastor JM, De-Leon-Ceriani D. A computational study on OME1 spray combustion under ECN Spray A conditions, Zhenjiang, China: ILASS-Asia; 2020.

[38] Zubel M, Ottenwälder T, Heuser B, Pischinger S. Combustion system optimization for dimethyl ether using a genetic algorithm. International Journal of Engine Research 2021;22:22–38. https://doi.org/10.1177/1468087419851577.

[39] Pickett LM, Siebers DL, Idicheria CA. Relationship Between Ignition Processes and the Lift-Off Length of Diesel Fuel Jets, SAE Technical Paper 2005-01-3843; 2005. https://doi.org/10.4271/2005-01-3843.

[40] Pastor JV, García-Oliver JM, Micó C, García-Carrero AA, Gómez A. Experimental Study of the Effect of Hydrotreated Vegetable Oil and Oxymethylene Ethers on Main Spray and Combustion Characteristics under Engine Combustion Network Spray A Conditions. Applied Sciences 2020;10:5460. https://doi.org/10.3390/app10165460.

[41] Svensson KI, Richards MJ, Mackrory AJ, Tree DR. Fuel Composition and Molecular Structure Effects on Soot Formation in Direct-Injection Flames Under Diesel Engine Conditions, SAE Technical Paper 2005-01-0381; 2005. https://doi.org/10.4271/2005-01-0381.

[42] Omari A, Heuser B, Pischinger S. Potential of oxymethylenether-diesel blends for ultra-low emission engines. Fuel 2017;209:232–7. https://doi.org/10.1016/j.fuel.2017.07.107.

[43] Heywood, John B. Internal combustion engine fundamentals. Second Edition. New York: McGraw-Hill; 2018.

Chapter 5

Dual alternative combustion: Spray and combustion characterization of HVO-LPG blends

Content

5.1 Introduction

This chapter will address the results of the combustion behavior and soot formation for a dual fuel combustion concept using Hydrotreated Vegetal Oil (HVO) and Liquified Protroleum Gas (LPG) which are considered alternative fuels [1–3].

The experiments were carried out in the High Pressure and High Temperature installation (HPHT) described in Chapter 3. The blend of both is stored in the same tank and it is injected through a common injection system using a single hole injector.

The main objective of this chapter is to evaluate under controlled ambient conditions the performance and soot emissions of fuel blends of liquid (HVO) and gaseous fuels (LPG) with potential to be used for dual fuel combustion in compression ignition engines for heavy duty transport. Thus, auto ignition, flame structure and soot formation are studied by means of high speed imaging techniques. The details of the experimental hardware is presented in the first section of this chapter, followed by the results which emphasize the effect of fuel composition on the evolution of the spray and combustion development as well as on soot formation. By last, the chapter ends with a summary and conclusions.

5.2 Experimental methodology

Different blends of HVO and LPG have been injected into a High Pressure and High Temperature installation [4–6] using a common-rail injection system which was modified to allow handling of the fuel blends and ensuring that evaporation in the injection system was avoided. The analysis of the effect of fuel composition on the ignition, flame development and soot emissions is made by applying three simultaneous high speed imaging techniques: schlieren imaging, broadband natural flame luminosity (NL) and high speed OH^* chemiluminescence imaging. The following paragraphs describe first the test facility, the injection system and the characteristics of the fuels used. Then, the test matrix and finally the implemented optical arrangement with emphasis on the experimental procedures followed for the measurement and analysis because the fundamentals of these techniques have been described in Chapter 4.

5.2.1 HVO-LPG injection system

A modified injection system based on a conventional common-rail system was used to inject fuel into the combustion vessel as sketched in Figure 5. 1. Considering that LPG is a gas at atmospheric pressure and ambient temperature and common-rail injection systems are designed to operate with liquid fuels, it was necessary to ensure that fuel was liquid at any point in the hydraulic circuit. For this, conventional LPG automotive fuel tanks were filled with the desired mixtures of HVO and LPG at a pressure of 7 bar. Fuel delivery to the rest of the circuit, i.e. to the common-rail system, was made by activating the low pressure pump inside the fuel tank. The rest of the injection system components are standard and it includes the high-pressure pump, a common rail with pressure regulator controlled by a PID

system and piezoelectric injector. In addition, a special injector holder is used to keep constant the injector tip temperature at the desired value through the whole test matrix [7].

To ensure that fuel was liquid at any point of the injection system avoiding the formation of fuel vapour bubbles that could alter the injected fuel behaviour, two heat exchangers were used as shown in Figure 5. 1. One of them was set just downstream of the pressurized fuel tank, before the high-pressure pump of the common-rail system. The second was set at the fuel return pipes to ensure that fuel was cooled down prior to drive it back to the pressurized tank. Both of them were instrumented to monitor pressure and temperature at any moment ensuring tests repeatability.

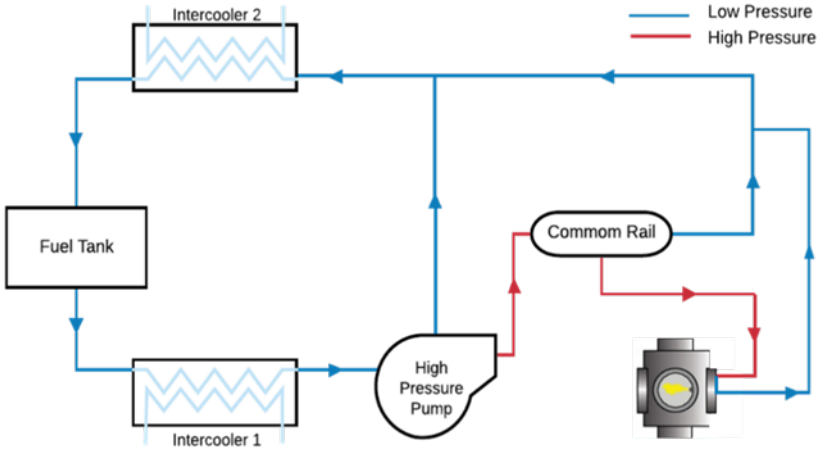

Figure 5. 1 High pressure injection system for HVO- LPG blends

In addition, to avoid any fuel leakage of gas to the laboratory atmosphere, both fuel returns from the high-pressure pump and from the injector were communicated and driven back to the tank. Besides, this allows to ensure that, due to the low amount of fuel injected during these tests, the composition of the fuel blend in the tank remained unchanged. All the low-pressure part of the hydraulic system was set to 7 bar and 290 K.

To perform a detailed characterization of the spray and combustion enhancing fuel effects, a single hole nozzle was used, so that isolated sprays were imaged. The nozzle used is a single-hole one with a 140 μm outlet diameter, a 1 mm long hole thickness and with a conical shape (K factor of 1.5). It has been used for some other studies during the last years [8,9].

5.2.2 Fuel characteristics

Four different fuels have been considered in this study as representative substitution rates in a hypothetical dual fuel combustion mode in a compression ignition engine. Pure HVO is considered as the High Reactivity Fuel (HRF) of the dual fuel combustion mode with a Derived Cetane Number close to conventional diesel fuel, LPG being the Low Reactivity Fuel (LRF). Thus, pure HVO is considered the reference fuel in this study and represents the zero substitution rate of the dual fuel mode. Then, three blends of HVO and LPG with

percentages of LPG of 25%, 50% and 75% in mass are considered to represent different rates of substitution.

The main properties for the two components of the blend, HVO and LPG, are detailed in Table 5. 1. All along the document, the four fuel are identified as "HVO" for pure HVO, and "7525", "5050" and "2575" for the blends with 25%, 50% and 75% of LPG respectively.

Characteristics	**HVO**	**LPG**
Density [kg/m^3]	779.1	502
Viscosity [mm^2/s]	2.7	0.0074
Lower heating value [MJ/kg]	44	45.79
Vapor Density [kg/m^3]	3.4	2,48x10^3
Vapor Pressure [bar]	0.87	15
Boiling Point [ºC]	(180)-(320)	(-42.1)-(3.7)
Flash Point [ºC]	>55	(-107.5)- (101.6)
Autoignition [ºC]	338	>400
Derived cetane number (IQT)	70.9	--
(A/F)st at 21% of O_2	14.55:1	15.63:1

Table 5. 1 Fuel properties

5.2.3 Operating conditions

For the four fuels, a set of parametric studies has been performed. Ambient density and ambient temperature were set as variables, as well as oxygen content and injection pressure. The injection strategy used was a single injection with an energizing time of 1500 µs, which provides an injection event long enough to study the development of the spray and flame under mixing controlled combustion. The fuel mass flow rate was 0.00381 kg/s

Four ambient conditions have been considered in the base test matrix summarized in Table 5. 2: Low Density (LD), Nominal Operation (NO), High Density (HD) and Low Temperature (LT). They have been considered as representative of LTC conditions, where dual fuel combustion has higher potential. Starting from a nominal operation (NO) with 22.8 kg/m^3 air density, a variation of temperature (800 and 900 K) at constant density and a variation of density (from 15.2 to 30.4 kg/m^3) at constant temperature were performed. In all cases, two rail pressures of 500 bar and 1000 bar were considered.

Operating condition	T [K]	ρ [kg/m^3]	O_2 [%]
Low Density (LD)	900	15.2	21
Nominal Operation (NO)	900	22.8	21
High Density (HD)	900	30.4	21
Low Temperature (LT)	800	22.8	21

Table 5. 2 Test Matrix

5.2.4 Optical set up

Aiming to analyse the effect of the LRF substitution rate upon spray development, ignition and soot formation, three different optical techniques have been applied simultaneously using the two opposed optical access windows in the vessel, trying to maximize the amount of information obtained. A sketch of the optical arrangement is shown in Figure 5. 2

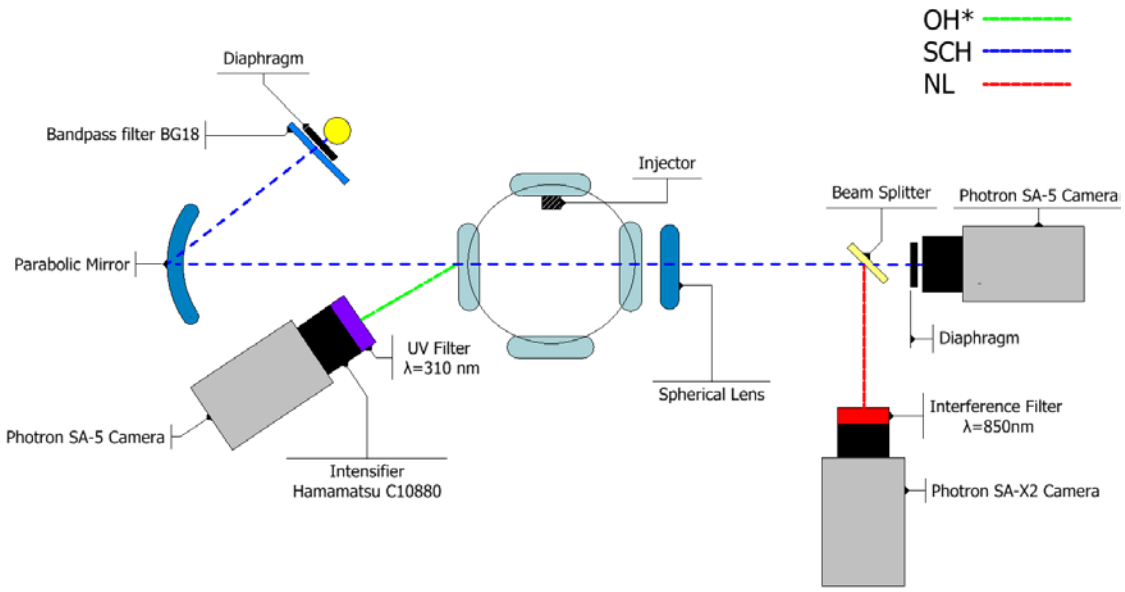

Figure 5. 2 Scheme for three optical technique used in the tests

5.2.4.1 Schlieren visualization

A high-speed, single-pass schlieren imaging setup, very similar to that described in detail in Chapter 4, was used to detect the spray and flame boundaries at any operating conditions. A scheme of the optical arrangement is shown in Figure 5. 2

A diffused point light obtained from a Xenon arc lamp with a liquid light guide and a pinhole was collimated by a parabolic mirror (f=610mm) which directs it through the combustion chamber. In addition, a BG18 band pass filter is used to restrict the spectrum of the Xenon lamp and avoid interference in the NL images commented later. A spherical lens (f=450mm) was placed on the other side of the chamber to focus the light onto a so-called Fourier plane, where a diaphragm was located with a cut-off diameter of 3 mm just before the high-speed camera (Photron Fastcam SA-5) equipped with a Carl Zeiss Makro-Planar T 100mm f/2 ZF2 camera lens. Images were recorded at a fixed frequency of 20 kfps, with a constant shutter time of 2.5 μs, a total magnification of 11 pixel/mm and a resolution of 1024x 368 pixels. A minimum of 30 injection cycles per test were recorded in any case.

The schlieren images have been used to depict a global phenomenological description of the injection and combustion process of the different fuel blends, which will be presented later. In addition, due to the fair space and time resolution of the Schlieren recordings, these images were also used to determine the real Start of Injection (SOI) for every case with sub-interframe temporal resolution. This was done by extrapolating the spray tip penetration measurable in the first injection frames to estimate the exact instant when fuel starts to exit from the nozzle hole. This SOI is used in all the results presented in this chapter as the temporal origin of any measured parameter with any cameras, since the three cameras used the same trigger signal.

As for the spray and combustion parameters measured from the Schlieren images, segmentation from the background is performed by applying the methodology described by Siebers [10], which has become a standard in the Engine Combustion Network [11]. This procedure has been described in Chapter 4. As well as, the criteria used to determine the ignition delay (ID), which it has been defined as the time where the maximum intensity increment occurs.

5.2.4.2 High-speed OH^* chemiluminescence imaging

The fundamentals of OH^* chemiluminescence have been described in Chapter 4. It has been indicated that OH^* radical is a good tracer of high temperature reactions zones, therefore the visualization of OH^* chemiluminescence at the base of the flame makes it possible to quantify the Lift-off length (LOL).

In this work, a high speed image intensifier (Hamamatsu C10880), coupled to a high speed camera (Photron Fastcam SA5) with a 1:1 relay lens, equipped with a UV f/4 100mm focal length lens (OUC 2.50 by Bernhard Halle Nachfl.) was used. An interference filter centred at 310nm (10nm FWHM) was placed in front of the camera to remove most of the radiation of the flame while keeping OH^* chemiluminescence. Images were taken at a fixed frequency of 15 kfps, with a resolution of 320x536 pixel, and a magnification of 3.4 pixel/mm. Shutter time was fixed in 33us and care was taken to ensure that light saturation, whenever occurred, did not affect the measurement of the LOL and was low enough as to not

imply any risk for the intensifier safety. Again, at least, 30 valid injection cycles per test were recorded in any case, at least.

Ignition delay was computed determining the first frame with light intensity, as a check to confirm the results obtained with the schlieren technique. As for the measurement of the LOL, the algorithm used is based on the Engine Combustion Network (ECN) recommended procedure described in [12], where the LOL was determined by finding the distances between the injector tip and the first axial locations above and below the spray centerline with intensity greater than 50% of the intensity peak of that zone. As it was explained in Chapter 4.

5.2.4.3 Natural luminosity

Natural luminosity (NL) technique registers the broadband radiation of the flame, which corresponds to the soot thermal luminosity during the diffusion combustion phase without using any particular optical filter [13,14]. In such cases, considering the spectral response of the camera, the light collected will be almost entirely the thermal radiation arising from small soot particles present in the flame and in some cases can include a minor contribution of other types of chemiluminescence radiation too, which can become significant only in low sooting flames cases. Then, qualitative and topological description of the sooting flame evolution can be obtained, but no quantitative description of the combustion intensity is expected since this is a line of-sight technique and consequently renders a variable that is integrated along the optical path, so spatial resolution is only possible as two dimensional distribution of the optical path integrated variable. It is well known that flame brightness does not depend only on soot concentration, but also on flame temperature [13]. However, for isolated sprays as those analyzed in this research if the only parameter changed is the fuel composition, it can be assumed that the temperature field in the flame at equivalent instants after ignition will not be too different. Thus, flame brightness can be a qualitative indicator of the amount of incandescent soot in the flame. Therefore, in this chapter, the images processing method is based on quantify the values of the grey levels of all the pixels in the image. First, an average background image (before start of combustion) is created to quantify the signal noise. This average background is subtracted from ach image. Then with an arbitrary threshold, a mask that contents the flame radiation is created. By last, the intensity levels of this mask are quantified in term of accumulated flame intensity along jet axis for each frame. Although with NL is not possible to do a quantitative analysis of soot formation, in this study NL has been used to do a qualitative and topological description of the sooting flame evolution by means of flame intensity.

In this experimental campaign, NL images are not images of flame broadband radiation, but of radiation at around 850nm (40nm FWHM) since an interference filter is used to avoid registering at the same time flame NL and the illumination light used for the schlieren. As a consequence, the spectrum fraction is severely reduced as well as the light collected. However, the analysis is exactly the same as with conventional broadband NL

images, since the only significant contribution of the flame in the near-IR spectrum comes from soot particles incandescence. It is well known that flame brightness does not depend only on soot concentration, but also on flame temperature [13]. However, for isolated sprays as those analysed in this work, if the only parameter changed is the fuel composition, it can be assumed that the temperature field in the flame at equivalent instants after ignition will not be too different. Thus, flame brightness can be a qualitative indicator of the amount of incandescent soot in the flame.

Natural Luminosity was recorded with a high-speed camera (Photron Fastcam SA-X2) at a fixed frequency of 20 kfps, with a resolution of 512x736 pixel, and a total magnification of 4.9 pixel/mm. Shutter time was adapted to the luminosity of each tested case to use properly the dynamic range of the camera. A minimum of 30 injection cycles per test were recorded in any case, too.

5.3 Auto ignition and macroscopic characteristics

Before entering into the detailed quantification on the effect that the HVO-LPG blend ratio has upon the spray features, the mixing process and soot formation, a phenomenological description of the injection and combustion process is given, paying attention to the effects clearly linked to the fuel composition.

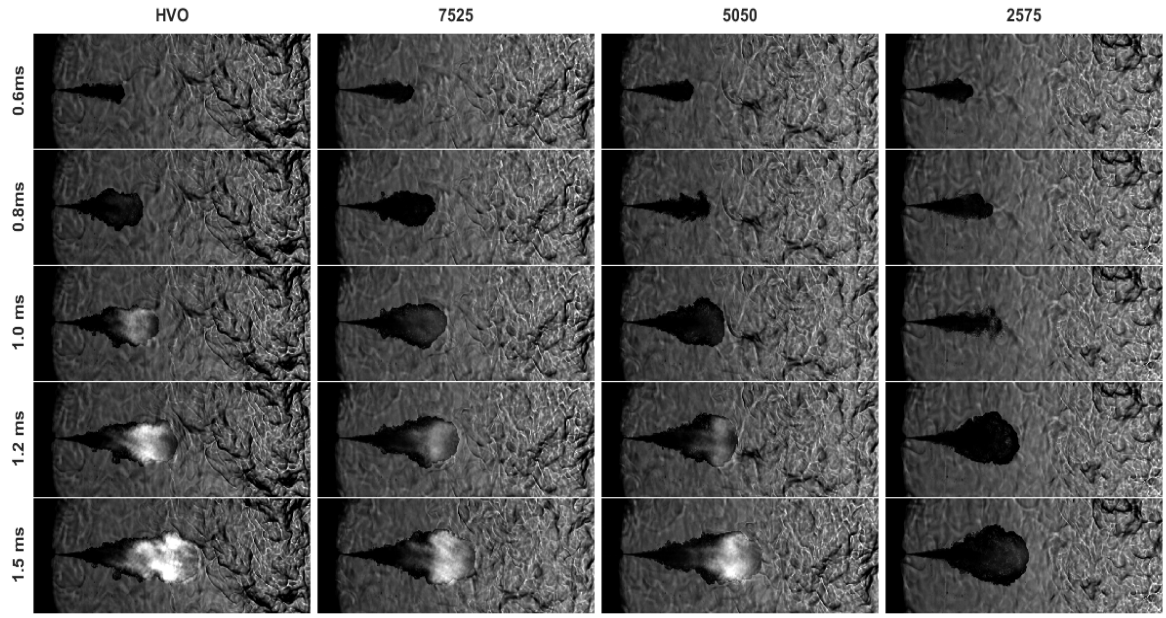

Figure 5. 3 Combustion evolution for the four blends tested at Nominal conditions (NO) and injection pressure of 500 bar

In Figure 5. 3 some frames of the high-speed images recorded using the schlieren technique are presented. These images show the evolution of the sprays and the combustion. The nozzle is located at the left hand side of the images and the sprays are injected at 500 bar

into a nearly stagnant flow with constant and uniform temperature field of 900 K and 22.8 kg/m^3 air density. Five frames have been selected to evidence the influence of the HVO-LPG ratio in the spray and flame development, before the end of the injection, i.e. when the spray is still mixing controlled. Images at the left column correspond to pure HVO, and the other three columns to the right are for increasing LPG proportion in the blend.

From top to bottom of any case the following events can be appreciated in the spray and flame development: in the first frames the spray in liquid or vapour phase appears as a dark shape that tends to increase in size as time evolves. When the first stage of the auto ignition process occurs the spray contrast of the schlieren images vanish (see, e.g. the third frame of the last column). Tip acceleration and radial expansion of the burning spray become evident in the following frame when high temperature ignition has already started. Certain time after ignition, incandescent soot appearance becomes evident and it can be seen as bright regions in the images.

Regarding the geometry of the spray, there are no significant differences before auto ignition for the four blends, which suggests similar characteristics of injection between the four fuels. However, two issues apparently linked to the ratio of LPG in the blend can be easily identified. First, ignition delay increases with LPG content in the blend, which indicates that LPG acts as an ignition inhibitor reducing burning propensity of HVO. A second effect is that the flame brightness decreases clearly when LPG rate increases, pointing out that LPG is a less sooting fuel than HVO. However, the Schlieren technique does not allow to perform the soot formation assessment. Although it is possible to appreciate the high luminosity of the HVO, it is necessary to use a specific optical technique to confirm which fuel has higher soot formation tendency. Therefore the Natural Luminosity technique has been used for this purpose.

5.3.1 Ignition delay (ID)

The ignition delay (ID) is defined as the time elapsed from the Start of Injection (SOI) and the Start of Combustion (SOC) and has been calculated from the Schlieren images following the procedure described in Chapter 4. This technique was chosen for this purpose, instead of high-speed OH^* chemiluminescence, because it was performed at a higher acquisition rate (better time resolution). Besides, both techniques were compared, and differences were below 0.05 ms, which could be due to the difference in time resolution of both techniques.

The influence of the different operating conditions upon the ignition delay has been widely studied in literature and a similar analysis will not be performed here. However, in order to check consistency of the experimental data of this work with the well-known spray physics, a comparison of the experimental data versus some correlations available in literature is given in Figure 5. 4. In particular, the correlation by Benajes [15] obtained for n-dodecane and represented in Equation 5.1

$$ID^* \propto exp\left(\frac{7523}{T_{amb}}\right) \cdot \rho_{amb}{}^{-1.35} \cdot (P_{inj} - P_{amb})^{-0.09} \cdot O_{2\%\,amb}{}^{-0.51} \qquad (5.1)$$

Where the constant inside the exponential term is related to the global activation energy of reactions. Equation 5.1 indicates that the ID is proportional to terms on the right. The correlation is completed with a constant term which reflects fuel properties contribution, and it will be not considered in this section, therefore the ID^* will be referred only to the proportionality. This correlation shows the effect of boundary conditions over the ignition delay [5,15], which decreases with increasing the temperature, as it accelerates oxidation reactions. ID also decreases with increasing density and injection pressure, as both parameters enhance the mixing and evaporation processes. In Figure 5. 4, operating conditions have been represented in ellipses with continuous lines.

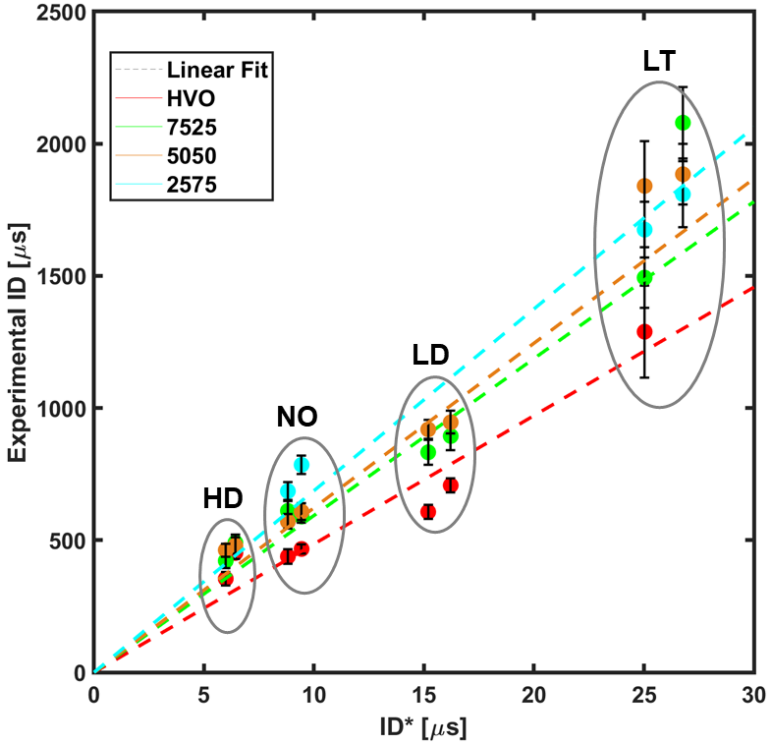

Figure 5. 4 Comparison of current experimental data with correlation calculated by Benajes [15] for dodecane

It is worth mentioning that the experiments in the work [15] were performed in the same facility as the present work, but using different fuel. In Figure 5. 4 is represented the experimental ignition delay versus the theoretical ignition delay (ID^*) obtained using the Equation 5.1. The slope obtained from linear fit (dashed lines) for each fuel corresponds to the missing constant in the Equation 5.1. Based on these correlation and linear fit, in Figure 5. 4 is observed that stratification exists by fuels, being the higher values of ID for HVO-LPG blends. HVO is the first to start combustion and the blend with the highest proportion

of gas (2575) is the last. Thus, LPG clearly increases ignition delay compared to the HVO, independent of the ambient or injection condition. For 15.2 kg/m^3 and: 22.8 kg/m^3 ambient density ID of blends with low (7525) and medium (5050) LPG ratio increased between 26% and 34% with respect to HVO at 500 bar of injection pressure, but fuel 2575 (high LPG ratio) showed an increase of 68%. However, for 30.4 kg/m^3 ambient density, the ID increase for the three blends in comparison with HVO is only around 6% to 8%. For the cases at 1000 bar of injection pressure the differences increase, reaching up to 50% of difference respect to HVO in LD operating condition, and the difference increase up to 40% in the NO and HD condition for HVO-LPG blends. In the case of low temperature (800 K), the differences between fuels vary from 15% and 40% for both injection pressure. For LT operating condition, the experimental data does not follow the linear correlation described by Equation 5.1. The effect of boundary conditions in comparison to other experimental points is the same as described previously. However, blends show larger variations than the ones predicted by the correlation. Moreover, when ambient temperature reduces, the ignition delay increases as well as its statistical uncertainty. At low temperature case, with ID of the order of 2000 µs, data scattering is higher in reference to other operating condition.

5.3.2 Spray tip penetration

Spray tip penetration and flame penetration were obtained from high-speed Schlieren images.

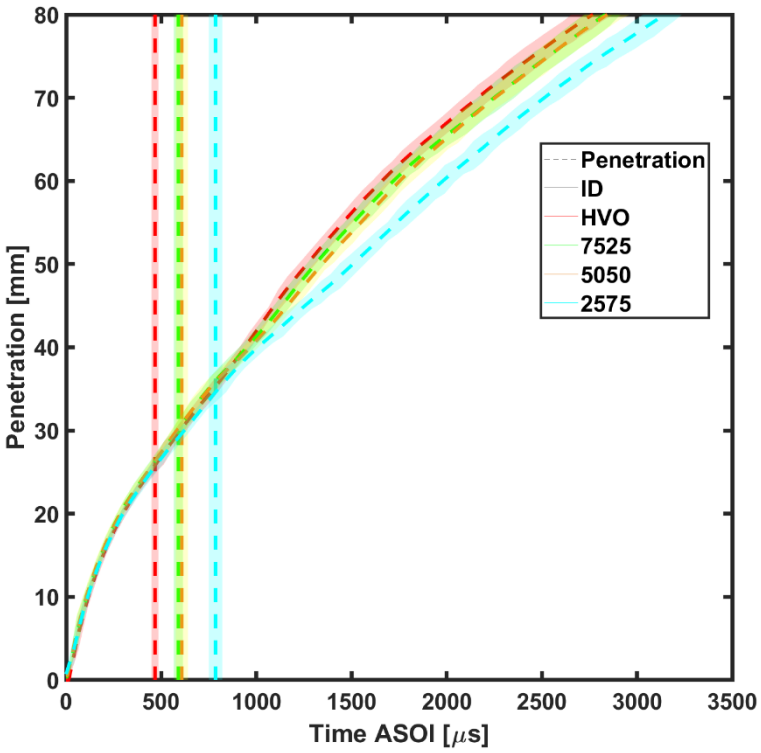

Figure 5. 5 Temporal evolution of vapor penetration for each blend at T=900K; ρ=22.8 kg/m^{3}and 500bar of injection pressure

Figure 5. 5 shows the temporal evolution of the vapor penetration obtained for each blend at nominal operating condition at 500 bar of injection pressure. It is possible to state that there is a first stage where vapor penetration is identical for all the blends (up to 480 µs) and, after a certain time (ignition time), some differences arise. This first stage corresponds to the ignition delay phase which extends for each blend until combustion starts, timing that has been marked in the graph as dashed vertical lines for each blend. During the period until ignition, attending to momentum flux conservation equations, there should be no effect of the fuel blends on the spray behavior as discussed in [16]; spray momentum flux at the nozzle orifice only depends on the pressure drop across the nozzle and on the orifice area, and none of them change throughout the experiment.

It is worth mentioning that, despite the physical properties of the fuel blend (mainly density and viscosity), do not affect spray tip penetration (until ignition stage), density may affect the fuel injection rate (which is not relevant in these experiments with long injections) while viscosity is related with fuel behavior inside the injection system. Consequently, it influences the hydraulic delay of the injector and the real Start of Injection (SOI) occurs later with the increasing proportion of LPG. As explained in the methodology section, the real SOI was determined by means of the high-speed Schlieren images and all curves in this paper have been shifted accordingly to refer them always to real SOI.

Despite differences observed in the hydraulic delay, injection process is not affected by the different properties of LPG and HVO as it is confirmed by the similarities observed in fuel penetration before the start of combustion.

After ignition, the flame penetration curves depart from each other because of the flame expansion described in previous works [8]. Not characteristic effect associated to fuel composition was observed in these experiments, other than the fact that the shorter the ignition delay, the faster the flame penetration [17].

5.3.3 Lift-off length

Flame Lift-off length plays an important role in the combustion and soot formation processes, since it is strongly related with the quality of fuel-air mixing process upstream of the combustion region [5,18]. Consequently, flame LOL is a parameter which is worthy to be studied in detail with these fuel blends.

As previously done with the ignition delay, a comparison of the raw experimental data obtained in this work with correlations available in literature is performed. The time interval to calculate the stable LOL was between 3200 µs and 3800 µs.

The correlation proposed by Benajes et al. [15] is shown in Figure 5. 6. It was obtained for n-dodecane, in the same facility and under similar conditions to the ones in this work. This correlation is represented by Equation 5.2:

$$LOL^{*} \propto T_{amb}{}^{-3.89} \cdot \rho_{amb}{}^{-1} \cdot \left(\sqrt{2 \cdot \frac{P_{inj} - P_{amb}}{\rho_{fuel}}}\right)^{0.54} \cdot O_{2\,amb}{}^{-1} \qquad (5.2)$$

It is worth mentioning that in Equation 5.2 a constant is missing, that converts the proportionality into a real value of LOL, therefore results of Equation 5.2 will be titled as LOL^{*} and the constant will depend on fuel used. In this study, the constant corresponds to slope obtained for the linear fit (dashed line) of each fuel.

The correlation shows that LOL decreases with increasing ambient temperature and density, as it reduces the amount of air required to burn the fuel injected. Besides, LOL increases with increasing injection pressure, as a higher injection velocity moves the reaction stabilization region [5, 15,19]. In addition, fuel density appears implicitly in the correlation, so that the lower the fuel density, the higher the LOL should be.

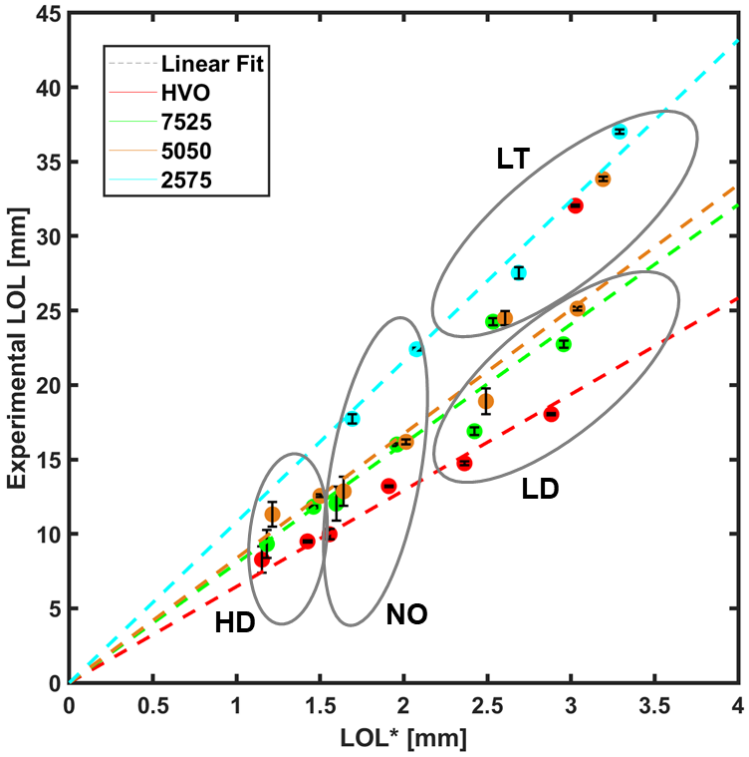

Figure 5. 6 Comparison of current experimental LOL data with correlations by Benajes [15] for each blend and operating condition

According to this, the shortest LOL should be obtained for HVO while increasing as LPG ratio in the blend increases. In this sense, experimental results show a stratification by fuels and by operating conditions, as it is represented in Figure 5. 6. Operating condition are represented with ellipses in continuous lines. A similar behaviour to the one described by Equation 5.2 is observed also with experimental data.

For 15.2 kg/m^3 and: 22.8 kg/m^3 ambient density, the difference of LOL between HVO-LPG blends and pure HVO was around 15% and 30%, while at 30.4 kg/m^3 the difference is still between 12% and 36%. For the LT condition, the observed differences are only between 5% and 15%. Besides, as it was observed for ID, these points show larger LOL values than the Equation 5.2 would predict for all the blends.

5.4 Soot formation

A brighter flame can be the consequence of either higher temperature in the flame, higher soot concentration, or both. However, natural flame luminosity has been used previously in the literature [13] for qualitative analysis of soot formation. For this reason, natural luminosity has been considered of interest for the analysis of soot formation behavior of the different fuels tested. On the assumption that fuels have similar flame temperature, the differences of luminosity only correspond to formed soot. Additionally, in previous work, the relationship between flame temperature and soot concentration has been studied and it was determined that both parameters are not directly linked and the higher flame temperature is not the governing factor for higher soot production [20].

High-speed flame emission images are presented in Figure 5. 7. It depicts the temporal evolution of natural luminosity for each fuel. From left to right, percentage of LPG increases. It is possible to observe that light radiation reduces significantly with the increase of LPG ratio, even when the LPG proportion is the lowest (second column from left to right). The first instant of time shown (1500 µs) corresponds to a time in which the combustion has started for all the blends. At this time, HVO has the highest light intensity**.** On the other hand, the flame of 2575 can hardly be seen. In addition, at 3500 µs (third row of the Figure 5. 7 seen from top to bottom) the difference in brightness is still very marked, as well as the flames are already developed for all fuels.

Considering the flames produced by the LPG, the maximum intensity levels are not reached (red color) compared to HVO. This can be explained by the fact that these blends start the combustion later than the HVO. Also, these blends have their flame Lift off at longer distance from the injector. As it was studied in [20], LOL is a governing factor for soot production. Longer LOL allows more air entrainment as it was discussed previously. For blends 7525 and 5050 is not clear which flame has higher luminosity. This can be explained by the fact that the difference between ID and LOL is not significant either. But what is quite clear is that adding LPG favors the reduction of luminosity and therefore the soot formation will be reduced.

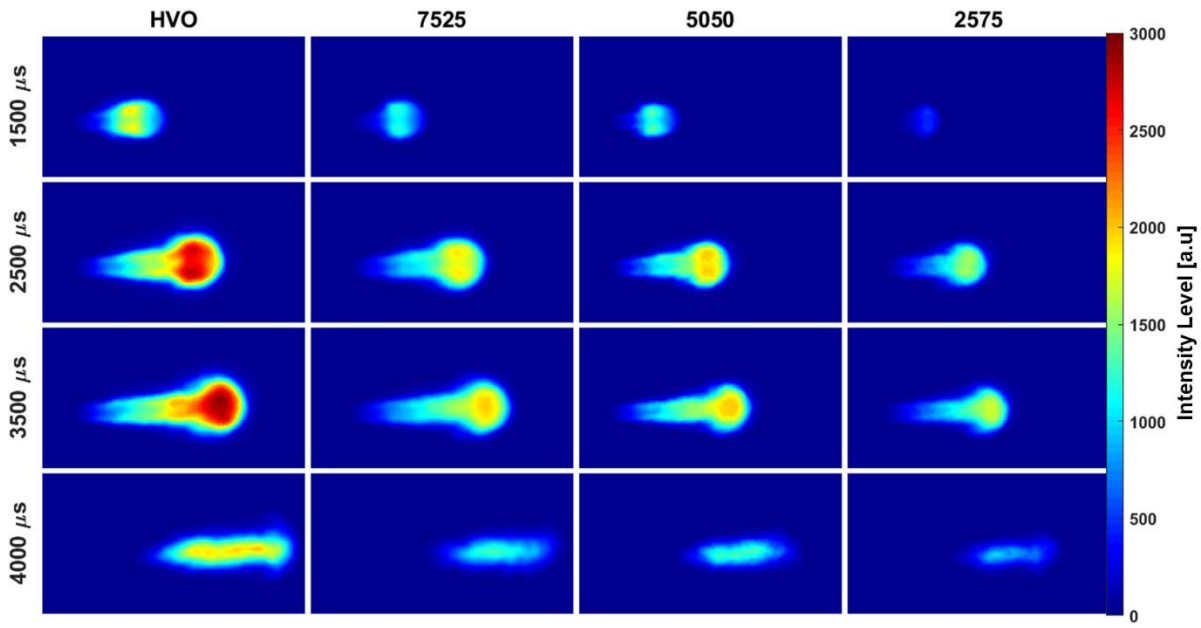

Figure 5. 7 Mean natural flame lumimosity for all fuels at 900K, ρ=22.8 kg/m^3 NO and 500 bar of injection pressure

In order to quantify the intensities in each fuel and make evident the effect of the addition of LPG, the values shown in Figure 5. 8 correspond to the mean accumulated intensity of the flame for all the fuels, at a certain instant, where the flame is stabilized, i. e. 3.5 ms after start of injection. In this figure, the two injection pressures and all the operating condition have been represented. It is possible to observe that adding LPG reduces the luminosity of the flame around 30% when the percentage of LPG in the mixture is the minimum tested (blend 7525). Additionally, during low temperature condition the luminosity observed for all fuels were quite small. As a consequence, the results are less accurate because it is difficult to detect the low flame intensity as the light radiation could be mistaken for the background noise of the images. And for that reason was not included in the analysis. Figure 5. 8 shows that increasing the injection pressure also reduces the intensity of the flame, as consequence of LOL increment. It is also possible to appreciate that when the density increases, the luminosity also increases. Xuan et al. in [20] indicates that a shorter Lift-off length (bigger Φ) has higher effect in the soot precursors than flame temperature which would result in a faster soot rise in the flame. Figure 5. 8 shows that, in general, differences between HD and NO operating condition are below or close to the standard deviation (represented by the error bars) which represents experimental variability. Thus, it is difficult to confirm the behavior described above between these two operating conditions.

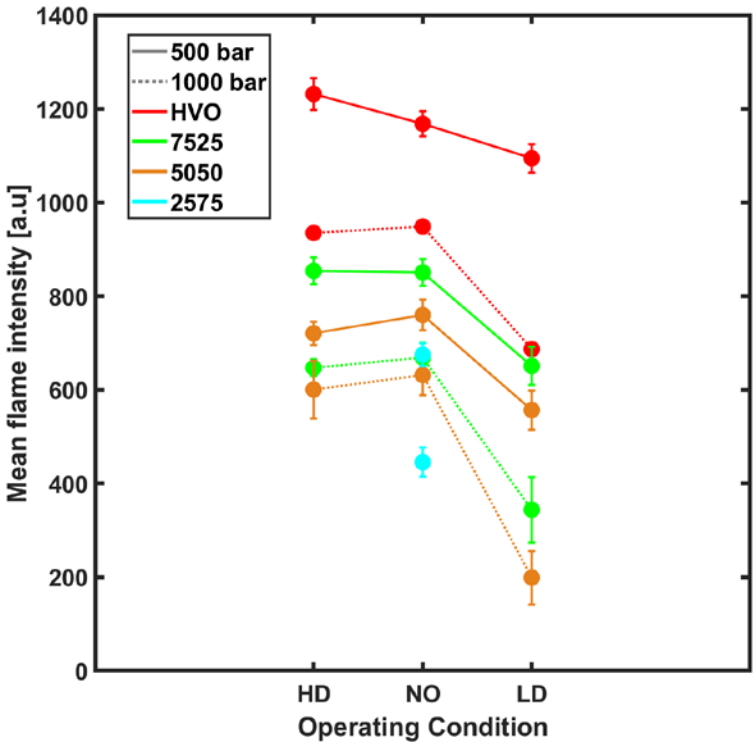

Figure 5. 8 Mean light intensity in the jet for all conditions at two injection pressure at 3200 µs ASOI

It is worth mentioning that blends with LPG have bigger ID and longer LOL than pure HVO. High values of both parameters favour less soot formation as more air is entrained and a better mixing is achieved upstream of the flame, which stabilizes at longer distances from the nozzle. This statement is supported by the calculations of the equivalence fuel-air ratio (Φ) at the spray axis, spray radius and Lift-off distance performed with a 1D spray model (DICOM) which is widely described in [21]. In DICOM the spray is assumed to be injected into a quiescent air volume, large enough so that the injected fuel does not change the conditions far away from the injector tip. The fuel stream has a uniform velocity profile at the tip of the nozzle. This flow exchanges its momentum with the ambient, and sets it moving. As a result of this, the spray increases its width with its axial distance. This phenomenon is modeled with two spray angles (one for the near-field and other angle for the far-field), with a transition occurring at a determined distance from the orifice. These parameters are inputs to the model as well as the fuel or blend composition, nozzle diameter, nozzle injection conditions (mass and momentum fluxes), and ambient condition (pressure, temperature, density and oxygen concentration). All these inputs come from the experiments. The outputs are the jet spray tip penetration as well as the mixture field at every simulated time instant. Other input is the spray cone angle that it is adjusted from comparison between penetration made by DICOM and the experimental penetration. In the current work, for HVO was used dodecane as surrogate while for LPG a blend of butane and propane was defined, according to the technical data sheet provided by supplier. Then blends were set according

to the mass fraction used in the experimental tests: 25%, 50% and 75% of LPG. The output is the air-fuel mixture field at every simulated time instant.

Fuel	LOL [mm]	Φ at spray axis
HVO	13.21	9.41
7525	16.00	7.05
5050	16.18	6.74
2575	22.4	3.93

Table 5. 3 Equivalence fuel air ratio (Φ) at LOL at NO operating condition and 1000 bar of injection pressure

To give a better understanding about effect of LPG on soot formation, Table 5. 3 represents the values of equivalent fuel-air ratio (Φ) at lift-off length at the spray axis when the flame is stabilized (3200 μs). Results correspond to NO at 1000 bar of injection pressure. The tendency is representative for the rest of operating condition. It is observed that an important difference of Φ between HVO and HVO-LPG blends exists. The larger LOL as LPG content increases means also more air when reactions start which explains the lower soot formed by them

.5.5 Summary and conclusions

This chapter collects and analysis all the results describing the spray development and combustion behavior for different blends of HVO and LPG under different ambient densities, temperatures and injection pressures. Measurements were carried out in the High Pressure and High Temperature installation and a dedicated injection system was implemented to inject the mixture of HVO and LPG at the same time. Optical setups included a schileren single pass combined with OH^* chemiluminescence and natural luminosity.

The most relevant findings lead to the following conclusions:

- The injection system implemented has shown a stable behavior, even when increasing LPG content. Spray penetration results suggest that no difference should be expected in terms of mass flow rate or spray momentum flux for the different blends used in this work.
- Ignition delay increases with the LPG content in the blend indicating that it acts as an ignition inhibitor of HVO. The sensitivity of the different blends to operation conditions was evaluated. For 25% and 50% LGP ratios, similar behavior was observed while larger differences were found when increasing LPG content to 75%.

- Flame Lift off length increases when increasing proportion of LPG. According with the correlation utilized, experimental results present similar variations as the ones predicted for different blend densities. As it was observed for ID, 25% and 50% LPG blends present a similar behavior while larger differences are observable for 75% LPG blend.
- The flame luminosity for blends is smaller than for pure HVO and it decreases when increasing LPG content. This can be related to less soot formation, as a consequence of more air entrainment due to larger ID and LOL.

References

[1] US EPA O. Alternative Fuels. US EPA, 2015. https://www.epa.gov/renewable-fuel-standard-program/alternative-fuels.

[2] Union PO of the E. Commission Regulation (EU) No 582/2011 of 25 May 2011 implementing and amending Regulation (EC) No 595/2009 of the European Parliament and of the Council with respect to emissions from heavy duty vehicles (Euro VI) and amending Annexes I and III to Directive 2007/46/EC of the European Parliament and of the Council, 2019. http://op.europa.eu/en/publication-detail/-/publication/4d2e52c3-41bc-11ea-9099-01aa75ed71a1/language-en/format-HTML (accessed April, 2020).

[3] ERTRAC Working Group. Energy Carriers for Powertrains for a clean and efficient mobility. European Road Transport Research Advisory Council (ERTRAC) Working Group: Energy and Environment; 2014.

[4] Viera A. Effect of multiple injection strategies on the Diesel spray formation and combustion using optical diagnostics. PhD thesis. Universitat Politècnica de València, 2019.

[5] Payri R, Salvador FJ, Manin J, Viera A. Diesel ignition delay and lift-off length through different methodologies using a multi-hole injector. Applied Energy 2016;162:541–50. https://doi.org/10.1016/j.apenergy.2015.10.118.

[6] Payri R, Gimeno J, Cardona S, Ayyapureddi S. Experimental study of the influence of the fuel and boundary conditions over the soot formation in multi-hole diesel injectors using high-speed color diffused back-illumination technique. Applied Thermal Engineering 2019;158:113746. https://doi.org/10.1016/j.applthermaleng.2019.113746.

[7] Gimeno J, Martí-Aldaraví P, Carreres M, Peraza JE. Effect of the nozzle holder on injected fuel temperature for experimental test rigs and its influence on diesel sprays. International Journal of Engine Research 2018;19:374–89. https://doi.org/10.1177/1468087417751531.

[8] Pastor JV, García-Oliver JM, García A, Micó C, Möller S. Application of optical diagnostics to the quantification of soot in n -alkane flames under diesel conditions. Combustion and Flame 2016;164:212–23. https://doi.org/10.1016/j.combustflame.2015.11.018.

[9] Pastor J, Garcia-Oliver JM, Garcia A, Nareddy VR. Characterization of Spray Evaporation and Mixing Using Blends of Commercial Gasoline and Diesel Fuels in Engine-Like Conditions, SAE Technical Paper 2017-01-0843; 2017. https://doi.org/doi:10.4271/2017-01-0843.

[10] Siebers DL. Liquid-Phase Fuel Penetration in Diesel Sprays, SAE Technical Paper 980809; 1998. https://doi.org/10.4271/980809.

[11] Engine Combustion Network | Engine Combustion Network Website, 2021. https://ecn.sandia.gov/.

[12] Siebers D, Higgins B. Flame Lift-Off on Direct-Injection Diesel Sprays Under Quiescent Conditions, SAE Technical Paper 2001-01-0530; 2001. https://doi.org/10.4271/2001-01-0530.

[13] Pastor JV, Garcia-Oliver JM, Garcia A, Pinotti M. Soot Characterization of Diesel/Gasoline Blends Injected through a Single Injection System in CI engines, SAE Technical Paper 2017-24-0048; 2017. https://doi.org/10.4271/2017-24-0048.

[14] Vera-Tudela Fajardo WM. An experimental study of the effects of fuel properties on diesel spray processes using blends of single-component fuels. PhD thesis. Universitat Politècnica de València, 2015.

[15] Benajes J, Payri R, Bardi M, Martí-Aldaraví P. Experimental characterization of diesel ignition and lift-off length using a single-hole ECN injector. Applied Thermal Engineering 2013;58:554–63. https://doi.org/10.1016/j.applthermaleng.2013.04.044.

[16] Kook S, Pickett LM. Liquid length and vapor penetration of conventional, Fischer–Tropsch, coal-derived, and surrogate fuel sprays at high-temperature and high-pressure ambient conditions. Fuel 2012;93:539–48. https://doi.org/10.1016/j.fuel.2011.10.004.

[17] Payri R, García-Oliver JM, Xuan T, Bardi M. A study on diesel spray tip penetration and radial expansion under reacting conditions. Applied Thermal Engineering 2015;90:619–29. https://doi.org/10.1016/j.applthermaleng.2015.07.042.

[18] Payri R, Viera JP, Gopalakrishnan V, Szymkowicz PG. The effect of nozzle geometry over ignition delay and flame lift-off of reacting direct-injection sprays for three different fuels. Fuel 2017;199:76–90. https://doi.org/10.1016/j.fuel.2017.02.075.

[19] Pickett LM, Siebers DL, Idicheria CA. Relationship Between Ignition Processes and the Lift-Off Length of Diesel Fuel Jets, SAE Technical Paper 2005-01-3843; 2005. https://doi.org/10.4271/2005-01-3843.

[20] Xuan T, Desantes JM, Pastor JV, Garcia-Oliver JM. Soot temperature characterization of spray a flames by combined extinction and radiation methodology. Combustion and Flame 2019;204:290–303. https://doi.org/10.1016/j.combustflame.2019.03.023.

[21] Desantes JM, Pastor JV, García-Oliver JM, Pastor JM. A 1D model for the description of mixing-controlled reacting diesel sprays. Combustion and Flame 2009;156:234–49. https://doi.org/10.1016/j.combustflame.2008.10.008.

Chapter 6

Commercial alternative combustion: Spray and combustion characterization of gasoline-diesel blends

Content

6.1 Introduction

This chapter will report the results of the experimental campaign in which the combustion behavior and soot formation of four different blends of commercial gasoline and diesel have been studied. The experiments were carried out in the optically accessible single cylinder engine described in Chapter 3 and under different diesel-like conditions, using a single injection system with the aim of characterizing the autoignition, mixing and combustion processes taking place inside the cylinder. The chapter will contribute with the understanding of the start of combustion and later combustion for diesel−gasoline blends whose potential for LTC strategies is promising. In addition, the limits of using gasoline−diesel blends will be addressed in terms of combustion effectiveness.

In this chapter the fuels and blends used will be described firstly. Then, the test matrix is presented, followed by a description of the experimental set up implemented to analyze the process. Finally, the results will be discussed, focusing first on the combustion performance and later on soot formation.

6.2 Experimental methodology

Experiments were carried out in the optically accessible single cylinder engine which was described in Chapter 3. This facility enables high-temperature and high-density conditions to be reached in a cylindrical shaped combustion chamber. It has one upper port for the fuel injector and four lateral orthogonal accesses. One is used for the pressure transducer while the other three are equipped with quartz optical windows through which the injection and combustion process are visualized. In this campaign an electronically controlled Bosch common-rail capable to achieve injection pressures up to 160 MPa and equipped with a piezoelectric injector of single-hole nozzle, was used. The outlet diameter of the nozzle is 140 μm with a conical shape (K factor of 1.5), which has also been used in different studies by the authors [1–4]. The injection frequency is low during operation and the injector holder is cooled, which allows the nozzle tip and injected fuel temperature to be constant. The injection was placed 3 CAD after TDC and the energizing time was 3 msec.

6.2.1 Fuel characteristics

Four different blends of commercial gasoline and diesel have been used for this study. Diesel is considered as the reference fuel due to high reactivity in this study and represents the zero-substitution rate. The other three blends contain 30%, 50% and 70% of gasoline in volume. Additives or lubricity improvers were not added to the blends. Throughout this chapter, the four blends are identified as “B0” for 100% of Diesel, and “3070”, “5050” and “7030” for the blends with 30%, 50% and 70% of gasoline respectively. The main properties for the two components are detailed in Table 6. 1.

Parameter	Gasoline	Diesel
Density at 15ºC [kg/m^3]	755	834
Viscosity [mm^2/sec]	At 18ºC [0.65]	at 40ºC [2.7]
Lower heating value [MJ⁄kg]	41.2	43.0
Auto ignition [ºC]	400°C	[254-285]
Research cetane number	--	53
Research Octane Number	103	--
$(A/F)_{st}$ at 21% of O_2	14.7:1	14.39:1

Table 6. 1 Fuel Properties

6.2.2 Operating conditions

Four ambient conditions have been considered for this study, which are summarized in Table 6. 2. An ambient density of 22.8 kg/m^3 at Top Dead Centre (TDC) was kept constant, while the temperature at TDC was varied, between Low Temperature (780 K), Medium Temperature (830 K) and High Temperature (870 K).

The oxygen concentration was modified to 15% at high temperature conditions to simulate Exhaust Gas Recirculation (EGR). This 15% O_2 concentration corresponds to an engine EGR rate between 28% and 70% for equivalence ratio values between 1 and 0.4 respectively. In all cases, three rail pressures of 500 bar, 1000 bar and 1500 bar were considered. Each fuel was tested under these operating conditions.

For all experiments performed within the present study, 30 injections have been recorded to reduce the measurement uncertainties due to engine operating variability.

The in-cylinder conditions required by the test plan were calculated using the methodology previously described by Pastor [5,6]. In that procedure, the thermodynamic conditions are calculated from the cylinder pressure using a first-law thermodynamic analysis considering blow-by, heat transfer and mechanical stress. Because of compression, air temperature and density vary with crank angle along the engine cycle and, consequently, during the injection event conditions are not constant. However, in this study it was assumed that temperature of the air interacting with the spray was constant and homogeneous and the values of temperature and density are averaged during a given time interval. For the purpose of this study, the average interval was considered that between the start of injection and ignition. During such interval, temperature variation was always lower than 1%."

Operating Condition	Injection Pressure [bar]	Temperature [K]	Density [kg/m^3]	Oxygen [%]]
LT	500/1000/1500	780	22.8	21
MT		830		21
HT		870		21
LO_2		870		15

Table 6. 2 Test Matrix

6.2.3 Pressure signal analysis

The in-cylinder pressure registered during the combustion cycles has been used to quantify ignition delay (ID). An AVL GU13P pressure transducer coupled to a Kistler 5011 charge amplifier is used for this purpose. The acquisition is synchronized through the flywheel encoder signal, corresponding to a 6 KHz sampling frequency. The system was configured so the motored cycle prior to the one with combustion was recorded. Thus, a difference between them is calculated (ΔP) and the ID is defined as the time elapsed between the injector's start of energizing (SOE) and the first instant when the pressure rise exceeds twice the standard deviation of time-averaged ΔP.

The pressure signal is also used to obtain a heat release (HR) and rate of heat release (RoHR). They were calculated based on the application of the first law of thermodynamics to combustion and motored cycles. It is assumed that the heat transfer is similar for both cycles. In addition, the total amount of fuel injected is negligible in comparison with the trapped air mass, so it is not affecting its thermodynamic properties.

6.2.4 Optical Set up

For the purpose of analysing the effect of the gasoline substitution rate on spray development and soot formation, two different optical techniques have been applied simultaneously: OH^* Chemiluminescence (OH^*) and Diffused Back Illumination (DBI). A sketch of the optical arrangement is shown in Figure 6. 1

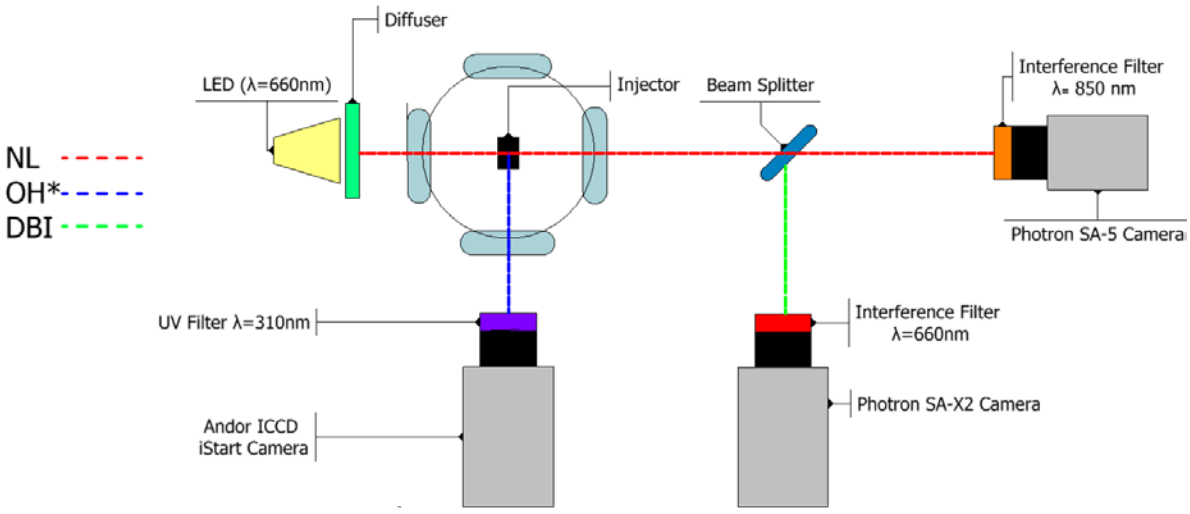

Figure 6. 1 Optical set up

6.2.4.1 High-speed OH* chemiluminescence imaging

The fundamentals of OH* Chemiluminescence have been described in Chapter 4. To summarize, the OH* radicals are good tracer of regions at high temperature regions in a flame [5,7], therefore to quantify the Lift-off length (LOL) is possible through the visualization of OH* Chemiluminescence at the base of the flame. The importance of this parameter lies in the close relationship with the amount of fuel–air mixing process upstream the combustion region. The image processing was done by means of a background segmentation, based on a threshold value, calculated as a percentage of the dynamic range of each image. That means that radiation and background are separated. Then, when the image that content just the radiation, the LOL in this campaign is defined as the average distance between the tip nozzle and the ten nearest pixels of the flame radiation.

In this experimental campaign, the OH* radiation was registered using an Andor Solis iStar ICCD intensified camera equipped with a 100mm focal length f/2 UV objective Bernhard Halle and a 310 nm interference filter (FWHM=10nm). A constant intensifier gating of 1 ms was used and only one image per injection event was recorded from 1 ms to 2 ms after start of energizing (ASOE) with an image resolution of 1024x1024 pixeles and a pixel/mm ratio of 9.1

6.2.4.2 Natural luminosity

Images of natural luminosity (NL) are those obtained by registering the broadband radiation of the flame without using any particular optical filter as it was mentioned in Chapter 5. Taking into consideration the spectral response of the camera, the light collected will almost entirely be in the visible and near infrared range, corresponding to the thermal radiation arising from small soot particles present in the flame. In some cases, it can include a minor contribution of other types of chemiluminescence radiation as well, which can

become significant only in low sooting flames. Qualitative and topological descriptions of the soot flame evolution can be obtained, but no quantitative description of the combustion or soot formation is expected. It is well known that flame radiation does not depend only on soot concentration, but also on flame temperature. Nevertheless, flame radiation can be considered as a qualitative indicator of the amount of incandescent soot in the flame [8–10].

In this work, NL images do not contain the whole broadband radiation spectrum. A bandpass filter centred at 850nm (FWHM = 40 nm) was used to avoid registering the light used for the DBI technique. In Figure 6. 1, the optical arrangement used for NL is shown. These images were recorded with a high-speed camera (Photron Fastcam SA5). The sampling rate was 25 kfps, with a resolution of 336x896 pixels. The exposure time was 40 μsec and a total magnification of 11 pixel/mm. As observed in the figure, a beam splitter with a 50% transmission rate was placed between the camera and the engine to redirect half of the light to the Diffused Back-Illumination extinction imaging (DBI) detector.

6.2.4.3 Diffused back-illumination extinction imaging

Diffused back-illumination extinction imaging (DBI) technique is based on measuring the amount of light attenuated by the soot particles within the flame, which is related to the soot concentration. The principles of this technique were described in Chapter 4 and in this section, the implemented arrangement will be described. Figure 6. 1 shows the optical setup. A red LED (λ = 660nm) was used in these experiments as the light source to create a high-power pulsed illumination. A diffuser was placed in front of the LED to create a diffused Lambertian intensity profile [11]. On the collection side, the transmitted light from the LED and the flame radiation went through a beam splitter with a 50% reflection rate. Then, half of the light was collected by a high-speed camera Photron SA-X2, with 0.29 μs exposure time, 336 × 896 pixels resolution, 25 kfps sampling frequency and a pixel/mm ratio of 11.

The images obtained were analyzed, taking into account that the total light registered by the camera includes two parts: the transmitted LED light intensity and the flame radiation. Due to the use of a bandpass filter centered at 660 nm (FWHM = 10nm), the crosstalk of flame radiation into the DBI signal is minimized. However, the flashing frequency of the LED was set as half of the camera frame rate to capture a flame image between every two consecutive LED pulses. Thus, flame luminosity was quantified and used to isolate the transmitted LED light from the total registered radiation. The light attenuation can then be related with the optical properties of soot cloud through the Lambert-Beer's law, as it was described in the Chapter 4.

In this chapter, the soot formation will be analyzed in terms of KL, which represents the integral value of the soot extinction coefficient along the light path.

To summarize, settings used for each technique are shown in Table 6. 3

Parameter	Optical Technique		
	OH*	NL	DBI
Camera	Andor Solis iStar ICCD	Photron Fastcam SA5	Photron SA-X2,
Exposure time (msec)	From 1 to 2	0.04	0.00029
Filter wavelength (nm)	310 ±10	850 ±40	660±10
Resolution (pixel)	1024x1024	336x896	336x896
Frame rate (kfps)	Single frame	25	25
Pixel/mm	9.1	11	11

Table 6. 3 Main characteristics of the optical techniques used

6.3 Effect of fuel composition on global combustion parameters

6.3.1 Auto-ignition effectiveness

Previous to the analysis of the effect of the different gasoline- diesel blend ratios over the combustion process, it has been considered important to address the feasibility of introducing a low reacting fuel, like gasoline, into a compression ignition engine. For this purpose, the effectiveness of auto ignition has been calculated for the four blends, under all operating conditions considered in this study. This parameter has been defined as the percentage of the cycles or repetitions carried out for each blend in which combustion takes place. The diagnostic has been based on the in-cylinder pressure signal, using the same criterion as the one described for ignition delay calculations.

From this analysis, it has been observed that the combustion takes place in 100% of the cases for fuels B0, 3070 and 5050. For 7030, due to the high proportion of gasoline in the mixture and its low reactivity, there are operating conditions in which combustion does not occur. These are low temperature (LT) and at low oxygen concentration (LO_2). For the first case, effectiveness was 73 % at 500 bar of injection pressure and as injection pressure increases, the effectiveness reduces to 13% at 1000 bar and 7 % at 1500 bar respectively. For the second case, no autoignition was observed.

6.3.2 Effect on ignition delay

Ignition delay was defined, through in-cylinder pressure, as the time elapsed between start of energizing (SOE) and the first instant when there is a pressure rise, when the start of

combustion is detected. Results shown in Figure 6. 2 correspond to the average of 30 cycles tested.

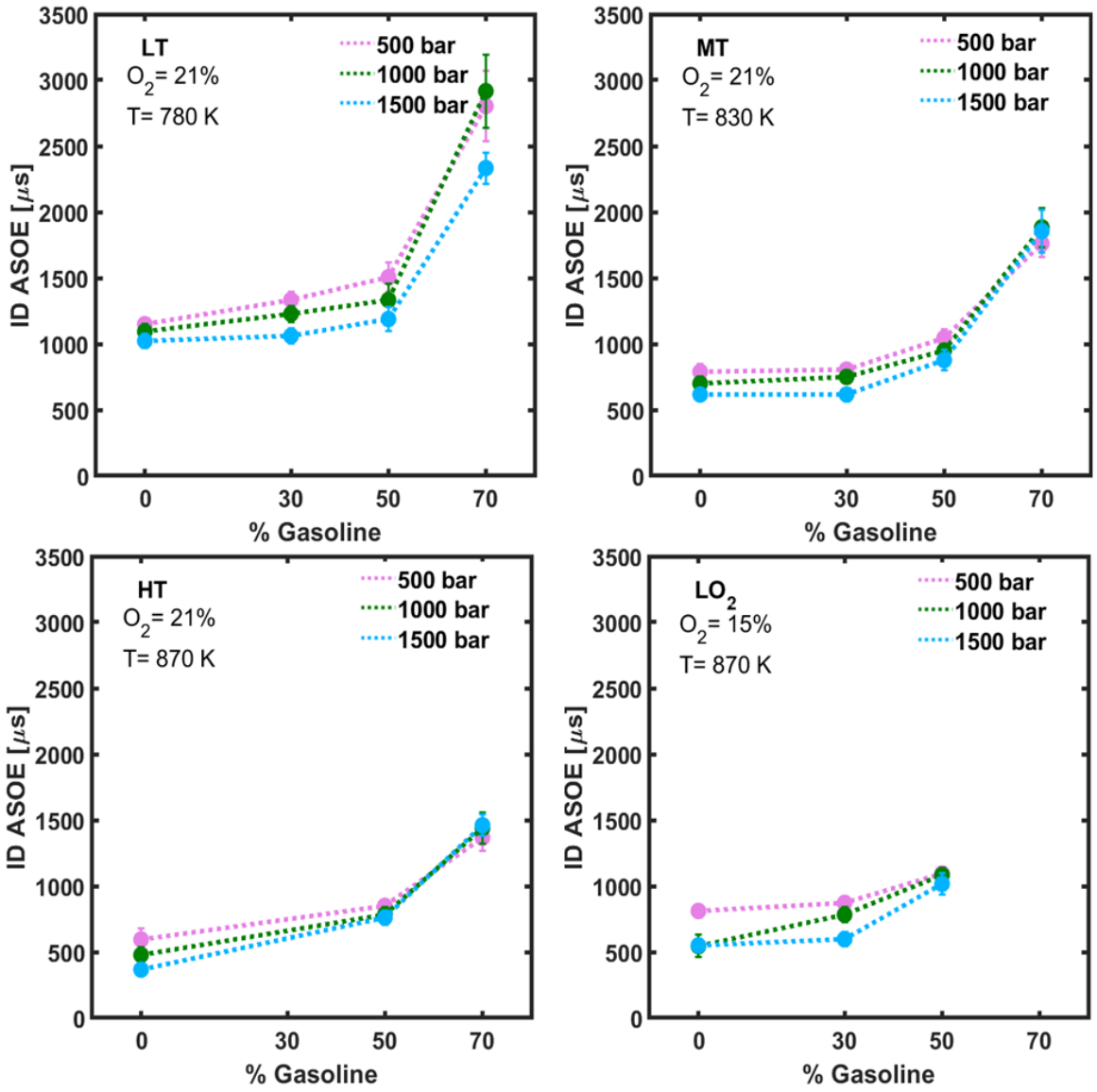

Figure 6. 2 Ignition delay related to gasoline blend ratio for each operating condition

The ignition delay can be observed in Figure 6. 2 for each blend, which is represented in the abscissa axis as the volume fraction of gasoline in the blend (in percent). In addition, the influence of operating conditions on the ignition delay is presented for the three injection pressures. It is worth mentioning that for LO_2, the ID values corresponding to 7030 have not been represented because there was not combustion in any cycle. For the LT case, effectiveness was very low and consequently standard deviation of ID in Figure 6. 2 is higher than for the other cases.

Figure 6. 2 also shows a clear correlation between the ignition delay and the reactivity of the fuel. Therefore, the ID for B0 is the lowest due to the high reactivity of the diesel and, in the opposite case, 7030, it is the highest. As a reference, for MT at 1000 bar of injection pressure, the increase in the ID between B0 and the blends is 50 µs, 250 µs and 1183 µs for 3070, 5050 and 7030. This represent an increment of 7% 35% and 270% respectively. Thus, the increase is not linear with the gasoline content. Furthermore, it is observed that the difference between 5050 and 7030 is bigger than difference between 3070 and 5050. It is expected that the cetane number would be reduced as the proportion of gasoline in the blend increases [12,13], which agrees with the behavior observed in this study. Additionally, Han [14] reports that cetane number is the most dominant factor on the ignition delay time. Another important observation is the change in the gradient between 5050 and 7030 for MT and HT conditions. The gradient is less steep for the HT operating condition. The difference between these two blends for MT conditions is around 933 µs (98%) whereas for HT it is 656 µs (83%), as the higher temperatures promote faster reaction rates.

The effect of temperature and injection pressure on ignition delay is in line with previous studies [15,16], which indicate that an increase of both parameters reduce the ID. On the other hand, a decrease in the oxygen concentration increases the ID due to the fact that the air-fuel blend is less reactive. However, in the case of 7030, the variation of injection pressure does not seem to have an effect on the ID, as the values are very close and the differences between each one is very small. The chemical characteristics of the blend cause a higher delay that avoid observing the effect of injection pressure.

6.3.3 Effect on heat release

Based on the in-cylinder pressure signal, the rate of heat release (RoHR) and the total heat release (HR) were calculated for the four blends and for the different operating conditions. Figure 6. 3 presents the evolution of both magnitudes during the combustion cycle for the blends and the operating conditions considered in this work.

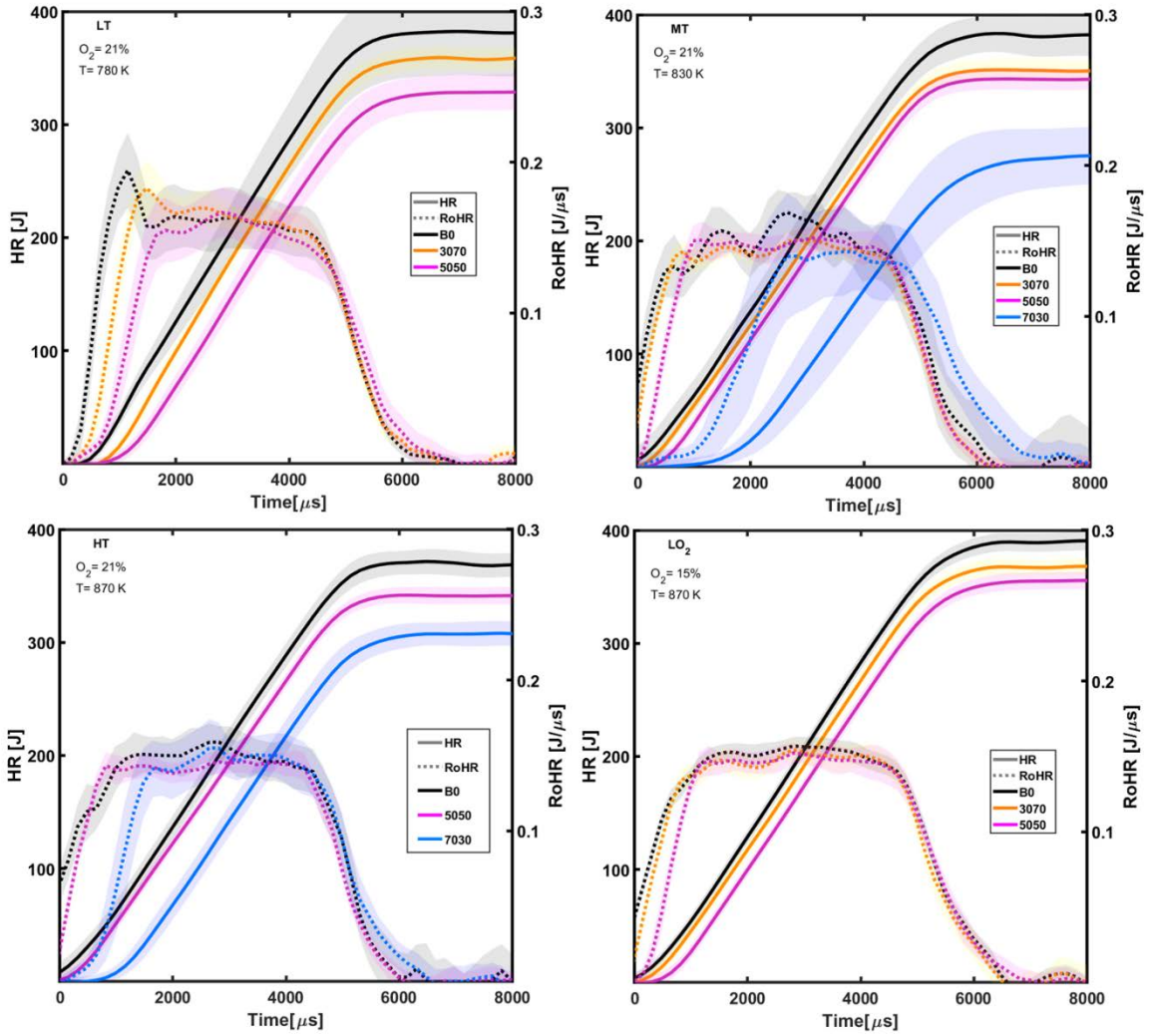

Figure 6. 3 Heat release (HR) and rate of heat release (RoHR) for each blend at different operating conditions and 1000 bar of injection pressure

In general, it is possible to see that an increase in the gasoline fraction in the blend reduces the heat released. Due to its lower reactivity, the ID increases and thus the energy from the fuel starts to be released later in the cycle. However, it can also be observed that combustion finishes more or less at the same time. As a consequence, the HR is lower. Furthermore, differences also arise when comparing the stabilized part of the RHR curves. As it was stated by Pastor [2], the mass flow rate of gasoline-diesel blend varied with the blend ratio. The more gasoline, the less fuel injected. The authors related this behavior mainly to differences in fuel density, based on Equation 6.1:

$$\dot{m}_{blend} = C_v \cdot \sqrt{2 \cdot (P_{inj} - P_{cc}) \cdot \rho_f} \cdot A_{eff} \quad (6.1)$$

Where $\dot{m}_{blend}$ corresponds to mass flow rate, ρ_f is the fuel density, C_v is the velocity coefficient, A_{eff} is the effective area of the orifice, P_{inj} is the injection pressure and P_{cc} is the pressure inside the combustion chamber. Additionally, results presented in [2] were obtained with the same injection system and operating conditions. Thus, they have been used in this paper to confirm the differences observed in RoHR between blends. Equation (6.2) shows the relationship between chemical rate of heat release (RoHR) and the mass flow rate of B0 and each one of the blends. RoHR corresponds only to the amount of energy available in the fuel, $\dot{m}_{B0}$ and ρ_{B0} refer to the mass flow rate and density of pure diesel and LHV_{blend} is the Low Heat Value for each blend assessed.

$$\boldsymbol{RoHR_{blend} = \dot{m}_{B0} \cdot \sqrt{\frac{\rho_{blend}}{\rho_{B0}}} \cdot LHV_{blend}} \tag{6.2}$$

Table 6. 4 shows the comparison between B0 and the other blends. The similarities observed between the experimental results and the calculations confirm the observed trends and justify that the differences of RoHR between the blends are due to their different densities and lower heating values.

Fuel	$RoHR_{blend}/RoHR_{B0}$ **Calculated (%)**	$RoHR_{blend}/RoHR_{B0}$ **Experimental (%)**
3070	91.34	91.80
5050	87.83	89.98
7030	69.11	71.95

Table 6. 4 Comparison between calculated and experimental rate of heat release with respect to B0 at MT operating conditions and 1000 bar of injection pressure

The lower RoHR is reflected directly in a reduction of the total HR. Therefore, the longer ID mentioned previously, together with the difference in rate of heat release, cause a reduction of the HR when the content in gasoline increases, reaching a difference of up to around 10% between B0 and 3070 and 5050, whereas in the case of 7030, the difference with respect to B0 is approximately 30% at the MT operating condition.

6.3.4 Effect on Lift-off length

Figure 6. 4 shows the Lift-off length (LOL) for each blend at the operating conditions defined in this paper. The abscissa axis represents the volume fraction of gasoline present in the blend as a percentage. Again, for LT and LO_2 operation conditions, LOL values corresponding to 7030 are not represented due to the low combustion effectiveness.

The trends observed for LOL are similar to those reported for ID. When the content of gasoline in the blend increases, the LOL increases too.

Analyzing the effects of boundary conditions, it can be observed that the results correspond to those found in the literature [15–17]. LOL decreases with increasing ambient temperature and density, as it reduces the amount of air required to burn the fuel injected.

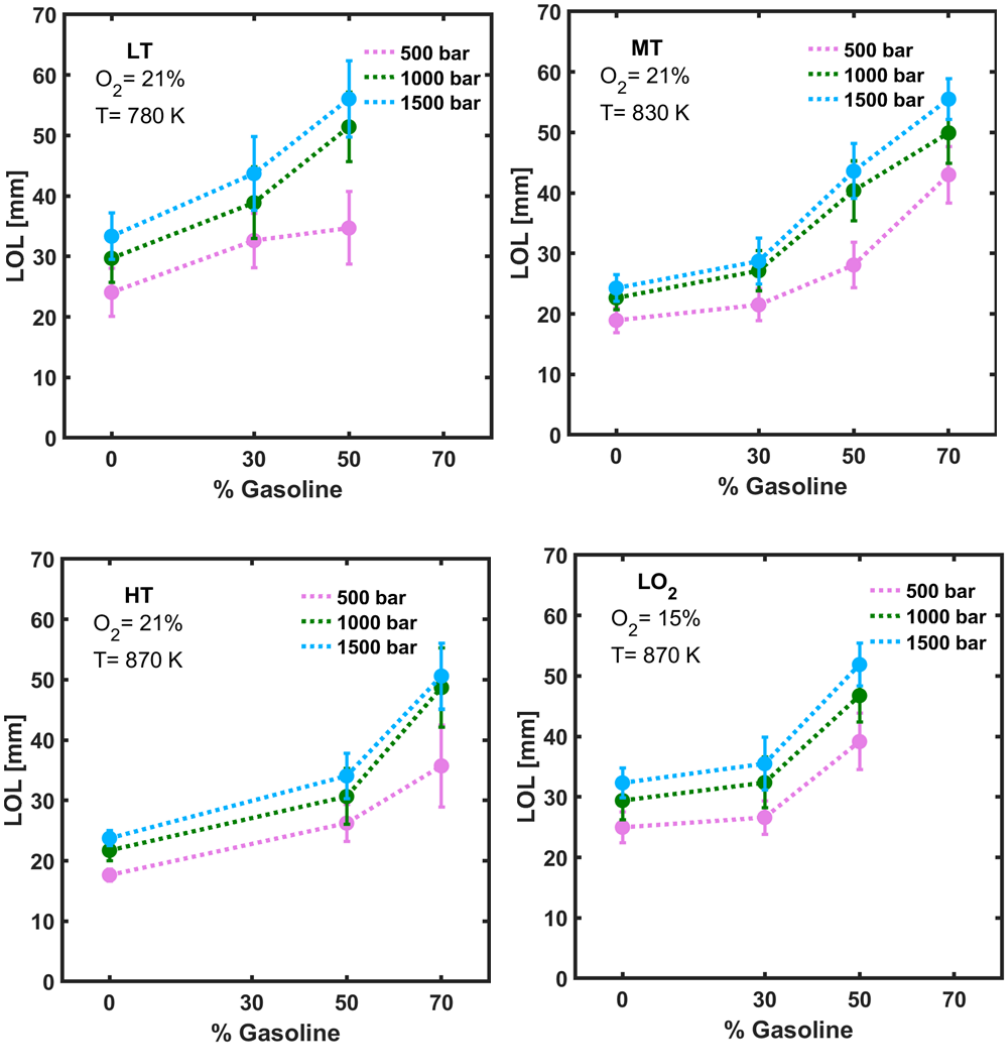

Figure 6. 4 Lift-off Length for each operating condition and each blend

In addition, Figure 6. 4 shows that the standard deviation is higher when the blends contains gasoline and therefore the gasoline addition made it difficult to achieve Lift-off stability.

6.4 Effect of fuel composition on soot formation

For the study of soot formation, the cases with a higher content of diesel (B0) and gasoline (7030) are represented, as well as an intermediate blend (5050) to verify the observed trend. Therefore, from now on, the analysis will be for B0, 5050 and 7030.

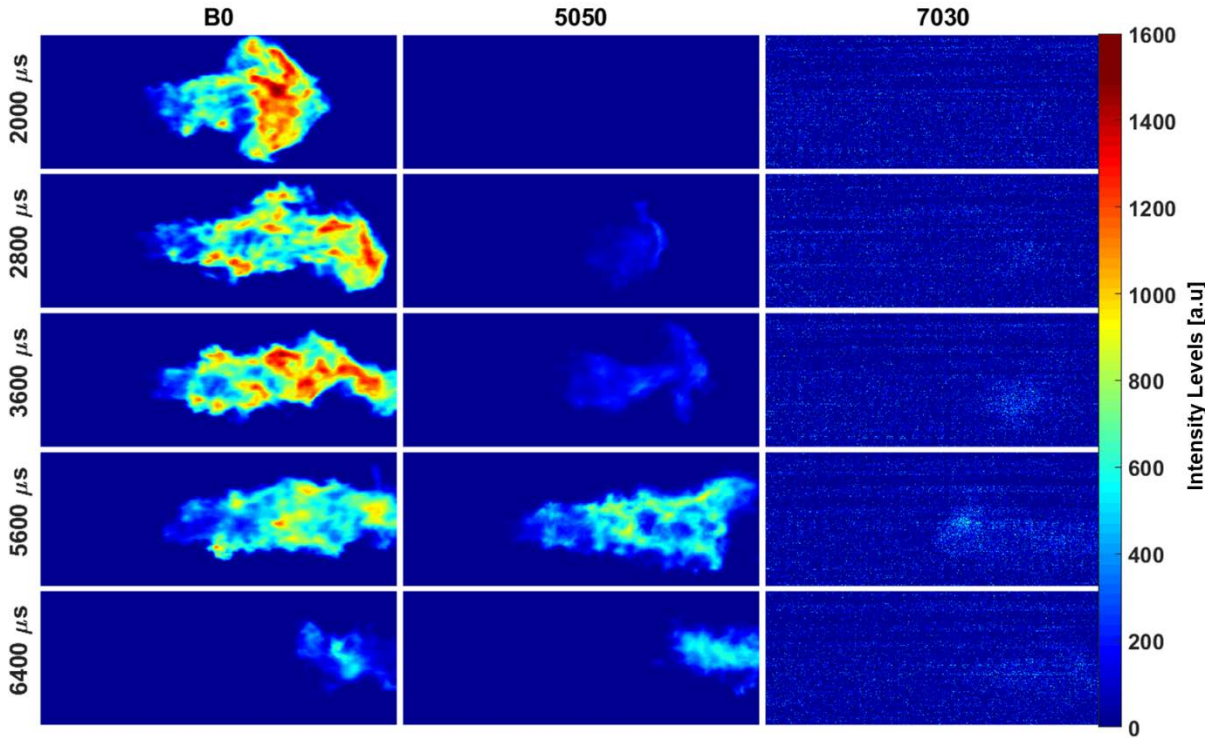

Figure 6. 5 Flame natural luminosity for blends tested at MT operating conditions and 1000 bar of injection pressure. 7030 intensity levels have been increased 30 times

Figure 6. 5 shows the flame natural luminosity for blends tested at MT operating conditions and 1000 bar of injection pressure. A temporal evolution is represented, by means of several frames recorded with the high-speed camera. For 7030, the luminosity did not reach sufficient intensity levels to be compared with others blends. For that reason, it has been increased 30 times and even so, it is not possible to observe the flame intensity of 7030. Images shown in Figure 6. 5 correspond to single combustion cycles.

The amount of natural radiation registered does not just depend on the soot concentration, but also on the temperature [9]. If it is considered that all blends have the same flame temperature, a qualitative analysis of soot formation can be done. Thus, in Figure 6. 5, it can be observed that soot formation decreases with the increase of gasoline in the blend. In addition, soot appears later and also farther from the injector. This is coherent with the results reported previously. Both ID and LOL increase with the gasoline volume fraction, allowing more air entrainment before combustion and hence a more homogeneous mixture, which leads to a decrease in soot formation.

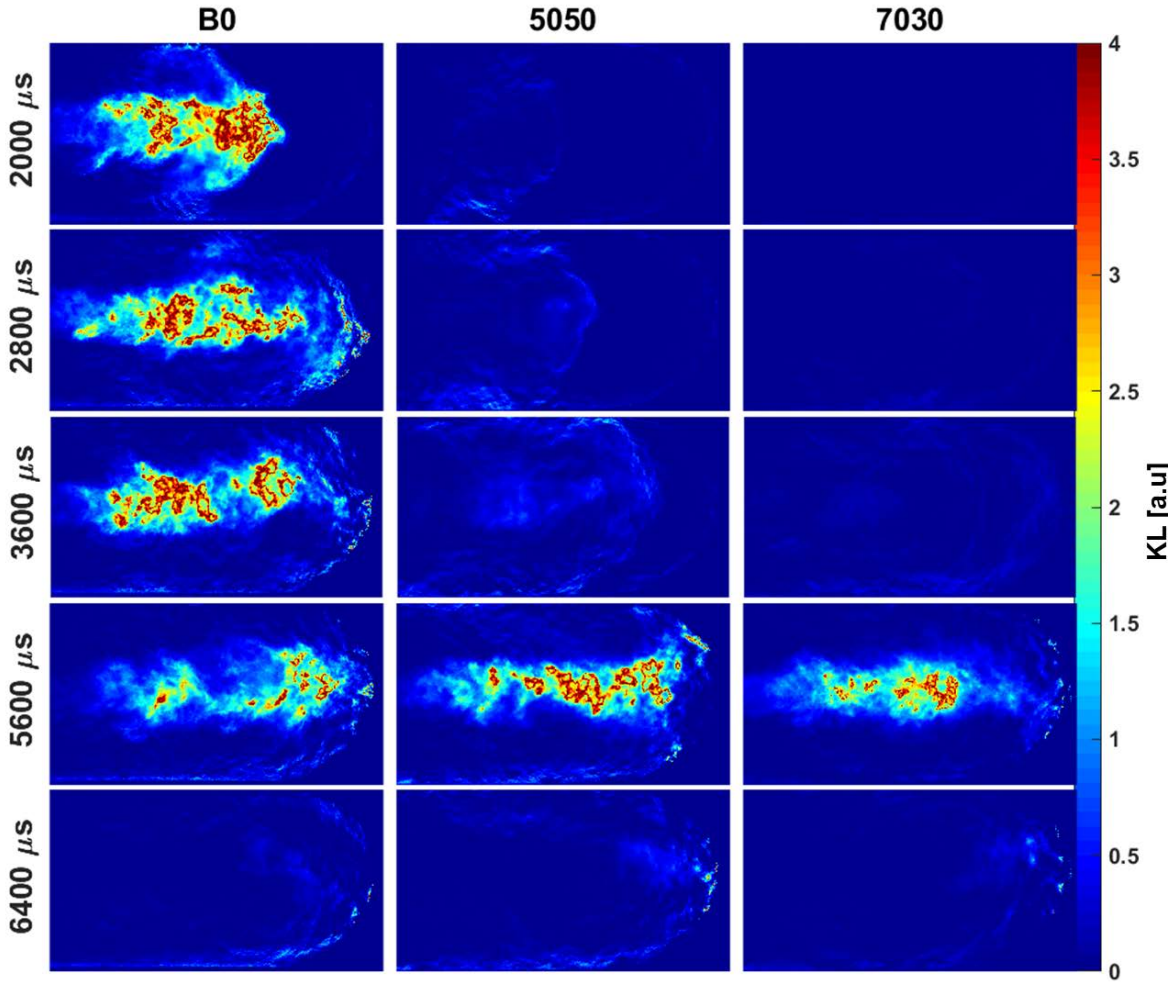

Figure 6.6. Light extinction for each blend at MT operating condition at 1000 bar of injection pressure. The scale (on right hand side) represent the KL parameter

In order to quantify the soot formed, images from DBI were used to determine the soot KL factor. It is an indicator of the flame soot concentration, as was explained in the methodology section. Figure 6.6 represents the light extinction obtained for each blend at the MT operating conditions and 1000 bar of injection pressure. These images correspond to a single combustion cycle; the same one that was used in Figure 6. 5 in the same time interval.

In Figure 6.6, it can be observed that the combustion behavior is similar to that studied with the pressure transducer and also with natural luminosity; when the gasoline content in the blend is greater, the combustion starts later and therefore the soot also appears later. In addition, an increase in the amount of gasoline produces a lower concentration of soot.

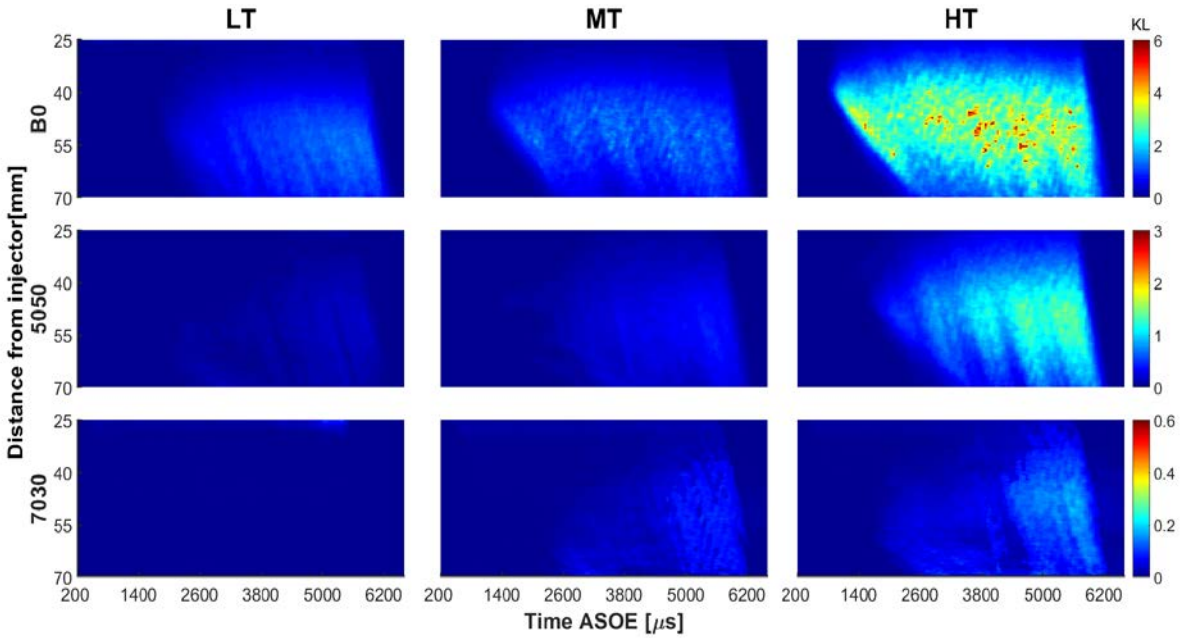

Figure 6. 6 Temporal and Spatial KL evolution at 1000 bar for LT, MT and HT operating conditions

Figure 6. 6 represents the spatial and temporal evolution of soot KL, as an average of the 30 repetitions tested. In this figure, the KL value is averaged along the radial direction of the flame. Thus, for each instant recorded, the corresponding KL image is transformed into a 1D-vector. After that, all vectors are concatenated to create a 2D-matrix of KL values, which correspond to each map shown in Figure 6. 6. As a result, the vertical axis represents the distance from the nozzle while the horizontal axis represents time ASOE. For a clear visualization of the map, a color scale has been used as a function of the KL values for each blend. Note that the 5050 and 7030 scales are 50% and 10% of the B0 scale respectively.

It can be observed in the maps that as the proportion of gasoline increases, the soot concentration decreases. This is due to the lower reactivity of gasoline, resulting in a longer ignition delay and a longer flame lift-off length, as was discussed previously. Regarding its evolution, it is possible to see that in general, the more gasoline content in the blend, the later the soot appears. Furthermore, its distribution is also less uniform along the cycle. For B0, as soon as soot is visible, the concentration remains at its maximum value almost up to the end of the combustion process. With respect to 7030, the first soot is detected around 2600 μs ASOE. However, its concentration starts increasing between 5000 μs and 6000 μs ASOE, when its maximum is reached.

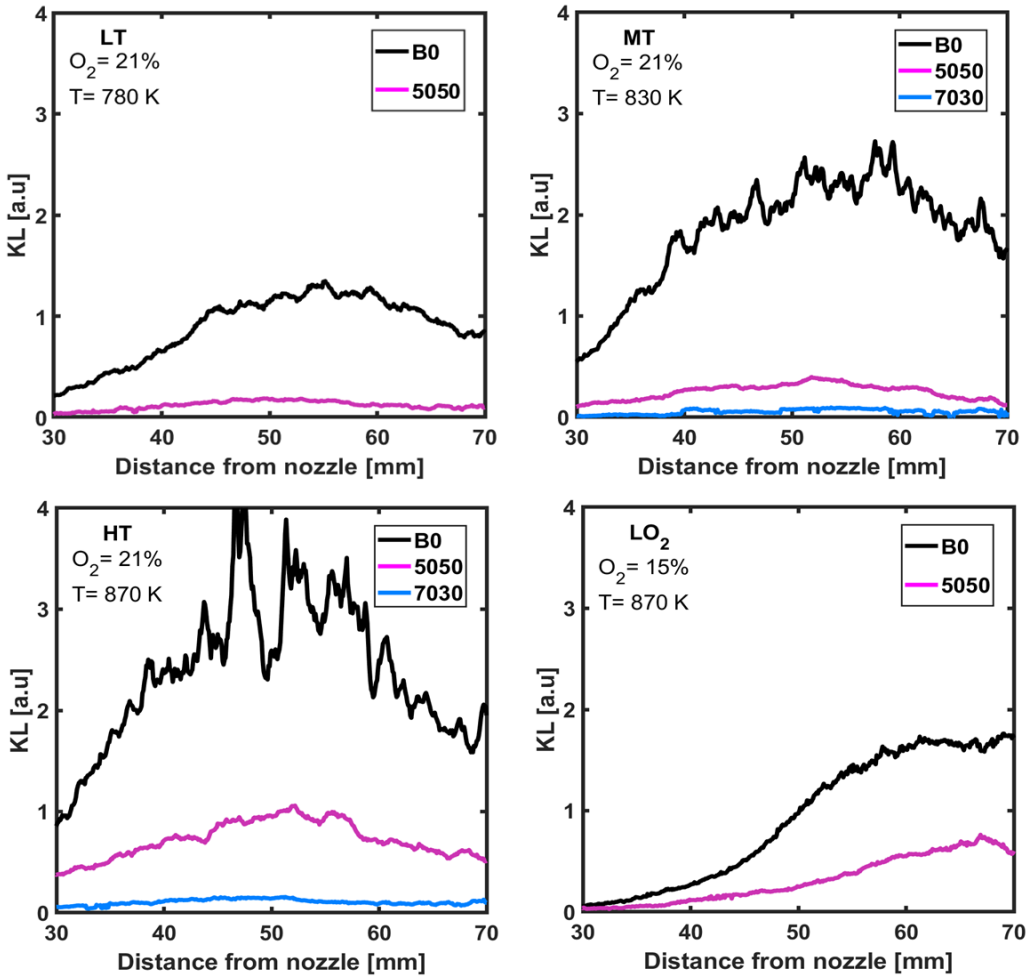

Figure 6. 7 KL evolution through spray axis at 1000 bar of injection pressure and at 5000 μs ASOE

In order to obtain a quantitative comparison, Figure 6. 7 shows the KL evolution along the flame axis at 5000 μs from the start of the energizing (ASOE). This time has been chosen to ensure that all blends reach a "stabilized" state (eliminating the influences of possible transient phenomena). Results correspond to the average of 30 cycles. The trends discussed previously are also observed in this figure. A higher temperature promotes more soot formation because of a faster combustion process, as the results shown for ID and LOL confirm. Furthermore, a higher percentage of gasoline in the blend ensures the soot reduction for any operating condition. By comparing B0 and 5050 in Figure 6. 7, it is also possible to observe that the difference between the maximum values are slightly larger when the temperature is higher. This could be because at higher temperatures, the diesel autoignition is faster, preventing the formation of a more homogeneous mixture and as consequence, the soot formation is favored

6.5 Summary and conclusions

Along this chapter, the behavior of different gasoline-diesel blends in an optically accessible single cylinder engine under different ranges of ambient gas temperature, oxygen concentration and injection pressures have been presented. It was used a single hole injector with conical shape (k=1.5) and outlet diameter of 140 μm. Measurements of ID, LOL, heat released, and soot formation were carried out by means of signal pressure and images obtained with OH^* chemiluminescence, Natural luminosity and Diffused back illumination. The most relevant findings lead to the following conclusions:

- It is possible to use gasoline-diesel blends in a compression ignition engine with similar characteristics to those used in this study. It was demonstrated that at least until 50% of gasoline in the blend, the combustion effectiveness is not affected, even in operating conditions with low temperatures and low oxygen concentration, where the reaction velocity is slow. At 70% of gasoline the combustion effectiveness was seriously reduced when the temperature and oxygen concentration were 780 K and 15% respectively
- Gasoline–diesel blends present lower reactivity compared to pure diesel. It decreases when increasing the gasoline ratio. As a consequence, the ignition delay and Lift-off length were affected, both increasing with the gasoline volume fraction. When gasoline was increased 30% in the blend, ID increased around 7% and LOL almost 20% at 830 K 1000 bar of injection pressure respect to B0. The tendency was similar for other temperature, oxygen concentration and injection pressure. For 50% of gasoline the increment was 35% for ID and 70% for LOL respect to B0. However, for 70% of gasoline the increment was very high: 2.7 times for ID and 2.15 times respect to B0 for 830 K and 1000 bar. Thus, the increment is not linear with the gasoline content.
- A delay in the start of combustion had an impact on heat release. It was observed that it started later in the cycle for the less reactive blends, but finished almost at the same time as the more reactive ones. On the other hand, the blend density affected the injection mass flow rate, which also has an impact on the amount of available energy and therefore the heat release during the whole cycle.
- As the gasoline content of the blended fuel was increased, the soot emission was reduced considerably. It has been related with the lower reactivity of the blends, which leads to more fuel-air mixing before auto ignition and therefore a more homogenous mixture. For 50% of gasoline in the blend, the KL was reduced 80% approximately when the temperature was 830 K and the injection pressure was 1000 bar. For 70% of gasoline the difference between KL values was around 90%. The tendency was similar in the other operating conditions.

References

[1] Pastor JV, García-Oliver JM, García A, Micó C, Möller S. Application of optical diagnostics to the quantification of soot in n -alkane flames under diesel conditions. Combustion and Flame 2016;164:212–23. https://doi.org/10.1016/j.combustflame.2015.11.018.

[2] Pastor J, Garcia-Oliver JM, Garcia A, Nareddy VR. Characterization of Spray Evaporation and Mixing Using Blends of Commercial Gasoline and Diesel Fuels in Engine-Like Conditions, SAE Technical Paper 2017-01-0843; 2017. https://doi.org/doi:10.4271/2017-01-0843.

[3] Pastor JV, García-Oliver JM, García A, Pinotti M. Effect of laser induced plasma ignition timing and location on Diesel spray combustion. Energy Conversion and Management 2017;133:41–55. https://doi.org/10.1016/j.enconman.2016.11.054.

[4] Pastor JV, García-Oliver JM, García A, Pinotti M. Laser induced plasma methodology for ignition control in direct injection sprays. Energy Conversion and Management 2016;120:144–56. https://doi.org/10.1016/j.enconman.2016.04.086.

[5] Pastor JV, Payri R, Gimeno J, Nerva JG. Experimental Study on RME Blends: Liquid-Phase Fuel Penetration, Chemiluminescence, and Soot Luminosity in Diesel-Like Conditions. Energy & Fuels 2009;23:5899–915. https://doi.org/10.1021/ef9007328.

[6] Pastor JV, García-Oliver JM, Nerva J-G, Giménez B. Fuel effect on the liquid-phase penetration of an evaporating spray under transient diesel-like conditions. Fuel 2011;90:3369–81. https://doi.org/10.1016/j.fuel.2011.05.006.

[7] Reyes M, Tinaut FV, Giménez B, Pastor JV. Effect of hydrogen addition on the OH* and CH* chemiluminescence emissions of premixed combustion of methane-air mixtures. International Journal of Hydrogen Energy 2018;43:19778–91. https://doi.org/10.1016/j.ijhydene.2018.09.005.

[8] Siebers D, Higgins B. Flame Lift-Off on Direct-Injection Diesel Sprays Under Quiescent Conditions, SAE Technical Paper 2001-01-0530; 2001. https://doi.org/10.4271/2001-01-0530.

[9] Pastor JV, Garcia-Oliver JM, Garcia A, Pinotti M. Soot Characterization of Diesel/Gasoline Blends Injected through a Single Injection System in CI engines, SAE Technical Paper 2017-24-0048; 2017. https://doi.org/10.4271/2017-24-0048.

[10] Pastor JV, García JM, Pastor JM, Buitrago JE. Analysis Methodology of Diesel Combustion by Using Flame Luminosity, Two-Colour Method and Laser-Induced Incandescence, SAE Technical Paper 2005-24-012; 2005. https://doi.org/10.4271/2005-24-012.

[11] Xuan T, Pastor JV, García-Oliver JM, García A, He Z, Wang Q, et al. In-flame soot quantification of diesel sprays under sooting/non-sooting critical conditions in an optical engine. Applied Thermal Engineering 2019;149:1–10. https://doi.org/10.1016/j.applthermaleng.2018.11.112.

[12] Wang J, Yang F, Ouyang M. Dieseline fueled flexible fuel compression ignition engine control based on in-cylinder pressure sensor. Applied Energy 2015;159:87–96. https://doi.org/10.1016/j.apenergy.2015.08.101.

[13] Yanowitz J. Compendium of Experimental Cetane Numbers. National Renewable Energy Laboratory (NREL); 2017.

[14] Han M. The effects of synthetically designed diesel fuel properties – cetane number, aromatic content, distillation temperature, on low-temperature diesel combustion. Fuel 2013;109:512–9. https://doi.org/10.1016/j.fuel.2013.03.039.

[15] Benajes J, Payri R, Bardi M, Martí-Aldaraví P. Experimental characterization of diesel ignition and lift-off length using a single-hole ECN injector. Applied Thermal Engineering 2013;58:554–63. https://doi.org/10.1016/j.applthermaleng.2013.04.044.

[16] Pickett LM, Siebers DL, Idicheria CA. Relationship Between Ignition Processes and the Lift-Off Length of Diesel Fuel Jets, SAE Technical Paper 2005-01-3843; 2005. https://doi.org/10.4271/2005-01-3843.

[17] Payri R, Salvador FJ, Manin J, Viera A. Diesel ignition delay and lift-off length through different methodologies using a multi-hole injector. Applied Energy 2016;162:541–50. https://doi.org/10.1016/j.apenergy.2015.10.118

Chapter 7

Conclusions and future works

Content

7.1 Introduction

The work carried out in this thesis has sought to assess the potential of alternative fuels on the soot formation, through the identification and quantification of the effect of their properties in the different stages of the combustion process. To achieve this, seven alternative fuels were selected based on their potential to reduce pollutants and their feasibility of implementation in internal combustion engines. These fuels come from fossil and renewable sources. These were: blends of diesel and gasoline, blends of Hydrotreated Vegetal Oil (HVO) and Liquefied Petroleum Gas (LPG), pure HVO and two oxymethylene ethers: OME_1 and OME_x. All of them have potential both in engine emission reduction and global CO_2 reduction as it was established in Chapter 2. In that chapter, these fuels were described in terms of physical-chemical properties, production, storage, distribution, performance and potential to be implemented in compression ignition engines. Also, pure diesel and dodecane were tested in this thesis to be used as reference fuels for comparisons. It is important to mention that dodecane is quite similar to diesel, although slight differences exist in terms of main combustion parameters and soot production. With the results obtained in this thesis, dodecane confirms to be a good surrogate for diesel and HVO.

The facilities where the experimental campaigns were carried out, as well as the single hole nozzle and the single injection strategy, were chosen with the aim to avoid uncertainties such as the interaction of the jet with cylinder wall and the interaction between jets and thus to simplify the analysis of the combustion and soot behavior of these alternative fuels. These facilities were described in Chapter 3. Moreover, a wide variety of optical techniques used for combustion analysis were also briefly described there.

The experimentation was carried out in three campaigns. In the first campaign, described in Chapter 4, the main spray and combustion characteristic were analyzed for HVO, OME_1 and OME_x. These characteristics were compared with those of commercial diesel and dodecane. The experiments were carried out in the High Pressure and High Temperature facility (HPHT) for two nozzles with orifice diameter of 89.4 µm (SA) and 189 µm (SD) similar to those used in light and medium duty diesel engines. The operating condition were defined using as baseline, the guidelines recommended by the Engine Combustion Network (ECN). The visualization techniques implemented were schileren, OH^* chemiluminescence, and Diffused Back Illumination (DBI). With these techniques autoignition, macroscopic combustion parameters and soot formation were studied. Results obtained for the dodecane with both SA and SD at the baseline condition: 900 K 1500 bar and 15% of O_2 are consistent with those found in the ECN database, which provides confidence in the reliability of the results of this study.

In the second campaign, detailed in Chapter 5, an alternative dual fuel combustion strategy was analyzed. The experiments were also carried out in the HPHT facility but it was necessary to adapt the injection system for injecting two fuels that in ambient conditions were in different phases. Those fuels were blends of HVO and LPG. Changing the fuel reactivity of the blend the main combustion parameter and soot formation were studied using schlieren, OH^* chemiluminescence and natural luminosity (NL).

In the last campaign, described in Chapter 6, a commercial alternative combustion was studied. The behavior of gasoline and diesel blends as well as their effect on combustion performance were analyzed. The experiments were carried out in the optically accessible single cylinder engine described in Chapter 3. The combustion effectiveness, autoignition, combustion behavior and soot formation were studied by means of a pressure transducer and optical techniques such as OH^* chemiluminescence, DBI and NL.

This chapter will summarize the main contributions and the main conclusions drawn from the research work. Then, a synthesis for all fuels tested will be presented in terms of theoretical correlations and thus to establish a comparison between them. At the end of this chapter, some suggestions for future works which could contribute with better understanding about combustion behavior and engine performance of alternative fuels assessed in this thesis will be proposed.

7.2 Main contributions of this thesis

A special contribution of this thesis has been the development of an extensive database for multiple fuels. It contains fundamental and useful combustion parameters that will help to the validation of new models and computational codes. This database includes values of liquid length, ignition delay and Lift-off length. Furthermore, the temporal evolution of parameters such as Lift-off length, vapor penetration, and flame penetration are part of this database. In addition, spatial distribution and temporal evolution of optical thickness (KL) parameter are also given for OME_1, OME_x, HVO, diesel and dodecane. Moreover, fundamental data has also been given for HVO-LPG and diesel-gasoline blends that will allow to validate CFD results for those fuels.

Additionally, this thesis has contributed methodologically as follows:

- It was possible to implement several visualization techniques simultaneously through spectral filtering of light. The optical arrangements were established in such a way that using dichroic mirror, and interference and bandpass filters, the useful wavelength could be collected for a certain technique. Therefore, in each experimental campaign, a minimum of three optical techniques were used.
- The criterion for obtaining the ignition delay (ID) from the Schlieren images was optimized. In this thesis, the ID was defined as the mean time where the minimum and maximum accumulated intensity increment occurs, instead of the time where the maximum occurs, which overestimated the ID value. This criterion was contrasted

with the raw images and compared with the ID obtained from the OH^* chemiluminescence technique. In both comparisons, the new criterion demonstrated to be quite accurate.

- The accuracy of DBI technique in terms of signal collection was improved in this thesis. Some high speed camera sensors are disturbed when they are excited with strong flashes of light. Thus the signal after a strong flash of light is not fully recorded. In other words, the accuracy is lost as a consequence of the loss of this signal radiation not registered by the camera. This phenomenon is known as "*image lag*". For this reason, the image acquisition methodology was optimized when the DBI technique was implemented in chapter 4. In this case, a configuration of “1 to 3” was used. This means that for each image with LED, three images without LED light were registered. It was confirmed that the last image without LED registered the entire flame radiation.
- A injection system was adapted to keep the fuel mixture in liquid phase throughout the entire injection line, even with the highest proportions of LPG in the mixture. This adaptation was designed to maintain the injection line at high pressure and low temperature and thus, avoid evaporation throughout the entire injection line. This system proved to be reliable, it behaved in a stable and repetitive manner throughout the experimental campaign. Although it has been a laboratory prototype, this opens the doors for the design of a much more developed commercial injection system in the future.

7.3 Conclusions of the experimental studies

In this part, the main conclusions for the experimental results are presented. The conclusions have been done in terms of auto-ignition, macroscopic combustion parameters and soot formation, first for pure fuels, then for blends of HVO-LPG and finally for diesel-gasoline blends.

7.3.1 Effect of fuel composition and nozzle diameter on a diffusion combustion spray

The analysis of combustion behavior of low carbon alternative fuels has been developed in Chapter 4. The main combustion characteristics were analyzed for Hydrotreated Vegetable Oil (HVO), oxymethylene ethers: OME_1 and OME_x.

Regarding the combustion behavior, it was found that:

- Changing the nozzle diameter produces the same effect for all fuels but not in the same proportion. Characteristics such as liquid length, vapor penetration, ignition delay and soot formation present higher values when the bigger nozzle diameter (SD) is used. However, as mentioned previously, the proportion of change depends on the chemical composition of the fuel. In the case of oxymethylene ethers (OME_1 and OME_x), as the combustion takes place in a lean stoichiometric environment, the effect

of changing the nozzle is not very significant in terms of characteristic spray parameters.

- Characteristics such as the liquid length correlate with the distillation temperature of each fuel, being the OME_1 the fuel with the lower distillation temperature and therefore, the shorter liquid length.
- In terms of vapor penetration, all fuels showed the same behavior before auto ignition because this parameter is governed by the momentum flux conservation at the nozzle orifice.
- The autoignition process is strongly dependent on fuel characteristics. The ID trend matches the cetane number. HVO ignites very close and earlier than diesel. However, OME_x ignites before the other fuels although its cetane number is not the highest, but its shorter ID is due to the oxygen in its molecular structure which improves its ignition. As it was expected, the ID for SD is higher than for SA. However, this trend was the opposite for OME_1, although it is true that it ignited after the other fuels, when the spray A was used, the ID was higher than SD. This is a consequence of its chemical composition, since for SA the equivalent ratio in the reaction zone is less or equal to 1, which means that there is an overmixing.
- When the flame Lift-off length was analyzed in the Chapter 4, it was determined that the longest LOL was for OME_1, which is quite far from OME_x and the other fuels. Conversely, OME_x has a closer behavior to HVO, diesel and dodecane in all operating conditions. The LOL follows the ID trend for diesel, HVO and OME_x. Higher ID produced longer LOL. However, for OME_1 although the SD had shorter ID than SA, when the LOL was analyzed, the LOL was longer with the SD. That means that LOL increases when the nozzle diameter increases too. However, increasing the orifice diameter worsen the air entrainment, this result in an increase of the equivalent ratio (Φ). Therefore, for smaller orifice diameters the mixing process improves, which means that vaporization process improves and the amount of air entrainment increases too, producing leaner mixtures.
- Regarding flame penetration for the different fuels, it was found that oxymethylene ethers: OME_1 and OME_x, stabilize early while HVO and diesel reach the flame stabilization later as a consequence of the fuel's stoichiometry. OME_1 flame stabilizes at lean air-fuel ratio therefore the flame length was the shortest.
- As a consequence of the low equivalence ratio of oxymethylene ethers, in addition to the oxygen content in their molecule and the absence of C-C bonds, no soot was detected at any operating condition for both nozzles. In the case of HVO, soot formation was observed in the whole test matrix, although the soot production was less than diesel. This is related with the absence of aromatic compounds in HVO formulation.

7.3.2 Dual fuel combustion of HVO-LPG blends

Implementing a dual injection system with two fuels in different phases at ambient conditions was possible. The combustion performance of different blends of Hydrotreated Vegetal Oil (HVO) and Liquified Petroleum Gas (LPG) was evaluated under compression ignition engine conditions in Chapter 5. The HVO was considered as the high reactivity fuel and the LPG was the low reactivity fuel.

Regarding combustion characteristics it was found that:

- The content of LPG in the blend did not affect the vapor penetration results. Before ignition, pure HVO and the blends HVO-LPG did not show differences respect to vapor penetration. As it is well known, this parameter depend on the momentum flux and this in turn depends on nozzle diameter. In this experimental campaign all blends were assessed with the same nozzle which justifies that no differences were observed.
- When the ignition delay was evaluated, the LPG demonstrated acting as an ignition inhibitor of HVO. Ignition delay increases with the LPG content. In the same way, the LOL increased when increasing proportion of LPG.
- The flame luminosity for blends was smaller than for pure HVO, and it decreased when LPG content was higher. This can be related to less soot formation, as a consequence of more air entrainment due to larger ID and LOL.

7.3.3 Combustion behavior of gasoline-diesel blends

The behavior of gasoline and diesel blends in different proportions: 30% 50% and 70% of gasoline as well as the effect on combustion performance were analyzed. The measurements were done using a pressure transducer and implementing optical techniques such as OH^* chemiluminescence, DBI and natural luminosity. The results obtained in this experimental campaign indicated that:

- The combustion effectiveness was 100% until 50% of gasoline in the blend. Increasing the content of gasoline in the blend over 50% affected this parameter in the operating points at low temperature and oxygen concentration. The blend reactivity decreased as the gasoline content increased.
- Parameters such as ignition delay and Lift-off length increased with the gasoline volume fraction but not linearly with gasoline content.
- The increment in the ID had an impact on heat released, although the start of combustion was delayed for less reactive blends, the combustion finished at the same time as the more reactive ones, because the density of the blends affected the injection mass flow rate, which also has an impact on the amount of available energy and therefore the heat release during the whole cycle.
- The total heat release for small proportions of gasoline in the mixture was not considerably affected. Therefore, using could represent a good solution to maintain the power and efficiency in engines

- Soot production was reduced with the increment of gasoline content. That is related with the lower reactivity of the blends which leads to more fuel-air mixing before auto ignition and therefore a more homogenous mixture. For 50% of gasoline in the blend, the KL was reduced 80% approximately at medium temperature (830 K). For 70% of gasoline the difference between KL values was around 90%.

The availability of these fuels in the market would allow to implement these blends as a short term solution to achieve the objectives of reducing pollutants in diesel engines. Moreover, the results presented in this thesis would allow predicting or estimating the engine's efficiency that is penalized when this blends are implemented.

7.4 Synthesis

The fuels analyzed in this thesis were studied in three experimental campaigns and in two different facilities, as it was mentioned previously. Therefore, establishing a direct comparison between them would not be correct, since the thermodynamic variations in each installation were different and they are not comparable. However, making a comparison based on existing theoretical correlations is possible and interesting. This allows to demonstrate the behavior in terms of characteristic combustion parameters such as the ignition delay and the Lift off length regardless of the installation where the fuels have been tested. Thus, in Figure 7. 1 the ignition delay (left) and Lift-off length (right) obtained in chapters 4, 5 and 6 are compared with the results obtained with the theoretical correlations for ID and LOL presented in Chapter 5. The ID* and LOL* in the axial axis represent the proportionality stated in equation 5.1 and 5.2.

$$\boldsymbol{ID^{*} \propto \exp\left(\frac{7523}{T_{amb}}\right) \cdot \rho_{amb}{}^{-1.35} \cdot (P_{inj} - P_{amb})^{-0.09} \cdot O_{2\%\,amb}{}^{-0.51}} \qquad (5.1)$$

$$\boldsymbol{LOL^{*} \propto T_{amb}{}^{-3.89} \cdot \rho_{amb}{}^{-1} \cdot \left(\sqrt{2 \cdot \frac{P_{inj} - P_{amb}}{\rho_{fuel}}}\right)^{0.54} \cdot O_{2\,amb}{}^{-1}} \qquad (5.2)$$

Where T_{amb}, ρ_{amb}, P_{amb}, $O_{2\%\,amb}$ represent the temperature, density, pressure and oxygen concentration of the ambient. The injection pressure and fuel density are represented as P_{inj}, ρ_{fuel} respectively

To convert ID* and LOL*in the experimental value (ID and LOL), it is necessary to determine the influence of fuel properties. That influence can be represented by a constant term which is indicated in Equations 7.1 and 7.2.

$$\boldsymbol{ID = A \cdot ID^{*}} \qquad (7.1)$$

$$LOL = B \cdot LOL^{*} \tag{7.2}$$

The influence of fuel properties expressed as A and B in Equations 7.1 and 7.2 can be observed as the slope of each curve in the Figure 7.1. Therefore, the terms A and B have been determined through a linear fit of the experimental values of ID and LOL.

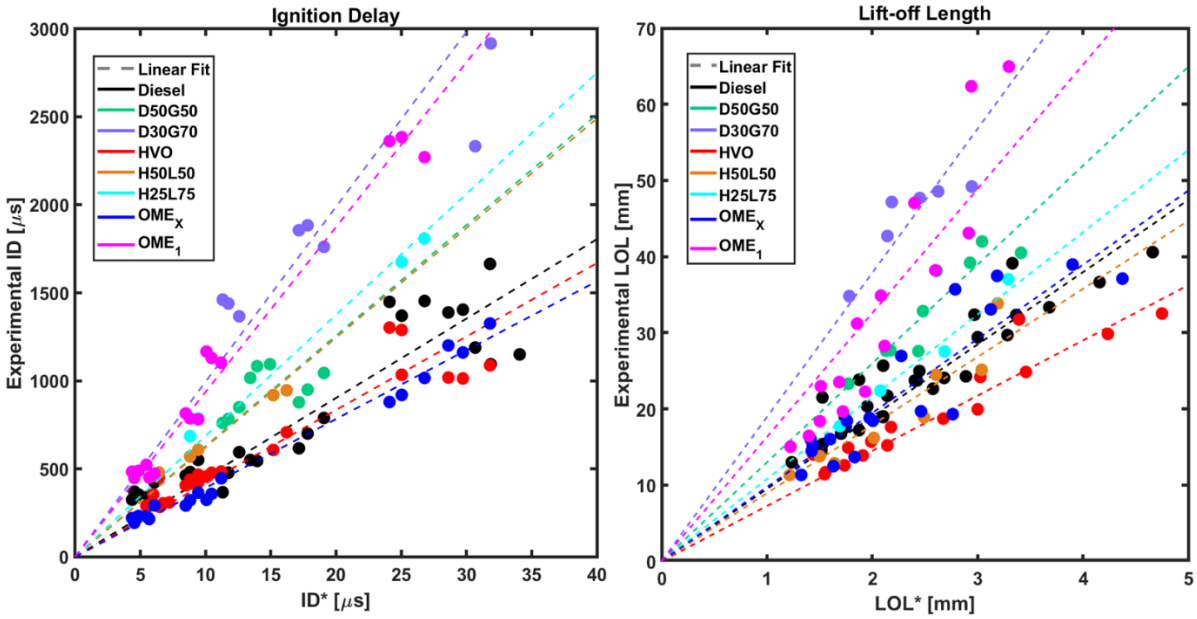

Figure 7. 1 Theoretical and experimental correlation for ID and LOL

To better understand the influence of fuel on ID and LOL, Figure 7. 2 depicts the constants A (purple bar) and B (yellow bar) and the chemical properties of the fuel more related to auto ignition and burning process such as cetane number (green bar), oxygen content (rose bar) and stoichiometric equivalence ratio (A/F)st (gray bar) for pure fuels. The aim is to evidence trends and the relationship between them. In the case of A belonging to ignition delay correlation, it can be seen an inverse trend with CN. Higher values of A correspond to those fuels whose reactivity is low such as OME1. On the contrary, the smallest values of A correspond to the OMEx and HVO. It is important to mention that although the highest cetane number corresponds to HVO, its oxygen content is null, unlike OMEx, which has a high cetane number and also a high oxygen content, which makes it the most reactive fuel within those studied in this thesis. Therefore, the constant A is highly dependent on the reactivity of the fuel (high CN and high oxygen content). In the case of blends with low reactivity fuels: gasoline and LPG, the values of A are between those for OME1 and diesel.

That is expected due to the fact that those blends have higher ignition resistance than high reactivity fuels such as diesel and HVO.

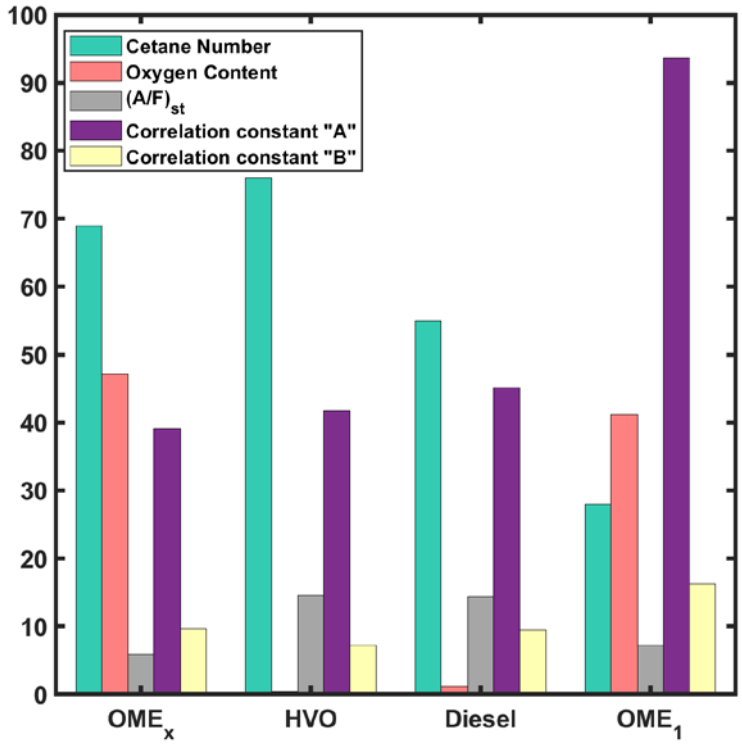

Figure 7. 2 Comparison of correlation constant A for determining the Ignition Delay respect to cetane number (CN)

For constant B belonging to LOL, the trend is not so clear. This does not appear to be related to a single fuel property. Although it is true that the biggest values correspond again to low-reactivity fuels such as OME_1, and the smallest value corresponds to HVO. However, for diesel and OME_x this trend is not clear. It does not correspond just to fuel reactivity (CN and oxygen content). This indicates that there are other fuel characteristics such as the stoichiometric air-fuel ratio $(A/F)_{st}$ that have a greater influence on LOL which is quite related with the mixing process. As it is observed in Figure 7. 2, OME_x has lower $(A/F)_{st}$ compared to diesel. Thus, B gets bigger when smaller is the $(A/F)_{st}$. This could be explain that B is bigger for OME_x than for diesel. In general terms, the LOL is influenced by the interaction of multiple fuel characteristics, including reactivity (CN and oxygen content) and the air-fuel ratio $(A/F)_{st}$.

Thus, the two dominant properties for A would be oxygen content and CN, but for B the stoichiometric air-fuel ratio also comes into play.

7.5 Future works

Undoubtedly, the use of alternative fuels is an excellent strategy to reduce pollutants in compression ignition engines, but there is still a long way to go to establish strategies to mitigate them and then to implement these fuels in commercial vehicles. For that, further analysis are needed. Therefore the following proposals are presented:

- The experimental database generated in this thesis could be used to develop and validate combustion computational models that provide detailed knowledge of the combustion process of these fuels. Furthermore, the soot production could also be studied by means of soot modeling since in this thesis experimental data about soot distribution was given.
- In this thesis two flame characteristics were analyzed: LOL and flame penetration by means of OH^* chemiluminescence. It was observed quite differences for oxygenated fuels respect to the other fuels. However, with this optical technique is not possible to provide further details about flame structure. The zones where chemical species such as OH and formaldehyde appear are not still identified. These species help to give more details about the pre-ignition process and combustion development. So there is still a gap in the characterization of oxygenated flames. Therefore, it is suggested to use advanced optical techniques such as Planar Laser-Induced Fluorescence (PLIF) to similar experiments to fill this gap. Furthermore, in this thesis the precursors of soot were not characterized either, only the radiation and attenuation of the soot formed was observed. With PLIF, those species could be identified and then studied. Additionally, it would also be so useful to characterize the NO formation zones and for that, PLIF technique could also be used. With all this information, a wide knowledge of HVO, OME_1 and OME_x flames could be established.
- The study carried out with these different fuels shows that they have potential not only in reducing CO_2 but also they have potential in reducing pollutant emissions under diffusion combustion conditions typical of a compression ignition engine. These alternative fuels were studied in terms of main combustion characteristics which would allow to estimate the necessary adjustments to be used in metal engines and thus obtain a better performance. In addition, it was possible to establish the differences of these alternative fuels with the conventional diesel, showing that HVO does not differ greatly from diesel in terms of characteristic parameters of combustion, but it does differ in terms of soot production, being less for the HVO. Although this fuel is already used in some heavy vehicles from Volvo, Scania and Mercedes Benz, they are often used mixed with diesel. Furthermore, in this thesis the mixture of oxymethylene ethers: OME_x turns out to be the most attractive fuel to be used in diffusion combustion. As it is the shortest auto ignition time, it would not imply drastic changes in the combustion setting in a real engine, although the material compatibility problems presented by oxymethylene ethers remain to be solved, but that was outside the scope of this thesis. The OME_x had combustion characteristics similar to diesel but did not produce soot in any of the operating conditions tested, which made it the most attractive of this experimental campaign. Therefore, HVO and OMEx are the most tractive fuels. However, more experimentation is needed to confirm that these fuels are still very interesting when they are implemented in real engines and if the trends observed in this thesis are still valid in terms of pollutants

formation and thermal efficiency for whole engine map. Therefore, it is proposed to test HVO and OME_x on a real engine.

- It would be interesting to study the effect produced by the jet to jet interaction, or the jet-wall interaction on combustion performance when HVO and OME_x are used since these effects have not been studied in this thesis. Furthermore, quantifying the NO emissions for understanding the soot-NO trade-off in the whole engine operating map would be useful for future commercial applications.
- Solving the technical problems related to the storage and supply of the HVO-LPG blends, this is quite attractive in terms of reducing pollutants. Adding LPG considerably reduces the soot formation. In addition they are two fuels whose supply chain is much more extended than that of other fuels (such as oxymethylene ethers for example). Although these are found as pure fuels in filling stations, the challenge with the mixture formation need to be solved. However, it would be interesting to evaluate the behavior of these mixtures in a real engine to confirm the trends found in this thesis and also quantify the benefit-challenge trade-off that these mixtures would involve in terms of consumption, efficiency or power when they are used.

The results provided in this thesis together with the proposals above described will contribute with the strategies focused on the decarbonization of transport sector.

References

Aakko P, Nylund N-O. Particle Emissions at Moderate and Cold Temperatures Using Different Fuels, SAE Technical Paper 2003-01-3285; 2003. https://doi.org/10.4271/2003-01-3285. **(Cited on page 31)**

Aatola H, Larmi M, Sarjovaara T, Mikkonen S. Hydrotreated Vegetable Oil (HVO) as a Renewable Diesel Fuel: Trade-off between NOx, Particulate Emission, and Fuel Consumption of a Heavy Duty Engine, SAE Int. J. Engines 1(1):1251-1262; 2008. https://doi.org/10.4271/2008-01-2500. **(Cited on page 31, 32, 96)**

Adam A, Leick P, Bittlinger G, Schulz C. Visualization of the evaporation of a diesel spray using combined Mie and Rayleigh scattering techniques. Exp Fluids 2009;47:439–49. https://doi.org/10.1007/s00348-009-0673-y. **(Cited on page 57)**

Akihama K, Takatori Y, Inagaki K, Sasaki S, Dean AM. Mechanism of the Smokeless Rich Diesel Combustion by Reducing Temperature, SAE Technical Paper 2001-01-0655; 2001. https://doi.org/10.4271/2001-01-0655. **(Cited on page 23)**

ANFAC | Informe Anual, 2019. https://anfac.com/informe-anual-2019/ (accessed June, 2021). **(Cited on page 29)**

Arcoumanis C, Bae C, Crookes R, Kinoshita E. The potential of di-methyl ether (DME) as an alternative fuel for compression-ignition engines: A review. Fuel 2008;87:1014–30. https://doi.org/10.1016/j.fuel.2007.06.007. **(Cited on page 33, 34)**

Asad U, Divekar P, Zheng M, Tjong J. Low Temperature Combustion Strategies for Compression Ignition Engines: Operability limits and Challenges, 2013, p. 2013-01–0283. https://doi.org/10.4271/2013-01-0283. **(Cited on page 23)**

Bae C, Kim J. Alternative fuels for internal combustion engines. Proceedings of the Combustion Institute 2017; 36:3389–413. https://doi.org/10.1016/j.proci.2016.09.009.**(Cited on page 5, 34, 36, 43)**

Baert RSG, Frijters PJM, Somers B, Luijten CCM, de Boer W. Design and Operation of a High Pressure, High Temperature Cell for HD Diesel Spray Diagnostics: Guidelines and Results, SAE Technical Paper 2009-01-0649; 2009. https://doi.org/10.4271/2009-01-0649. **(Cited on page 50)**

Bayraktar H, Durgun O. Investigating the effects of LPG on spark ignition engine combustion and performance. Energy Conversion and Management 2005; 46:2317–33. https://doi.org/10.1016/j.enconman.2004.09.012. **(Cited on page 5)**

Benajes J, Garcia-Oliver JM, Pastor JM, De-Leon-Ceriani D. A computational study on OME1 spray combustion under ECN Spray A conditions, Zhenjiang, China: ILASS-Asia; 2020. **(Cited on page 104)**

Benajes J, Payri R, Bardi M, Martí-Aldaraví P. Experimental characterization of diesel ignition and lift-off length using a single-hole ECN injector. Applied Thermal Engineering 2013;58:554–63. https://doi.org/10.1016/j.applthermaleng.2013.04.044 **(Cited on page 20, 21, 88, 89, 105, 125, 126, 146, 149)**

Bermúdez V, García JM, Juliá E, Martínez S. Engine with Optically Accessible Cylinder Head: A Research Tool for Injection and Combustion Processes. SAE Technical Papers, SAE Technical Paper 2003-01-1110; 2003. https://doi.org/10.4271/2003-01-1110. **(Cited on page 52)**

Bjørgen KOP, Emberson DR, Løvås T. Combustion and soot characteristics of hydrotreated vegetable oil compression-ignited spray flames. Fuel 2020;266:116942. https://doi.org/10.1016/j.fuel.2019.116942. **(Cited on page 31, 83)**

Boronat Colomer V. Dual-Fuel Dual-Mode combustion strategy to achieve high thermal efficiency, low NOx and smoke emissions in compression ignition engines. PhD thesis. Universitat Politècnica de València, 2018. **(Cited on page 7)**

Bortel I, Vávra J, Takáts M. Effect of HVO fuel mixtures on emissions and performance of a passenger car size diesel engine. Renewable Energy 2019; 140:680–91. https://doi.org/10.1016/j.renene.2019.03.067. **(Cited on page 6, 32)**

Bredenoord. HVO diesel as a sustainable solution. Bredenoord, 2019. https://www.bredenoord.com/en/knowledge/hvo-diesel/ (accessed July, 2021). **(Cited on page 32)**

Bruneaux G. Combustion structure of free and wall-impinging diesel jets by simultaneous laser-induced fluorescence of formaldehyde, poly-aromatic hydrocarbons, and hydroxides. International Journal of Engine Research 2008;9:249–65. https://doi.org/10.1243/14680874JER00108. **(Cited on page 58, 59, 61)**

Cairns A, Stansfield P, Fraser N, Blaxill H, Gold M, Rogerson J, et al. A Study of Gasoline-Alcohol Blended Fuels in an Advanced Turbocharged DISI Engine. SAE Int J Fuels Lubr 2009;2:41–57. https://doi.org/10.4271/2009-01-0138. **(Cited on page 33)**

European Environment Agency, Carbon dioxide emissions from Europe's heavy-duty vehicles, 2018. https://www.eea.europa.eu/themes/transport/heavy-duty-vehicles/carbon-dioxide-emissions-europe. **(Cited on page 3)**

Chemical looping combustion. Wikipedia, 2021. **(Cited on page 28)**

Choi MY, Mulholland GW, Hamins A, Kashiwagi T. Comparisons of the soot volume fraction using gravimetric and light extinction techniques. Combustion and Flame 1995;102:161–9. https://doi.org/10.1016/0010-2180(94)00282-W. **(Cited on page 85)**

European Parliament and Council, Commission Regulation with respect to emissions from heavy duty vehicles (Euro VI); 2011. **(Cited on page 3)**

Crusius S, Müller M, Stein H, Goral T. Oxy-methylen-di-methylether (OMEx) as an alternative for diesel fuel and blend compound: properties, additizing and compatibility with fossil and renewable fuels, Esslingen: 12th International Colloquium Fuels - Conventional and Future Energy for Automobiles; 2019, p. 8. **(Cited on page 6, 34, 71)**

Dec JE, Canaan RE. PLIF Imaging of NO Formation in a DI Diesel Engine, SAE Technical Paper 980147; 1998. https://doi.org/10.4271/980147. **(Cited on page 62)**

Dec JE, Coy EB. OH Radical Imaging in a DI Diesel Engine and the Structure of the Early Diffusion Flame, SAE Technical Paper 960831; 1996. https://doi.org/10.4271/960831. **(Cited on page 23, 49, 55, 99)**

Dec JE, Espey C. Chemiluminescence Imaging of Autoignition in a DI Diesel Engine, SAE Technical Paper 982685; 1998. https://doi.org/10.4271/982685. **(Cited on page 20, 55)**

Dec JE, A Conceptual Model of DI Diesel Combustion Based on Laser-Sheet Imaging, SAE Technical Paper 970873; 1997. https://doi.org/10.4271/970873. **(Cited on page 21, 22, 58, 59)**

Dec JE, Advanced compression-ignition engines—understanding the in-cylinder processes. Proceedings of the Combustion Institute 2009;32:2727–42. https://doi.org/10.1016/j.proci.2008.08.008. **(Cited on page 4, 23)**

Desantes JM, Garcia-Oliver JM, Novella R, Pachano L. A numerical study of the effect of nozzle diameter on diesel combustion ignition and flame stabilization. International Journal of Engine Research 2020;21:101–21. https://doi.org/10.1177/1468087419864203. **(Cited on page 104)**

Desantes JM, Pastor JV, García-Oliver JM, Briceño FJ. An experimental analysis on the evolution of the transient tip penetration in reacting Diesel sprays. Combustion and Flame 2014;161:2137–50. https://doi.org/10.1016/j.combustflame.2014.01.022. **(Cited on page 77)**

Desantes JM, Pastor JV, García-Oliver JM, Pastor JM. A 1D model for the description of mixing-controlled reacting diesel sprays. Combustion and Flame 2009;156:234–49. https://doi.org/10.1016/j.combustflame.2008.10.008. **(Cited on page 132)**

Desantes JM, Pastor JV, Pastor JM, Juliá JE. Limitations on the use of the planar laser induced exciplex fluorescence technique in diesel sprays. Fuel 2005;84:2301–15. https://doi.org/10.1016/j.fuel.2005.05.009. **(Cited on page 57)**

Dimethyl Ether, 2021. https://dieselnet.com/tech/fuel_dme.php (accessed May, 2021). **(Cited on page 33, 35)**

Dimitriadis A, Seljak T, Vihar R, Žvar Baškovič U, Dimaratos A, Bezergianni S, et al. Improving PM-NOx trade-off with paraffinic fuels: A study towards diesel engine optimization with HVO. Fuel 2020; 265:116921. https://doi.org/10.1016/j.fuel.2019.116921. **(Cited on page 6)**

Domenech Llopis V. Study of new strategies for combustion control in partially premixed modes in compression ignition engines (in Spanish). PhD thesis. Universitat Politècnica de València, 2013. **(Cited on page 7)**

Engine Combustion Network | Engine Combustion Network Website, 2021. https://ecn.sandia.gov/. **(Cited on page 8, 71, 73, 74, 79, 81, 86,122**

ERTRAC Working Group. Energy Carriers for Powertrains for a clean and efficient mobility. European Road Transport Research Advisory Council (ERTRAC) Working Group: Energy and Environment; 2014. **(Cited on page 26, 28, 29, 30, 31)**

Espey C, Dec JE, Litzinger TA, Santavicca DA. Planar laser rayleigh scattering for quantitative vapor-fuel imaging in a diesel jet. Combustion and Flame 1997;109:65–86. https://doi.org/10.1016/S0010-2180(96)00126-5. **(Cited on page 57)**

European Commission. A European Green Deal, 2019. https://ec.europa.eu/info/strategy/priorities-2019-2024/european-green-deal_en (accessed July 15, 2021). **(Cited on page 5)**

European Commission. Directorate General for Research and Innovation. Alternative fuels: expert group report. LU: Publications Office; 2017. **(Cited on page 5)**

Flynn PF, Durrett RP, Hunter GL, zur Loye AO, Akinyemi OC, Dec JE, et al. Diesel Combustion: An Integrated View Combining Laser Diagnostics, Chemical Kinetics, And Empirical Validation, SAE Technical Paper 1999-01-0509; 1999. https://doi.org/10.4271/1999-01-0509. **(Cited on page 21, 22, 55)**

FolletoCorporativo_Balearia, 2021. https://www.balearia.com/es/grupo-balearia/#page=12 (accessed June, 2021). **(Cited on page 29)**

European Road Transport Research Advisory Council (ERTRAC) Working Group: Energy and Environment, Future Light and Heavy Duty ICE Powertrain Technologies, 2016. **(Cited on page 5, 27)**

European Road Transport Research Advisory Council, Future Light duty Powertrain Technologies and Fuels, 2011. **(Cited on page 6, 27)**

García A, Monsalve-Serrano J, Villalta D, Lago Sari R, Gordillo Zavaleta V, Gaillard P. Potential of e-Fischer Tropsch diesel and oxymethyl-ether (OMEx) as fuels for the dual-mode dual-fuel concept. Applied Energy 2019; 253:113622. https://doi.org/10.1016/j.apenergy.2019.113622. **(Cited on page 6)**

García Oliver JM, Contributions to the study of the j turbulent combustion process of jets in direct injection diesel engines (in Spanish). PhD thesis. Universitat Politècnica de València, 2004. **(Cited on page 19,20, 21, 22, 23, 56)**

Gaydon AG, The Spectroscopy of Flames. Dordrecht: Springer Netherlands; 1974. https://doi.org/10.1007/978-94-009-5720-6. **(Cited on page 79)**

Ghandhi JB, Heim DM. An optimized optical system for backlit imaging. Review of Scientific Instruments 2009;80:056105. https://doi.org/10.1063/1.3128728. **(Cited on page 56)**

Gimeno J, Martí-Aldaraví P, Carreres M, Peraza JE. Effect of the nozzle holder on injected fuel temperature for experimental test rigs and its influence on diesel sprays. International Journal of Engine Research 2018;19:374–89. https://doi.org/10.1177/1468087417751531. **(Cited on page 20, 56, 119)**

Guo H, Hosseini V, Neill WS, Chippior WL, Dumitrescu CE. An experimental study on the effect of hydrogen enrichment on diesel fueled HCCI combustion. International Journal of Hydrogen Energy 2011;36:13820–30. https://doi.org/10.1016/j.ijhydene.2011.07.143. **(Cited on page 37)**

Han M, The effects of synthetically designed diesel fuel properties – cetane number, aromatic content, distillation temperature, on low-temperature diesel combustion.

Fuel 2013;109:512–9. https://doi.org/10.1016/j.fuel.2013.03.039. **(Cited on page 146)**

Hartikka T, Kuronen M, Kiiski U. Technical Performance of HVO (Hydrotreated Vegetable Oil) in Diesel Engines, SAE Technical Paper 2012-01-1585; 2012. https://doi.org/10.4271/2012-01-1585. **(Cited on page 31)**

Härtl M, Seidenspinner P, Jacob E, Wachtmeister G. Oxygenate screening on a heavy-duty diesel engine and emission characteristics of highly oxygenated oxymethylene ether fuel OME1. Fuel 2015; 153:328–35. https://doi.org/10.1016/j.fuel.2015.03.012. **(Cited on page 6, 36)**

Heindl R, Eichlseder H, Spuller C, Gerbig F, Heller K. New and Innovative Combustion Systems for the H2-ICE: Compression Ignition and Combined Processes. SAE International Journal of Engines, SAE Int. J. Engines 2(1):1231-1250; 2009. https://doi.org/10.4271/2009-01-1421 **(Cited on page 36, 37)**

Heywood, John B. Internal combustion engine fundamentals. Second Edition. New York: McGraw-Hill; 2018.**(Cited on page 110)**

Huber GW, O'Connor P, Corma A. Processing biomass in conventional oil refineries: Production of high quality diesel by hydrotreating vegetable oils in heavy vacuum oil mixtures. Applied Catalysis A: General 2007;329:120–9. https://doi.org/10.1016/j.apcata.2007.07.002 **(Cited on page 31)**

Hydrogen vehicle. Wikipedia 2021. **(Cited on page 37)**

Inagaki K, Fuyuto T, Nishikawa K, Nakakita K, Sakata I. Dual-Fuel PCI Combustion Controlled by In-Cylinder Stratification of Ignitability, SAE Technical Paper 2006-01-0028; 2006. https://doi.org/10.4271/2006-01-0028. **(Cited on page 4)**

Jacobs TJ, Assanis DN. The attainment of premixed compression ignition low-temperature combustion in a compression ignition direct injection engine. Proceedings of the Combustion Institute 2007;31:2913–20. https://doi.org/10.1016/j.proci.2006.08.113. (**Cited on page 23)**

Jeon J, Bae C. The effects of hydrogen addition on engine power and emission in DME premixed charge compression ignition engine. International Journal of Hydrogen Energy 2013;38:265–73. https://doi.org/10.1016/j.ijhydene.2012.09.177. **(Cited on page 36, 37)**

Kamimoto T, Bae M. High Combustion Temperature for the Reduction of Particulate in Diesel Engines, SAE Technical Paper 880423; 1988. https://doi.org/10.4271/880423. **(Cited on page 23)**

Kim MY, Yoon SH, Ryu BW, Lee CS. Combustion and emission characteristics of DME as an alternative fuel for compression ignition engines with a high pressure injection system. Fuel 2008;87:2779–86. https://doi.org/10.1016/j.fuel.2008.01.032. **(Cited on page 34)**

Kokjohn SL, Hanson RM, Splitter DA, Reitz RD. Experiments and Modeling of Dual-Fuel HCCI and PCCI Combustion Using In-Cylinder Fuel Blending. SAE International

Journal of Engines, vol. 2, 2009, p. 24–39. https://doi.org/10.4271/2009-01-2647. **(Cited on page 4)**

Kook S, Pickett LM. Liquid length and vapor penetration of conventional, Fischer–Tropsch, coal-derived, and surrogate fuel sprays at high-temperature and high-pressure ambient conditions. Fuel 2012;93:539–48. https://doi.org/10.1016/j.fuel.2011.10.004.**(Cited on page 87, 90, 103, 128)**

Kosaka H, Aizawa T, Kamimoto T. Two-dimensional imaging of ignition and soot formation processes in a diesel flame. International Journal of Engine Research 2005;6:21–42. https://doi.org/10.1243/146808705X7347. **(Cited on page 23, 59)**

Lago Sari R, Dual-mode dual-fuel combustion implementation on a real medium duty engine platform. PhD thesis. Universitat Politècnica de València, 2021. **(Cited on page 8)**

Lambert's cosine law. Wikipedia 2021. **(Cited on page 83)**

Lee S, Kim C, Lee S, Lee J, Kim J. Diesel injector nozzle optimization for high CNG substitution in a dual-fuel heavy-duty diesel engine. Fuel 2020;262:116607. https://doi.org/10.1016/j.fuel.2019.116607. **(Cited on page 29)**

Lequien G, Berrocal E, Gallo Y, Themudo e Mello A, Andersson O, Johansson B. Effect of Jet-Jet Interactions on the Liquid Fuel Penetration in an Optical Heavy-Duty DI Diesel Engine, SAE Technical Paper 2013-01-1615; 2013. https://doi.org/10.4271/2013-01-1615. **(Cited on page 87)**

Li D, He Z, Xuan T, Zhong W, Cao J, Wang Q, et al. Simultaneous capture of liquid length of spray and flame lift-off length for second-generation biodiesel/diesel blended fuel in a constant volume combustion chamber. Fuel 2017;189:260–9. https://doi.org/10.1016/j.fuel.2016.10.058. **(Cited on page 87)**

Liu H, Wang Z, Zhang J, Wang J, Shuai S. Study on combustion and emission characteristics of Polyoxymethylene Dimethyl Ethers/diesel blends in light-duty and heavy-duty diesel engines. Applied Energy 2017;185:1393–402. https://doi.org/10.1016/j.apenergy.2015.10.183.**(Cited on page 36)**

Low Temperature Combustion 2021. https://dieselnet.com/tech/engine_ltc.php (accessed April, 2021). **(Cited on page 26**)

Lu X, Han D, Huang Z. Fuel design and management for the control of advanced compression-ignition combustion modes. Progress in Energy and Combustion Science 2011;37:741–83. https://doi.org/10.1016/j.pecs.2011.03.003. **(Cited on page 4)**

Maes N, Skeen SA, Bardi M, Fitzgerald RP, Malbec L-M, Bruneaux G, et al. Spray penetration, combustion, and soot formation characteristics of the ECN Spray C and Spray D injectors in multiple combustion facilities. Applied Thermal Engineering 2020;172:115136. https://doi.org/10.1016/j.applthermaleng.2020.115136. **(Cited on page 104)**

Manente V, Tunestal P, Johansson B, Cannella WJ. Effects of Ethanol and Different Type of Gasoline Fuels on Partially Premixed Combustion from Low to High Load, SAE Technical Paper 2010-01-0871; 2010. https://doi.org/10.4271/2010-01-0871. **(Cited on page 4)**

Manin J, Bardi M, Pickett LM. Evaluation of the liquid length via diffused back-illumination imaging in vaporizing diesel sprays, Fukuoka, Japan: The Eighth International Conference on Modeling and Diagnostics for Advanced Engine; 2012. **(Cited on page 56)**

Manin J, Pickett LM, Skeen SA. Two-Color Diffused Back-Illumination Imaging as a Diagnostic for Time-Resolved Soot Measurements in Reacting Sprays. SAE International Journal of Engines, SAE Int. J. Engines 6(4):1908-1921; 2013. https://doi.org/10.4271/2013-01-2548. **(Cited on page 61)**

Manin J, Analysis of mixing processes in liquid and vaporized diesel sprays through lif and rayleigh scattering measurements. PhD thesis. Universitat Politècnica de València, 2011. **(Cited on page 56)**

Manin J. High-speed mixing measurements, ECN 5, 2017. **(Cited on page 57)**

Marinov NM, Pitz WJ, Westbrook CK, Vincitore AM, Castaldi MJ, Senkan SM, et al. Aromatic and Polycyclic Aromatic Hydrocarbon Formation in a Laminar Premixed n-Butane Flame. Combustion and Flame 1998;114:192–213. https://doi.org/10.1016/S0010-2180(97)00275-7. **(Cited on page 96)**

McCormick RL, Graboski MS, Alleman TL, Herring AM, Tyson KS. Impact of Biodiesel Source Material and Chemical Structure on Emissions of Criteria Pollutants from a Heavy-Duty Engine. Environmental Science & Technology 2001;35:1742–7. https://doi.org/10.1021/es001636t.**(Cited on page 30)**

Micó C, Development of measurement and visualization techniques for characterization of mixing and combustion processes with surrogate fuels. PhD thesis. Universitat Politècnica de València, 2015. **(Cited on page 10, 52, 53, 55, 56, 60)**

Ministerio para la Transición Ecológica y el Reto Demográfico - ¿Qué gasolina debo repostar?, 2021. https://energia.gob.es/Gasolinas/Paginas/tipos-gasolina.aspx (accessed July, 2021). **(Cited on page 32)**

Monsalve Serrano J, Dual-fuel compression ignition: towards clean, highly efficient combustion. PhD thesis. Universitat Politècnica de València, 2016. **(Cited on page 7)**

Motores marinos a gas natural. Gasnam, 2021. https://gasnam.es/maritimo/motores-marinos-a-gas-natural/ (accessed June, 2021). **(Cited on page 29)**

Mueller CJ, Musculus MP. Glow Plug Assisted Ignition and Combustion of Methanol in an Optical DI Diesel Engine, SAE Technical Paper 2001-01-2004; 2001. https://doi.org/10.4271/2001-01-2004. **(Cited on page 60)**

Murtonen T, Aakko-Saksa P, Kuronen M, Mikkonen S, Lehtoranta K. Emissions with Heavy-duty Diesel Engines and Vehicles using FAME, HVO and GTL Fuels with

and without DOC+POC Aftertreatment, SAE Int. J. Fuels Lubr. 2(2):147-166; 2010. https://doi.org/10.4271/2009-01-2693. **(Cited on page 32)**

Murugesa Pandian M, Anand K. Comparison of different low temperature combustion strategies in a light duty air cooled diesel engine. Applied Thermal Engineering 2018;142:380–90. https://doi.org/10.1016/j.applthermaleng.2018.07.047. **(Cited on page 23)**

Musculus MPB, Miles PC, Pickett LM. Conceptual models for partially premixed low-temperature diesel combustion. Progress in Energy and Combustion Science 2013;39:246–83. https://doi.org/10.1016/j.pecs.2012.09.001. **(Cited on page 19, 24, 25, 49)**

Musculus MPB, Multiple Simultaneous Optical Diagnostic Imaging of Early-Injection Low-Temperature Combustion in a Heavy-Duty Diesel Engine, SAE Technical Paper 2006-01-0079; 2006. https://doi.org/10.4271/2006-01-0079. **(Cited on page 25)**

Naccarato F, Potenza M, de Risi A. Simultaneous LII and TC optical correction of a low-sooting LPG diffusion flame. Measurement 2014;47:989–1000. https://doi.org/10.1016/j.measurement.2013.09.013. **(Cited on page 61)**

Napolitano P, Alfè M, Guido C, Gargiulo V, Fraioli V, Beatrice C. Particle emissions from a HD SI gas engine fueled with LPG and CNG. Fuel 2020; 269:117439. https://doi.org/10.1016/j.fuel.2020.117439. **(Cited on page 5)**

Nerva J-G, An Assessment of fuel physical and chemical properties in the combustion of a Diesel spray. PhD thesis. Universitat Politècnica de València, 2013. **(Cited on page 7, 52)**

Niaz S, Manzoor T, Pandith AH. Hydrogen storage: Materials, methods and perspectives. Renewable and Sustainable Energy Reviews 2015;50:457–69. https://doi.org/10.1016/j.rser.2015.05.011. **(Cited on page 36)**

Niethammer B, Wodarz S, Betz M, Haltenort P, Oestreich D, Hackbarth K, et al. Alternative Liquid Fuels from Renewable Resources. Chemie Ingenieur Technik 2018;90:99–112. https://doi.org/10.1002/cite.201700117. **(Cited on page 35)**

Niven RK, Ethanol in gasoline: environmental impacts and sustainability review article. Renewable and Sustainable Energy Reviews 2005;9:535–55. https://doi.org/10.1016/j.rser.2004.06.003. **(Cited on page 33)**

O'Connor J, Musculus M. Optical Investigation of Multiple Injections for Unburned Hydrocarbon Emissions Reduction with Low-Temperature Combustion in a Heavy-Duty Diesel Engine. vol. 1, 8th US National Combustion Meeting 2013. Western States Section/Combustion Institute; 2013, p. 467–91. **(Cited on page 24, 25)**

Oh H, Bae C, Min K. Spray and Combustion Characteristics of Ethanol Blended Gasoline in a Spray Guided DISI Engine under Lean Stratified Operation. SAE International Journal of Engines, SAE Int. J. Engines 3(2):213-222; 2010. https://doi.org/10.4271/2010-01-2152. **(Cited on page 33)**

Omari A, Heuser B, Pischinger S. Potential of oxymethylenether-diesel blends for ultra-low emission engines. Fuel 2017;209:232–7. https://doi.org/10.1016/j.fuel.2017.07.107. **(Cited on page 107)**

Pachano L, CFD modeling of combustion and soot production in diesel sprays. PhD thesis. Universitat Politècnica de València, 2020. **(Cited on page 8, 102,103,108)**

Park SH, Lee CS. Combustion performance and emission reduction characteristics of automotive DME engine system. Progress in Energy and Combustion Science 2013;39:147–68. https://doi.org/10.1016/j.pecs.2012.10.002. (**Cited on page 34)**

Pastor J, Garcia-Oliver JM, Garcia A, Nareddy VR. Characterization of Spray Evaporation and Mixing Using Blends of Commercial Gasoline and Diesel Fuels in Engine-Like Conditions, SAE Technical Paper 2017-01-0843; 2017. https://doi.org/doi:10.4271/2017-01-0843. **(Cited on page 54, 102, 119, 139, 147, 148)**

Pastor JV, García JM, Pastor JM, Buitrago JE. Analysis Methodology of Diesel Combustion by Using Flame Luminosity, Two-Colour Method and Laser-Induced Incandescence, SAE Technical Paper 2005-24-012; 2005. https://doi.org/10.4271/2005-24-012. **(Cited on page 61, 143)**

Pastor JV, García-Oliver JM, García A, Micó C, Möller S. Application of optical diagnostics to the quantification of soot in n -alkane flames under diesel conditions. Combustion and Flame 2016;164:212–23. https://doi.org/10.1016/j.combustflame.2015.11.018. **(Cited on page 54, 61, 119, 128,139)**

Pastor JV, Garcia-Oliver JM, Garcia A, Morales López A. An Experimental Investigation on Spray Mixing and Combustion Characteristics for Spray C/D Nozzles in a Constant Pressure Vessel, SAE Technical Paper 2018-01-1783; 2018. https://doi.org/10.4271/2018-01-1783. **(Cited on page 73, 104)**

Pastor JV, García-Oliver JM, García A, Pinotti M. Effect of laser induced plasma ignition timing and location on Diesel spray combustion. Energy Conversion and Management 2017;133:41–55. https://doi.org/10.1016/j.enconman.2016.11.054. **(Cited on page 54, 139)**

Pastor JV, García-Oliver JM, García A, Pinotti M. Laser induced plasma methodology for ignition control in direct injection sprays. Energy Conversion and Management 2016;120:144–56. https://doi.org/10.1016/j.enconman.2016.04.086. **(Cited on page 54, 139)**

Pastor JV, Garcia-Oliver JM, Garcia A, Pinotti M. Soot Characterization of Diesel/Gasoline Blends Injected through a Single Injection System in CI engines, SAE Technical Paper 2017-24-0048; 2017. https://doi.org/10.4271/2017-24-0048. **(Cited on page 60, 123, 124, 130,143,150)**

Pastor JV, García-Oliver JM, López JJ, Vera-Tudela W. An experimental study of the effects of fuel properties on reactive spray evolution using Primary Reference Fuels. Fuel 2016;163:260–70. https://doi.org/10.1016/j.fuel.2015.09.064.**(Cited on page 91)**

Pastor JV, García-Oliver JM, Micó C, García-Carrero AA, Gómez A. Experimental Study of the Effect of Hydrotreated Vegetable Oil and Oxymethylene Ethers on Main Spray and Combustion Characteristics under Engine Combustion Network Spray A Conditions. Applied Sciences 2020;10:5460. https://doi.org/10.3390/app10165460. **(Cited on page 107)**

Pastor JV, García-Oliver JM, Nerva J-G, Giménez B. Fuel effect on the liquid-phase penetration of an evaporating spray under transient diesel-like conditions. Fuel 2011;90:3369–81. https://doi.org/10.1016/j.fuel.2011.05.006. **(Cited on page 140)**

Pastor JV, López JJ, Juliá JE, Benajes JV. Planar Laser-Induced Fluorescence fuel concentration measurements in isothermal Diesel sprays. Opt Express, OE 2002;10:309–23. https://doi.org/10.1364/OE.10.000309. **(Cited on page 56)**

Pastor JV, Pastor JM, Gimeno J, Nerva J-G. The effect of Biodiesel fuel blend rate on the Liquid-phase fuel penetration in Diesel engine conditions, SAE Technical Paper 2009-24-0051; 2009. https://doi.org/10.4271/2009-24-0051. **(Cited on page 53)**

Pastor JV, Payri R, Garcia-Oliver JM, Briceno FJ. Analysis of transient liquid and vapor phase penetration for diesel sprays under variable injection conditions. Atomization and Sprays 2011;21:503–20. https://doi.org/10.1615/AtomizSpr.2011003721. **Cited on page 56)**

Pastor JV, Payri R, Garcia-Oliver JM, Briceño FJ. Schlieren Methodology for the Analysis of Transient Diesel Flame Evolution. SAE International Journal of Engines, SAE Int. J. Engines 6(3):1661-1676; 2013. https://doi.org/10.4271/2013-24-0041. **(Cited on page 58)**

Pastor JV, Payri R, Garcia-Oliver JM, Nerva J-G. Schlieren Measurements of the ECN-Spray A Penetration under Inert and Reacting Conditions, SAE Technical Paper 2012-01-0456; 2012. https://doi.org/10.4271/2012-01-0456. **(Cited on page 58)**

Pastor JV, Payri R, Gimeno J, Nerva JG. Experimental Study on RME Blends: Liquid-Phase Fuel Penetration, Chemiluminescence, and Soot Luminosity in Diesel-Like Conditions. Energy & Fuels 2009;23:5899–915. https://doi.org/10.1021/ef9007328. **(Cited on page 53, 140, 142)**

Payri F, Pastor JV, Nerva J-G, Garcia-Oliver JM. Lift-Off Length and KL Extinction Measurements of Biodiesel and Fischer-Tropsch Fuels under Quasi-Steady Diesel Engine Conditions, SAE Int. J. Engines 4(2):2278-2297; 2011. https://doi.org/10.4271/2011-24-0037. **(Cited on page 52)**

Payri R, García-Oliver JM, Bardi M, Manin J. Fuel temperature influence on diesel sprays in inert and reacting conditions. Applied Thermal Engineering 2012;35:185–95. https://doi.org/10.1016/j.applthermaleng.2011.10.027 **(Cited on page 51)**

Payri R, García-Oliver JM, Xuan T, Bardi M. A study on diesel spray tip penetration and radial expansion under reacting conditions. Applied Thermal Engineering 2015;90:619–29. https://doi.org/10.1016/j.applthermaleng.2015.07.042. **(Cited on page 128)**

Payri R, Gimeno J, Cardona S, Ayyapureddi S. Experimental study of the influence of the fuel and boundary conditions over the soot formation in multi-hole diesel injectors using high-speed color diffused back-illumination technique. Applied Thermal Engineering 2019;158:113746. https://doi.org/10.1016/j.applthermaleng.2019.113746. **(Cited on page 51, 118)**

Payri R, Salvador FJ, Manin J, Viera A. Diesel ignition delay and lift-off length through different methodologies using a multi-hole injector. Applied Energy 2016;162:541–50. https://doi.org/10.1016/j.apenergy.2015.10.118. **(Cited on page 88, 89, 118,126, 128, 149)**

Payri R, Viera JP, Gopalakrishnan V, Szymkowicz PG. The effect of nozzle geometry over ignition delay and flame lift-off of reacting direct-injection sprays for three different fuels. Fuel 2017;199:76–90. https://doi.org/10.1016/j.fuel.2017.02.075. **(Cited on page 128)**

Payri R, Viera JP, Pei Y, Som S. Experimental and numerical study of lift-off length and ignition delay of a two-component diesel surrogate. Fuel 2015;158:957–67. https://doi.org/10.1016/j.fuel.2014.11.072. **(Cited on page 87)**

Pélerin D, Gaukel K, Härtl M, Jacob E, Wachtmeister G. Potentials to simplify the engine system using the alternative diesel fuels oxymethylene ether OME1 and OME3−6 on a heavy-duty engine. Fuel 2020;259:116231. https://doi.org/10.1016/j.fuel.2019.116231. **(Cited on page 35, 36)**

Pérez-Sánchez EJ, Garcia-Oliver JM, Novella R, Pastor JM. Understanding the diesel-like spray characteristics applying a flamelet-based combustion model and detailed large eddy simulations. International Journal of Engine Research 2020;21:134–50. https://doi.org/10.1177/1468087419864469. **(Cited on page 104)**

Pickett LM, Kook S, Williams TC. Transient Liquid Penetration of Early-Injection Diesel Sprays, SAE Int. J. Engines 2(1):785-804; 2009. https://doi.org/10.4271/2009-01-0839. **(Cited on page 102)**

Pickett LM, Siebers DL, Idicheria CA. Relationship Between Ignition Processes and the Lift-Off Length of Diesel Fuel Jets, SAE Technical Paper 2005-01-3843; 2005. https://doi.org/10.4271/2005-01-3843. **(Cited on page 21, 105, 129, 146**

Pickett LM, Siebers DL. Non-Sooting, Low Flame Temperature Mixing-Controlled DI Diesel Combustion, SAE Technical Paper 2004-01-1399; 2004. https://doi.org/10.4271/2004-01-1399. **(Cited on page 93, 99)**

Pickett LM, Siebers DL. Orifice Diameter Effects on Diesel Fuel Jet Flame Structure. J Eng Gas Turbines Power 2005;127:187–96. https://doi.org/10.1115/1.1760525. **(Cited on page 91)**

Pittermann R, Spectroscopic Analysis of the Combustion in Diesel and Gas Engines. MTZ Worldw 2008;69:66–73. https://doi.org/10.1007/BF03227907. **(Cited on page 59, 60)**

Plee SL, Ahmad T. Relative Roles of Premixed and Diffusion Burning in Diesel Combustion, SAE Technical Paper 831733; 1983. https://doi.org/10.4271/831733. **(Cited on page 20)**

Reducir las emisiones de los automóviles: nuevos objetivos de CO2 | Noticias | Parlamento Europeo, 2018. **(Cited on page 3)**

Reif, K. Gasoline Engine Management. Wiesbaden: Springer Fachmedien Wiesbaden; 2015. https://doi.org/10.1007/978-3-658-03964-6. **(Cited on page 27)**

Renewable Diesel / HVO: Why are we not heading to a Malthusian trap /? | LinkedIn, 2021. https://www.linkedin.com/pulse/renewable-diesel-hvo-why-we-heading-malthusian-trap-fabien-hillairet-1e/ (accessed July, 2021). **(Cited on page 32)**

Review of evidence on health aspects of air pollution – REVIHAAP project: final technical report, 2017. http://www.euro.who.int/en/health-topics/environment-and-health/air-quality/publications/2013/review-of-evidence-on-health-aspects-of-air-pollution-revihaap-project-final-technical-report. **(Cited on page 3)**

Reyes M, Tinaut FV, Giménez B, Pastor JV. Effect of hydrogen addition on the OH* and CH* chemiluminescence emissions of premixed combustion of methane-air mixtures. International Journal of Hydrogen Energy 2018;43:19778–91. https://doi.org/10.1016/j.ijhydene.2018.09.005. **(Cited on page 58, 79,142)**

Ritchie H, Roser M. CO_2 and Greenhouse Gas Emissions. Our World in Data, 2017. **(Cited on page 3)**

Saxena P, Jawale S, Joshipura MH. A Review on Prediction of Properties of Biodiesel and Blends of Biodiesel. Procedia Engineering 2013;51:395–402. https://doi.org/10.1016/j.proeng.2013.01.055. **(Cited on page 30)**

Semelsberger TA, Borup RL, Greene HL. Dimethyl ether (DME) as an alternative fuel. Journal of Power Sources 2006;156:497–511. https://doi.org/10.1016/j.jpowsour.2005.05.082. **(Cited on page 34)**

Settles GS, Schlieren and Shadowgraph Techniques: Visualizing Phenomena in Transparent Media. Springer Science & Business Media; 2012. **(Cited on page 57, 75)**

Siebers D, Higgins B. Flame Lift-Off on Direct-Injection Diesel Sprays Under Quiescent Conditions, SAE Technical Paper 2001-01-0530; 2001. https://doi.org/10.4271/2001-01-0530. **(Cited on page 21, 94, 96, 105,123)**

Siebers DL, Liquid-Phase Fuel Penetration in Diesel Sprays, SAE Technical Paper 980809; 1998. https://doi.org/10.4271/980809. **(Cited on page 77,102,122)**

Siebers DL, Scaling Liquid-Phase Fuel Penetration in Diesel Sprays Based on Mixing-Limited Vaporization, SAE Technical Paper 1999-01-0528; 1999. https://doi.org/10.4271/1999-01-0528. **(Cited on page 125)**

Singh D, Sharma D, Soni SL, Inda CS, Sharma S, Sharma PK, et al. A comprehensive review of biodiesel production from waste cooking oil and its use as fuel in compression ignition engines: 3rd generation cleaner feedstock. Journal of Cleaner Production 2021;307:127299. https://doi.org/10.1016/j.jclepro.2021.127299. **(Cited on page 30)**

Singh S, Musculus MPB, Reitz RD. Mixing and flame structures inferred from OH-PLIF for conventional and low-temperature diesel engine combustion. Combustion and Flame 2009;156:1898–908. https://doi.org/10.1016/j.combustflame.2009.07.019. **(Cited on page 59)**

Sjöholm J, High Repetition Rate Laser Diagnostics for Combustion Applications. PhD thesis. Lund University, 2012. **(Cited on page 61, 62)**

Skeen SA, Manin J, Dalen K, Pickett LM. Extinction-based Imaging of Soot Processes over a Range of Diesel Operating Conditions. Internal combustion and gas turbine engines, 2013, p. 1–13. **(Cited on page 61)**

Smallwood GJ, Clavel D, Gareau D, Sawchuk RA, Snelling DR, Witze PO, et al. Concurrent Quantitative Laser-Induced Incandescence and SMPS Measurements of EGR Effects on Particulate Emissions from a TDI Diesel Engine, SAE Technical Paper 2002-01-2715; 2002. https://doi.org/10.4271/2002-01-2715. **(Cited on page 61)**

Soler A, Role of e-fuels in the European transport system - Literature review. Brussels: Concawe; 2020. **(Cited on page 6)**

Sugiyama K, Goto I, Kitano K, Mogi K, Honkanen M. Effects of Hydrotreated Vegetable Oil (HVO) as Renewable Diesel Fuel on Combustion and Exhaust Emissions in Diesel Engine, SAE Int. J. Fuels Lubr. 5(1):205-217; 2011. https://doi.org/10.4271/2011-01-1954. **(Cited on page 31, 32)**

Svensson KI, Richards MJ, Mackrory AJ, Tree DR. Fuel Composition and Molecular Structure Effects on Soot Formation in Direct-Injection Flames Under Diesel Engine Conditions, SAE Technical Paper 2005-01-0381; 2005. https://doi.org/10.4271/2005-01-0381. **(Cited on page 107)**

Syed MT, Sherif SA, Veziroğlu TN, Sheffield JW. An economic analysis of three hydrogen liquefaction systems. International Journal of Hydrogen Energy 1998;23:565–76. https://doi.org/10.1016/S0360-3199(97)00101-8. **(Cited on page 36)**

Syngaschem BV. https://www.syngaschem.com/ (accessed April, 2021). **(Cited on page 27)**

Thorlabs - Search, 2021. https://www.thorlabs.com/search/thorsearch.cfm?search=shortpass%20dichroic%20mirror (accessed July, 2021). **(Cited on page 81)**

Uhl M, Schießl R, Maas U, Dreizler A. Time Resolved Spray Characterisation in a Common Rail Direct-Injection Production Type Diesel Engine Using Combined Mie/LIF Laser Diagnostics, SAE Technical Paper 2003-01-1040; 2003. https://doi.org/10.4271/2003-01-1040. **(Cited on page 56)**

Ulrich A, Kathrin H, Philipp H, Jörg S. Refuels – Raw Materials, Processes and Applications for Synthetic Fuels. COMSYN European 2nd Generation Biofuels - Opportunities and Applications 2018. **(Cited on page 35)**

Union PO of the E. Commission Regulation (EU) No 582/2011 of 25 May 2011 implementing and amending Regulation (EC) No 595/2009 of the European Parliament and of the Council with respect to emissions from heavy duty vehicles (Euro VI) and amending Annexes I and III to Directive 2007/46/EC of the European

Parliament and of the Council, 2019. http://op.europa.eu/en/publication-detail/-/publication/4d2e52c3-41bc-11ea-9099-01aa75ed71a1/language-en/format-HTML (accessed April, 2020). **(Cited on page 118)**

US EPA O. Alternative Fuels. US EPA, 2015. https://www.epa.gov/renewable-fuel-standard-program/alternative-fuels. **(Cited on page 118)**

Vera-Tudela Fajardo WM, An experimental study of the effects of fuel properties on diesel spray processes using blends of single-component fuels. PhD thesis. Universitat Politècnica de València, 2015. **(Cited on page 7, 102, 103, 123)**

Viera A, Effect of multiple injection strategies on the Diesel spray formation and combustion using optical diagnostics. PhD thesis. Universitat Politècnica de València, 2019. **(Cited on page 50, 51, 76, 118)**

Wang J, Yang F, Ouyang M. Dieseline fueled flexible fuel compression ignition engine control based on in-cylinder pressure sensor. Applied Energy 2015;159:87–96. https://doi.org/10.1016/j.apenergy.2015.08.101. **(Cited on page 146)**

Wang Z, Liu H, Zhang J, Wang J, Shuai S. Performance, Combustion and Emission Characteristics of a Diesel Engine Fueled with Polyoxymethylene Dimethyl Ethers (PODE3-4)/ Diesel Blends. Energy Procedia 2015; 75:2337–44. https://doi.org/10.1016/j.egypro.2015.07.479. **(Cited on page 6)**

Wannatong K, Akarapanyavit N, Siengsanorh S, Chanchaona S. Combustion and Knock Characteristics of Natural Gas Diesel Dual Fuel Engine, SAE Technical Paper 2007-01-2047; 2007. https://doi.org/10.4271/2007-01-2047. **(Cited on page 29)**

Wei L, Geng P. A review on natural gas/diesel dual fuel combustion, emissions and performance. Fuel Processing Technology 2016;142:264–78. https://doi.org/10.1016/j.fuproc.2015.09.018. **(Cited on page 29)**

Welch AB, Wallace JS. Performance Characteristics of a Hydrogen-Fueled Diesel Engine with Ignition Assist, SAE Technical Paper 902070; 1990. https://doi.org/10.4271/902070. **(Cited on page 37)**

Wu Y, Ferns J, Li H, Andrews G. Investigation of Combustion and Emission Performance of Hydrogenated Vegetable Oil (HVO) Diesel. SAE International Journal of Fuels and Lubricants, SAE Int. J. Fuels Lubr. 10(3):2017; 2017. https://doi.org/10.4271/2017-01-2400. **(Cited on page 32)**

Xuan T, Desantes JM, Pastor JV, Garcia-Oliver JM. Soot temperature characterization of spray a flames by combined extinction and radiation methodology. Combustion and Flame 2019;204:290–303. https://doi.org/10.1016/j.combustflame.2019.03.023. **(Cited on page 81, 130, 131)**

Xuan T, Pastor JV, García-Oliver JM, García A, He Z, Wang Q, et al. In-flame soot quantification of diesel sprays under sooting/non-sooting critical conditions in an optical engine. Applied Thermal Engineering 2019;149:1–10. https://doi.org/10.1016/j.applthermaleng.2018.11.112. **(Cited on page 143)**

Xuan T. Optical investigations on diesel spray dynamics and in-flame soot formation. PhD thesis. Universitat Politècnica de València, 2017. **(Cited on page 8, 52, 61, 83)**

Xue J, Grift TE, Hansen AC. Effect of biodiesel on engine performances and emissions. Renewable and Sustainable Energy Reviews 2011;15:1098–116. https://doi.org/10.1016/j.rser.2010.11.016. **(Cited on page 31)**

Yang B, Xi C, Wei X, Zeng K, Lai M-C. Parametric investigation of natural gas port injection and diesel pilot injection on the combustion and emissions of a turbocharged common rail dual-fuel engine at low load. Applied Energy 2015;143:130–7. https://doi.org/10.1016/j.apenergy.2015.01.037. **(Cited on page 29)**

Yanowitz J, Compendium of Experimental Cetane Numbers. National Renewable Energy Laboratory (NREL); 2017. **(Cited on page 146)**

Yuvenda D, Sudarmanta B, Wahjudi A, Muraza O. Improved combustion performances and lowered emissions of CNG-diesel dual fuel engine under low load by optimizing CNG injection parameters. Fuel 2020;269:117202. https://doi.org/10.1016/j.fuel.2020.117202. **(Cited on page 35)**

Zhao H, Ladommatos N. Optical diagnostics for soot and temperature measurement in diesel engines. Progress in Energy and Combustion Science 1998;24:221–55. https://doi.org/10.1016/S0360-1285(97)00033-6. **(Cited on page 57, 60)**

Zhao M, Experimental and Numerical Study of OH Chemiluminescence in Hydrogen Diffusion Flames. Combustion and Flame 2018;197:369–77. https://doi.org/10.1016/j.combustflame.2018.08.019. **(Cited on page 58)**

Zhen X, Wang Y. An overview of methanol as an internal combustion engine fuel. Renewable and Sustainable Energy Reviews 2015;52:477–93. https://doi.org/10.1016/j.rser.2015.07.083. **(Cited on page 32, 33)**

Zubel M, Ottenwälder T, Heuser B, Pischinger S. Combustion system optimization for dimethyl ether using a genetic algorithm. International Journal of Engine Research 2021;22:22–38. https://doi.org/10.1177/1468087419851577. **(Cited on page 105)**

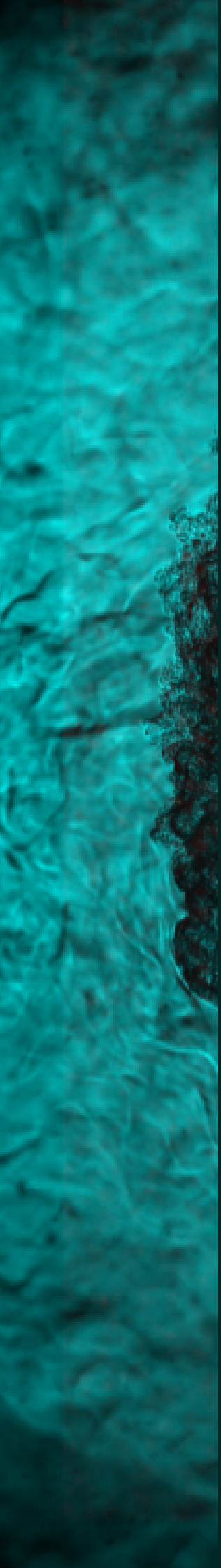

UNIVERSITAT POLITÈCNICA DE VALÈNCIA

EXPERIMENTAL STUDY OF THE FUEL EFFECT ON DIFFUSION COMBUSTION AND SOOT FORMATION UNDER DIESEL ENGINE-LIKE CONDITIONS

DOCTORAL THESIS

PRESENTED BY:

ALBA ANDREINA GARCÍA CARRERO

SUPERVISED BY:

JOSÉ VICENTE PASTOR SORIANO

NOVEMBER 2021

DEPARTAMENTO DE MÁQUINAS Y MOTORES TÉRMICOS